Mathematical modelling of haematopoiesis and blood diseases

Ivan Demin

UNIVERSITÉ DE LYON

ÉCOLE DOCTORALE InfoMaths

INFORMATIQUE ET MATHÉMATIQUES

T H È S E

pour obtenir le titre de

Docteur en Sciences

de l'Université Claude Bernard Lyon 1

Mention : MATHÉMATIQUES APPLIQUÉES

Présentée et soutenue par

Ivan DEMIN

Modélisations mathématiques de l'hématopoïèse et des maladies sanguines

Thèse dirigée par Vitaly VOLPERT et Charles DUMONTET

préparée à l'Université Lyon 1

soutenue le 11 décembre 2009

Jury :

Président :	Olivier GANDRILLON	Directeur de recherches au CNRS, Université Lyon 1
Rapporteurs :	Jean CLAIRAMBAULT	Directeur de recherches à INRIA, Rocquencourt
	Pierre MAGAL	Professeur, Université de Bordeaux
Directeurs :	Vitaly VOLPERT	Directeur de recherches au CNRS, Université Lyon 1
	Charles DUMONTET	PUPH, CHU Lyon
Examinatrice :	Narcisa APREUTESEI	Professeure, Université de Iasi, Roumanie

Remerciements

Tout d'abord, je souhaite exprimer ma profonde gratitude à mes deux directeurs de thèse, Vitaly Volpert et Charles Dumontet, pour le sujet de thèse qu'ils m'ont proposé et leur encadrement. Le travail sous leur direction m'a permis d'étudier un grand spectre de modèles et de méthodes modernes en mathématiques appliquées. Mon directeur principal, Vitaly, était toujours très disponible, ce qui a permis de rendre mon travail efficace. La collaboration avec Charles m'a appris beaucoup de choses sur d'autres disciplines que les mathématiques, en particulier sur la recherche clinique.

Je tiens à remercier également mes deux rapporteurs, Jean Clairambault et Pierre Magal. Je suis très honoré qu'ils aient accepté de relire mon manuscrit. Les remarques qu'ils ont faites m'ont permis d'améliorer la présentation et la qualité de mon travail.

Ensuite je voudrais exprimer ma reconnaisance au président du jury, Olivier Gandrillon. J'ai beaucoup collaboré avec lui tout au long de ma thèse concernant la partie biologique. Je remercie également Narcisa Apreutesei pour son rôle d'examinatrice de ma thèse.

J'ai fait ma thèse à l'Institut Camille Jordan, dans le groupe de Modélisation Mathématique en Médecine et en Biologie. Je voudrais donc remercier tous les membres de ce groupe, en particulier, Fabien Crauste, Stéphane Génieys, Laurent Pujo-Menjouet et Samuel Bernard. A chaque réunion où nous avons discuté de mon projet de recherche, ils m'ont toujours fait des suggestions très intéressantes dont j'ai essayé de tenir compte dans mes modèles. Je remercie encore une fois Olivier Gandrillon, qui a répondu présent à chaque fois que j'avais des questions et qui m'a donné des explications toujours très claires sur l'erythropoïèse et sa régulation. Et, en particuler, je souhaite remercier Fabien Crauste avec qui j'ai collaboré le plus pendant ma thèse. Sans lui, cela aurait été beaucoup plus difficile de bien terminer la première partie de ma thèse. Merci, Fabien. J'adresse également mes remerciements à mon camarade Pierre Crepel qui était toujours de bonne humeur. C'était un plaisir de le croiser dans les couloirs ou de passer lui dire bonjour.

Le bon déroulement d'une thèse ne dépend pas que de l'activité scientifique. Il est aussi important d'avoir les bonnes personnes autours de soi. Je tiens donc à remercier mes amis de l'université, Nastia, Nicolas, Polina, Vladimir et Loan avec qui j'ai pu partager les bons

moments et les moments difficiles. Une bonne activité physique est également nécessaire pour restituer les forces. Je remercie mon équipe de football "Objectifs Jeunes" et, en particulier, son capitaine Mohamed, grâce à qui j'ai pu me détendre sur le terrain. Je voudrais aussi remercier mes amis de mon autre equipe, "CBP", au sein de laquelle il était toujours agréable de jouer le dimanche matin.

Enfin, je remercie ma famille, qui m'a toujours apporté son soutien, m'a encouragé et a toujours cru en moi. Un très grand merci à ma chérie, Clara, avec tout mon amour. C'est grâce à elle que j'ai pu tenir ces trois ans de travail intense.

à la recherche française

Table des matières

Introduction

1 Biology and mathematical modelling of haematopoiesis

1.1 Haematopoiesis

Haematopoiesis is the process of blood cell production. In human adults, it occurs within the bone marrow, whereas in mice haematopoietic organs are located in the bone marrow and in the spleen. Blood cell production begins with haematopoietic stem cells (HSCs), which are multi-

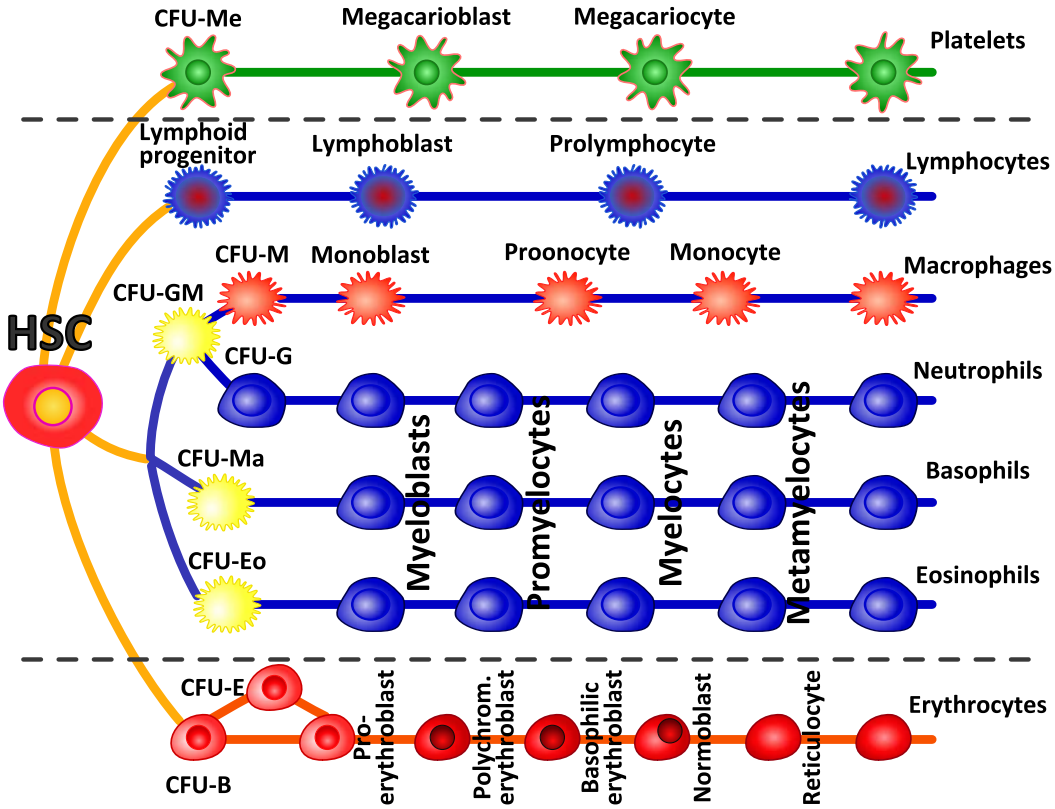

FIGURE 1 – Haematopoiesis scheme.

potent cells with self-renewal capacity and the ability to generate all blood cell types [22, 124]. Stem cells were discovered by Till and McCulloch [109] in 1961. More information about stem cells and their history can be found in [56]. Several types of stem cells can be distinguished :

✓ **totipotent stem cells** can differentiate into embryonic and extraembryonic cell types. Such cells can construct a complete, viable organism. Cells produced by the first few divisions of the fertilised egg are also totipotent ;

- ✓ **pluripotent stem cells** are the descendants of totipotent cells and can differentiate into almost all cells ;
- ✓ **multipotent stem cells** can differentiate into a number of closely related cells ;
- ✓ **oligopotent stem cells** can differentiate into only a few cells, such as lymphoid or myeloid stem cells ;
- ✓ **unipotent stem cells** can produce only one cell type, their own (for example skin, liver).

The number of HCSs is very small and they are difficult to identify. About 90% of HSCs remain in quiescent stage and do not proliferate. All blood cells originate from HSCs and can be divided into three categories (Figure 1) :

$\rightsquigarrow$ **Erythrocytes** (red blood cells, RBC) are simple cells filled with haemoglobin. Their main function is to transport oxygen to organs. In humans erythrocytes do not contain nucleus. The process of red blood cell production is called erythropoiesis.

$\rightsquigarrow$ **Leukocytes** (white blood cells) are cells of the immune system that defend the organism against various infectious diseases and foreign debris. They are produced through leukopoiesis and are divided into three subtypes :

- ✓ **granulocytes** possess granules in their cytoplasm. They phagocytose and destruct small foreign organisms ;
- ✓ **monocytes** move from blood to infected organs and phagocytose microbes, whole cells and also small pollutants ;
- ✓ **lymphocytes** are responsible for the specific recognition of foreign agents and their subsequent removal from the organism. They are divided into two groups, T and B lymphocytes. T lymphocytes are agents of cellular immunity that recognise infected cells and destroy them. B lymphocytes are involved in so-called humoral immunity. They destroy foreign substances.

$\rightsquigarrow$ **Platelets** (trombocytes) are produced by fragmentation of megakaryocytes. They play a fundamental role in haemostasis and blood coagulation.

In humans all these cells represent about 45% of blood volume, the rest of 55% is plasma composed mostly of water. Life time of white blood cells is about 24 hours, one week for platelets and about 120 days for red blood cells. One liter of blood contains 5×10^{12} of RBCs, 10^9 of WBCs and 3×10^{11} of platelets. Almost the whole volume of circulating blood cells is

occupied by RBCs.

1.2 Erythropoiesis

The focus of this work is, in particular, red blood cell lineage. Erythropoiesis is the process by which red blood cells are produced.

Haematopoietic stem cells differentiate into immature erythroid cells, called erythroid progenitors, which are undifferentiated cells committed to erythroid lineage. Then, through maturation and differentiation stages, erythroid progenitors become reticulocytes, which are almost mature red blood cells. These latter end their maturation to become red blood cells and enter the blood stream.

Erythropoiesis consists in a series of cell divisions through which erythroid cells acquire differentiation characteristics. This process allows the production of sufficient amount of erythrocytes to transport oxygen to organs. Erythropoiesis can sometimes exhibit disorders, such as excessive proliferation of immature cells, as observed in acute leukaemias [64, 74]. Such disorders can be caused by alteration of intracellular regulatory networks, which control cell fate (e.g. Madan et al. [70]), that is self-renewal (the ability to produce daughter cells of the same maturity [123]), differentiation (the ability to produce more mature daughter cells) or apoptosis (programmed cell death). Hence, the regulation of erythropoiesis depends on a precise control of cell fate by means of intracellular proteins and growth factors.

Usually self-renewal is considered to be a property of stem cells. However recent studies [51, 83] have shown that erythroid progenitors, which are committed stem cells, also possess this ability. Differentiation allows the production of two daughter cells, one of which at least being more mature than the mother cell. Apoptosis is a programmed cell death [108]. It is a particular form of cell death, different from necrosis, which is controlled by various regulatory mechanisms.

One of the most well studied growth factors, playing an important role in erythropoiesis regulation, is erythropoietin (Epo), a glucoprotein released by the kidney in response to hypoxia, that is a lack of oxygen in tissues. Glucocorticoids (GCs) are lipophilic hormones involved in the regulation of various physiological responses, and in particular in stress erythropoiesis. They

are known to favour cell proliferation [129]. Growth factors operate by activating membrane receptors on cell surface to trigger intracellular protein activation.

Recently, Rubiolo et al. [96] proposed a description of the regulatory network that controls erythroid progenitor fate : some proteins are involved in a self-renewal loop, some others in a differentiation/apoptosis loop, see Figure 4. The first loop self-activates and inhibits the second one, whereas the second loop can inhibit the first one and, depending on Epo levels, induce either erythroid progenitor differentiation or apoptosis. Self-renewal loop relies on proteins of the MAPK family, the other loop is mainly controlled by Fas, a protein of the tumour-necrosis factor family.

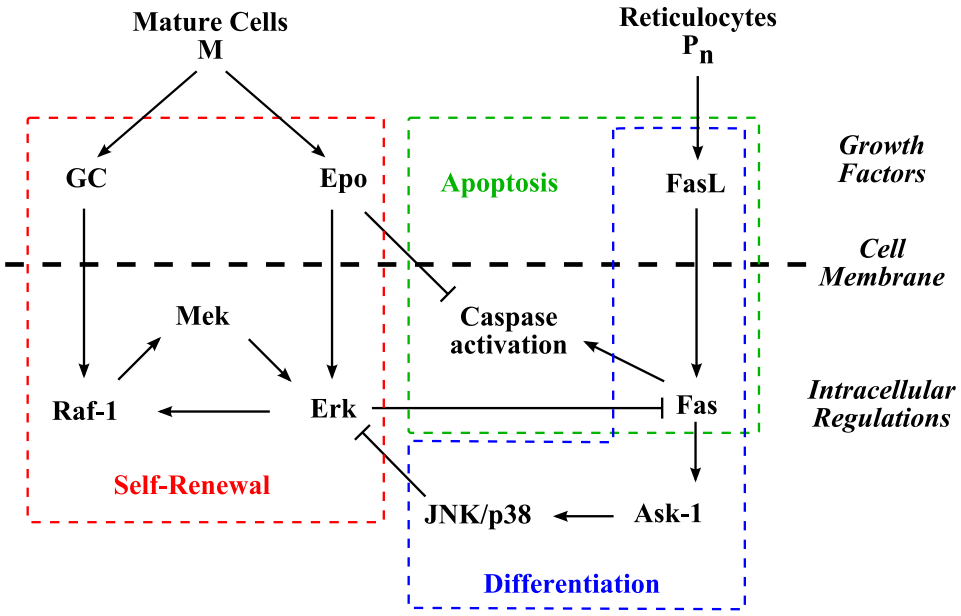

FIGURE 2 – Summary of intracellular protein interactions that determine erythroid progenitor fate, partially adapted from [96].

Cells in the bone marrow are known to exchange different signals that regulate cell behaviour. Hence, it is important to take into account spatial distribution of cells. In the next section we discuss spatial organisation of the bone marrow.

1.3 Spatial structure of the bone marrow

Bone marrow is a flexible tissue located in the hollow interior of bones. It is located mainly in flat bones, such as the hip bone, breast bone, skull, ribs, vertebrae, and in the cancellous material at the epiphyseal ends of the long bones such as the femur and humerus.

Bone marrow cells have a certain spatial structure. Animal studies support the hypothesis that the HSCs and progenitor cells are localised much closer to the bone trabecula surfaces and decrease in concentration within deeper regions of bone marrow [80, 107]. Works by Frassoni et al. [47], Lord [66], and Cui et al. [37] on the mouse femoral shaft have demonstrated a clear spatial gradient in the distribution of different cell lines responding to marrow growth factors as a function of distance inside the femoral medullary cavity.

One of recent studies of spatial distribution of cells in the bone marrow was published by Watchman et al. [122]. The objective of this work was to directly measure the spatial concentration of HSCs and progenitor cells within human disease-free bone marrow. The authors obtained that haematopoietic $CD34^+$ cells (stem cells committed to erythroid lineage) were located along a linear spatial gradient with a maximal areal concentration localised within the first 50μm of the bone surfaces.

For erythroid progenitors, an important role play erythroblastic islands. Erythroblastic islands are specific microenvironmental compartments, within which erythroblasts proliferate and differentiate. They have been firstly described by M. Bessis [18]. In the center of such an island a macrophage is located surrounded by a ring of developing erythroblasts in various stages of differentiation, ranging from CFU-E (immature erythroid progenitors) to young reticulocytes [72]. Erythroblastic islands are uniformly distributed throughout the bone marrow and contain variable number of erythroblasts. Rat femurs have about 10 cells per island, whereas islands harvested from human bone marrow contain 5–30 erythroblasts. The interaction between different components of these structures is essential through all stages of maturation. It is suggested that during early stages of maturation, macrophages provide nutrients and proliferative signals to erythroblasts, during late stages macrophages promote enucleation and phagocytose injected nuclei. Both macrophages and erythroblasts display adhesive interactions that maintain island integrity. These interactions enable regulatory feedbacks between cells within

islands and also trigger intracellular signaling pathways that regulate gene expressions. Some feedbacks between mature and immature erythroblasts as well as between macrophages and immature erythroblasts carry out controls of apoptosis. The process of enucleation which is governed by macrophages decreases the adhesion between the macrophages and well differentiated erythroblasts (reticulocytes). These latter detach from the islands and are taken away by the blood stream.

Different disorders can appear during these complex processes of cell production, among which leukaemias. In the next section we discuss leukaemias and their treatment.

1.4 Leukaemias and treatments

Up to now, cancer was the second cause of death in developed countries, after cardiovascular diseases (CVDs). Since 1980's and by 2004 the number of deaths due to CVDs has decreased twice while that due to cancer has decreased only by 10%. Statistics on deaths in France shows that cancer has become the first cause of death in 2004 and will certainly keep this position. Among cancers, leukaemia occupies the third place [8].

Leukaemia is a cancer of blood or bone marrow and is characterised by abnormal proliferation of precursor cells or haematopoietic stem cells within the bone marrow. Leukaemia can be acute (rapid increase of immature blood cells) or chronic (excessive production of relatively mature blood cells). Leukaemias are generally classified according to the type of blood cells affected. Four most common kinds of leukaemia are acute lymphoblastic leukaemia (ALL), chronic lymphocytic leukaemia (CLL), chronic myeloid leukaemia (CML) and acute myeloid leukaemia (AML). In 1970th so-called French-American-British (FAB) classification of leukaemias was elaborated. In this work the attention is focused on the AML, FAB classification for AML can be found in Figure 3.

Acute leukaemias, by its definition, develop abruptly and require urgent treatment, it progresses rapidly and is typically fatal within weeks or months if left untreated. The first step in diagnosis is the enumeration of blast cells (immature progenitors) in the blood and examination of their cytologic features. In [16, 106] more information about leukaemia diagnosis can be found. AML (known also as acute myelogenous leukaemia or acute nonlymphocytic leu-

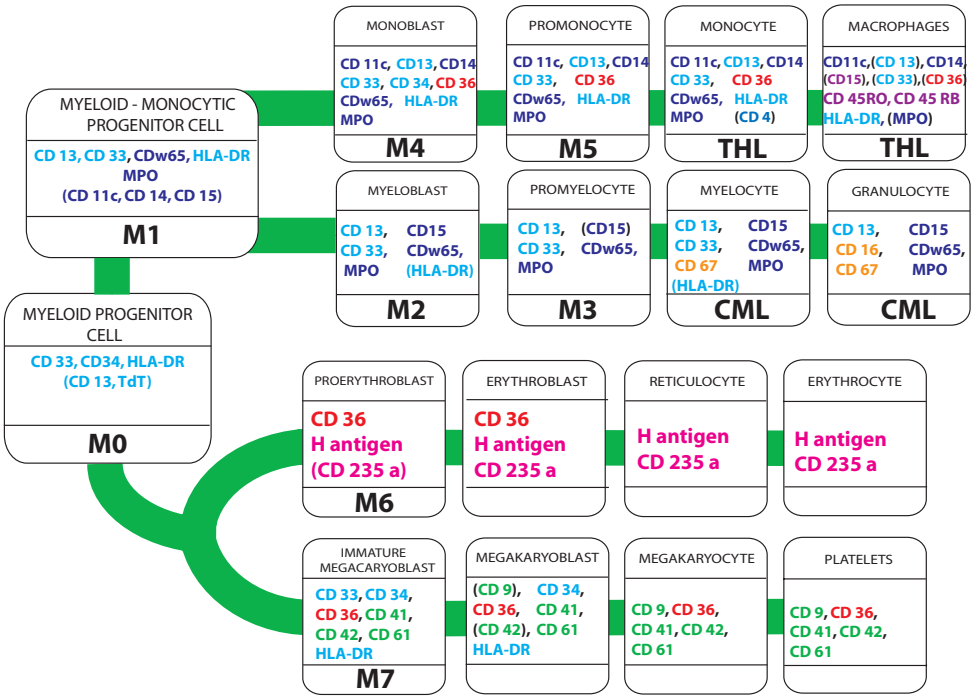

FIGURE 3 – Myeloid cell differentiation - Schematic figure of myeloid differentiation including the corresponding leukaemia and non-Hodgkin lymphomas as well as cell markers involved in each stage, adapted from [86].

kaemia) is a subtype of leukaemia in which myeloid lineage is involved. It is rare in childhood (15% of childhood AL), but is much more frequent than ALL in adults [16] with median age above 60 years. Usual symptoms of AML are fatigue, weight loss, shortness of breath, easy bruising and bleeding and increased risk of infection. Although several risk factors for AML have been identified, the specific cause of AML remains unclear.

The treatment of acute leukaemia consists generally of chemotherapy with or without stem cell transplantation [24, 100]. Two phases of treatment are usually applied, the standard first phase of AML treatment is induction chemotherapy. The goal is to bring the disease into remission, when the patient's blood counts return to normal and bone marrow samples show no sign of disease, i.e. less than 5% of cells are leukaemic. Induction chemotherapy is very intense and usually lasts one week, followed by three or more weeks for the patient to recover from the treatment. The second phase is consolidation chemotherapy, the goal is to destroy any remaining leukaemic cells.

The majority of cytotoxic drugs that are used in chemotherapy are not specific to malignant cells. They affect normal bone marrow cells as well, which is its great disadvantage. Generally, chemotherapy drugs are cycle-active agents, it kills all cells that are in S phase of cell cycle. Hence, such a treatment has many side effects. Stem cell transplantation is a powerful technique but many side effects persist in early and late phases after the transplantation [112].

One of the standard and most important drugs currently available for the treatment of AML is AraC (1-β-D-arabinofuranosylcytosine, cytarabine, cytosine arabinoside), see [61, 97]. AraC is administered in combination with other drugs, usually daunorubicin or idarubicin. It is also active against other haematologic malignancies, including acute lymphoblastic leukaemia (ALL) and non-Hodgkin's lymphoma. AraC is a cytotoxic nucleoside analog that has some differences in chemical structure with respect to physiological nucleosides. Its metabolism and mechanism of action are relatively well known [58], but its efficacy is limited by numerous resistances that occur during treatment [58, 102]. For example, AraC shows virtually no activity with isolated leukaemic stem cells [57].

Active form of AraC is its triphosphate AraCTP, which competes with deoxycytidine triphosphate (dCTP) for incorporation into DNA. When incorporated, AraCTP blocks DNA synthesis and thus cell proliferation. At high intracellular concentrations, AraCTP is cytotoxic, at

low intracellular concentrations there is still a pronounced cytostatic effect. The numbers of killed malignant as well as normal cells are determined by intracellular AraCTP concentrations. Thus, crucial importance has the knowledge of relationship between administered AraC and intracellular AraCTP concentrations. The measurements of intracellular concentrations of nucleoside analogs imply complex procedures. One of the approaches to measure several intracellular nucleosides simultaneously has been recently developed and approved [34]. It is not clear which dose of AraC is optimal for concrete patient, though some standard protocols are usually applied. Some trials are currently being carried out, in which clinicians try to find out optimal conditions of treatment. For example, in [61] the authors study if high-dose AraC treatment is more effective for patient survival than standard dose AraC treatment. Mathematical modelling can be a good additional utility for that kind of research.

In the next section we present an overview of the works on mathematical modelling of haematopoiesis and erythropoiesis. In Section 1.6 we discuss possible ways to model leukaemia treatment.

1.5 Mathematical modeling of haematopoiesis and erythropoiesis

Mathematical modelling of haematopoiesis and HSC dynamics has been attracting much attention since the end of the 1970's. One of the first models was proposed by Mackey [67] in 1978, which described periodic haematopoiesis at the cellular level by delay equations. The approach proposed in [67] was later used in many works devoted to the description of oscillatory behaviours within haematopoietic systems. In [17] Bernard et al. focused on the white blood cell production to bring an explanation to oscillatory phenomena observed in patients with cyclical neutropenia. A global model of haematopoietic cell dynamics has been proposed by Colijn and Mackey [32, 33] in 2005. Other works on haematopoiesis modelling have been proposed by Loeffler and his collaborators since the beginning of the 1980's, see [91, 93].

Pioneering models of erythropoiesis regulation were proposed by Wichmann and Loeffler [126] in 1985. They modelled the dynamics of haematopoietic stem cells, erythroid progenitors and erythroid precursors (reticulocytes). The authors considered feedback controls from reticulocytes on progenitors and from progenitors on stem cells, confronted their models with

experimental data on stress erythropoiesis (bleeding, irradiation) and fitted model parameters. Later Wulff et al. [128] and Wichmann et al. [127] improved Wichmann and Loeffler's models. In 1995, Bélair et al. [15] proposed a model of erythropoiesis, partially based on previous works by Mackey [67, 68] and his collaborators [69] on haematopoietic stem cell dynamics. In [15] the authors proposed an age-structured model describing erythroid cell dynamics, including an explicit control of differentiation by erythropoietin. This model was then improved in [71]. Other works inspired by [15] proposed mathematical models of erythropoiesis [1, 2, 12]. The erythropoietin-mediated inhibition of apoptosis has been considered in Adimy and Crauste [3]. The authors focused on the appearance of periodic haematological diseases (such as periodic chronic myeloid leukemia [46]).

It is however noticeable that in all above-mentioned papers self-renewal ability is associated with haematopoietic stem cells only. Relatively new feature in erythropoiesis modelling is related to self-renewal ability of erythroid progenitors. In [36] the authors concluded that adding self-renewing capacity to erythroid progenitors allows a better fit of experimental data on induced anaemia.

Modelling of regulatory networks involved in cell decision has been the subject of recent analysis of lineage specification. As it is known, erythrocytes and platelets have one myeloid progenitor in common, called MEP (for Megakaryocytic-Erythroid Progenitor). As a result of a competition between two proteins (PU.1 and GATA-1), the MEP differentiates either into an erythroid progenitor or into a megakaryocytic progenitor. This choice has been modelled by Roeder and Glauche [92] and Huang et al. [55]. In both studies, models proposed by the authors demonstrated a bistable behaviour. This idea has been further developed in Chickarmane et al. [30].

Cell-to-cell interactions inside bone marrow play a crucial role for haematopoiesis regulation. One of the appropriate approaches that would allow taking into account these interactions is the individual based modelling. This considers each cell as an independent element of the whole system and, thus, every cell can have its own properties and protein concentrations. Some IBM models of growth of cell populations were presented in [50]. In [43] the authors discussed individual based models of growth of unstructured cell populations, that is spatial structure formation of monolayers and multicellular spheroids. In [26] the authors compared two alternative

theoretical approaches for simulating the growth of cell aggregates in vitro : individual based models and continuous models.

There is an extensive literature devoted to modelling of solid tumors. Cell proliferation results in the motion of the medium described by Darcy's law or Navier-Stokes equations, see [7, 49, 87]. The PDE models of cell motion can be justified by probabilistic methods (see [27] and the references therein). In [44] the authors described cell concentrations within the bone marrow by reaction-diffusion equations and their motion by Darcy's law.

1.6 PK/PD modelling

Pharmacokinetic-pharmacodynamic (PK/PD) models study drug distribution and efficacy. Such models include accurate description of drug delivery to the specific organs being treated and introduce an insight into the understanding of the drug action. In the future it promises an important tool for designing new drugs and protocols applicable for treatment of certain diseases. Once the drug is delivered to the organ being treated it penetrates through the cell membrane. Inside cells a scheme of metabolism provides detailed description of drug transformation into its active form. This set of events constitutes pharmacokinetics. Pharmacodynamics, in turn, describes how active metabolite of the drug acts on diseased organs [111].

PK/PD modelling and simulations can be used as an applied tool to provide more insignts into efficacy and safety of new drugs faster and at a lower cost, it can be helpful through all clinical and preclinical phases of drug development. Let us give an example from the current practice of PK/PD involvement into the drug design process. CPX-351 (cytarabine/daunorubicin liposome injection) is a liposomal formulation of a synergistic, fixed combination of AraC and daunorubicin encapsulated within the liposomes for intravenous infusion. The two drugs leak out much easier when liposomes are situated inside bone marrow. CPX-351 is currently under Phase II of clinical trial. The paper [14] provides a pharmacokinetic model of CPX-351 liposome injection in the mouse. The authors studied leak rates from liposomes in plasma and bone marrow, which allowed the prediction of free drug concentrations. In [88] an interested reader will find a review of PK/PD applications for drug development and its use in pharmacological industry.

Sometimes modelers use the term WBPBPKPD, which stands for the Whole Body Physiologically Based PK/PD modelling. An interesting work was presented in [113], in which the authors studied a WBPBPKPD model of the drug called capecitabine, which is a triple prodrug of 5-FU. More general model of this type can be found in [121]. In [31] the author remarks that developing such WBPBPKPD models needs a lot of experimental work *in vitro* as well as *in vivo* and that this modelling is very drug specific.

Modelling of leukaemia and its treatment attracts much attention since 1970s. For example in paper [94] by Rubinow et al., the authors proposed a dynamic mathematical model of the acute myeloblastic leukaemic state, in which normal neutrophils (granulocytes) and their precursors, and leukemic myeloblasts, proliferate as distinct but interacting cell populations, G_0 compartment (resting cells) is considered for each population. In [95] Rubinow et al. introduced a model of chemotherapy and by calculations they demonstrated that small changes in the protocol can have significant effects on efficacy of treatment. They then found optimal treatment protocol. Another mathematical model of AML can be found in [4], in which cell populations are supposed to have Gompertzian dynamics. In [89] Ribba et al. considered a mathematical model of treatment of non-Hodkin's lympoma. The authors investigated drug pharmacokinetics (PK) in order to determine drug concentrations in the vasculature at any given time and drug pharmacodynamics (PD). They then investigated qualitatively some treatment regimens.

Recently, the work [25] was published, in which the authors considered a simple PK/PD model of treatment of non-small cell lung cancer and breast cancer. The integrated model contains four major components : PK model, biomarker model, model of signal transduction and tumour response model (PD). Some experiments were carried out in parallel with cell lines that allowed the estimation of certain model parameters.

In [65, 76] Morrison and his collaborators proposed a very accurate PK/PD model of AML treatment with AraC. They introduced a model of drug distribution in the body, drug metabolism and drug action on DNA synthesis. The authors estimated all constants for L1210 cell line (lymphocytic leukaemia cells derived from mice) and carried out computer simulations of treatment. A PK/PD model presented in this thesis is based on these works.

2 Summary of the results

The thesis deals with several aspects of haematopoiesis modelling and with modelling of leukaemia treatment. Some of the results are published in [19, 20, 35, 40, 41, 42]. The work consists of four chapters.

In the first chapter we present two multiscale models of haematopoiesis regulation. In the second chapter we consider spatial models of haematopoiesis. Third chapter is devoted to individual based modelling approach. The last chapter of the work describes a PK/PD model of leukaemia treatment with AraC.

Multi-scale modelling of erythropoiesis. Haematopoiesis is a process of blood cell production, which occurs mainly in the bone marrow. All blood cells are divided into three groups : red blood cells, white blood cells and platelets. The process of production of red blood cells is called erythropoiesis. We developed two mathematical models that describe haematopoiesis regulation, one more specific to erythropoiesis. Normal erythropoiesis is maintained by the balance between self-renewal, differentiation and apoptosis. There are a number of intracellular proteins and growth factors that control this balance. The scheme of the intracellular regulatory network can be found in Figure 4. Two intracellular proteins, Erk and Fas, are supposed to be determinant for regulation of self-renewal, differentiation and apoptosis.

Two models of the intracellular regulatory network, which governs these processes, are proposed. We first consider a general bistable dynamic system, which can be applied to haematopoiesis modelling as well. Then, we describe the intracellular regulatory network as a set of chemical reactions and obtained the following system,

$$\begin{cases} \dfrac{dE}{dt} &= \left(\alpha(Epo, GC) + \beta E^k\right)(1-E) - aE - bEF, \\ \dfrac{dF}{dt} &= \gamma(P_n)(1-F) - cEF - dF, \end{cases}$$

where E and F are Erk and Fas concentrations, functions $\alpha(Epo, GC)$ and $\gamma(P_n)$ describe feedback controls. We conclude that this system has a bistable behaviour for certain parameter values.

We consider several compartments of erythroid progenitors according to maturity, denoted

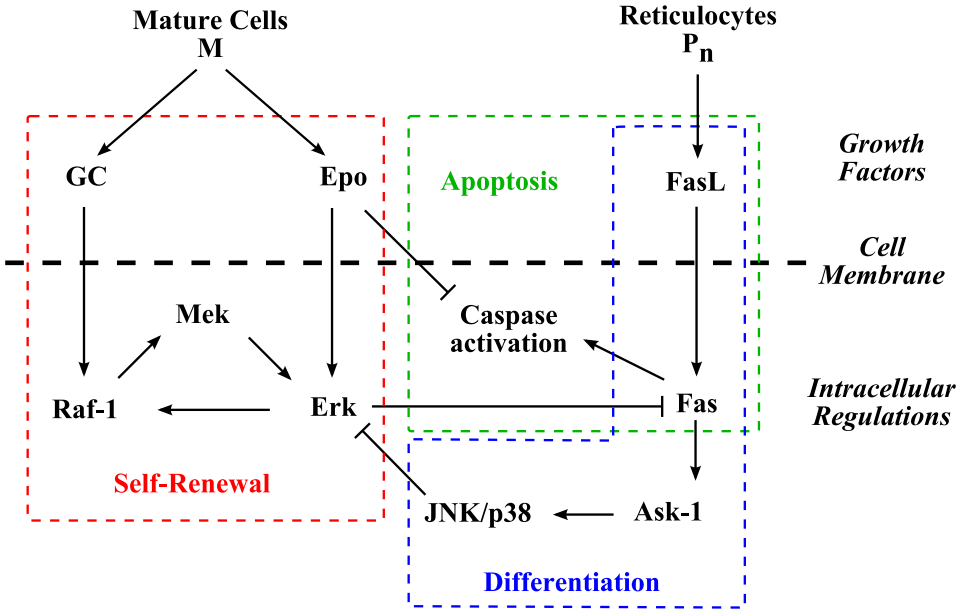

FIGURE 4 – Summary of intracellular protein interactions that determine erythroid progenitor fate, partially adapted from [96].

by $P_1, \ldots, P_n$, and a population of erythrocytes, denoted by M, see Figure 5. For each sub-

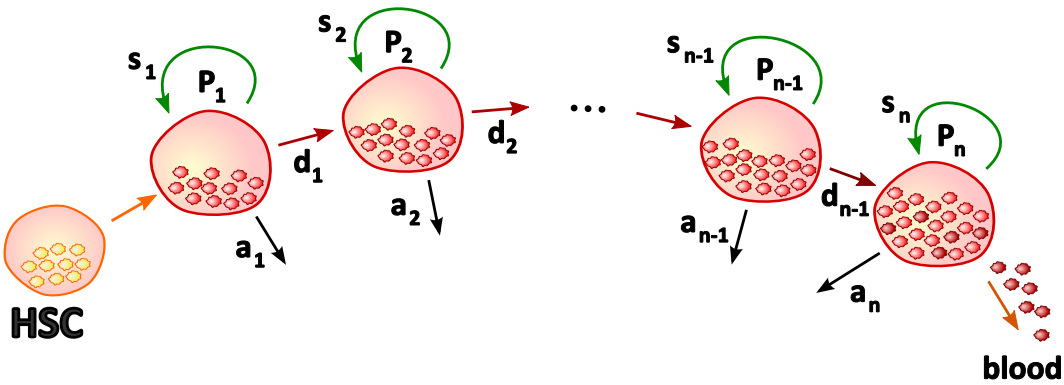

FIGURE 5 – Differentiation scheme of erythroid progenitors. P_i, $i = 1, \ldots, n$, denotes the number of progenitors in the i-th sub-population per μl of blood, and by s_i, d_i and a_i their rates of self-renewal, differentiation and apoptosis, respectively.

population of progenitors we introduce self-renewal, differentiation and apoptosis rates, s_i, d_i and a_i. Dynamics of erythroid progenitors are described by the following differential equations,

$$\frac{dP_1}{dt} = HSC + s_1 P_1 - d_1 P_1 - a_1 P_1,$$

where HSC accounts for the cell influx from the stem cell compartment, and for $i = 2, \ldots, n$,

$$\frac{dP_i}{dt} = 2d_{i-1}P_{i-1} + s_iP_i - d_iP_i - a_iP_i.$$

Dynamics of erythrocyte count satisfies

$$\frac{dM}{dt} = d_nP_n - \delta M,$$

where δ is the natural mortality rate of erythrocytes.

Regulation of erythropoiesis is realised through several feedback controls, which are turned on in stress situations, e.g. anaemia, lack of red blood cells. We introduce into the model two growth factors, erythropoietin (Epo) and glucocorticoids (GC). Their dynamics are described by

$$\frac{dEpo}{dt} = f_{Epo}(M) - k_{Epo}\,Epo,$$
$$\frac{dGC}{dt} = f_{GC}(M) - k_{GC}\,GC,$$

where k_{Epo} and k_{GC} are degradation constants, and f_{Epo} and f_{GC} are production terms, determined by the number of erythrocytes. We choose Michaelis-Menten functions to describe these dependencies.

The rates are controlled through intracellular regulatory network, based on Erk and Fas. We consider as well a direct inhibition of apoptosis by Epo, independently of the intracellular network. Hence, functions the s_i, d_i and a_i are defined as

$$s_i = s(E_i, F_i), \quad d_i = d(E_i, F_i), \quad a_i = a(E_i, F_i)\, f_{aEpo}(Epo),$$

The function f_{aEpo} describes a direct mechanism of apoptosis inhibition by Epo. We considered Hill function to describe it.

We thus obtain two models of erythropoiesis. The first one is a general model which can be extended to haematopoiesis, it is presented in [40]. The second one contains more precise description of the intracellular network involved in erythropoiesis regulation. The objective of

this work is to evaluate the roles of the feedback controls in order to provide more insights into the regulation of erythropoiesis. This work is presented in [35].

For each model we find steady states and their stability using Implicit Function Theorem. To test the models, we carry out computer simulations of anaemia, that is a lack of red blood cells. The obtained results are confronted with experimental data on induced by phenylhydrazine anaemia in mice, see Figure 20. The second model allows the conclusion that feedback by Epo on apoptosis rate, independently of the intracellular network based on Erk and Fas, is determinant during early stages after anaemia induction, whereas intracellular regulatory network is important later. These two models can be found in Chapter I.

Spatial models of erythropoiesis. Bone marrow has a particular structure. Current research in this field provides more and more insights into its spatial composition. A part of the work is dedicated to spatial models of erythropoiesis.

We describe erythropoiesis by a system of reaction-diffusion-convection equations in a porous medium,

$$\frac{\partial c_i}{\partial t} + \nabla.(c_i v) = d\Delta c_i + k(c_{i-1} - c_i), \quad i = 1, \dots, n, \quad c_0 = 0,$$
$$\Delta P = k(c_1 + \dots + c_n), \quad \nabla P = \nu v,$$

which is considered in the domain

$$\Omega = (0, L_x) \times (0, L_y)$$

with boundary conditions

$$\frac{\partial P}{\partial x}(0, y) = 0, \quad \frac{\partial P}{\partial y}(x, 0) = 0, \quad \frac{\partial P}{\partial y}(x, L_y) = 0, \quad P(L_x, y) = 0,$$
$$c_1(0, y) = 1, \quad \frac{\partial c_1}{\partial y}(x, 0) = 0, \quad \frac{\partial c_1}{\partial y}(x, L_y) = 0, \quad \frac{\partial c_1}{\partial x}(L_x, y) = 0,$$
$$\frac{\partial c_i}{\partial x}(0, y) = 0, \quad \frac{\partial c_i}{\partial y}(x, 0) = 0, \quad \frac{\partial c_i}{\partial y}(x, L_y) = 0, \quad \frac{\partial c_i}{\partial x}(L_x, y) = 0,$$
$$i = 2, \dots, n.$$

where c_i denotes concentration of cells in i-th sub-population, v is the velocity of the medium, d is diffusion coefficient. Reaction functions are determined from the populational model introduced above.

Using Leray-Schauder method we prove the existence of a stationary solution in 1D case, that is a solution of the following system,

$$dc_i'' - (c_i p')' + k(c_{i-1} - c_i) = 0, \quad i = 1, ..., n, \quad c_0 = 0$$
$$p'' = \nu \left(\sum_{k=1}^{n-1} (s_i + d_i)c_i + (s_n - d_n)c_n \right),$$

together with the boundary conditions

$$c_1(0) = 1, \;\; c_i'(0) = 0 \;\; i = 2, ..., n,$$
$$c_i'(L) = 0, \;\; i = 1, .., n,$$
$$p'(0) = 0, \;\; p(0) = 0.$$

To do so we introduce the following homotopy,

$$dc_i'' - \tau(c_i p')' + (\tau 2 d_{i-1} c_{i-1} - b_i c_i) = 0, \;\; c_0 = 0, \;\; i = 1, ..., n, \quad \tau \in [0, 1],$$
$$p'' = \nu \sum_{k=1}^{n} k_i c_i,$$

and find a priori estimates of solutions of this system, which allows the application of Leray-Schauder method.

Computer simulations in 2D case are carried out using COMSOL MULTIPHYSICS software. In leukaemic case, malignant cells propagate as a travelling wave. We describe their distribution in the bone marrow the following equation,

$$\frac{\partial s}{\partial t} + \nabla.(sv) = d_s \Delta s + k_s s,$$

with the same boundary conditions as for other cells,

$$\frac{\partial s}{\partial x}(0,y)=0, \quad \frac{\partial s}{\partial y}(x,0)=0, \quad \frac{\partial s}{\partial y}(x,L_y)=0, \quad \frac{\partial s}{\partial x}(L_x,y)=0.$$

We calculate wave speed of malignant cell propagation in two ways, using direct numerical calculations and analytical approximations. We then compared results of the two methods of wave speed calculation. This work was presented in the paper [41].

Cells in the bone marrow exchange bio-chemical signals. This communication has direct impact on cell behaviour and is important for erythropoiesis regulation. A cell can perceive signals from other cells that are located in certain neighbourhood. We study the existence of a solution of the following non-local reaction-diffusion equation, which describes such a cell communication,

$$\frac{\partial u}{\partial t}=\frac{\partial^2 u}{\partial x^2}+J(u)\,u(1-u)-\alpha u, \quad x\in\mathbb{R},$$

where

$$J(u)=\int_{-\infty}^{\infty}\phi(x-y)u(y,t)dy.$$

Here $\phi(x)$ is a non-negative function with a bounded support, $\phi(x-y)$ shows how the cells located at the point y influence the cells located at the point x.

We prove the existence of solution in the form of travelling wave $u(x,t)=w(x-ct)$. In [10] the authors proved the existence of solutions in the form of monotone travelling waves for a similar integro-differential equation, in which function ϕ had a small support $[-\varepsilon_0,\varepsilon_0]$. We construct a homotopy with parameter $\tau\in[0,1]$ that relies our equation to the equation with function ϕ having a small support. A solution in the form of travelling wave satisfies

$$w''+cw'+J_\tau(w)w(1-w)-\alpha w=0 \tag{0.1}$$

with

$$J_\tau(u)=\int_{-\infty}^{\infty}\phi_\tau(x-y)u(y)dy,$$

where

$$\phi_\tau(x)=\frac{(\varepsilon_0-1)\tau+1}{\varepsilon_0}\,\phi\left(\frac{((\varepsilon_0-1)\tau+1)x}{\varepsilon_0}\right)$$

We are interested in solutions with the following conditions at infinities,

$$\lim_{x\to\pm\infty} w(x) = w_{\pm}. \tag{0.2}$$

We work in Hölder weighted spaces. Obviously, any function $u \in C^{k+\alpha}_{\mu}(\mathbb{R})$ tends to zero at infinity. On the other hand, we look for solutions of Equation (0.1) with the limits (0.2). Therefore, we introduce an infinitely differentiable function $\psi(x)$ such that $\psi(x) = w_+$ for $x \geqslant 1$ and $\psi(x) = w_-$ for $x \leqslant -1$ and put $w = u + \psi$. Hence we can write Equation 0.1 in the form

$$(u+\psi)'' + c(u+\psi)' + J(u+\psi)(u+\psi)(1-u-\psi) - \alpha(u+\psi) = 0.$$

We consider the operator $A(u)$ corresponding to the left-hand side of the previous equation,

$$A_\tau(u) = (u+\psi)'' + c(u+\psi)' + J_\tau(u+\psi)(u+\psi)(1-u-\psi) - \alpha(u+\psi)$$

Again, we use Leray-Schauder method to prove the existence of waves. In order to construct the topological degree for operator $A_\tau(u)$ acting in weighted Hölder spaces,

$$A : C^{2+\alpha}_{\mu}(\mathbb{R}) \to C^{\alpha}_{\mu}(\mathbb{R}), \quad \mu(x) = 1 + x^2$$

with norms

$$\|u\|_{C^{2+\alpha}_{\mu}(\mathbb{R})} = \|u\mu\|_{C^{2+\alpha}(\mathbb{R})},$$

we demonstrate that it is proper and its linearised operator L is Fredholm with zero index. Note that due to the invariance of solutions $u(x+h)$ obtained by a translation of the solution $u(x)$, they are not bounded in the weighted Hölder space $C^{2+\alpha}_{\mu}(\mathbb{R})$. This makes impossible to find a priori estimate of solutions. In order to get rid of this invariance, we apply a functionalisation of parameter c. We introduce functional

$$c(u) = \ln \int_R (u(x) + \psi(x) - w_+)^2 \sigma(x) dx,$$

where $\sigma(x)$ is an increasing function, with $\sigma(-\infty) = 0$, $\sigma(+\infty) = 1$ and

$$\int_{-\infty}^{0} \sigma(x)dx < \infty.$$

We find a priori estimates of solutions that allows the application of Leray-Schauder method [42].

These two models can be found in Chapter II.

Individual based modelling approach. Cell-to-cell communications are very important for the erythropoiesis regulation. One of the appropriate approaches that would allow taking into account this communication is the individual based modelling. This considers each cell as an independent element of the whole system and, thus, allows considering communications of every single cell with its neighbours that can provide additional insights into the behaviour of cell populations.

In Section 10 a multi-agent software that describes such a communication is presented [20]. It allows us to numerically study spatial distribution of erythroid progenitors in the bone marrow, see Section 11. Using this software we demonstrate that cell division can generate random cell motion, see Section 12. Random cell motion, in turn, can be described by a diffusion term when dealing with continuous models [19]. This modelling together with the description of the software are presented in Chapter III.

PK/PD modelling of AML treatment with AraC. Acute myeloid leukaemia, known also as non-lymphocytic or myelogenous leukaemia, is a type of leukaemia characterised by abnormal proliferation of immature myeloid cells. One of the most common and effective chemotherapeutic agents against AML is AraC (cytosine arabinoside, cytarabine), which is used in combination with other drugs. Pharmacokinetics-pharmacodynamics approach is one of modern ways to study drug efficiency for treatment of certain diseases. The last part of the work is devoted to the PK/PD modelling of AML treatment with AraC.

We built a mathematical model of AraC distribution in the body and of its action. The model consists of two parts. First part describes pharmacokinetics of AraC, that is drug delivery to the bone marrow, penetration through cell membrane and its metabolism, which is a set of interactions between the drug and intracellular proteins, its degradation, phosphorylation and

deamination. We consider AraC distribution between two compartments, blood and bone marrow. Using Michaelis-Menten kinetics we describe metabolism of AraC. Its scheme is presented in Figure 6. Dynamics of extracellular AraC concentration in blood (a_b) and in bone marrow (a_m) are given by

$$\begin{aligned}\frac{da_b}{dt} &= I(t) - k_{bm}(a_b - a_m) - \gamma_b a_b,\\ \frac{da_m}{dt} &= k_{bm}(a_b - a_m) - k_{hENT1}(a_m - a_{mi}) - \gamma_m a_m,\end{aligned}$$

where $I(t)$ determines treatment protocol, γ_b and γ_m are clearance constants in blood and in bone marrow, k_{bm} describes the rate of AraC distribution between the two compartments, k_{hENT1} describes thansmembrane transport of AraC in the bone marrow. This simple model allows us to take into account transmembrane transport of AraC.

Dynamics of intracellular AraC (a_{mi}) and AraCTP (ap_3) concentrations are given by

$$\begin{aligned}\frac{da_i}{dt} &= k_{hENT1}(a - a_{mi}) - \dot{r}_p + \dot{r}_{dp} - \dot{r}_{da},\\ \frac{dap_3}{dt} &= (\dot{r}_p - \dot{r}_{dp})/\widetilde{\alpha},\end{aligned}$$

where phosphorylation rate of AraC is given by

$$\dot{r}_p \equiv \left[\frac{d(ap_1 + ap_2 + ap_3)}{dt}\right]_p = \frac{V_k}{1 + \frac{K_m}{a_{mi}}\left(1 + \frac{c}{K_i} + \frac{dC}{K_I} + \frac{ap_3}{K_i'}\right) + K_m\left(\frac{c}{K_i K_m'} + \frac{ap_3}{K_i' K_m''}\right)},$$

dephosphorylation rate is given by

$$\dot{r}_{dp} \equiv \left[\frac{d(ap_1 + ap_2 + ap_3)}{dt}\right]_{dp} = \left(1 + \frac{1}{\alpha_1\alpha_2} + \frac{1}{\alpha_1}\right)\left[\frac{d\,ap_3}{dt}\right]_{dp} = \frac{V_{dp}}{1 + \frac{\alpha_1\alpha_2 K_{dp}}{ap_3}},$$

and deamination rate is given by

$$\dot{r}_{da} = \frac{da}{dt} = \frac{V_{da}}{1 + \frac{K_{da}}{a_{mi}}}.$$

Second part of the modelling is pharmacodynamics. We consider the following spatial mo-

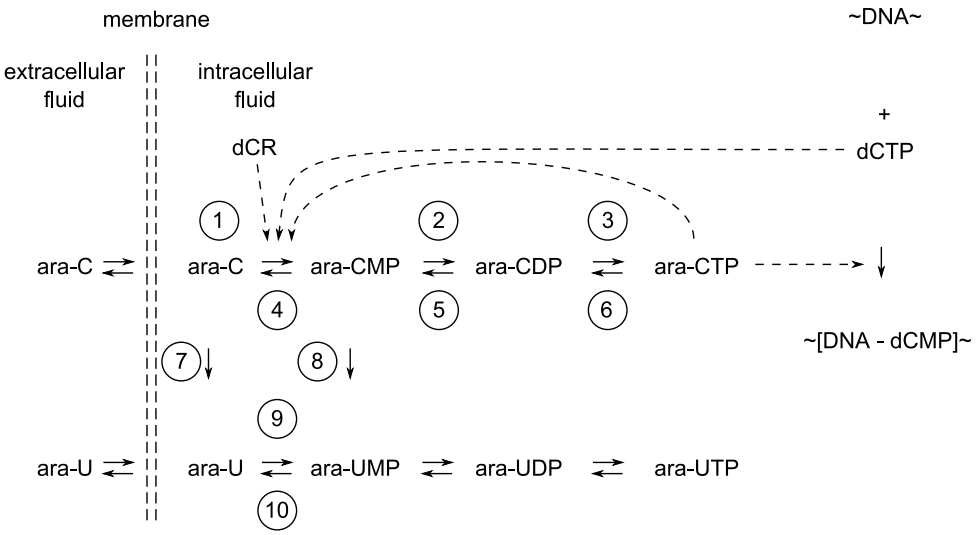

FIGURE 6 – The metabolism of AraC, adapted from [76].

del of erythroleukaemia,

$$\begin{cases} \dfrac{\partial P}{\partial t} &= D_P \dfrac{\partial^2 P}{\partial x^2} + H + (s-d)P(P_0 - P - Q) - aP, \\ \dfrac{\partial Q}{\partial t} &= D_Q \dfrac{\partial^2 Q}{\partial x^2} + (s_m - d_m)Q(P_0 - P - Q) - a_m Q, \end{cases}$$

where P denotes normal cell population and Q denotes malignant cell population, H denotes the influx of haematopoietic stem cells, s, d and a are respectively self-renewal, differentiation and apoptosis rates (s_m, d_m and a_m are the rates for malignant cells). We suppose that cell concentrations cannot surpass certain threshold value P_0. We find conditions of existence of leukaemic equilibrium (P_m^*, Q_m^*) for the system without diffusion terms. Then we demonstrate that this equilibrium is globally assimptotically stable in the sense that any solution with the initial condition $(P_0(x), Q_0(x))$, where $P_0(x) \geqslant \varepsilon$, $Q_0(x) \geqslant \varepsilon$, ε is a positive constant, converges uniformly to $(P, Q) = (P_m^*, Q_m^*)$ as $t \to \infty$.

We describe the drug action as a dependence of the three rates on AraCTP concentration.

$$s = s(ap_3), \quad d = d(ap_3), \quad a = a(ap_3),$$

We then carry out simulations of WBPBPK model and PK/PD and test different treatment pro-

tocols. The work has been developed in the frame of ANR project AnaTools and is presented in Chapter IV.

Première partie

Multi-scale Modelling of Erythropoiesis

This part of the work is devoted to mathematical modelling of erythropoiesis. We propose two multi-scale models, in which we bring together erythroid progenitor dynamics and intracellular regulatory network that determines erythroid cell fate. First model is based on a general bistable system which describes intracellular regulatory network. In the second model we describe intracellular regulatory network as a set of chemical reactions. All erythroid progenitors are divided into several sub-populations according to their maturity. Two intracellular proteins, Erk and Fas, are supposed to be determinant for regulation of self-renewal, differentiation and apoptosis. We consider two growth factors, erythropoietin and glucocorticoids, and describe their dynamics. Several feedback controls are introduced in the model. We carry out computer simulations of anaemia and compare the obtained results with available experimental data on induced anaemia in mice. The main objective of this work is to evaluate the roles of the feedback controls in order to provide more insights into the regulation of erythropoiesis. Feedback by Epo on apoptosis is shown to be determinant in the early stages of the response to anaemia, whereas regulation through intracellular regulatory network, based on Erk and Fas, appears to operate on a long-term scale.

3 Intracellular regulatory network

In a recent paper, Rubiolo et al. [96] investigated the differentiation process of erythroid progenitors. In particular, they identified key proteins involved in self-renewal and differentiation/apoptosis, see Figure 7. Differentiation and apoptosis appear to be controlled by the same proteins. In fact, different proteins are involved both in cell differentiation and cell apoptosis, however, depending on external conditions, cells undergo either differentiation or apoptosis. For example, Epo has been shown to inhibit erythroid progenitor apoptosis [63]. Hence, when Epo levels are low, erythroid progenitors preferentially die by apoptosis, whereas with high Epo levels they differentiate.

Rubiolo et al. [96] showed that self-renewal was controlled by the self-activated cascade Raf-1 - Mek - Erk, whereas differentiation was controlled by the cascade Fas - Ask-1 - Jnk/p38, Fas triggering also cell apoptosis. This latter protein cascade is inhibited by the former, and vice versa. Hence erythroid progenitor self-renewal and differentiation/apoptosis processes are

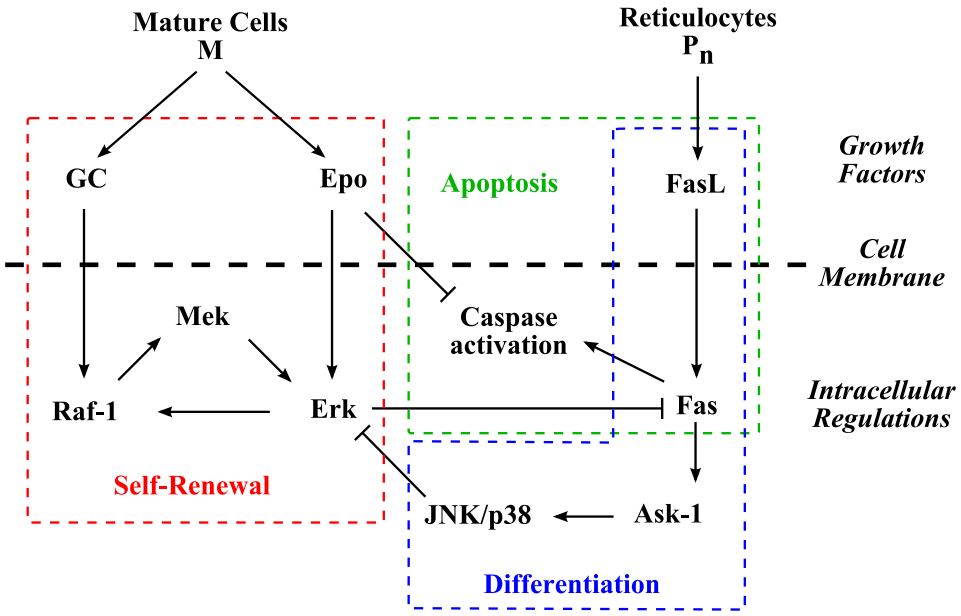

FIGURE 7 – Summary of intracellular protein interactions that determine erythroid progenitor fate, partially adapted from [96].

controlled by two inhibitor loops, one being self-activating. Two proteins are of particular interest : Erk and Fas. The former is the cornerstone of the inhibition of differentiation and apoptosis. Erk (Extracellular signal-Regulated Kinase) is a member of the MAPK family, also known as the classical MAP kinase, it regulates cell proliferation and differentiation. Fas belongs to the tumour necrosis factor family (TNF), it induces cell apoptosis. We focus our attention on the interaction between these two proteins, that are key regulators of erythroid progenitor fate.

As mentioned in Figure 7, external signals activate intracellular proteins. Epo is known to have the dual action of being both a mitogen and a survival factor [103]. The molecular mechanisms involved have been clarified (for a review, see [98]) : Epo prevents apoptosis of erythroid progenitors through Stat5/GATA-1/Bcl-xL pathway [53], that is largely independent of the ERK pathway [28, 79, 105]. Self-renewal promoting activity of Epo, on the contrary, seems to rely mainly on the activation of the ERK kinase [96, 104]. We therefore decided to integrate separately these two aspects of Epo action in the model : prevention of apoptosis is modelled as a direct mechanism, i.e. the molecular players are not explicitly taken into account. This feedback is assumed to be independent of the intracellular regulatory network based on Erk and Fas interactions. This is introduced in Section 5.1, Equation (1.18). On the contrary,

self-renewal is modelled as an ERK-dependent mechanism. GCs are involved in regulation of stress erythropoiesis [13, 51]. They activate self-renewing loop by increasing the level of Raf-1 expression.

One source term of activation appears in Figure 7 concerning the differentiation/apoptosis part. Fas-ligand, denoted by FasL, a membrane protein, activates the transmembrane protein Fas. De Maria et al. [39] suggested the existence of a negative regulatory feedback between mature and immature erythroid progenitors, in which mature cells exert a cytotoxic effect on immature cells. Mature erythroid progenitors, called reticulocytes, express FasL, which stimulates activation of Fas in immature erythroid progenitors. Sensitivity to FasL decreases with cell maturation. Other external factors, such as c-Kit, the protein associated with the stem cell factor (SCF) [77], proteins from the JAK family [114], etc., regulate the levels of activated intracellular proteins. Yet, we cannot take all these proteins into account, and we focus, in the following, on Epo, GCs, and FasL.

Further we discuss two different approaches to describe the intracellular regulatory network. First approach considers a bistable system that describes interaction between Erk and Fas (Section 3.1). In the second approach we make transition from a linear system describing interactions presented in Figure 7 to a nonlinear system that can have either monostable or bistable behaviour depending on parameter values (Section 3.2). Consider the first approach.

3.1 General bistable system

We focus our attention on two proteins, Erk and Fas, and we suppose that their expression levels determine the values of self-renewal, differentiation and apoptosis rates. Note that these proteins are present in cells in two forms, activated and inactivated. We are interested in the activated protein forms. There exist maximum values for Erk and Fas activated forms that cannot be surpassed. So, we denote by E the ratio of activated Erk form to its maximum value, by F the ratio of Fas activated form to its maximum value. This guarantees the variables E and F to be between 0 and 1, that is favorable for mathematical analysis and not limiting for modelling. To describe the competition between Erk and Fas we consider the following system that has a

bistable behaviour,

$$\begin{cases} \dfrac{dE}{dt} =(E-a)(b-E-c(F-a)), \\ \dfrac{dF}{dt} =(F-a)(b-F-c(E-a)), \end{cases} \tag{1.1}$$

where a, b and c are positive constants, $a < b$ and $c > 1$. The system has four steady states, $(E^1, F^1) = (a, a)$, $(E^2, F^2) = (a, b)$, $(E^3, F^3) = (b, a)$, $(E^4, F^4) = \left(\frac{b+ac}{1+c}, \frac{b+ac}{1+c}\right)$. The steady states (E^2, F^2) and (E^3, F^3) are stable. The steady state $(E^2, F^2) = (a, b)$ corresponds to Fas domination, which means that the cell rather chooses differentiation or apoptosis than self-renewal, and the steady state $(E^3, F^3) = (b, a)$ corresponds to Erk prevalence, which means that the cell undergoes rather self-renewal. Thus (E^3, F^3) is associated with cell proliferation, whereas (E^2, F^2) is associated with cell differentiation and apoptosis. The two other steady states, (E^1, F^1) and (E^4, F^4), are unstable. A detailed mathematical analysis of a system similar to the system above can be found in [78].

If in this system we add external sources of activation : the activation of ERK-cascade due to Epo and GCs denoted by α and FasL-related activation of Fas denoted by γ, then it becomes,

$$\begin{cases} \dfrac{dE}{dt} =(E-a)(b-E-c(F-a)) + \alpha, \\ \dfrac{dF}{dt} =(F-a)(b-F-c(E-a)) + \gamma. \end{cases} \tag{1.2}$$

In the next section we consider a specific system that describes intracellular protein interactions presented in Figure 7 as a set of chemical reactions.

3.2 From linear behaviour to bistability

Denote by R, M, E, F, A and J the levels of activated forms of Raf-1, Mek, Erk, Fas, Ask-1 and Jnk/p38, respectively. We describe the reactions of either activation/suppression of expression or activation by means of linear ordinary differential equations. Enzymatic activation is expressed by a positive linear term, whereas suppression of expression or suppression of activation appears as a negative linear term. When modelling intracellular regulation mechanisms, external signal sources are considered as constants. We denote by λ_{GC} the source of glucocorticoids stimulating Raf-1 activation, by λ_{Epo} the source of erythropoietin activating

Erk, and by λ_{FL} the external source of FasL stimulating Fas activation. Then, the following system describes the regulatory network summarised in Figure 7,

$$\left\{\begin{array}{lcllcl} \dfrac{dR}{dt} &=& \lambda_{GC} + k_1 E - k_2 R, & \dfrac{dF}{dt} &=& \lambda_{FL} - k_8 E - k_9 F, \\ \dfrac{dM}{dt} &=& k_3 R - k_4 M, & \dfrac{dA}{dt} &=& k_{10} F - k_{11} A, \\ \dfrac{dE}{dt} &=& \lambda_{Epo} + k_5 M - k_6 E - k_7 J, & \dfrac{dJ}{dt} &=& k_{12} A - k_{13} J. \end{array}\right. \tag{1.3}$$

The last term in each equation stands for degradation. All constants k_i, $i = 1, \ldots, 13$, are positive.

In order to focus on Erk and Fas dynamics, we suppose that all reactions except those for Erk and Fas are rapid. This allows obtaining equations for Erk and Fas, while keeping all the information contained in System (1.3). Rapid reactions are then in steady state with respect to slow reactions, which provides

$$\left\{\begin{array}{lcllcl} R &=& \dfrac{\lambda_{GC} + k_1 E}{k_2}, & A &=& \dfrac{k_{10}}{k_{11}} F, \\ M &=& \dfrac{k_3}{k_4} R, & J &=& \dfrac{k_{12}}{k_{13}} A. \end{array}\right. \tag{1.4}$$

Using values of R, M, J and A in (1.4) in equations for E and F in (1.3), the following linear system describing interactions between activated Erk and activated Fas is obtained,

$$\left\{\begin{array}{lcl} \dfrac{dE}{dt} &=& \alpha + \beta E - aE - bF, \\ \dfrac{dF}{dt} &=& \gamma - cE - dF, \end{array}\right. \tag{1.5}$$

where

$$\alpha = \lambda_{Epo} + \frac{k_3 k_5}{k_2 k_4} \lambda_{GC}, \quad \beta = \frac{k_1 k_3 k_5}{k_2 k_4}, \quad \gamma = \lambda_{FL},$$

and

$$a = k_6, \quad b = \frac{k_7 k_{10} k_{12}}{k_{11} k_{13}}, \quad c = k_8, \quad d = k_9.$$

All coefficients a, b, c, d and α, β, γ are nonnegative. First terms on the right hand side of System (1.5) account for activation of Erk and Fas by external factors (α and γ) and by self-

activation (βE). Other terms describe suppression of activation.

System (1.5) is a linear system of ordinary differential equations. It has a unique steady state, whose stability depends upon the parameter values. We are particularly interested in the instability of this steady state. Indeed, when it is unstable, either there is an unlimited growth of activated Erk concentration, and the cell finally undergoes self-renewal, or an unlimited growth of activated Fas concentration, and the cell undergoes either differentiation or apoptosis. In reality, this growth is limited, due to cell division for instance. Hence, this linear system appears well adapted to the description of Erk and Fas interactions, even if it is biologically limited.

Since we aim at using this system coupled with a description of cell population dynamics, which is reported in Section 4, and also for the model to be more biologically realistic, we make some additional assumptions on the dynamics of Erk and Fas concentrations.

First, as described in Figure 7, Fas acts on Erk by suppressing its expression and conversely Erk suppresses Fas activation. In agreement with mass action law, we assume the rates of these suppressions, coefficients b and c in System (1.5), are proportional to the concentration of E and F respectively, so that the terms $-bF$ and $-cE$ become $-bEF$ and $-cEF$. This assumption allows, in particular, the Problem (1.5) to be well-posed in the sense that E and F cannot become negative contrary to the original system.

The second term in the right-hand side of the first equation in (1.5), describing Erk self-activation, is replaced with βE^k, where $k \geqslant 1$. This considers a nonlinear rate of Erk production. The choice of this nonlinearity can be discussed. In particular, as observed in Figure 7, Erk self-activation is obtained through a kinase cascade, that could be appropriately fitted with Michaelis-Menten functions (smooth positive increasing s-shaped functions). Qualitatively, both assumptions are equivalent. Yet, the choice we make allows an easier analysis of the final System (1.6), and consequently its deeper study.

Third, due to limited resources, we assume there exist maximal values that limit productions of Erk and Fas. Denote by E_0 the maximum value of activated Erk, and by F_0 the maximum value of activated Fas. System (1.5) now reads as

$$\left\{ \begin{array}{rcl} \dfrac{dE}{dt} & = & (\alpha + \beta E^k)(E_0 - E) - aE - bEF, \\ \dfrac{dF}{dt} & = & \gamma(F_0 - F) - cEF - dF. \end{array} \right. \tag{1.6}$$

To find steady states of System (1.6), we should solve

$$\frac{dE}{dt} = 0 \qquad \text{and} \qquad \frac{dF}{dt} = 0,$$

that is

$$F = \frac{(\alpha + \beta E^k)(E_0 - E)}{bE} - \frac{a}{b} \qquad \text{and} \qquad F = \frac{\gamma F_0}{cE + d + \gamma}. \tag{1.7}$$

Depending on the parameter values, (1.7) can have one to three solutions. Indeed, denote by ξ and χ the following functions,

$$\xi(E) = \frac{(\alpha + \beta E^k)(E_0 - E)}{bE} - \frac{a}{b} \qquad \text{and} \qquad \chi(E) = \frac{\gamma F_0}{cE + d + \gamma}. \tag{1.8}$$

Then one easily obtains that χ is a bounded positive decreasing function, mapping the interval $[0, E_0]$ into $[\gamma F_0/(cE_0 + d + \gamma), \gamma F_0/(d + \gamma)]$. The function ξ satisfies

$$\lim_{E \to 0} \xi(E) = +\infty \qquad \text{and} \qquad \xi(E_0) = -\frac{a}{b} < 0.$$

Consequently, System (1.6) has at least one steady state.

The analysis of the variations of function ξ, easy though tedious, shows that for some values of the parameters ξ is decreasing, hence System (1.6) has only one steady state. For other parameter values however, ξ is not monotonous and up to three steady states may exist. In particular, to obtain existence of three steady states it is necessary that $k > 1$.

The case of three steady states is shown in Figure 8. The points A and C are stable nodes, the point B is a saddle. The point A corresponds to high levels of activated Fas and low levels of activated Erk, whereas the point C corresponds to low levels of activated Fas and high levels of activated Erk. Hence, the point A is associated with erythroid progenitor differentiation or apoptosis, the point C with erythroid progenitor self-renewal.

The basins of attraction of the points A and C are separated by the separatrix of the point B. If the initial condition is chosen in a random way on the plane (E, F), then the probability for the trajectory to go to the point A or to the point C depends on the areas of their basins of attraction. Let us denote these probabilities by p_A and p_C, respectively. It can be easily verified

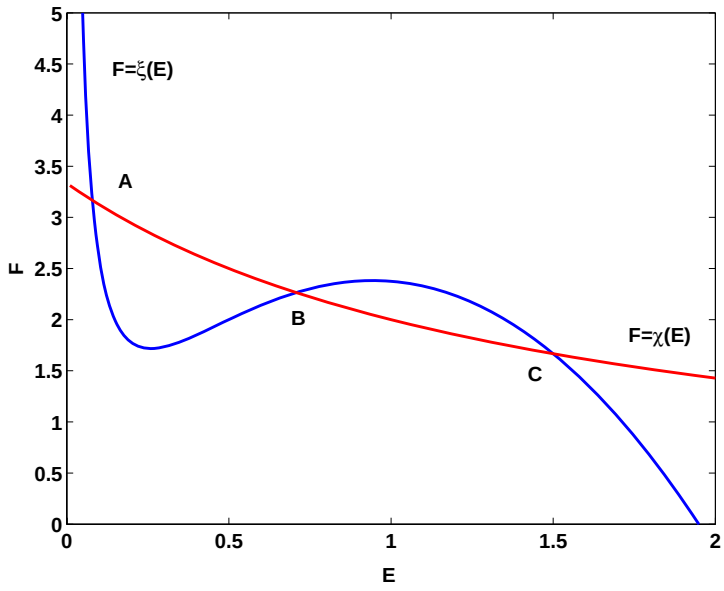

FIGURE 8 – Curves defined by (1.8). Three intersection points determine steady states of System (1.6). Two of them, A and C, are stable.

that p_A increases with the increase of γ and decreases with the increase of α. Moreover,

$$p_A = \begin{cases} 0, & \text{if } \gamma \leqslant \gamma_1, \\ 1, & \text{if } \gamma \geqslant \gamma_2, \end{cases}$$

where γ_1 and γ_2 are some given values, $\gamma_1 < \gamma_2$, which depend on α. We note that $p_A + p_C = 1$. Hence, if γ is sufficiently large the erythroid progenitor will undergo differentiation or apoptosis, whereas if γ is sufficiently small it will self-renew.

When there is only one steady state, it is asymptotically stable, and corresponds either to a high level of activated Fas (with low level of activated Erk), or to a high level of activated Erk (with low level of activated Fas). These situations may be obtained when $\gamma > \gamma_2$, for instance, or $\gamma < \gamma_1$. Equivalently, this corresponds to a movement upwards of the curve $F = \chi(E)$ in Figure 8 ($\gamma > \gamma_2$) or downwards ($\gamma < \gamma_1$).

If α and γ are not constant but dynamically depend on growth factors, then, during a response to a stress, values of α and γ can be such that temporarily System (1.6) goes from three steady states to only one steady state, and all cells undergo either self-renewal or differentiation/apoptosis.

4 Erythroid progenitor dynamics

Since erythroid cell sensitivity to external signals strongly depends on the maturity, we consider several erythroid progenitor differentiation stages, called sub-populations, characterised by their maturity. We suppose there are n erythroid progenitor sub-populations, with $n > 1$ fixed. Let us denote by P_i, $i = 1, \ldots, n$, the number of progenitors in the i-th sub-population per μl of blood, and by s_i, d_i and a_i their rates of self-renewal, differentiation and apoptosis, respectively. For the sake of simplicity we consider only symmetric cell division. Then, progenitor self-renewal produces two daughter cells with the same maturity as the mother cell, thus, the two cells belong to the same sub-population. Differentiation produces two cells, which are more mature, and then belong to the next sub-population, see Figure 9. Dynamics of erythroid

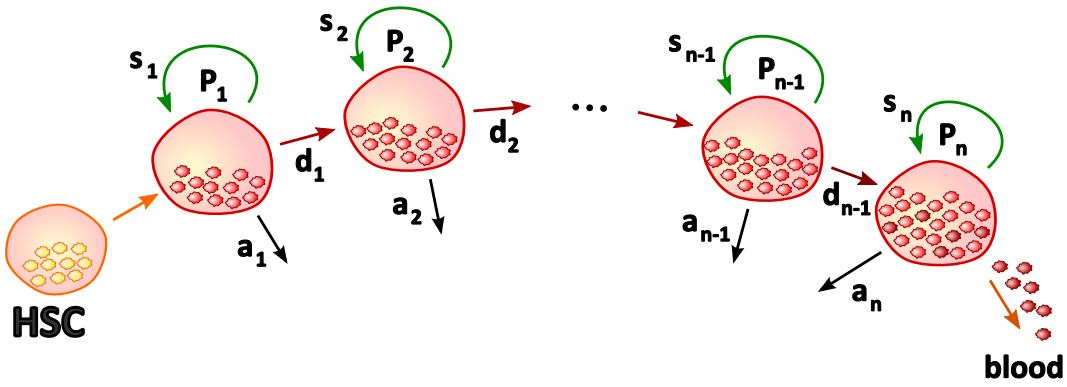

FIGURE 9 – Differentiation scheme of erythroid progenitors. P_i, $i = 1, \ldots, n$, denotes the number of progenitors in the i-th sub-population per μl of blood, and by s_i, d_i and a_i their rates of self-renewal, differentiation and apoptosis, respectively.

progenitors are described by the following system of differential equations,

$$\frac{dP_1}{dt} = HSC + s_1 P_1 - d_1 P_1 - a_1 P_1, \tag{1.9}$$

where HSC accounts for the cell influx from the stem cell compartment, and for $i = 2, \ldots, n$,

$$\frac{dP_i}{dt} = 2d_{i-1} P_{i-1} + s_i P_i - d_i P_i - a_i P_i. \tag{1.10}$$

Moreover, we denote by M the number of erythrocytes per μl of blood, which satisfies

$$\frac{dM}{dt} = d_n P_n - \delta M, \tag{1.11}$$

where δ is the natural mortality rate of erythrocytes.

The term red blood cell (RBC) refers to an erythroid cell which circulates in the blood flow and carries oxygen to tissues. It can be an erythrocyte or a reticulocyte. During normal erythropoiesis very few reticulocytes circulate in the blood. For this reason and since we do not consider spatial aspects of erythropoiesis that could allow distinguishing between circulating reticulocytes and reticulocytes in the bone marrow, we assume that RBC count equals erythrocyte count. RBC count is determinant for the release of various growth factors in the blood stream. For instance, due to a lack of oxygen, kidneys release Epo. RBCs also induce the release of glucocorticoids in stress situations [13]. Denote by Epo and GC the blood levels of erythropoietin and glucocorticoids respectively. They are supposed to satisfy ordinary differential equations [15, 71],

$$\frac{dEpo}{dt} = f_{Epo}(M) - k_{Epo}\, Epo, \tag{1.12}$$

$$\frac{dGC}{dt} = f_{GC}(M) - k_{GC}\, GC, \tag{1.13}$$

where k_{Epo} and k_{GC} are degradation constants, and f_{Epo} and f_{GC} are production terms. They depend on the number of erythrocytes, and are supposed to be positive, bounded, decreasing functions, since the more erythrocytes the lower erythropoietin and glucocorticoid levels.

In the next section we couple intracellular protein dynamics with cell population dynamics, and obtain multi-scale models of erythropoiesis.

5 Models of erythropoiesis

5.1 Coupling the two scales

To simplify the modelling, we neglect variations in cell cycle durations, so cell cycle lengths are supposed to be constant, equal to T_c. Each cell cycle ends up with either self-renewal,

differentiation or apoptosis. Then, on every time unit

$$s_i + d_i + a_i = \frac{1}{T_c}.$$

Since erythroid progenitors perform one cell cycle in about 24 hours [36], and the time unit considered in this paper is also 24 hours, we suppose $T_c = 1$ and the above equality becomes

$$s_i + d_i + a_i = 1. \tag{1.14}$$

Let us specify how these rates are defined. This is used later in this section and in Section 6. Denote by p_s the probability of self-renewal provided that the cell does not undergo apoptosis. Then the probability of differentiation p_d, provided that the cell does not undergo apoptosis, is $p_d = 1 - p_s$. Since cell cycle time is fixed and equals one time unit, we can then write s and d (subscripts are deliberately omitted) as

$$s = (1 - a)p_s, \quad d = (1 - a)(1 - p_s). \tag{1.15}$$

The term $1-a$ accounts for the rate of survival to apoptosis. Consequently, s denotes the overall self-renewal rate, which is in fact expressed by the probability of self-renewal of non-apoptotic cells p_s multiplied by the rate of survival $1 - a$. The same holds for the differentiation rate.

As described in Section 3, self-renewal, differentiation and apoptosis rates depend on one hand on the intracellular protein regulatory network inherent to each erythroid progenitor, and on another hand apoptosis is inhibited by Epo. Proteins Erk and Fas have been previously identified as the main regulators of erythroid progenitor fate, see Section 3. Erk induces self-renewal, and inhibits differentiation and apoptosis, whereas Fas inhibits self-renewal and induces differentiation or apoptosis, depending on Epo blood concentration. In the first model, concentrations of Erk and Fas, denoted by E and F, satisfy System (1.2), in the second model the satisfy System (1.6), where constants α and γ account for external sources of Erk and Fas activators, respectively. As mentioned in Section 3, the source of Erk activator consists mainly in erythropoietin and glucocorticoids. Hence, we assume α is an increasing function of Epo and

GC,

$$\alpha = \alpha(Epo, GC).$$

Parameter γ stands for activation of Fas by FasL, which is expressed on surface of reticulocytes. Hence, we assume γ depends on P_n, which correspond to reticulocytes, and the sensitivity of γ to P_n decreases with maturity level i, so that

$$\gamma = \gamma_i(P_n),$$

and γ_i is a positive, bounded and increasing function.

Finally, before stating the system verified by concentrations E and F, let us present the last assumption. As explained in the previous section, quantities of Erk and Fas are supposed to have maximum values, denoted by E_0 and F_0 respectively. Usually, exact quantities of Erk and Fas in erythroid cells cannot be measured, rather relative levels of activated Erk and Fas are provided. Hence, in order to render this model more comprehensible, we normalise activated Erk and Fas quantities, denoting by E and F the ratios E/E_0 and F/F_0. This guarantees the variables E and F to be between 0 and 1. Thus, E_i and F_i, the levels of activated Erk and Fas in the i-th progenitor sub-populations, satisfy the following system, obtained from (1.6),

$$\left\{ \begin{array}{rcl} \dfrac{dE_i}{dt} & = & \left(\alpha(Epo, GC) + \beta E_i^k\right)(1 - E_i) - aE_i - bE_iF_i, \\ \dfrac{dF_i}{dt} & = & \gamma_i(P_n)(1 - F_i) - cE_iF_i - dF_i, \end{array} \right. \tag{1.16}$$

where β, a, b, c and d respectively stand for βE_0^k, aE_0, bE_0F_0, cE_0F_0 and dF_0. Note that all cells of a sub-population are assumed to express the same levels of activated Erk and Fas. This is a strong hypothesis, because in reality, different progenitors with the same maturity express different levels of Erk and Fas indicating stochasticity in protein expression. This stochasticity certainly plays an important role in erythropoiesis, yet in this model we do not take it into account.

The same normalisation can be done for System (1.2),

$$\begin{cases} \dfrac{dE}{dt} =(E-a)(b-E-c(F-a))+\alpha(Epo,GC), \\ \dfrac{dF}{dt} =(F-a)(b-F-c(E-a))+\gamma_i(P_n). \end{cases} \tag{1.17}$$

For example, for the first equation of the system, if $\alpha = 0$, then $E < b$ if initial condition $E_{init} < E_0 = b$. If $\alpha > 0$, then $E < E_0 = 0.5(a+b+\sqrt{(a-b)^2+4\alpha_{\max}})$. So we solve this system, obtain (E, F) and do the normalisation to use (E, F) in the system.

One may observe the complexity of erythropoiesis through the model we propose. Erythroid progenitors and erythrocytes contribute to the control of growth factor concentrations in blood, which in turn regulate intracellular mechanisms of cell fate (self-renewal, differentiation, apoptosis). We complete the model of erythropoiesis by specifying how intracellular regulatory mechanisms influence erythroid progenitor fate.

As described in Section 3, self-renewal, differentiation and apoptosis rates depend on levels of activated Erk and Fas, denoted by E_i and F_i, the subscript i referring to a given subpopulation. Moreover, apoptosis rate is also inhibited by Epo independently of the intracellular network based on Erk and Fas. Hence, functions s_i, d_i and a_i are defined as

$$s_i = s(E_i, F_i), \quad d_i = d(E_i, F_i), \quad a_i = a(E_i, F_i)\, f_{aEpo}(Epo), \tag{1.18}$$

where functions s, d and a define self-renewal, differentiation, and apoptosis rates, respectively, for given Erk and Fas levels. The function f_{aEpo} describes a direct mechanism of apoptosis inhibition by Epo, which is independent of the intracellular regulatory network. It is assumed to be bounded, positive and decreasing.

Dynamics of erythroid progenitors, described by Equations (1.9)–(1.10), are then coupled to protein levels (1.17) in the first model (to protein levels (1.16) in the second model) through erythrocyte dynamics in (1.11), growth factor concentration evolution in (1.12)–(1.13), and self-renewal, differentiation and apoptosis rates definitions in (1.14) and (1.18). This set of equations forms the multi-scale models of erythropoiesis we study below.

5.2 Existence of steady states

5.2.1 General bistable model

We begin with the analysis of the system consisting of (1.9)-(1.11), (1.1) written for each cell sub-population and (1.12)-(1.13). Denote this system by Σ_1. Once the system is examined, we establish the correspondence between the steady states of the System Σ_1 and the steady states of the System (1.9)-(1.11), (1.17), (1.12)-(1.13) (denoted by Σ_2). This allows us to find steady states of the System Σ_2 and their stability.

The System Σ_1 is decoupled into three parts (because the System (1.1) does not contain the terms $\alpha(Epo, GC)$ and $\gamma_i(P_n)$). The first one describes Erk-Fas interaction, the second one describes sub-population dynamics and the third one describes Epo and GCs dynamics. Denote by (E_i^*, F_i^*) the values of (E_i, F_i) in a steady state, $i = 1, \dots, n$, and introduce the notations

$$s_i^* = s(E_i^*, F_i^*), \quad d_i^* = d(E_i^*, F_i^*), \quad a_i^* = a(E_i^*, F_i^*) f_{aEpo}(Epo^*).$$

Then $(P_1^*, \dots, P_n^*, M^*)$, given by

$$P_1^* = \frac{HSC}{d_1^* + a_1^* - s_1^*}, \qquad P_i^* = \frac{2d_{i-1}^* P_{i-1}^*}{d_i^* + a_i^* - s_i^*},\ i = 2, \dots, n, \qquad M^* = \frac{d_n^* P_n^*}{\delta},$$

is the corresponding steady state of the second subsystem. The condition of the existence of this steady state, taking into account (1.14), is $s_i^* < 1/2,\ i = 1, \dots, n$, i.e. during normal erythropoiesis erythroid progenitors self-renew with a rate less than 50%.

Finally, (Epo^*, GC^*), given by

$$Epo^* = \frac{f_{Epo}(M^*)}{k_{Epo}}, \qquad GC^* = \frac{f_{GC}(M^*)}{k_{GC}},$$

is the corresponding steady state of the third subsystem. Since System (1.1) has 4 steady states and we consider n cell sub-populations, we conclude that the System Σ_1 has 4^n steady states. To study their stability we linearise the system about a steady state. The resulting matrix is decoupled into three sub-matrices (one part corresponds to the first subsystem, one part to the second subsystem and one part to the third subsystem, see Figure 10). The second sub-matrix

FIGURE 10 – Matrix of the System Σ_1 linearised about one of its steady states (see text for details). Symbol x stands for a non-zero element. The matrix has three sub-matrices located on its diagonal and zeros above. First sub-matrix corresponds to the subsystem describing E_i, F_i interactions, second sub-matrix corresponds to the cell sub-population dynamics and the third one corresponds to the growth factor dynamics. Eigenvalues of this matrix are eigenvalues of the three sub-matrices.

E_1	x	x	...	0	0	0	...	0	0	0	0
F_1	x	x	...	0	0	0	...	0	0	0	0
...			...			0	...	0	0	0	0
E_n	0	0	...	x	x	0	...	0	0	0	0
F_n	0	0	...	x	x	0	...	0	0	0	0
P_1			↑			x	...	0	0	0	0
...			1st sub-matrix				...			0	0
P_n						0	...	x	0	0	0
M			2nd sub-matrix →			0	...	x	x	0	0
Epo										x	0
GC								3rd sub-matrix →		0	x

is a triangle matrix with negative diagonal elements, the third sub-matrix is a diagonal matrix with negative diagonal elements. So all eigenvalues of the linearised matrix, except maybe the eigenvalues of the first sub-matrix, are negative real numbers. Hence the eigenvalues of the first sub-matrix determine stability of the full System Σ_2.

The first sub-matrix contains n times the matrix of the System (1.1) linearised about one of its steady states, once for each cell sub-population. We have noted that the stable steady states of the System (1.1) are $(E^*, F^*) = (\alpha, \beta)$ and $(E^*, F^*) = (\beta, \alpha)$. This means that stable steady states of the System Σ_1 are determined by $(E_i^*, F_i^*) = (\alpha, \beta)$ and $(E_i^*, F_i^*) = (\beta, \alpha)$, $i = 1, \ldots, n$. Since only two of four steady states of the System (1.1) are stable, the System Σ_1 has 2^n stable steady states. Then the System Σ_2, like the System Σ_1, has also 2^n stable steady states defined by $(\widetilde{E}_i^*, \widetilde{F}_i^*)$, $i = 1, \ldots, n$, that are small perturbations of those mentioned above. Consequently, some sub-populations are characterised by a domination of Erk, the others by a domination of Fas. Let us discuss some biological limitations that we have to take into account.

During the process of maturation, erythroid progenitors lose their ability to self-renew [38], thus immature cells are more inclined to self-renewal and mature ones are more inclined to differentiation. Hence, among all possible stable steady states only those which are characterised by a

certain integer number $k,\ 1 \leqslant k \leqslant n$, such that cells in sub-populations $P_1, \ldots, P_{k-1}$ preferentially self-renew (Erk dominates in cells of these sub-populations) and cells in sub-populations $P_k, \ldots, P_n$ preferentially differentiate (Fas dominates in cells of these sub-populations) are biologically reasonable. It reduces the number of biologically meaningful stable steady states to n. It seems natural to expect that in normal erythropoiesis the number of mature cells is larger than the number of immature cells, so we impose the conditions $P_i^* > P_{i-1}^*$, that are equivalent to

$$\frac{2d_{i-1}^*}{1-2s_i^*} > 1, \quad i = 2, \ldots, n.$$

Thus the multi-scale model has, generally speaking, several (from 1 up to n) stable steady states that satisfy all biological conditions discussed above.

5.2.2 Model with erythropoiesis-specific intracellular system

We investigate the existence of steady states for the system formed with (1.9)–(1.14), (1.16) and (1.18). It should be noted that existence of such solutions is not straightforward. Indeed, denote by P_i^* the steady state values of (1.9)–(1.10), M^* the steady state value of (1.11), Epo^* and GC^* the steady state values of (1.12)–(1.13), and E_i^* and F_i^* the steady state values of (1.16). We also introduce the notations

$$s_i^* = s(E_i^*, F_i^*), \quad d_i^* = d(E_i^*, F_i^*), \quad a_i^* = a(E_i^*, F_i^*) f_{aEpo}(Epo^*).$$

Then, P_i^*, $i = 1, \ldots, n$, exist if and only if

$$\begin{cases} (d_1^* + a_1^* - s_1^*)P_1^* &= HSC, \\ (d_i^* + a_i^* - s_i^*)P_i^* &= 2d_{i-1}^* P_{i-1}^*, \qquad i = 2, \ldots, n. \end{cases}$$

Hence, using (1.14), P_i^* exists for $i = 1, \ldots, n$ provided that

$$s_i^* < \frac{1}{2},$$

and P_i^* is given by

$$P_1^* = \frac{HSC}{1-2s_1^*}, \qquad P_i^* = \frac{2d_{i-1}^*}{1-2s_i^*}P_{i-1}^*,\ i = 2,\dots,n.$$

Then, M^*, Epo^* and GC^* are uniquely defined by

$$M^* = \frac{d_n^*}{\delta}P_n^*, \quad Epo^* = \frac{f_{Epo}(M^*)}{k_{Epo}}, \quad GC^* = \frac{f_{GC}(M^*)}{k_{GC}}.$$

Yet, implicitly, all the above steady state values, and in particular P_n^*, Epo^* and GC^*, are functions of E_i^* and F_i^*, for $i = 1,\dots,n$, through the steady state values of the different rates s_i^*, d_i^* and a_i^*. Since E_i^* and F_i^* are solutions of system

$$\begin{cases} \left(\alpha(Epo^*, GC^*) + \beta(E_i^*)^k\right)(1-E_i^*) - aE_i^* - bE_i^*F_i^* &= 0, \\ \gamma_i(P_n^*)(1-F_i^*) - cE_i^*F_i^* - dF_i^* &= 0, \end{cases}$$

which has been shown to have 1 to 3 solutions when α and γ are constant (see Section 3.2), it follows that determining steady states for the full model is equivalent to solving a system in the form

$$\begin{cases} E_i^* &= \varphi_i(E_1^*,\dots,E_n^*,F_1^*,\dots,F_n^*), \\ F_i^* &= \psi_i(E_1^*,\dots,E_n^*,F_1^*,\dots,F_n^*), \end{cases}$$

for all $i = 1,\dots,n$. Functions φ_i and ψ_i are some unknown functions. In a general case such a system cannot be solved.

For the sake of simplicity, suppose α is given by

$$\alpha(Epo, GC) = \alpha_0 + f(Epo) + g(GC),$$

where $\alpha_0 > 0$ accounts for Erk activation when erythropoietin and glucocorticoids are low. Since erythropoietin and glucocorticoids are not the only activators of Erk, this assumption is biologically reasonable. Functions f and g are bounded nonnegative increasing functions, for instance, of Michaelis-Menten type, with $f(0) = g(0) = 0$. Similarly, suppose γ_i is given by

$$\gamma_i(P_n) = \gamma_0 + \mu_i\bar{\gamma}(P_n),$$

where γ_0 is a constant source of Fas activation independent of mature progenitor cell production of Fas ligand, and μ_i is a parameter accounting for sensitivity of Fas activation to cell maturity. The function $\bar{\gamma}$ is assumed to be nonnegative, bounded and increasing, with $\bar{\gamma}(0) = 0$ and $\gamma(P_n) \leqslant 1$.

With these assumptions, we can apply the Implicit Function Theorem to find steady states of the full model. Suppose that in the steady state, values of Epo^* and GC^* are such that $f(Epo^*)+g(GC^*)$ is very small, close to zero. Moreover, μ_i are supposed to be small parameters.

We first note that the following system,

$$\left\{ \begin{array}{rcl} \left(\alpha_0 + \beta(E_i^*)^k\right)(1-E_i^*) - aE_i^* - bE_i^*F_i^* &=& 0, \\ \gamma_0(1-F_i^*) - cE_i^*F_i^* - dF_i^* &=& 0, \end{array} \right. \tag{1.19}$$

has one to three solutions, depending on the values of α_0 and γ_0. This has been obtained in Section 3.2, for $\alpha = \alpha_0$ and $\gamma = \gamma_0$, see System (1.7). Denote by $(E^{*,0}, F^{*,0})$ one of these potential solutions. Then for every pair $(E^{*,0}, F^{*,0})$, there exists a unique value of s_i^*, d_i^* and a_i^*, and consequently of P_i^*, $i = 1, \ldots, n$, M^*, Epo^* and GC^*.

As μ_i increases away from zero, the Implicit Function Theorem gives the existence of steady states for the full model. These steady states are small perturbations of the above mentioned steady states, based on $(E^{*,0}, F^{*,0})$. Hence, stability does not change, and steady states of the full system are stable (respectively, unstable) if steady states of (1.9)–(1.14), (1.18) and (1.19) are stable (respectively, unstable). And (1.19) has up to 2 stable steady states for all $i = 1, \ldots, n$.

We can then state that full system formed with (1.9)–(1.14), (1.16) and (1.18) has up to 2^n stable steady states. This number may appear large, yet it does not take into account biological constraints.

During the process of maturation, erythroid progenitors lose their ability to self-renew [38], thus immature cells are more inclined to self-renewal and mature ones are more inclined to differentiation. Hence, among all possible stable steady states only those, characterised by a certain integer j, $1 \leqslant j \leqslant n$, such that cells in the first j sub-populations (corresponding to variables P_1 to P_j) preferentially self-renew (let us call them self-renewing sub-populations), and cells in the last $n-j$ sub-populations (corresponding to variables P_{j+1} to P_n) preferentially differentiate (let us call them differentiating sub-populations), are biologically reasonable. It

reduces the number of biologically meaningful stable steady states to n. Moreover, it seems natural to expect that in normal erythropoiesis the number of mature cells is larger than the number of immature cells, so we impose the conditions $P_i^* < P_{i+1}^*$, which are equivalent to

$$\frac{2d_i^*}{1-2s_{i+1}^*} > 1, \qquad i = 1, \dots, n-1.$$

Thus the multi-scale model formed with (1.9)–(1.14), (1.16) and (1.18) has, generally speaking, several (from 1 up to n) stable steady states, which satisfy the biological constraints discussed above.

The next section is devoted to numerical simulations. The attention is focused, in particular, on anaemia situations.

6 Simulations of anaemia

A typical situation of stress erythropoiesis is anaemia : a lack of red blood cells, or haemoglobin. It can be either induced, for instance by killing erythrocytes, which can be obtained with phenylhydrazine, or by bleeding, or disease-related. A number of haematological diseases are characterised by or associated with severe anaemia, such as aplastic anaemia or some leukaemias.

6.1 General bistable model

To carry out simulations we have to specify the shape of the functions $s(E,F)$, $d(E,F)$, $a(E,F)$ and $f_{aEpo}(Epo)$ in (1.18). We suppose that $\alpha(Epo,GC) = \alpha_0 + f(Epo) + g(GC)$, so we should specify $f_E(Epo),\ f_G(GC)$. We suppose as well that $\gamma_i(P_n) = \mu_i\gamma(P_n)$. We should specify as well $f_{Epo}(M)$ in (1.12) and $f_{GC}(M)$ in (1.13). To define the functions $s(E,F)$ and $d(E,F)$ it is sufficient to fix $p_s(E,F)$ and $a(E,F)$, see (1.15). For simplicity we consider that the functions $p_s(E,F)$ and $a(E,F)$ are functions of one variable, $p_s(E,F) = p_s(F-E)$ and

TABLE 1 – Parameters for functions defined by (1.20). Functions of two types (Hill and Michaelis-Menten) are described in the table. Parameter b expresses the maximum value, parameter θ is a threshold value, with the same units as function variable units, parameter n is the sensitivity (dimensionless quantity). Parameter units are specified in parenthesis after the value.

function name	function type	b	θ	n
$\widetilde{f}_{aEpo}(Epo)$	Hill	1.2	$6.3\,(\text{U.ml}^{-1})$	3
$f_E(Epo)$	Michaelis	$0.04\,(\text{d}^{-1})$	$100\,(\text{U.ml}^{-1})$	6
$f_G(Epo)$	Michaelis	$0.03\,(\text{d}^{-1})$	$250\,(\text{U.ml}^{-1})$	10
$f_F(P_n)$	Michaelis	$1\,(\text{d}^{-1})$	$20\,(\text{cells.}\,\mu\text{l}^{-1})$	1
$f_{Epo}(M)$	Hill	$7130\,(\text{U.ml}^{-1}.\text{d}^{-1})$	$225\,(\text{cells.}\,\mu\text{l}^{-1})$	7
$f_{GC}(M)$	Hill	$2930\,(\text{U.ml}^{-1}.\text{d}^{-1})$	$320\,(\text{cells.}\,\mu\text{l}^{-1})$	6

$a(E,F) = a(F-E)$. We consider

$$\begin{cases} a(x) = (a_{max} - a_{min})\dfrac{(x+1)^{n_a}}{1+(x+1)^{n_a}} + a_{min} \\ p_s(x) = (s_{max} - s_{min})\dfrac{1}{1+(x+1)^{n_s}} + s_{min} \end{cases}, \quad x \in [-1,1],$$

with $a_{min} = 0.1\,\text{d}^{-1}$, $a_{max} = 0.48\,\text{d}^{-1}$, $s_{min} = 0.1$, $s_{max} = 0.57$ and $n_a = 6, n_s = 5$.

Functions $f_E(Epo)$, $f_G(GC)$, $f_F(P_n)$, $f_{Epo}(M)$ and $f_{GC}(M)$ are either Hill or Michaelis-Menten functions (g_1 and g_2 in (1.20) respectively) and are defined by three parameters indicated in Table 1.

$$g_1(x) = b\frac{x^n}{\theta^n + x^n}, \quad g_2(x) = b\frac{\theta^n}{\theta^n + x^n}. \tag{1.20}$$

Epo cannot suppress apoptosis completely, thus we consider that the function $f_{aEpo}(Epo)$ has a minimum value different from zero, $f_{aEpo}(Epo) = 0.2 + \widetilde{f}_{aEpo}(Epo)$, where $\widetilde{f}_{aEpo}(Epo)$ is Hill function with parameters mentioned in Table 1. Erythrocyte lifespan is considered to be 40 days (average lifespan of an erythrocyte in mice), thus $\delta = 1/40\,\text{d}^{-1}$. Parameters $\alpha = 0.1$, $\beta = 0.6$, $\gamma = 2.7$, $\mu_1 = 0.04$, $\mu_i = 3\mu_{i-1}/4$, $i = 2,\ldots,n$ are dimensionless quantities. Epo and GCs elimination constants are $k_{Epo} = 7.1295\,\text{d}^{-1}$ and $k_{GC} = 5.8714\,\text{d}^{-1}$. Parameters are chosen to describe erythropoiesis in mice.

As discussed above, the model has several, up to n, stable steady states. In the k-th possible stable steady state, cells in sub-populations $P_1,\ldots,P_{k-1}$ self-renew and in sub-populations

$P_k, \ldots, P_n$ differentiate, thus we can say that a steady state is characterised by a number k. This number stands for the number of self-renewing sub-populations plus one. Then, for parameters of the system mentioned above, the steady state value of erythrocyte count in the stable steady state with k self-renewing sub-populations is about one order larger than the steady state value of erythrocyte count in the stable steady state with $k-1$ self-renewing sub-populations. Thus, taking into consideration the realistic proportion between the daily influx of HSC and erythrocyte count we can choose only one of the possible steady states that would meet this criterion. The exact proportion between the daily influx of HSC and erythrocyte count cannot be determined, yet we can estimate the order of the proportion. To our knowledge this proportion is of order 10^5 [36]. For the parameters mentioned above, the appropriate configuration is four immature sub-populations with Erk domination and four mature sub-populations with Fas domination.

Anaemia is a critical lack of haemoglobin that can be caused by erythrocyte loss. Thus, to model an anaemia, as initial conditions in the simulations we take steady state values for all variables except for erythrocyte count, for which we take an underestimate value (about 30% of the steady state value).

Left picture in Figure 11 represents cell sub-population dynamics on a logarithmic scale. We carry out simulations for $n = 8$ progenitor sub-populations. Four immature progenitor sub-populations preferentially self-renew (dot lines), four mature ones preferentially differentiate (solid lines). We can see the amplification by about one order from one self-renewing sub-population to another one, and an overshoot in erythrocyte count following the anaemia. This has already been noticed in [36]. In the right picture, dynamics of E_i and F_i, $i = 1, \ldots, n$, perturbed during anaemia, are presented. Erk dominates in self-renewing cells, Fas dominates in differentiating cells. Figure 12 shows weak self-renewal rate in differentiating sub-populations, important self-renewal rate in self-renewing sub-populations, apoptosis rate is about 45% for differentiating cells and about 10% for self-renewing cells. Differentiation rate does not differ much from one cell sub-population to another, except during the days following the anaemia. During anaemia mature progenitors self-renew twice more intensively than in normal situation, with maximum rate about 18%, apoptosis rate is weak for all cells during anaemia. After about 35 days the three rates come back with damped oscillations to their normal values. In Figure 13 growth factor dynamics are presented. We observe elevated levels (Epo levels increase by about

three orders) during anaemia that come back to the normal state after 5 days.

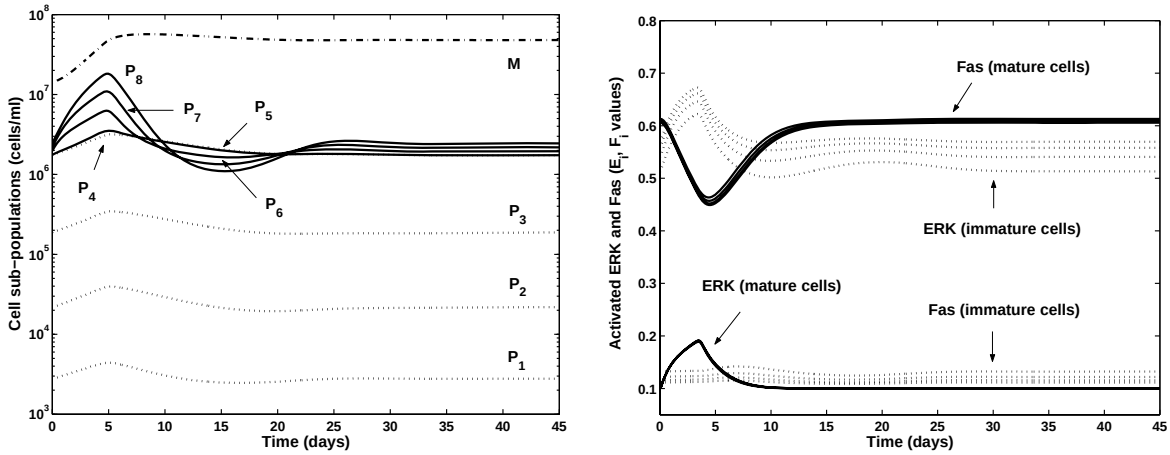

FIGURE 11 – Results of anaemia simulations over 45 days. Left : cell sub-population dynamics, presented on log scale. Right : E_i and F_i dynamics. Parameter $n = 8$, i.e. the simulations are carried out with eight progenitor maturation levels. Four immature progenitor sub-populations, inclined to self-renewal, are described by dot lines, four others, mature cell sub-populations, are illustrated with solid lines. Dash-dot line represents the dynamics of erythrocytes. Initial conditions for variables $P_1, \ldots, P_8$ equal their steady state values, initial condition for erythrocyte count is the value that equals 30% of its steady state value. This number is chosen in accordance with simulations of an anaemia presented in [36]. It takes 6 days to come back to normal erythrocyte count that is followed by an overshoot. The return after the overshoot to the steady state is slow because of the small value of erythrocyte elimination constant (erythrocyte lifespan, that is equal to 40 days, is assumed to be not modified during anaemia). Erk and Fas quantities are importantly modified during anaemia, and within 15 days they return to their normal values.

6.2 Model with erythropoiesis-specific intracellular system

6.2.1 Parameter values

The nature of the induced anaemia can be very different, according to the method used to urge it. [45] noticed that the way haematocrit evolves following the anaemia induction, and in particular the speed of the return to the equilibrium, strongly depends on its strength. In other words, the more red blood cells are removed from the body, the stronger response to anaemia is. Results of experiments on mice with phenylhydrazine-induced anaemia obtained in [29] are presented in Figure 14. One can observe that, following the anaemia, the erythrocyte count

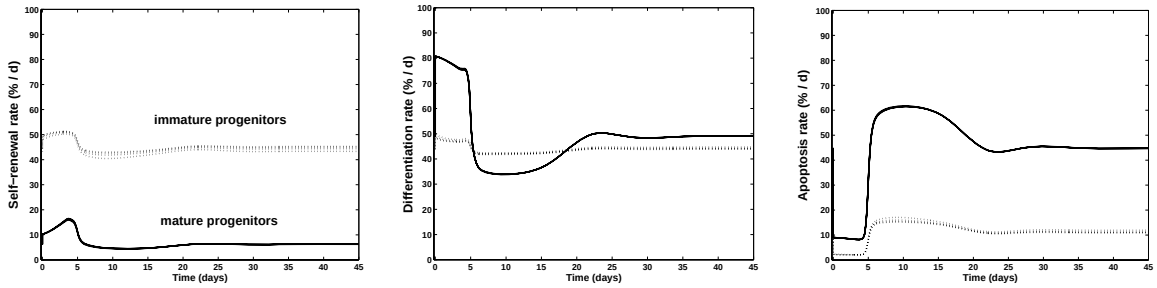

FIGURE 12 – Three rates during anaemia simulations. Left : self-renewal rate. Center : differentiation rate. Right : apoptosis rate. Dot lines correspond to immature cell sub-populations, solid lines describe the three rates in mature cell sub-populations. The rates are almost the same within all immature (mature) sub-populations. Feedbacks by Epo and GCs on Erk activation and feedback by Epo on apoptosis rate modify the self-renewal rate that increases twice in mature progenitors during anaemia. During anaemia the majority of mature progenitors differentiate with weak apoptosis rate to gain normal erythrocyte count as fast as possible. The three rates are strongly perturbed during the first 6 days.

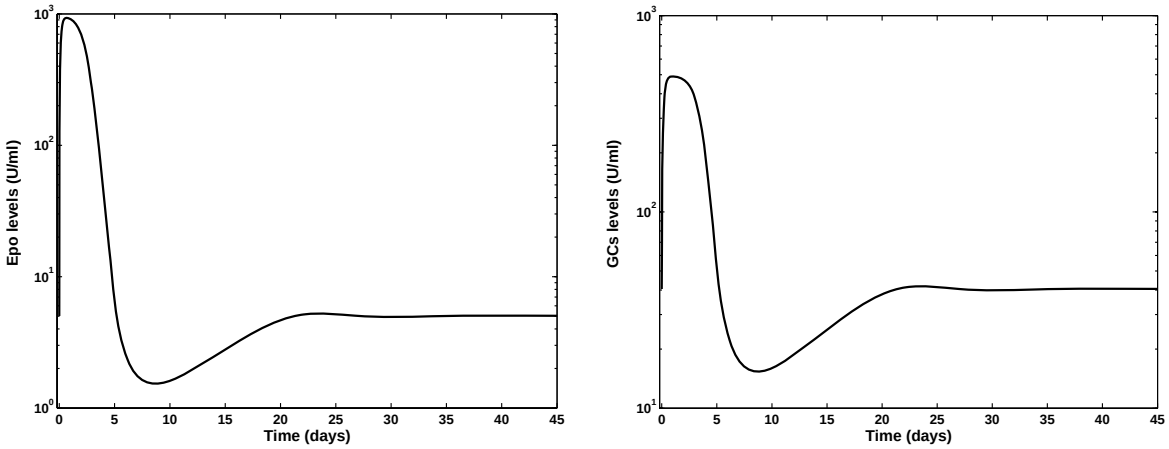

FIGURE 13 – Growth factor dynamics on log scale during anaemia. Left : Epo levels. Right : GCs levels. Epo concentration increases by about 3 orders due to the lack of haemoglobin (corresponds to lack of red blood cells) in the blood. After about 5 days it returns to its normal values. A small undershoot with respect to normal values is observed on day 8.

quickly increases and, although still not at its equilibrium, decreases once again on day 11 before finally reaching normal values from day 18 up to the end of experiments. This surprising decrease (days 11 to 18) will be investigated in Section 6.2.2 : we will look for feedback controls responsible for it.

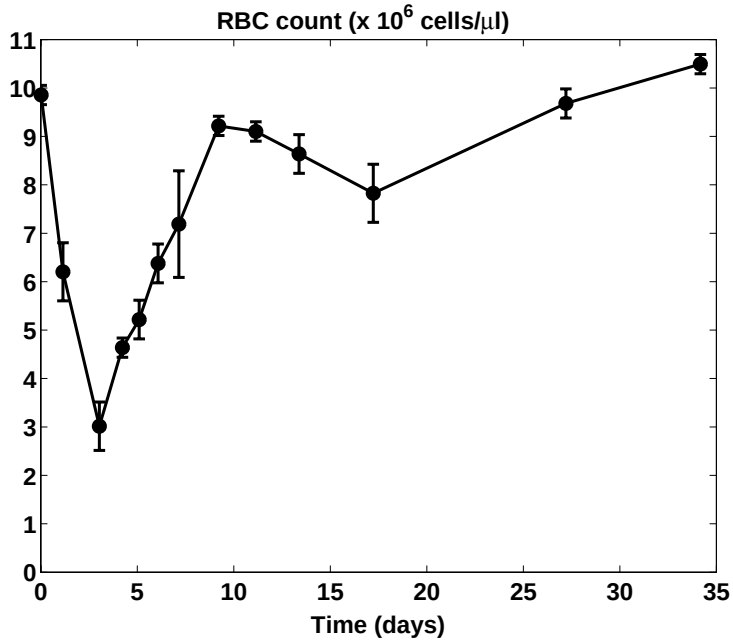

FIGURE 14 – Phenylhydrazine-induced anaemia in mice, adapted from [29]. Two injections (60mg/kg) are administered intraperitoneally at days 0 and 1. Mean values among six mice are presented with error bars. Initial value of red blood cell count (before starting the experiment) is about 10^7 cells.μl^{-1}.

We consider the model of erythropoiesis that consists of Equations (1.9)-(1.11) describing immature and mature blood cell dynamics, Equations (1.12)-(1.13) describing growth factors dynamics, and Equation (1.16) accounting for intracellular regulatory mechanisms.

We determine functions and parameter values of the model. Some parameters are rather easily accessible, whereas other parameters and most feedback functions are usually unavailable. We distinguish between these two kinds of values.

Estimations based on existing data. Among easily accessible parameter values, the mortality rate of erythrocytes (δ in equation (1.11)) is the first for which a value can be assigned. Since erythrocyte average lifespan in mice equals 40 days, we chose $\delta = 1/40$ d^{-1}.

Let now focus on growth factor dynamics system (1.12)-(1.13). In mice the half-life of erythropoietin is about 180 minutes [85]. The half-life of glucocorticoids ranges in a wide interval, yet 90 minutes can be considered as reasonable for short-term glucocorticoids [129] (that is glucocorticoids acting for a short time), like cortisol, which are likely to be involved in stress erythropoiesis [13]. Using the definition of half-life, we compute degradation constants : consider a substance that degrades with constant rate ν, then its dynamics can be described by the equation,

$$\frac{dx}{dt} = -\nu x,$$

whose solution is $x(t) = x_0 e^{-\nu t}$. The half-life is the time $T_{1/2}$ such that

$$x(T_{1/2}) = \frac{x_0}{2},$$

which gives $\nu = \ln(2)/T_{1/2}$. Using the above estimations for the half-life of erythropoietin and glucocorticoids, we obtain the following values for the degradation constants,

$$k_{Epo} = 5.55 \text{ d}^{-1}, \qquad k_{GC} = 11.1 \text{ d}^{-1}.$$

The functions f_{Epo} and f_{GC} in (1.12) and (1.13), accounting for growth factor production terms, are supposed to be Hill functions [15, 71],

$$f_{Epo}(M) = f^0_{Epo} \frac{\theta^{q_E}_{Epo}}{\theta^{q_E}_{Epo} + M^{q_E}}, \qquad f_{GC}(M) = f^0_{GC} \frac{\theta^{q_G}_{GC}}{\theta^{q_G}_{GC} + M^{q_G}}.$$

During anaemia Epo blood concentrations increase by 2-3 orders [90]. To our knowledge, variations of glucocorticoids are less important, but exact values are not available. We then chose parameters of functions $f_{Epo}(M)$ and $f_{GC}(M)$ that allowed us to obtain such variations of Epo and GCs in anaemia simulations we carried out. All these parameters are listed in Table 2.

As obtained in Section 5.2.2, the model we consider has from 1 up to n stable steady states. Not all steady states are biologically meaningful and one of these numerous steady states can be selected by taking into consideration a realistic proportion between the daily influx of haematopoietic stem cells (input of the model) and erythrocyte count in mice (output of the model).

TABLE 2 – Values of the parameters used to numerically compute erythrocyte count and growth factor levels. N.U means "no unit is relevant".

Parameter		Value	Unit
δ	mortality rate of erythrocytes	0.025	d^{-1}
k_{Epo}	degradation rate of Epo	5.55	d^{-1}
k_{GC}	degradation rate of GC	11.1	d^{-1}
f^0_{Epo}	maximum value of f_{Epo}	7130	$\text{mU}.\mu\text{l}^{-1}$
θ_{Epo}	threshold value of f_{Epo}	4.63×10^6	$\text{cells}.\mu\text{l}^{-1}$
q_E	sensitivity of f_{Epo}	7	N.U.
f^0_{GC}	maximum value of f_{GC}	2930	$\text{mU}.\mu\text{l}^{-1}$
θ_{GC}	threshold value of f_{GC}	7.69×10^6	$\text{cells}.\mu\text{l}^{-1}$
q_G	sensitivity of f_{GC}	6	N.U.

From [36], the ratio M^*/HSC between normal erythrocyte count and HSC daily influx can be estimated in the order of 10^5. The number of self-renewing sub-populations (see discussion at the end of Section 5.2.2) allows to select the appropriate steady state. We carried out several simulations with different numbers of self-renewal-inclined sub-populations and we obtained a correct ratio M^*/HSC for $n = 8$ and the case of 4 immature preferentially self-renewing sub-populations, and consequently 4 mature differentiation-inclined sub-populations.

Intracellular regulatory network. Let first focus on the part of the intracellular regulatory system (1.16) independent of feedback functions. Variables E and F are dimensionless and the parameter values we use are deduced from numerical simulations since no data are available in the literature. They are

$$\begin{aligned} k &= 2, & \beta &= 40\ \text{d}^{-1}, & a &= 2\ \text{d}^{-1}, \\ b &= 40\ \text{d}^{-1}, & c &= 10\ \text{d}^{-1}, & d &= 2.5\ \text{d}^{-1}. \end{aligned} \tag{1.21}$$

With these values, the intracellular regulatory network may have three steady states for given α and γ (Figure 8), two steady states being stable.

As mentioned in previous sections, System (1.16), describing intracellular regulatory network, in which α stands for Erk activation by Epo and GCs, and γ stands for Fas activation by FasL, can have either one or two stable steady states. Thus, primordially bistable system can

temporarily lose its bistability when values of parameters α and γ change, like in stress situations. For the parameters of the intracellular regulatory network mentioned in (1.21), we found numerically the set of (α, γ) values, for which System (1.16) has a bistable behaviour (domain D_1 in Figure 15).

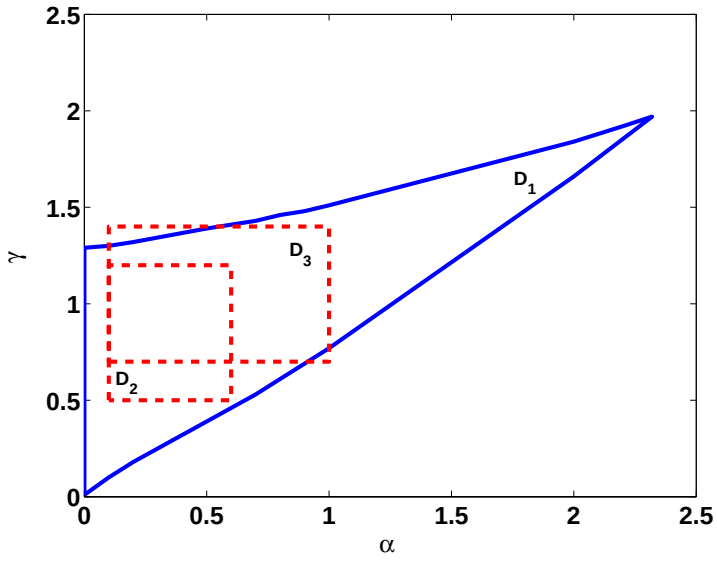

FIGURE 15 – Intracellular system (1.16) has a bistable behaviour for (α, γ) inside D_1. Two examples of (α, γ) variations are tested numerically, domains D_2 and D_3, when bistability can be temporarily lost.

After determining system parameters (see below), we numerically tested two cases : first when intracellular regulatory network always keeps a bistable behaviour during anaemia, independently of the values of α and γ, and second when for some extreme values of α and γ the bistability is temporarily lost and the intracellular regulatory network has only one stable steady state. The first case corresponds to variations of α and γ in the rectangular domain D_2 in Figure 15 that is entirely inside the bistability area. The second case corresponds, for instance (this is what was tested), to variations of α and γ in the domain D_3 that partially exits D_1. If a system trajectory goes through these out-of-D_1 parts of D_3, then the bistability of System (1.16) is lost for the corresponding values of (α, γ). We investigated the consequences of these two distinct situations on the response to anaemia.

In the second case the response of the system was stronger but qualitatively the same as the one obtained in the first case. We tried to increase out-of-D_1 parts of domain D_3 through

which the trajectory goes and we obtained that beyond certain thresholds (i.e. if the trajectory stays long enough outside the domain D_1), the solution could not come back to its initial state, the solution changed an attractor and went definitely to another steady state, or in other words, the system switched to single stable steady state regimen. The system would then lose its biological meaning (the balance between self-renewal and differentiation would be broken) and consequently we decided to focus only on the first case (α and γ range in D_2) and we present numerical simulations only for this case.

Let now concentrate ourselves on the choice of functions α and γ.

For the sake of simplicity, we supposed that FasL exerts the same feedback control on Fas activation for all progenitor sub-populations, which implies that $\gamma_i(P_n)$ in (1.16) is independent of $i : \gamma_i(P_n) = \gamma(P_n)$ for all $i = 1, \ldots, n$.

The system trajectory represented on (α, γ)-plane stays inside domain D_2 during erythrocyte recovery. The domain D_2 is characterised by $\alpha \in [0.1, 0.6]$, $\gamma \in [0.5, 1.2]$, see Figure 15. Recall that $\alpha = \alpha(Epo, GC)$ and $\gamma = \gamma(P_n)$. We suppose $\alpha(Epo, GC) = \alpha_0 + f(Epo) + g(GC)$, where α_0 is constant and $f(Epo)$, $g(GC)$ are Hill functions,

$$f(Epo) = f_{max}\frac{Epo^{q_f}}{\theta_f^{q_f} + Epo^{q_f}}, \quad g(GC) = g_{max}\frac{GC^{q_g}}{\theta_g^{q_g} + GC^{q_g}}. \tag{1.22}$$

Function $\gamma(P_n)$ is supposed to be a Hill function, given by

$$\gamma(P_n) = \gamma_{min} + (\gamma_{max} - \gamma_{min})\frac{P_n^{q_\gamma}}{\theta_\gamma^{q_\gamma} + P_n^{q_\gamma}}. \tag{1.23}$$

No information could allow us to determine the shape of such functions. The choice of Hill functions lies on the interest of these functions in describing kinase cascades and, more generally, biological phenomena with saturation effects. Parameter values of functions $\alpha(Epo, GC)$ and $\gamma(P_n)$ are given in Table 3. They were deduced from numerical simulations.

TABLE 3 – Parameters of the intracellular regulatory network, functions $\alpha(Epo, GC) = \alpha_0 + f(Epo) + g(GC)$ and $\gamma(P_n)$, defined in (1.22) and (1.23). N.U means "no unit is relevant".

Parameter		Value	Unit
k	sensitivity of Erk self-activation	2	N.U.
β	rate of Erk self-activation	40	d^{-1}
a	Erk degradation rate	2	d^{-1}
b	suppression of Erk expression rate	40	d^{-1}
c	suppression of Fas expression rate	10	d^{-1}
d	Fas degradation rate	2.5	d^{-1}
α_0	constant Erk activation rate	0.1	d^{-1}
f_{max}	maximum value of $f(Epo)$	0.25	d^{-1}
q_f	sensitivity of $f(Epo)$	6	N.U.
θ_f	threshold value of $f(Epo)$	100	$\text{mU.}\mu\text{l}^{-1}$
g_{max}	maximum value of $g(GC)$	0.25	d^{-1}
q_g	sensitivity of $g(GC)$	2	N.U.
θ_g	threshold value of $g(GC)$	49.4	$\text{mU.}\mu\text{l}^{-1}$
γ_{min}	minimum value of $\gamma(P_n)$	0.5	d^{-1}
γ_{max}	maximum value of $\gamma(P_n)$	1.2	d^{-1}
q_γ	sensitivity of $\gamma(P_n)$	3	N.U.
θ_γ	threshold value of $\gamma(P_n)$	1.14×10^6	$\text{cells.}\mu\text{l}^{-1}$

Self-renewal, differentiation and apoptosis rates. From Equations (1.14), (1.15) and (1.18), self-renewal, differentiation and apoptosis rates are given, for $i = 1, \ldots, n$, by

$$\begin{cases} s_i &= (1 - a_i)\, p_s(E_i, F_i), \\ d_i &= 1 - s_i - a_i, \\ a_i &= a(E_i, F_i)\, f_{aEpo}(Epo). \end{cases} \tag{1.24}$$

The dependence upon Erk and Fas is defined through function $p_s(E, F)$, which describes how the probability of self-renewal depends upon Erk and Fas, and function $a(E, F)$, which describes how apoptosis rate depends on Erk and Fas. The direct action of Epo on apoptosis rate is determined by $f_{aEpo}(Epo)$. Hence, the three functions p_s, a and f_{aEpo} entirely determine the three rates.

The function f_{aEpo} is supposed to be decreasing and bounded. In order to describe the effect of large Epo variations (quick changes from 5 to 1000 $\text{mU.}\mu\text{l}^{-1}$), we chose a Hill function of

the logarithm of Epo, given by,

$$f_{aEpo}(Epo) = 0.2 + \frac{0.73 \times 1.1^{9.2}}{1.1^{9.2} + (\log_{10}(Epo))^{9.2}}, \tag{1.25}$$

the parameters being dimensionless, except the threshold value 1.1, which is expressed in mU.μl^{-1}. Parameters have been chosen so that $f_{aEpo}(Epo)$ in the steady state Epo^* equals 0.9 and numerical simulations fit correctly experimental data from Figure 14.

For the sake of simplicity, we supposed functions $p_s(E, F)$ and $a(E, F)$ to be functions of one variable, $p_s(E, F) = p_s(E - F)$ and $a(E, F) = a(F - E)$. The function p_s is supposed to take larger values when Erk levels are high, whereas the value of a is more important when Fas levels are high. Consequently, both functions are supposed to be increasing. Moreover, they are positive and we assumed the following form,

$$z(x) = z_{min} + \frac{(z_{max} - z_{min})(x + 1)^{n_z}}{\theta_z^{n_z} + (x + 1)^{n_z}}, \quad x \in [-1, 1].$$

Before giving values of the parameters z_{min}, z_{max}, n_z and θ_z associated with functions p_s and a, let us illustrate how the roles of Erk and Fas are investigated through these functions.

Let us recall that we assumed functions γ_i do not depend on the index i. Hence, from (1.16) it follows that all sub-populations have the same steady state values (E^*, F^*), which do not depend on i. Moreover, by assuming that α and γ evolve in the restricted domain D_2, we ensure the existence of two stable steady states for System (1.16), one in which Erk levels are higher than Fas levels, and the other one with higher Fas levels. These two steady states (E^*, F^*) provide two distinct values of the variable $F^* - E^*$, one positive and one negative. The positive value is associated with cell differentiation, whereas the negative one corresponds to cell self-renewal. Hence, the positive value of $F^* - E^*$ characterises differentiation-inclined erythroid progenitors, that is mature cells, and the negative one self-renewal-inclined erythroid progenitors, that is immature cells.

During anaemia, concentrations of Erk and Fas vary, therefore values of $F - E$ vary as well. Carrying out simulations however, we observed that variations of $F - E$ were limited to neighborhoods of the two stationary points $F^* - E^*$, and did not range in the whole interval $[-1, 1]$. This means that variations of functions $p_s(E - F)$ and $a(F - E)$ are only relevant

on these neighborhoods of $F^* - E^*$. Consequently, in order to determine the roles of Erk and Fas on the response to anaemia, we considered three cases describing three different ways of acting on self-renewal, differentiation and apoptosis rates, based on variations of p_s and a in the neighborhoods of the steady state values.

In the first case $p_s(E-F)$ and $a(F-E)$ vary slightly on both neighborhoods of the steady states. In the second case $p_s(E-F)$ (respectively $a(F-E)$) varies a lot near the steady state corresponding to Erk prevalence, i.e. $F^* - E^* < 0$ (respectively, Fas prevalence, i.e. $F^* - E^* > 0$), and is almost constant near the other steady state. Biologically it can be interpreted as follows : in critical situations Erk and Fas importantly modify the progenitor self-renewal rate of immature but not of mature cells, and apoptosis rate is strongly modified in mature cells but not in immature ones. The third case is opposite to the second one. It should be noted that the assumption on the three rates that confines them in the interval $[0, 1]$, limits maximum values of functions p_s and a, so the fourth possible case, when the functions vary a lot on both neighborhoods is ineligible. Simulations indicated that the response obtained in the first case is weak, that is the system takes more time to come back to the equilibrium. Second case seemed to us biologically more realistic than the third one, hence we chose to use only the second case for the numerical simulations. Nevertheless, it can be noted that the simulation of the third case showed a weaker response, i.e. slower erythrocyte count dynamics, though the rates displayed different dynamics.

In order to obtain a good fit of experimental data, functions $p_s(E-F)$ and $a(F-E)$ used for the simulations are

$$p_s(x) = 0.1 + \frac{1.2 \times x^{40}}{1.7^{40} + x^{40}}, \quad a(x) = 0.12 + \frac{1.02 \times x^{40}}{1.5^{40} + x^{40}}.$$

Units of 0.12 and 1.02 for function a are d^{-1}, other parameters are dimensionless values.

Steady state values. Since we are going to confront the simulation results with experimental data presented in Figure 14, we tried to get equilibrium value of erythrocyte count $M^* = 10^7$ cells.$\mu\mathrm{l}^{-1}$. This implied $HSC = 80$ cells.$\mu\mathrm{l}^{-1}$.d^{-1}. As initial condition for the number of erythrocytes we took 30% of its equilibrium value, which corresponds to the anaemia presented in

Figure 14 (see value of RBC count on day 3). Equilibrium values are taken as initial conditions for all other system variables. Steady state values of the main system components, obtained through the simulation, are presented in Table 4.

TABLE 4 – Steady state values of the main variables of the system.

Steady states		Value	Units
Erythrocyte count	M^*	10^7	cells.μl^{-1}
Reticulocyte count	P_8^*	4.75×10^5	cells.μl^{-1}
Erythropoietin level	Epo^*	5.7	mU.μl^{-1}
Glucocorticoids level	GC^*	44.6	mU.μl^{-1}
Fas $-$ Erk level for immature cells	$F^* - E^*$	-0.66	N.U.
Fas $-$ Erk level for mature cells	$F^* - E^*$	0.48	N.U.
Activation rate of Erk $\alpha(Epo^*, GC^*)$	α^*	0.21	d^{-1}
Activation rate of Fas $\gamma(P_n^*)$	γ^*	0.55	d^{-1}
Self-renewal rate of immature cells	s^*	0.44	d^{-1}
Self-renewal rate of mature cells	s^*	0.06	d^{-1}
Differentiation rate of immature cells	d^*	0.45	d^{-1}
Differentiation rate of mature cells	d^*	0.53	d^{-1}
Apoptosis rate of immature cells	a^*	0.11	d^{-1}
Apoptosis rate of mature cells	a^*	0.41	d^{-1}

As shown in Table 4, in normal erythropoiesis reticulocyte count is 20-fold smaller than erythrocyte count. Progenitor sub-populations $P_1, \ldots, P_7$ are much smaller than P_8 (not shown here). The model predicts that 44% of immature progenitors self-renew per day (only 6% of mature progenitors per day), which allows the conclusion that mature progenitors mainly lost their ability to self-renew. Apoptosis rate is high in mature cells (41% d^{-1}), whereas it is only 11% d^{-1} in immature cells. About 53% of mature and 45% of immature progenitors differentiate per day, providing that the differentiation remains important in all erythroid cells. Thus, in normal erythropoiesis, immature progenitor sub-populations are characterised by weak apoptosis and comparable self-renewal and differentiation rates. Mature progenitors, however, preferentially differentiate with high apoptosis.

The next section is devoted to numerical simulations of phenylhydrazine-induced anaemia.

6.2.2 Simulation of phenylhydrazine-induced anaemia and comparison with experimental data

Using parameter values obtained in the previous section, we numerically computed solutions of system formed with Equations (1.9) to (1.13) and Equation (1.16), for an anaemia-induced situation : it is assumed that at the beginning of the numerical computations (day 0) the erythrocyte count is lower than its equilibrium value (30% of its equilibrium) due to previous phenylhydrazine injections. Simulations were carried out using MATLAB and results are presented in Figures 16 to 20.

First, dynamics of main variables of the system and of some relevant rates are illustrated : erythrocyte and reticulocyte counts in Figure 16, erythropoietin and glucocorticoid levels in Figure 17, Erk and Fas levels in Figure 18, self-renewal, differentiation and apoptosis rates in Figure 19. Explanations on the dynamics of the system are proposed. Then results are confronted to experimental data from Figure 14 in Figure 20.

All simulations start at day zero. For the sake of clarity, equilibrium values are shown on days -1 to 0.

Erythrocyte and reticulocyte counts. Erythrocyte count (solid line) and reticulocyte count (dash line) dynamics are presented in Figure 16.

Following the anaemia, erythrocyte count quickly increases and reaches a maximum value (lower than the equilibrium value) after 7 days, then stays there up to day 10. Afterwards, erythrocyte count slowly decreases (days 10 to 17). Quick increase is observed between days 17 to 21, followed by a gradual return to the equilibrium. Although erythrocyte count globally increases between day 0 and day 30, it should be noted that 30 days after anaemia the erythrocyte count is still below its equilibrium value.

At day 0, the reticulocyte count increases to reach a maximum value that equals approximately four-fold of its equilibrium value on day 4, then comes back to its steady state and keeps on decreasing. On day 17, when erythrocyte count is decreasing, the number of reticulocyte increases once again, though less importantly this time.

The first increase of reticulocyte count (up to day 4) is due to a strong increase of mature progenitor differentiation, see Figure 19.B. Explanations on the behavior of erythrocyte and

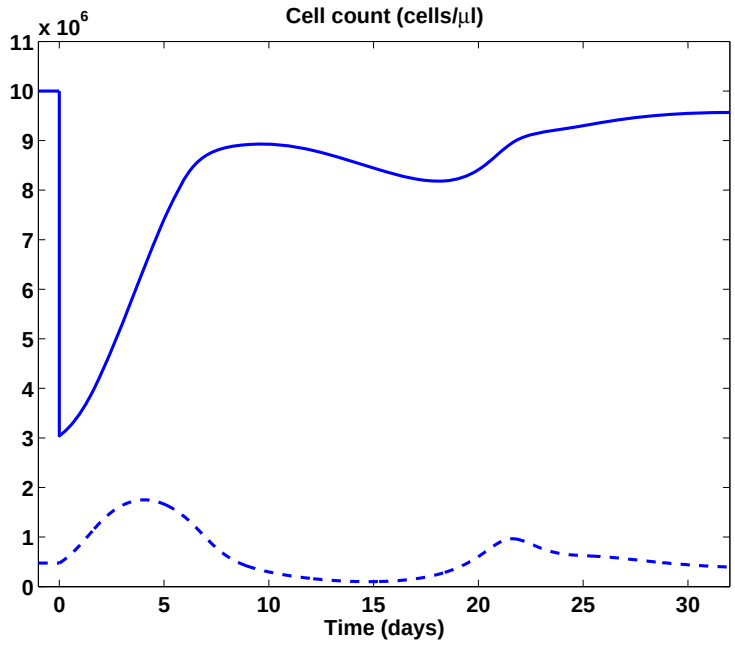

FIGURE 16 – Anaemia simulation. Erythrocyte and reticulocyte count dynamics. Solid curve represents erythrocyte count, dash curve represents reticulocytes. Equilibrium value of erythrocyte count used in the simulation is $M^* = 10^7$cells.μl^{-1}.

reticulocyte counts on day 17 are however less straightforward and will be given later in this section, when confronting the results with experimental data.

Growth factors dynamics. In Figure 17, erythropoietin and glucocorticoid dynamics are shown. Growth factor levels are strongly perturbed (large increase) during the first five days following the anaemia, this perturbation being characterised by a sharp increase of both concentrations on day 1, when the organism lacks erythrocytes. Then values of Epo and GCs levels smoothly return to their equilibria, with small perturbations, in particular they both increase once again on day 17, due to the fall in erythrocyte count (Figure 16).

As it will be noted in the following sections, two different actions of Epo and GCs appear in the response to anaemia. First, in the early stages of the response to anaemia (between days 0 and 5) mainly Epo inhibits apoptosis (Figure 19), leading to high proliferation of immature progenitors. Second, from day 6 up to the end of the response, Epo and GCs levels are closer to their equilibrium values and they regulate erythropoiesis mainly through Erk-Fas regulation (Figure 18).

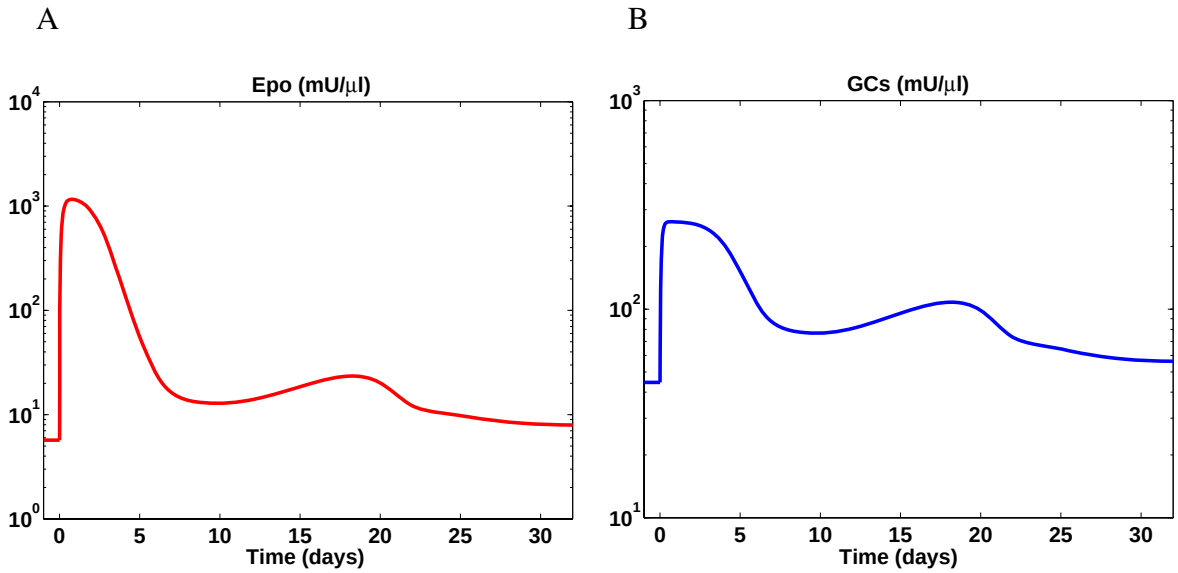

FIGURE 17 – Anaemia simulation. Dynamics of growth factors, shown on logarithmic scale.

Erk and Fas levels. Dynamics of variable $F - E$ and feedback controls expressed by α and γ are presented in Figure 18. Values of $F - E$ in all mature (respectively, in all immature) sub-populations are similar because the feedback by FasL has been supposed to be the same on all cells (see Section 6.2.1).

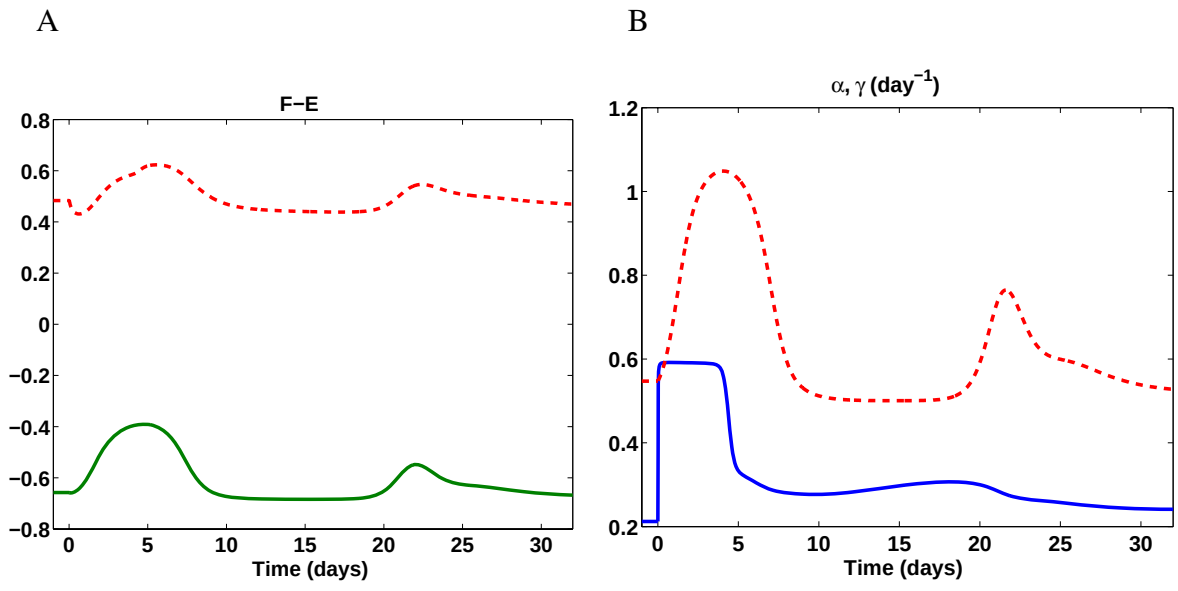

FIGURE 18 – Anaemia simulation. Panel A : Dynamics of $F - E$ for self-renewing (green solid curve) and differentiating (red dash curve) sub-populations. Panel B : Dynamics of $\alpha(Epo, GC)$ (blue solid curve) and $\gamma(P_n)$ (red dash curve).

On the first day following anaemia the quantity $F - E$ decreases. This is more clearly observed for mature cells (red dash curve), yet it also occurs for immature cells (green solid curve). This is due to high values of α (Panel B), the feedback function controling Erk production. Then, $F - E$ increases and reaches its extreme values after 5-6 days following anaemia induction. As one can observe on Panel A, between days 9 and 19 the difference $F - E$ has values below its equilibria, which is due to the regulation through α and γ.

Production of Erk, the feedback control expressed by α, is at its maximum during the first four days, while γ (production of Fas) is increasing. Then, α sharply decreases almost down to its equilibrium, while γ decreases smoothly and reaches its minimum value, where it stays from day 10 up to day 18. On day 18, a new increase of γ is observed, due to the increase of the reticulocyte count (Figure 16). Two different behaviors are observed in α and γ dynamics : fast changes (α on days 1 and 4) and modest variations (γ between days 1 and 8, and days 18 and 25). Fast changes of α are directly due to sharp Epo and GCs dynamics (see Figure 17), while modest γ dynamics is due to modest evolution of reticulocyte count (see Figure 16).

Self-renewal, differentiation and apoptosis rates. Self-renewal, differentiation and apoptosis rates are presented in Figure 19. The three rates exhibit important fluctuations. Their dynamics for immature and mature cell populations are different.

Self-renewal rate varies a lot for all cells. At first sight, it seems not to be the case for mature cells, yet self-renewal equilibrium value is small and the variations represent a two-fold increase of the equilibrium value. Such important variations are also observed for the two other rates. Moreover, two different types of changes in values of the rates appear in Figure 19. First, sharp variations appear between days 0 and 1 : they are strong, for instance, for mature sub-populations (red dash curves in Figure 19). Then, after day 1, variations are more gradual, sometimes with large amplitudes.

Taking into account the nature of the feedback controls, we conclude that sudden sharp variations in the three rates right after the induction of anaemia are due to direct inhibition of apoptosis by Epo, independently of the intracellular network based on Erk and Fas, and gradual variations that occur later (after day 2) are due to Erk and Fas regulation. During the first six days these gradual variations are observed for the self-renewal rate (Panel A) and the diffe-

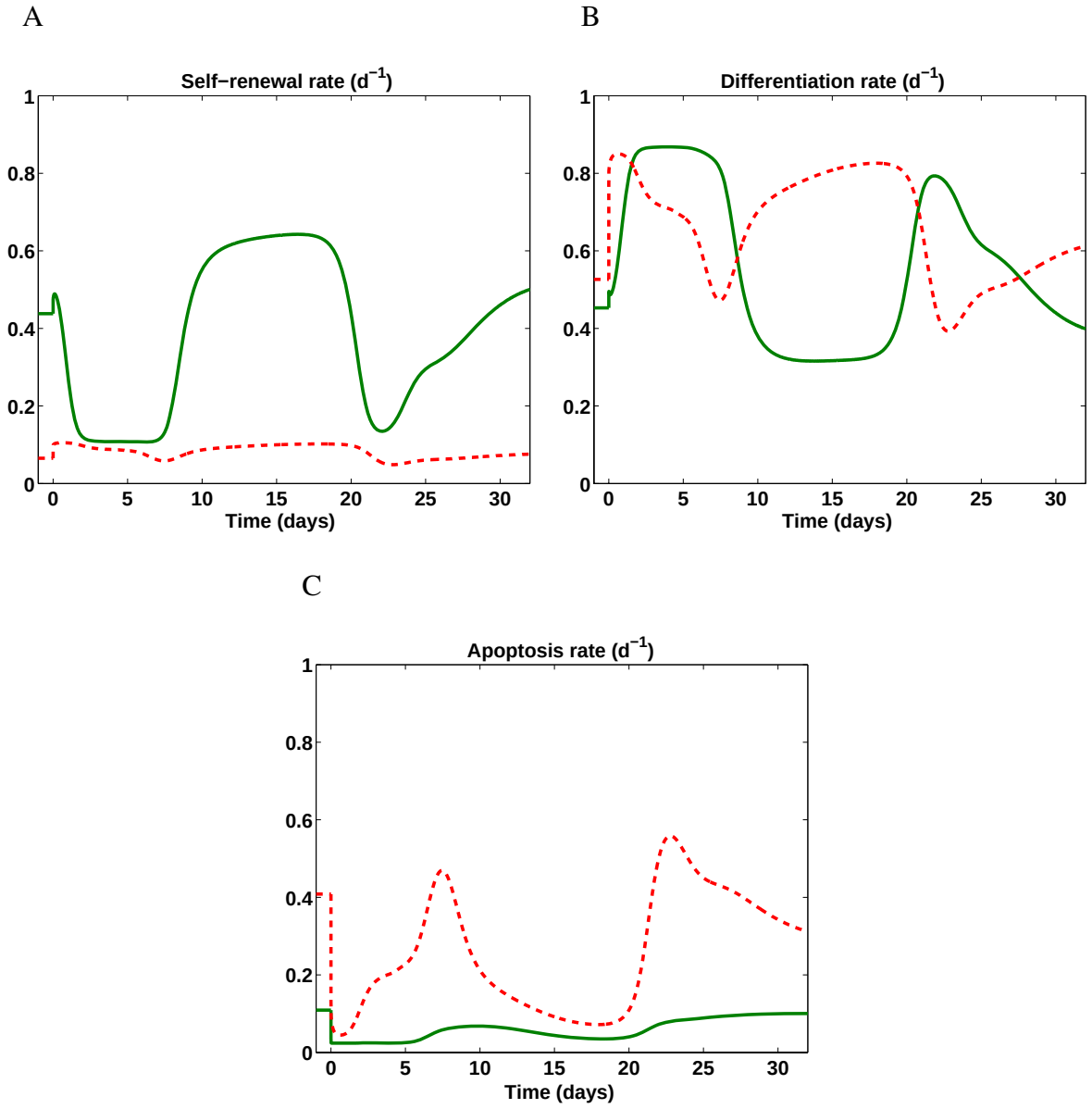

FIGURE 19 – Anaemia simulation. Self-renewal, differentiation and apoptosis rates of immature self-renewing (green solid curve) and mature differentiating (red dash curve) sub-populations.

rentiation rate (Panel B) of immature cells. During days 6-32, the three rates keep on varying gradually, which is due to Erk and Fas variations. These fluctuations are important, suggesting a strong dependence of the rates on Erk and Fas (which at the same time vary modestly), and last longtime (40-45 days, not shown here). These conclusions must however be completed by the fact that the influence of Epo on apoptosis rate is observed as long as its levels are not back to equilibrium value, especially for immature self-renewing sub-populations (Figure 19.C).

It should be noted as well that differentiation in our model is a choice by default, i.e. a cell that is protected against apoptosis and which does not self-renew differentiates.

Confrontation to experimental data. Simulation results and experimental data are presented in Figure 20. The blue dash curve represents the simulation discussed above (Figure 16), the black solid line represents the outcome of experiments by [29] (Figure 14).

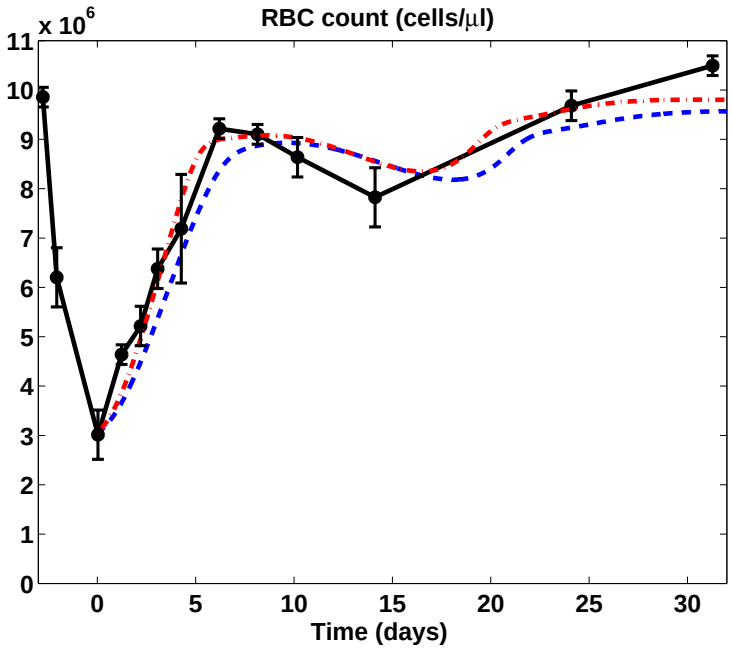

FIGURE 20 – Anaemia simulations. Erythrocyte count dynamics obtained by [29] in experiments on induced anaemia in mice (black circled solid line), obtained in simulations carried out with $\delta = 1/40$ d^{-1} (blue dash curve) and with $\delta = 1/30$ d^{-1} (red dash-dot curve).

Let focus on the simulated blue dash curve. First, from day 0 to day 7, the computed erythrocyte count increases as fast as observed in the experiments, with only one day delay. From day

10, simulated erythrocyte count decreases in spite of its low value (lower than equilibrium). Similar phenomenon is observed in the experiments (black solid line) from day 8 to 15. The cause of such a decrease in cell numbers although the erythrocyte count is still lower than normal is investigated in the following.

In Figure 16, reticulocyte count starts decreasing at day 4. Figure 19 shows that during first four days apoptosis rate is below its equilibrium for mature cells, whereas both self-renewal and differentiation rates are above their equilibrium values. This results in an increase of the number of mature progenitors (not shown here). However, for immature cells the picture is a bit different, self-renewal rate increases a little bit on the first day and then decreases a lot due to high $F-E$ values (Figure 18.A), differentiation rate is higher than at equilibrium, apoptosis rate is lower than at equilibrium. This results in a decrease of the number of immature progenitors (not shown here). Hence, on day 4 the system starts lacking immature cells to maintain the increase of mature progenitors that triggers a decrease of the latter and, thus, of reticulocytes. Apoptosis of mature progenitors is high during days 6-8 (Figure 19.C), whereas differentiation rate is low (Panel B) and self-renewal is about its steady state (Panel A). This makes reticulocyte count decrease even faster (Figure 16), go below its equilibrium on day 8, where it stays up to day 19. This, in turn, decreases the supply of mature erythrocytes that results in the reduction of erythrocyte count observed between day 10 and day 18. Thus, our model suggests that this decrease of erythrocyte count is a consequence of low self-renewal rate of immature cells during first seven days and of the high apoptosis of mature cells during days 6-8. This, in turn, is due to a high value of $F-E$ (Figure 18.A) and not to Epo control of apoptosis, which is below its equilibrium during these days and should, in contrary, decrease apoptosis rate (Figure 21). Consequently, this decrease (days 10-18) of the erythrocyte count can be explained by Erk-Fas regulation. It can be compared to the quick increase of erythrocyte count following the anaemia, which is clearly due to an inhibition of progenitor apoptosis by Epo, independently of Erk-Fas regulation.

The above analysis enlightens two different and clear mechanisms of erythropoiesis regulation : first, inhibition of apoptosis by Epo in the early stages of the response to anaemia, and second, a more moderate regulation on the long-term of erythroid progenitor self-renewal, differentiation and apoptosis based on intracellular regulation (Erk and Fas).

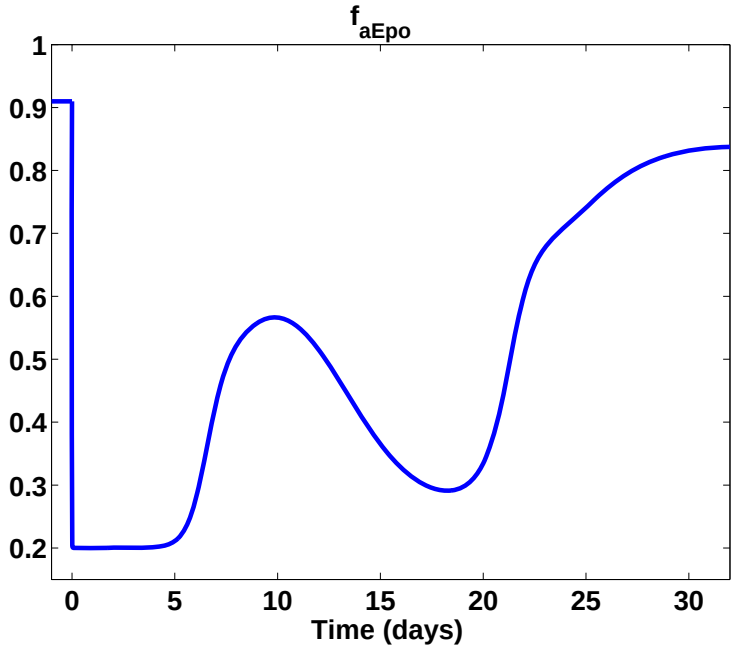

FIGURE 21 – Anaemia simulation. Function $f_{aEpo}(Epo)$.

Although close to experimental data, the simulated erythrocyte count (blue dash curve) does not appear to be the best fit to the data. Focusing on the nature of the anaemia, that is the consequences of phenylhydrazine use, we can obtain better results.

Phenylhydrazine is known to damage cell membrane, which results in reduced lifetime of erythrocytes following the injections. We tested this assumption with our model, assuming a mortality rate of erythrocytes $\delta = 1/30$ d^{-1}, which means the average lifetime of an erythrocyte is reduced to 30 days under the action of phenylhydrazine. Red dash-dot curve in Figure 20 represents erythrocyte count in this case. It provides a better fit of the data, with a stronger slope on the first days (days 1 to 5), a smaller undershoot afterward and a faster return to the equilibrium. It should be noted that the current modification of the value of δ does not alter the above analysis and conclusions, it only allows a better fit of the data. For both simulations presented in Figure 20, one feature of experimental curve is however not well approached : the undershoot in both simulations (observed around day 18) is slower, occurs later and is also smaller than the one obtained in the experiments (observed around day 14).

We confronted our model with other experimental data on phenylhydrazine-induced anaemia, presented in [36]. In these experiments, haematocrit values were measured during 45 days

after anaemia induction. The model used in this work does not a priori provide haematocrit, but only erythrocyte count. Haematocrit $H(t)$ is defined by

$$H(t) = \frac{vM(t)}{vM(t) + \text{Plasma volume}},$$

where $vM(t)$ represents the volume of erythrocytes in the blood. In [36] we assumed that the plasma volume was not modified during the experiments and considering normal haematocrit H^* (assumed to equal 50%) and erythrocyte count M^* we obtained

$$H^* = \frac{vM^*}{vM^* + \text{Plasma volume}},$$

which provides

$$\text{Plasma volume} = \frac{1 - H^*}{H^*} vM^*.$$

Consequently, haematocrit can be deduced from the erythrocyte count,

$$H(t) = \frac{M(t)}{M(t) + (1 - H^*)M^*/H^*}.$$

This is displayed in Figure 22.

To obtain an overshoot on day 5 as presented in Figure 22, it was necessary to modify functions $f_{aEpo}(Epo), p_s(E - F)$ and $a(F - E)$. In particular, the minimum value of f_{aEpo} has been dropped from 0.2 down to 0.1, see (1.25), functions $p_s(E - F)$ and $a(F - E)$ have been modified to have smaller variations on the relevant intervals of $F - E$. One can observe that experimental results are properly reproduced by the model, although the decrease following the peak in haematocrit values is slower in the model. Erythrocyte lifespan must be reduced from 40 days to 15 days to obtain these results, similarly to what has been done in [36].

Hence, this model is able to reproduce features of a simpler model, and also leads to more insights into regulatory mechanisms of erythropoiesis.

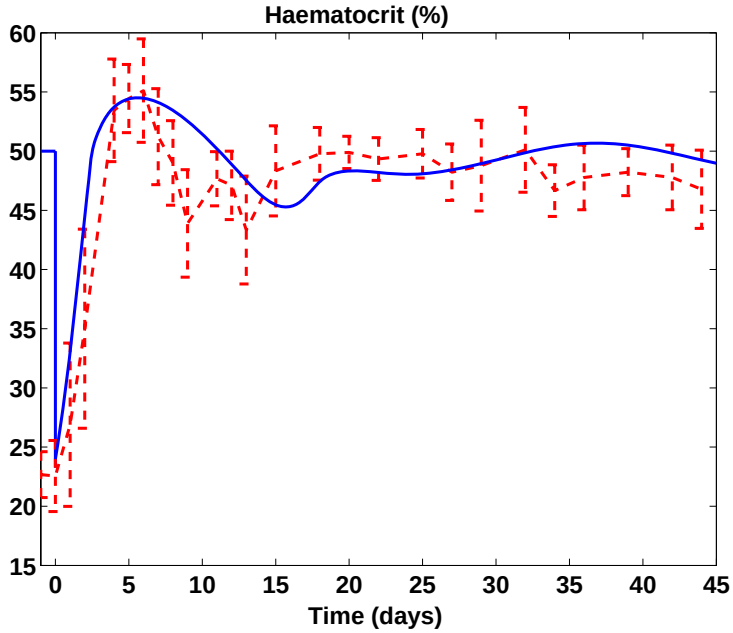

FIGURE 22 – Anaemia simulation. Haematocrit dynamics. Blue solid line represents simulation results, red dash line represents results of experiments on induced anaemia in mice obtained in [36]. Normal haematocrit is assumed to equal 50%, lifetime of erythrocytes is 15 days.

7 Discussion

In this chapter we presented two multi-scale mathematical models of erythropoiesis taking into account several biological aspects known nowadays. The objective of the first model was to bring together all available biological information in a mathematical model. Intracellular regulatory network has been described by a bistable system. Results of simulations were not confronted with experimental data. Second model is based on the first model. It is more precise and contains more biological information. Some model parameters have been taken from the literature, others have been chosen to qualitatively represent erythropoiesis regulation. Second model has been better studied numerically, i.e. more simulations have been carried out. The results were confronted with two different experimental data sets on induced anaemia. The objective of the second model was to study roles of different feedback mechanisms in the regulation of erythropoiesis. The results of the second model were deeper analysed.

In the first model intracellular regulatory network, determining cell choice between self-renewal, differentiation and apoptosis, was supposed to have bistable behaviour. Erk and Fas

were considered as key proteins determining progenitor fate choice. We considered several progenitor compartments and erythrocyte compartment that allowed the construction of populational dynamics with regulation by feedbacks from erythrocyte compartment to progenitor compartments through two growth factors, Epo and GCs. Epo was supposed to implement two feedbacks, it controlled Erk levels in cells and regulated apoptosis rate. Reticulocytes implemented feedback on progenitors by means of FasL. An essential feature considered in the model was the ability of progenitors to self-renew. The resulting mathematical model was analysed, we found steady states and their stability using Implicit Function Theorem. The considered model had several stable steady states, but only one among them satisfied all biological conditions. We carried out simulations of anaemia situation. The numerical results were in agreement with our expectations.

In the second approach, intracellular model was based on the scheme proposed in [96] and was obtained as a transition from a simple linear model to a non-linear bistable system. Again, two intracellular proteins, Erk and Fas, were supposed to be determinant for cell fate. Cell cycles were supposed to be constant and equaled one day. We considered several compartments of erythroid progenitors and a population of erythrocytes. A new feature, which we took into account in the model, is self-renewal ability of erythroid progenitors. For each sub-population of progenitors, we defined self-renewal, differentiation and apoptosis rates. We introduced as well two growth factors, Epo and GCs. Connections between the two modelling scales were provided by several feedback controls : Erk and Fas determined self-renewal, differentiation and apoptosis rates ; Epo and GCs were controlled by erythrocyte count ; Epo directly inhibited apoptosis rate independently of Erk activation. These feedback controls are turned on in critical situations. The resulting mathematical model was analysed, we found steady states and their stability. Then, simulations of anaemia were carried out and the results were confronted with experimental data. This allowed the evaluation of the roles of the feedback controls in response to anaemia : feedback by Epo on apoptosis, independently of the intracellular network based on Erk and Fas, was found to be determinant in the early stage of the response, to quickly increase the number of erythrocytes, whereas feedback control through the intracellular regulatory network, introduced in Section 3.2, is more important later in the response, when the erythrocyte count almost reached its equilibrium value, to regulate on a long-term the response to the stress.

Epo, however, has a permanent influence on progenitor apoptosis.

An additional feature brought by the model concerns apoptosis rate. The presented simulation provided that the apoptosis rate in mature sub-populations equals $a^* = 0.41$ d^{-1}. Thus, the model suggests that in normal erythropoiesis, 41% of produced mature erythroid progenitors undergo apoptosis daily. The model shows that in stress situations, like anaemia, organism reacts by temporarily suppressing apoptosis that allows fast recovery of erythrocytes (Figure 19).

Other simulations (not shown here) were carried out as well, to test hypotheses not presented here. For instance, consequences of the loss of bistability of intracellular network were investigated. The response of the system in this case was qualitatively the same as the one obtained in the simulations presented in Section 6. As mentioned in the previous section, different shapes for the probability function p_s and the apoptosis function a were considered. The presented simulation has shown a better fit, other simulations (not presented here) provided weaker response. We also tried different feedback functions f_{aEpo}, to evaluate the role of the feedback by Epo on apoptosis rate in response to the anaemia (strong or weak sensitivity of apoptosis to Epo). We also carried out simulations of less severe anaemia, with initial value of erythrocyte count being equal to 0.7 of steady state value. Obtained dynamics of erythrocyte count was qualitatively the same.

All the simulations were performed under the assumption that cell cycle durations were constant, equal to one day. Although there is no evidence that cell cycles vary during response to a stress, nor that such variations could be important, this assumption appears restrictive. In particular, it is responsible in part for the delay observed in the first days of the response for the increase of the erythrocyte count. Hence, considering that cell cycles can be shortened during stress erythropoiesis could enhance the results of the proposed model, by allowing a better fit to the data, and consequently more relevance of the predicted parameters.

The modelling presented in this chapter is novel and introduce some new insights into erythropoiesis regulation in critical situations.

Deuxième partie

Spatial Models of Erythropoiesis

8 Spatial distribution of cell populations in the process of erythropoiesis

Bone marrow has a particular structure. Current research in this field provides more and more insights into its spatial composition. This part of the work is devoted to spatial modelling of erythropoiesis. We take into account spatial cell distribution inside the bone marrow and cell motion resulting from cell proliferation. Immature erythrocytes appear and push each other through the medium formed by other cells and by porous matrix. In the process of this motion, cells increase their maturity. Mature blood cells are pushed out into blood vessels going through the marrow, see Figure 23. Thus, normal haematopoiesis implies certain spatial cell organisation

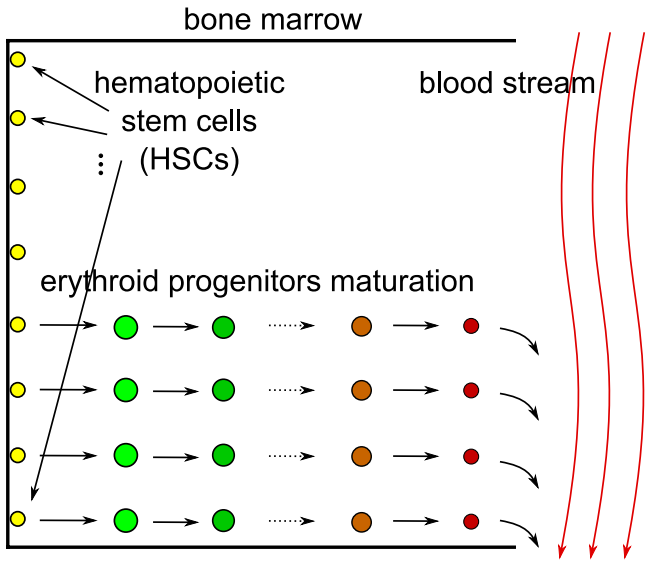

FIGURE 23 – Spatial structure of the bone marrow.

according to their maturity level. There are little experimental results about spatial distribution of blood cells in the bone marrow. It is known that stem cell can be localised and form a stem cell niche [75, 81, 84, 99, 110]. One of recent studies of spatial distribution of cells in the bone marrow was published by Watchman et al. [122]. The authors obtained that haematopoietic $CD34^+$ cells (stem cells committed to erythroid lineage) were located along a linear spatial gradient with a maximal areal concentration localised close to the bone surfaces.

Excessive proliferation of immature cells, which can be related to certain blood diseases including leukaemia, changes normal cell distribution in the marrow. If proliferation of malignant cells is sufficiently fast, then the tumour grows and can fill the whole marrow. The propagation of leukaemic cells corresponds to travelling wave solutions of reaction-diffusion-convection equations. We study in this model spatial cell distribution for both normal and leukaemic haematopoiesis.

In this work we describe cell concentrations by reaction-diffusion-convection equations and their motion by Darcy's law. The difference with the works cited before is related in particular to some specific features of cell production in the process of haematopoiesis. A close problem was studied in [44] in the 1D spatial case. In this work we are particularly interested by propagation of 2D waves which correspond to leukaemia development in the bone marrow.

The work is organised as follows. In Section 8.1 we present reaction-diffusion equations in porous media which describe evolution of cell populations. This model is briefly discussed in the general framework and more specifically for erythroid progenitors. In Section 8.2 we prove the existence of a stationary solution in the 1D case. This solution gives a stationary cell distribution in the cross-section of the bone marrow considered as a 2D rectangular domain. In the leukaemic case, this 1D solution can become unstable. The region filled by malignant cells will propagate and fill the whole domain. We study this phenomenon numerically in Section 8.3. We give an analytical approximation for the speed of the travelling wave and compare it with the numerical results.

8.1 Models of cell populations

8.1.1 Equations of continuous mechanics

We consider a cell population in a porous medium. In particular, this can be blood cells in the bone marrow. Let us denote by c_i, $i = 1, ..., n$ the concentrations of different cell types, that is the mass fraction of cells of the i-th type in a unit volume. Cell population is considered as a continuous medium. The evolution of the concentrations is governed by the following equation

$$\frac{\partial c_i}{\partial t} + \nabla.(\mathbf{v}c_i) = d\Delta c_i + F_i, \tag{2.1}$$

where $\mathbf{v}$ is the velocity of the medium, d is the diffusion coefficient and F_i is the production rate of the i-th type of cells. The diffusion terms describes random cell motion. Let ϕ be the total cell concentration, that is

$$\phi = c_1 + ... + c_n. \tag{2.2}$$

Taking a sum of all equations in (2.1), we obtain that ϕ satisfies the equation

$$\frac{\partial \phi}{\partial t} + \nabla.(\mathbf{v}\phi) = d\Delta\phi + \sum_{i=1}^{n} F_i. \tag{2.3}$$

Let us consider cells as spherical particles which consist of an external elastic membrane and which are filled by an incompressible fluid. Let us suppose for simplicity that all particles have the same size and denote their diameter by r and the volume by v_0. Consider next a sufficiently small cube with the side a and the volume V. Denote by p the pressure, that is the force acting from the particles on the sides of the cube. Let N be the number of particles inside the cube. If $N < N_0 = (a/r)^3$, then the particles can be distributed in such a way inside the cube that there is no repulsion between them and no force on the sides of the cube. The maximal number of particles can be estimated by $N_{max} = V/v_0$. In this case the cube is filled by an incompressible fluid. If the number of particles is between N_0 and N_{max}, then the pressure is a function of N.

Thus, the pressure p is a function of the total cell concentration ϕ :

$$p(\phi) = \begin{cases} 0 & , \quad \phi \leqslant \phi_0 \\ p_0(\phi) & , \quad \phi_0 < \phi < \phi_{max} \end{cases},$$

where $p_0(\phi)$ is some given function, ϕ_0 and ϕ_{max} are positive parameters. If $\phi = \phi_{max}$, then from (2.3) we obtain the following equation

$$\nabla.\mathbf{v} = \frac{1}{\phi_{max}} \sum_{i=1}^{n} F_i. \tag{2.4}$$

In the case without sources ($F_i = 0, i = 1, ..., n$), we obtain an incompressible medium.

The pressure-concentration dependence is shown in Figure 24. The equation of state can be

written as

$$H(p, \phi) = 0, \tag{2.5}$$

where the function H is such that $H(p(\phi), \phi) = 0$.

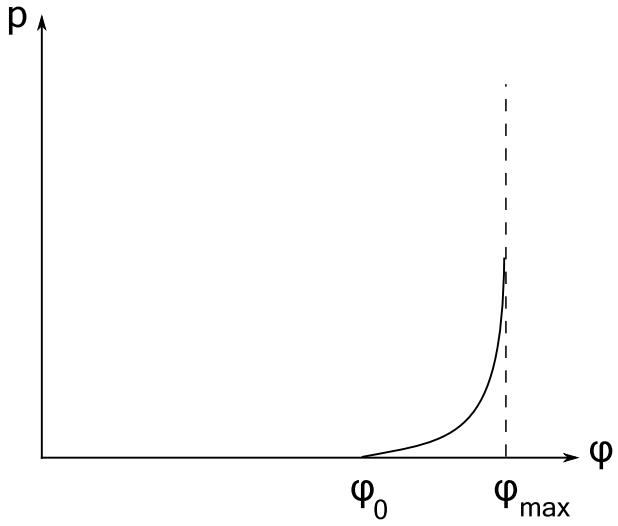

FIGURE 24 – The pressure-concentration dependence in the equation of state.

If we consider a porous medium, then convective motion is described by Darcy's law :

$$\frac{\rho}{\epsilon}\frac{\partial \mathbf{v}}{\partial t} = -\nabla p - \frac{\mu}{K}\mathbf{v}, \tag{2.6}$$

Here p is the pressure, ρ the density, ϵ the porosity of the medium, K the permeability and μ the viscosity. System of equations (2.1), (2.3), (2.5), (2.6) should be considered in some domain and completed by appropriate initial and boundary conditions.

8.1.2 Cell proliferation, differentiation, apoptosis

Here we specify the functions F_i used in the previous section. They describe the rates of production or disappearance of various cell types. Consider a single cell lineage which consists of n sub-populations with the following properties. The cells in each sub-population P_i are identical to each other. They can self-renew with the rate s_i, differentiate with the rate d_i or die by apoptosis with the rate a_i, see Figure 9. By self-renewal we understand here that two daughter cells are identical to the mother cell. In the case of differentiation, daughter cells

belong to the next sub-population P_{i+1}. We assume that there is an influx of cells to the first sub-population P_1 with a constant rate S. These cells can come from stem cell compartment or from other immature cell populations. Finally, the cells of the last sub-population P_n can differentiate into other cells or leave the system. This situation corresponds to the development of erythroid progenitors in the bone marrow, as discussed in previous chapter.

Under these assumptions, homogeneous in space concentrations c_i of cell sub-populations P_i and c_D of dead cells are described by the following system of equations :

$$\frac{dc_1}{dt} = S + (s_1 - d_1 - a_1)c_1 \equiv F_1, \tag{2.7}$$

$$\frac{dc_i}{dt} = (s_i - d_i - a_i)c_i + 2d_{i-1}c_{i-1} \equiv F_i, \quad i = 2, ..., n, \tag{2.8}$$

$$\frac{dc_D}{dt} = a_1c_1 + \ldots + a_nc_n \equiv F_D. \tag{2.9}$$

The rates of cell self-renewal, differentiation and apoptosis are determined by intracellular regulatory networks and can be influenced by surrounding cells, by the whole cell population and by external regulatory mechanisms based on hormones and growth factors. We do not consider here intracellular regulatory networks (see previous chapter for more detailed discussion) and suppose that these rates can be only influenced by surrounding cells. This means that the coefficients s_i, d_i, a_i can depend on $c_1, ..., c_n$. In particular, we will take into account the limitation on cell proliferation. When the total cell concentration $c_\Sigma = c_1 + ... + c_n$ approaches some maximal value c_{max}, cells produce signals which reduce their proliferation rate :

$$s_i = s_i^0(c_{max} - c_\Sigma), \quad d_i = d_i^0(c_{max} - c_\Sigma). \tag{2.10}$$

It is also possible that cells accelerate their own proliferation or proliferation of other cells. In the case of linear self-acceleration, instead of (2.8) we will have

$$s_i = s_i^0c_i(c_{max} - c_\Sigma), \quad d_i = d_i^0c_i(c_{max} - c_\Sigma). \tag{2.11}$$

In this case

$$F_1(c) = S + (s_1^0 - d_1^0)\, c_1^m(c_{max} - c_\Sigma) - a_1c_1,$$

$$F_i(c) = (s_i - d_i)\, c_i^m (c_{max} - c_\Sigma) + 2d_{i-1}(c_{max} - c_\Sigma)c_{i-1} - a_i c_i, \quad i = 2, ..., n,$$

where $c = (c_1, ..., c_n)$, $m = 1, 2$. We note that the restriction on cell proliferation by the total number of cells may not take place. In particular, this can be the case for malignant cells. Similar models can be written for several cell lineages.

8.1.3 Summary of the models

Depending on the value of cell concentration, we obtain the models which differ by the equations of motion. If $c_\Sigma \leqslant \phi_0$, then $p = 0$. From (2.6) it follows that $\mathbf{v} = \mathbf{0}$ and the model is reduced to reaction-diffusion system (2.1) without convective terms. The condition on c_Σ will be verified if $c_{max} < \phi_0$.

If $c_\Sigma < \phi_{max}$, then $p = p_0(\phi)$. The model is given by equation (2.1) and

$$\frac{\rho}{\epsilon}\frac{\partial \mathbf{v}}{\partial t} = -\nabla p_0(c_\Sigma) - \frac{\mu}{K}\mathbf{v}.$$

Under the quasi-stationary approximation, the last equation is replaced by

$$\mathbf{v} = -\frac{K}{\mu}\,\nabla p_0(c_\Sigma).$$

If we consider a linear approximation of the function p_0, we obtain $\mathbf{v} = -\kappa\nabla(c_1 + ... + c_n)$ (cf. [44]), where $\kappa = K/\mu$ is a positive parameter.

If $c_\Sigma = \phi_{max}$, then the model is given by equations (2.1), (2.4), (2.6). It is possible to have all three cases $c_\Sigma \leqslant \phi_0$, $\phi_0 < c_\Sigma < \phi_{max}$, $c_\Sigma = \phi_{max}$ at the same time, each one in some subdomain. The boundaries between the subdomains can depend on time.

8.2 Incompressible medium

Let us consider the case $c_\Sigma = \phi_{max}$. Then, in the 1D case, we obtain the system of equations

$$\frac{\partial c_i}{\partial t} + \frac{\partial (v c_i)}{\partial x} = d\,\frac{\partial^2 c_i}{\partial x^2} + F_i(c), \quad i = 1, ..., n, \tag{2.12}$$

$$\frac{\partial v}{\partial x} = \frac{1}{\phi_{max}} \left(\sum_{i=1}^{n} F_i(c) + F_D(c) \right). \tag{2.13}$$

We consider it in the bounded interval $0 \leqslant x \leqslant L$ with the boundary conditions

$$x = 0 : c_1 = c_1^0, \frac{\partial c_i}{\partial x} = 0,\ i = 2, ...n, \quad x = L :\ \frac{\partial c_i}{\partial x} = 0,\ i = 1, ..., n. \tag{2.14}$$

This problem is supplemented with the condition $\frac{\partial v}{\partial x} = 0$ at $x = 0$ and is also supplemented with some suitable positive initial data. Up to a normalisation of the parameters, we will assume in the sequel that $c_1^0 = 1$. Denote

$$F_i = (s_i - d_i - a_i)c_i + 2d_{i-1}c_{i-1}, \quad c_0 = 0, \quad i = 1, \ldots, n,$$

$$F = F_1 + \ldots + F_n + F_D = \sum_{k=1}^{n-1} (s_i + d_i)c_i + (s_n - d_n)c_n.$$

Then stationary solutions of Problem (2.12)-(2.14) satisfy the following system of equations :

$$dc_i'' - (c_i p')' + F_i(c) = 0, \quad i = 1, ..., n, \tag{2.15}$$

$$p'' = \nu F, \tag{2.16}$$

together with the boundary conditions

$$\begin{aligned} &c_1(0) = 1, \quad c_i'(0) = 0 \quad i = 2, ..., n, \\ &c_i'(L) = 0, \quad i = 1, .., n, \\ &p'(0) = 0, \quad p(0) = 0. \end{aligned} \tag{2.17}$$

Here $v = p'$, $\nu = \mu/(K\phi_{max})$. We obtain the following result.

Theorem 1. *Let us suppose that*

$$d_i + a_i - s_i \geqslant 0, \quad i = 1, \ldots n, \text{ and } s_n - d_n \geqslant 0.$$

Then System (2.15)-(2.17) *has a solution* $(c_{1,0}, .., c_{n,0}, p_0) \in C^2([0, L])^{n+1}$ *such that*

$$c_{i,0} \geqslant 0, \quad \forall\, i = 1, ..., n. \tag{2.18}$$

Proof. The proof of this theorem is based on the Leray-Schauder method. A similar problem but with different boundary conditions was considered in [44].

Denote $b_i = d_i + a_i - s_i$, $i = 1, \dots n$, $k_i = s_i + d_i$, $i = 1, \dots n-1$ and $k_n = s_n - d_n$ and suppose that all b_i and k_i are positive. With these notations System (2.15)-(2.16) becomes

$$dc_i'' - (c_i p')' + (2d_{i-1}c_{i-1} - b_i c_i) = 0, \quad c_0 = 0, \quad i = 1, ..., n,$$

$$p'' = \nu \sum_{k=1}^{n} k_i c_i.$$

Let us consider the system depending on a parameter τ :

$$dc_i'' - \tau(c_i p')' + (\tau 2d_{i-1}c_{i-1} - b_i c_i) = 0, \quad c_0 = 0, \quad i = 1, ..., n, \tag{2.19}$$

$$p'' = \nu |k_1 c_1 + \ldots + k_n c_n|, \tag{2.20}$$

together with boundary conditions (2.17). Here $\tau \in [0, 1]$ is the homotopy parameter. If $\tau = 1$, then we obtain the previous problem. For $\tau = 0$ we obtain a model problem with known properties.

Consider a solution of Problem (2.15), (2.16) and (2.17). Show first that $c_i \geqslant 0$. The equation for c_1 is

$$dc_1'' - \tau c_1' p_1' - (\tau p'' + b_1)c_1 = 0, \quad c_1(0) = 1, \quad c_1'(L) = 0. \tag{2.21}$$

Since $(\tau p'' + b_1)$ is positive, then $c_1(x)$ cannot have negative minima. Indeed, let x_0 be a point of a local minimum of the function $c_1(x)$. Then, in this point $c_1''(x_0) > 0$ and $c_1'(x_0) = 0$. Substituting it into Equation (2.21) we obtain that $c_1(x) \geqslant 0$. Let us show that the case where exists $x_0 \in (0, L)$ such that $c_1(x) \geqslant 0$ for $x \in (0, x_0)$ and $c_1(x) < 0$ for $x \in (x_0, L)$ is not possible as well. In this case we would have $c_1''(L) > 0$ that would provide $c_1(L) > 0$. Thus, $c_1(x) \geqslant 0, \ \forall x \in [0, L]$. Repeating this reasoning for every $i = 2, \dots, n$ we obtain that $c_i \geqslant 0$.

Thus, Equation (2.20) is transformed into the following one :

$$p'' = \nu(k_1c_1 + \ldots + k_nc_n).$$

The second step is to obtain a priori estimates of these solutions. Let us multiply Equation (2.19) by c_i and integrate it over $(0, L)$. Then we obtain

$$\int_0^L dc_i''c_i dx - \int_0^L \tau(c_ip')'c_i dx + \int_0^L (\tau 2d_{i-1}c_{i-1} - b_ic_i)c_i dx = 0$$

$$d\int_0^L (c_i')^2 dx + b_i\int_0^L c_i^2 dx + dc_i'(0)c_i(0) + \frac{\tau\nu}{2}\int_0^L c_i^2(k_1c_1 + \ldots + k_nc_n)dx =$$
$$= -\frac{\tau}{2}c_i^2(L)p'(L) + 2\tau d_{i-1}\int_0^L c_{i-1}c_i dx$$

Denote by C positive constants that do not depend on the solution. Since $p'(L) = \int_0^L (c_1 + \ldots + c_n)dx$, then $p'(L) \geqslant 0$ and

$$C\|c_i\|_{H^1}^2 \leqslant -dc_i'(0)c_i(0) + 2\tau d_{i-1}\int_0^L c_{i-1}c_i dx \leqslant -dc_i'(0)c_i(0) + 2d_{i-1}\int_0^L c_{i-1}c_i dx.$$

For $i = 1$ we have

$$C\|c_1\|_{H^1}^2 \leqslant -dc_1'(0), \tag{2.22}$$

while for $i \geqslant 2$,

$$C\|c_i\|_{H^1}^2 \leqslant 2d_{i-1}\int_0^L c_{i-1}c_i dx \leqslant 2d_{i-1}\|c_{i-1}\|_{L^2}\|c_i\|_{L^2} \leqslant 2d_{i-1}\|c_{i-1}\|_{L^2}\|c_i\|_{H^1},$$

and, therefore,

$$C\|c_i\|_{H^1} \leqslant 2d_{i-1}\|c_{i-1}\|_{L^2}.$$

By induction, we obtain that for $i \geqslant 2$ the following estimate holds :

$$\|c_i\|_{H^1} \leqslant C\|c_1\|_{H^1}. \tag{2.23}$$

In order to estimate $c_1'(0)$, let us integrate the equation for c_1 over $(0, L)$. We obtain the equality

$$-dc_1'(0) = \tau p'(L)c_1(L) + b_1 \int_0^L c_1 dx.$$

We have

$$p'(L) = \nu \int_0^L (k_1 c_1 + \ldots + k_n c_n) dx.$$

The Hölder inequality provides the following estimate :

$$p'(L) \leqslant C(\|c_1\|_{L^2} + \ldots + \|c_n\|_{L^2}).$$

Using (2.23), we obtain

$$p'(L) \leqslant C\|c_1\|_{L_2}.$$

The function c_1 satisfies the problem

$$dc_1'' - \tau c_1' p_1' - (\tau p'' + b_1)c_1 = 0, \quad c_1(0) = 1, \quad c_1'(L) = 0.$$

Since $p'' \geqslant 0$, then from the maximum principle we obtain that $c_1 \leqslant 1$, and then $c_1(L) \leqslant 1$. This allows obtaining the following estimate :

$$-dc_1'(0) \leqslant C\|c_1\|_{L^2}.$$

Finally, due to (2.22) we conclude that $\|c_i\|_{H_1}^2 \leqslant C$ for $i = 1, \ldots, n$. This bound provides an estimate of p in space H^3. Due to Sobolev embedding theorem, we obtain an estimate in $C^2[0, L]$ of the function p and due to equation (2.19) we obtain a bound in $C^1[0, L]$ for c_i.

Consider now the Banach space Y defined by

$$Y = \left(C^1([0,L])\right)^n \times C^2([0,L]),$$

endowed with the norm

$$\|(c_1,\ldots,c_n,p)\|_Y = \|c_1\|_{C^1([0,L])} + \ldots + \|c_n\|_{C^1([0,L])} + \|p\|_{C^2([0,L])}.$$

Consider the mapping $T_\tau : Y \to Y$ defined by $T_\tau((\widetilde{c}_1,\ldots,\widetilde{c}_n),q) = ((c_1,\ldots,c_n),p)$, where $(c_1,\ldots,c_n,p)$ is the solution of the linear system

$$dc_i'' - b_i c_i = \tau((\widetilde{c}_i q')' - 2d_{i-1}\widetilde{c}_{i-1}), \quad c_0 = 0, \quad i = 1,...,n, \tag{2.24}$$

$$p'' = \nu(k_1 c_1 + \ldots + k_n c_n), \tag{2.25}$$

together with boundary conditions (2.17). From the elliptic regularity it follows that the mapping T_τ is a compact operator.

Next, from the above a priori estimates it follows that there exists such constant $M > 0$ that for any $\tau \in [0,1]$, (C,p) is a fixed point of the operator T_τ implies that $\|C,p\|_Y < M$. Then, if we consider $B = B_Y(0,M)$, then the topological degree $deg(I - T_\tau, B, 0)$ is well defined and from the homotopy invariance we have

$$deg(I - T_0, B, 0) = deg(I - T_1, B, 0). \tag{2.26}$$

The operator T_0 corresponds to the constant operator

$$T(\widetilde{C}, q) = (c_1^0,\ldots,c_n^0,p^0),$$

where $c_i^0 \equiv 0$, $i \geqslant 2$, the function c_1^0 is given by resolution of the equation

$$dc_1'' - b_1 c_1 = 0, \quad c_1(0) = 1, \quad c_1'(L) = 0$$

and $p^0(x) = \int_x^L \int_0^s (c_1^0(t))dtds$. Thus we obtain that $deg(I - T_0, B, 0) = 1$ and, due to (2.26), system (2.15)-(2.17) has a solution. This completes the proof of the theorem.

□

8.3 Numerical simulations

In this section we present numerical simulations of the system considered in the previous section but in the 2D space. We suppose for simplicity that all parameters k_i defined in the proof of Theorem 1 are equal to each other. We denote them by k. The system of equations

$$\frac{\partial c_i}{\partial t} + \nabla.(c_i v) = d\Delta c_i + k(c_{i-1} - c_i), \quad i = 1, \ldots, n, \quad c_0 = 0,$$
$$\Delta P = k(c_1 + \ldots + c_n), \quad \nabla P = \nu v$$

is considered in the domain

$$\Omega = (0, L_x) \times (0, L_y)$$

with the boundary conditions

$$\frac{\partial P}{\partial x}(0, y) = 0, \quad \frac{\partial P}{\partial y}(x, 0) = 0, \quad \frac{\partial P}{\partial y}(x, L_y) = 0, \quad P(L_x, y) = 0,$$
$$c_1(0, y) = 1, \quad \frac{\partial c_1}{\partial y}(x, 0) = 0, \quad \frac{\partial c_1}{\partial y}(x, L_y) = 0, \quad \frac{\partial c_1}{\partial x}(L_x, y) = 0,$$
$$\frac{\partial c_i}{\partial x}(0, y) = 0, \quad \frac{\partial c_i}{\partial y}(x, 0) = 0, \quad \frac{\partial c_i}{\partial y}(x, L_y) = 0, \quad \frac{\partial c_i}{\partial x}(L_x, y) = 0,$$
$$i = 2, \ldots, n.$$

The boundary conditions for the pressure mean that the vertical component v_y of the velocity vanishes at the top and at the bottom of the rectangular domain. The horizontal component of the velocity v_x equals zero at the left boundary because there is no convective flux. This means that stem cells are attached to the left boundary and provide a constant concentration of immature cells c_1. Cell proliferation inside the domain results in cell flow outside the domain through the right boundary where the pressure is zero.

Computer simulations are carried out using COMSOL Multiphysics 3.4 software. This software uses finite element methods. We do not list technical parameters of the calculations for the

sake of brevity. The simulations are carried out for three cell populations c_1, c_2 and c_3, $L_x = 10$, $L_y = 20$, $d = 0.1$, $k = 15$.

Hereafter we present simulations of the stationary solution the existence of which was proved in the previous section, simulations of wave propagation and the calculation of the wave speed.

8.3.1 Stationary solution

We first present simulations of the stationary problem. Note that the stationary solution does not depend on the variable y. Hence, the solution of the 2D problem considered as a function of x coincides with the 1D stationary solution. Its existence is proved in Section 8.2. Left image of the Figure 25 represents cell population distributions, the right image shows the pressure distribution.

Recall that the domain Ω represents a bone marrow in which the wall $x = 0$ is the wall with stem cells fixed on it, the boundary $x = L_x$ is the boundary between the bone marrow and the blood stream. Mature cells pass it and leave the bone marrow into the blood stream. Cells of population c_i are considered to be more mature than those of population c_{i-1}. As we can see from the left image of Figure 25, the majority of cells located on the left boundary $x = 0$ are immature cells of population c_1, whereas among cells leaving the bone marrow mature cells are present in bigger quantity.

8.3.2 2D waves

Suppose that malignant cells appear at some moment of time. These cells lose (or decrease) their ability to differentiate and excessively self-renew. Their distribution in the bone marrow can be described by the following equation :

$$\frac{\partial s}{\partial t} + \nabla.(sv) = d_s \Delta s + k_s s,$$

with the same boundary conditions as for other cells :

$$\frac{\partial s}{\partial x}(0, y) = 0, \quad \frac{\partial s}{\partial y}(x, 0) = 0, \quad \frac{\partial s}{\partial y}(x, L_y) = 0, \quad \frac{\partial s}{\partial x}(L_x, y) = 0.$$

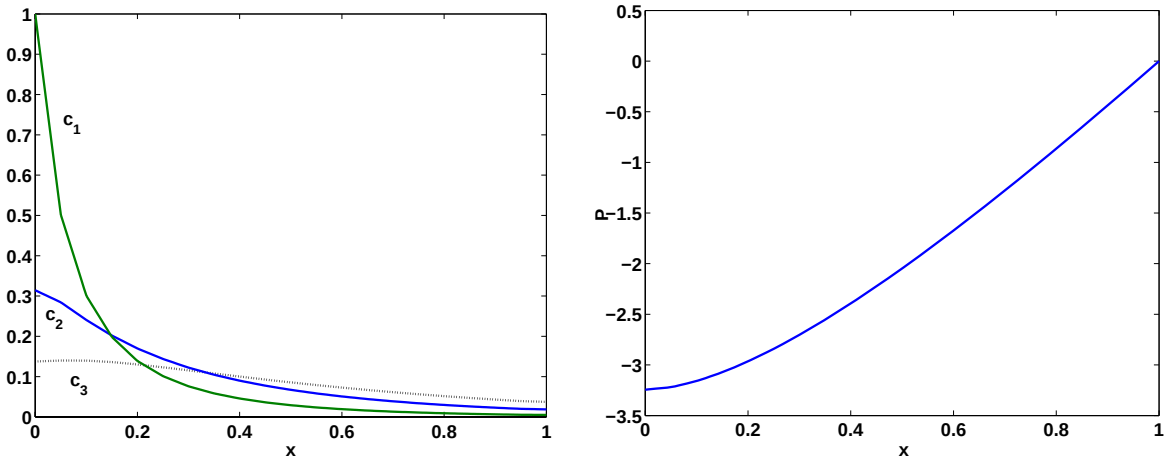

FIGURE 25 – Stationary solution as a function of the variable x (it does not depend on y). Simulations are carried out for three cell populations. Left : cell population distributions. Right : pressure distribution.

In this section we present simulations of propagations of the region filled by malignant cells. As initial condition for malignant cell population we consider a function that is zero everywhere in the domain except for a small area inside the domain, the nidus from which malignant cells start developing. An example of numerical simulations is given in Figure 26. The values of the parameters are the same as above. We can see that the concentration of malignant cells gradually grows and propagates along the bone marrow as a travelling wave. At the first stage of the development the tumour propagates along the x-direction (along the flow), at the second stage along the y-direction (perpendicular to the flow).

Wave propagation occurs if the stationary solution discussed above becomes unstable. The stability of the stationary solution for a similar problem is studied in [44].

The speed of the propagation depends on the diffusion coefficients d and d_s of normal and malignant cells, and on the parameters k and k_s. We study the speed of propagation in the section.

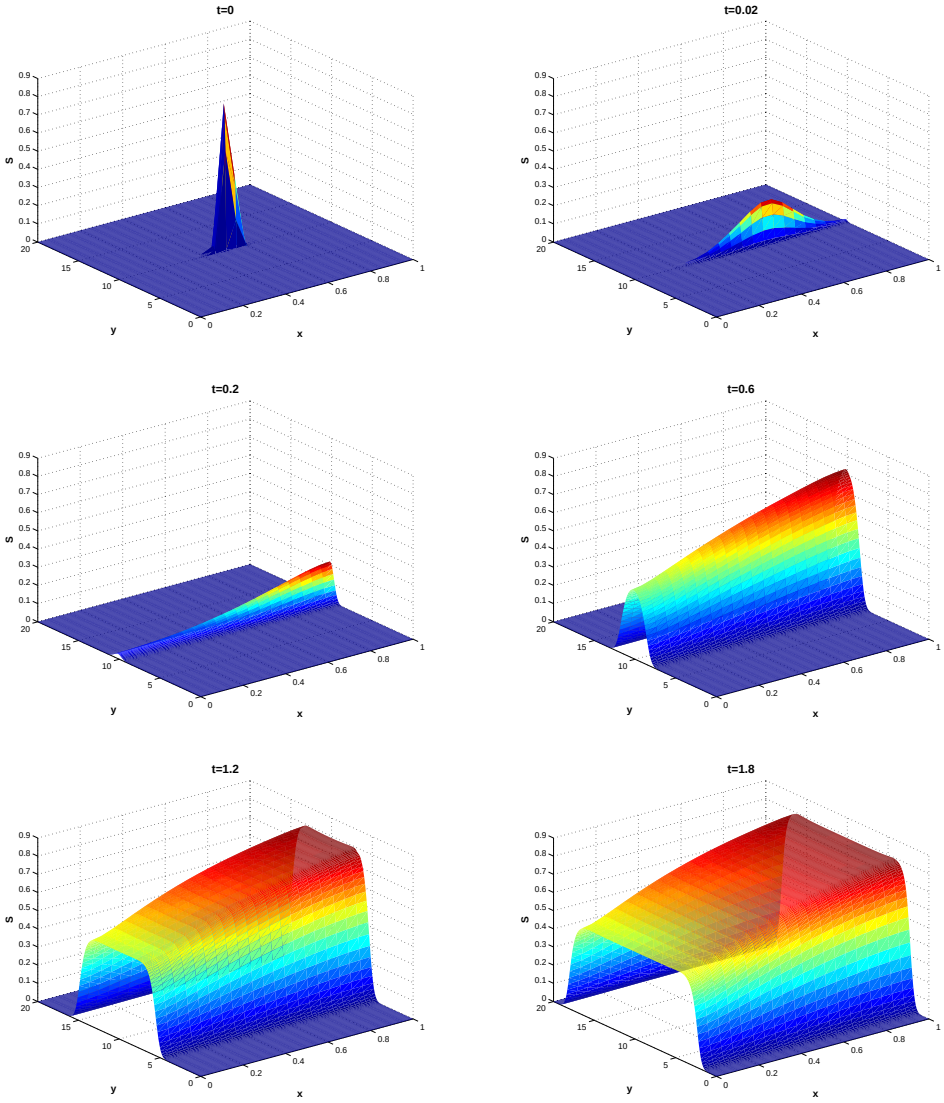

FIGURE 26 – Propagation of malignant cells in the bone marrow. Their concentration at times $t = 0, 0.02, 0.2, 0.6, 1.2$ and 1.8. Malignant cells propagate and finally occupy the whole bone marrow.

8.3.3 Wave speed

From mathematical point of view, wave propagation should be studied in the infinite strip $\Omega = (0, L) \times \mathbb{R}$. We consider the system of equations

$$\frac{\partial c_i}{\partial t} + \nabla.(c_i \mathbf{v}) = d\Delta c_i + k(c_{i-1} - c_i), \quad i = 1, .., n, \quad c_0 = 0. \tag{2.27}$$

$$\frac{\partial s}{\partial t} + \nabla.(s\mathbf{v}) = d_s \Delta s + k_s s, \tag{2.28}$$

$$\nabla.\mathbf{v} = k(c_1 + ... + c_n) + k_s s, \quad \nabla p = \nu \mathbf{v}, \tag{2.29}$$

in this domain together with boundary conditions

$$c_1(0, y) = 1, \quad \partial_x s(0, y) = \partial_x c_i(0, y) = 0 \text{ for } y \in \mathbb{R} \text{ and } i = 2, .., n, \tag{2.30}$$

$$\partial_x s(L, y) = \partial_x c_i(L, y) = 0 \text{ for } y \in \mathbb{R} \text{ and } i = 1, .., n, \tag{2.31}$$

$$\frac{\partial p}{\partial x}(0, y) = 0, \quad p(L, y) = 0 \text{ for } y \in \mathbb{R}. \tag{2.32}$$

In order to find an analytical approximation of the wave front speed we suppose first that there exists a one-dimensional disease free stationary solution

$$(c_{i,0}, s_0, p_0, v_0) = (c_{i,0}(x), 0, p_0(x), v_0(x)).$$

It corresponds to solutions of the stationary problem in the interval $(0, L)$:

$$\begin{aligned}
&(c_{i,0} v_0)' = d c_{i,0}'' + k(c_{i-1,0} - c_{i,0}), \quad i = 1, .., n, \quad c_0 = 0 \\
&v_0' = k(c_{1,0} + ... + c_{n,0}), \quad p_0' = \nu v_0 \\
&c_{1,0}(0) = 1, \quad c_{i,0}' = 0 \text{ for } i = 2, .., n \\
&c_{i,0}'(L) = 0, \quad p_0'(0) = 0, \quad p_0(L) = 0.
\end{aligned}$$

This stationary solution is supposed to be stable with respect to the system without malignant

cells. This means that the eigenvalue problem : find $\lambda \in \mathbb{C}$, $c_1, .., c_n$ and v satisfying

$$\begin{aligned}
&\lambda c_i + (c_{i,0}v)' + (c_i v_0)' = dc_i'' + k(c_{i-1} - c_i), \quad i = 1, .., n, \quad c_0 = 0 \\
&v' = k(c_1 + ... + c_n), \quad p' = \nu v \\
&c_1(0) = 0, \quad c_i'(0) = 0 \text{ for } i = 2, .., n \\
&c_i'(L) = 0, \quad p'(0) = 0, \quad p(L) = 0,
\end{aligned} \tag{2.33}$$

has solutions only with a negative real part, $\Re\lambda < 0$.

We now consider travelling wave solutions of Problem (2.27)-(2.32), that are solutions in the form

$$(c_1, .., c_n, s, p, \mathbf{v})(t, x, y) = (\widetilde{c_1}, .., \widetilde{c_n}, \widetilde{s}, \widetilde{p}, \widetilde{\mathbf{v}})(x, y - ct),$$

where $c > 0$ is the wave speed. In order to simplify the notations, we omit the tilde. Setting $z = y - ct$, we obtain that the travelling wave solution satisfies the following problem in the moving frame :

$$d\Delta c_i + c\frac{\partial c_i}{\partial z} - \nabla.(c_i \mathbf{v}) + k(c_{i-1} - c_i) = 0, \quad i = 1, .., n, \quad c_0 = 0.$$

$$\begin{aligned}
d_s \Delta s + c\frac{\partial s}{\partial z} - \nabla.(s\mathbf{v}) + k_s s = 0, \\
\nabla.\mathbf{v} = k(c_1 + ..c_n) + k_s s, \quad \nabla p = \nu \mathbf{v},
\end{aligned} \tag{2.34}$$

together with the boundary conditions

$$c_1(0, z) = 1, \quad \partial_x s(0, z) = \partial_x c_i(0, z) = 0 \text{ for } z \in \mathbb{R} \text{ and } i = 2, .., n,$$

$$\partial_x s(L, z) = \partial_x c_i(L, z) = 0 \text{ for } z \in \mathbb{R} \text{ and } i = 1, .., n,$$

$$\frac{\partial p}{\partial x}(0, z) = 0, \quad p(L, z) = 0 \text{ for } z \in \mathbb{R}.$$

We are looking for a travelling wave that connects the disease free stationary state when unstable (with respect to the complete model) to what we expect to be a stationary solution, which

corresponds to the disease, that is

$$\lim_{z\to+\infty}(c_1,..,c_n,s,p,\mathbf{v})(x,z)=(c_{1,0}(x),..,c_{n,0}(x),0,p_0(x),v_0(x)), \tag{2.35}$$

$$\partial_y p(x,\pm\infty)=0 \text{ for } x\in(0,L),$$

and we assume that

$$\partial_y(c_1,..,c_n)(x,\pm\infty)=0 \text{ for } x\in(0,L).$$

To find the wave speed, we assume that the solution has an exponential behaviour as $z\to+\infty$. More precisely we suppose that

$$s(z,x)\approx e^{-\mu z}\overline{s}(x)\ \ z\to+\infty.$$

Since the function $s(z,x)$ is assumed to be positive, one obtains the conditions

$$\mu\in(0,\infty),\ \ \overline{s}\geqslant 0.$$

We substitute the solution in this form into (2.34) and using condition (2.35), we obtain that

$$\begin{aligned}&(d_s\mu^2-c\mu)\overline{s}+d_s\partial_y^2\overline{s}-(\overline{s}v_0(x))'+k_s\overline{s}=0,\\&\overline{s}'(0)=0,\ \ \overline{s}'(L)=0.\end{aligned}$$

Consider the operator

$$\mathcal{L}s=d_s\partial_y^2 s-(sv_0(x))'+k_s s,\ \ s'(0)=0,\ \ s'(L)=0. \tag{2.36}$$

Then, $\overline{s}$ is its eigenvector and $c\mu-d_s\mu^2$ is an associated eigenvalue. Since $\overline{s}\geqslant 0$, then we conclude that it is an eigenvector associated with the principal eigenvalue $\lambda_p>0$ of the operator $\mathcal{L}$, i.e., $\mathcal{L}\overline{s}=\lambda_p\overline{s}$, and μ satisfies

$$c\mu-d_s\mu^2=\lambda_p,\ \ \mu>0.$$

This equation has a real and positive solution if and only if $c^2 - 4d_s\lambda_p \geqslant 0$, that is for any c such that

$$c \geqslant c^* \text{ with } c^* = 2\sqrt{d_s\lambda_p}. \tag{2.37}$$

Finally, we expect that c^* corresponds to the spreading rate of the malignant cells.

Numerical computations of c^* for $n = 3$ and $L_x = 1$ and direct numerical computations of the speed of front propagation of malignant cells c_{num} are presented in Table 5. Wave speed obtained by the analytical approximation is in a good agreement with the wave speed found by direct numerical calculations.

TABLE 5 – Comparison between analytical approximation of the wave speed and numerical simulations. The values of the parameters are $d = 0.1$, $k = 15$ and $d_s = 0.8$. Analytical approximation is obtained through linearisation of the equation.

k_s	8	10	12	14	16	18	20
c^*	2.06	3.26	4.13	4.84	5.46	6.02	6.53
c_{num}	1.98	3.20	4.06	4.80	5.49	6.15	6.83

Since λ_p is the principal eigenvalue of the operator $\mathcal{L}$ defined by (2.36), one can conclude that λ_p depends linearly on k_s. Then from (2.37) we obtain that $(c^*)^2$ linearly depends on k_s. We verify this dependence for analytical and numerical computations. For the values given in Table 5, we test this linear dependence between k_s and c^2_{num}. The results are presented in Figure 27.

8.4 Discussion

We studied a spatial model of erythropoiesis. The model consisted of a system of reaction-diffusion-convection equations in the porous medium described by Darcy's law. We proved the existence of a 1D solution. If we introduce malignant cells, which have a higher proliferation rate than normal cells, then one-dimensional cell distribution can lose its stability. This corresponds to the appearance of tumour. We carried out numerical simulations of tumour growth, that is of malignant cell propagation. This propagation has a form of a two-dimensional travelling wave. The speed of the wave was calculated in two ways. Firstly, we linearised the system

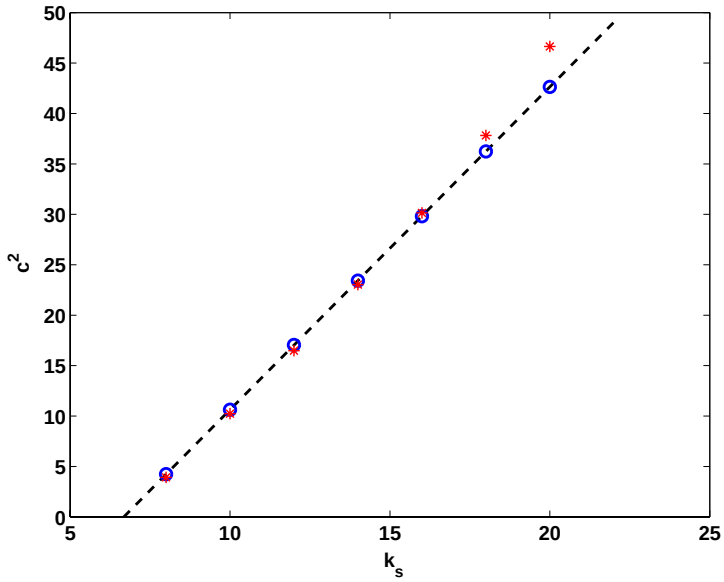

FIGURE 27 – Dependence of c^2 on k_s. Circles : analytical approximation, asterisks : direct numerical simulations.

and obtained an eigenvalue problem. It allowed us to find the minimal wave speed from the condition of positivity of the corresponding eigenfunction. Secondly, we found the wave speed in direct numerical simulations. These two approaches are in a good agreement, see Table 5.

9 Nonlocal reaction-diffusion equation

In this section we study a nonlocal reaction-diffusion equation arising in population dynamics. We prove the existence of travelling wave solutions using the Leray-Schauder method. In order to do this we define topological degree and obtain a priori estimates of solutions in weighted Hölder spaces.

9.1 Introduction

We study the integro-differential equation

$$\frac{\partial u}{\partial t} = \frac{\partial^2 u}{\partial x^2} + J(u)\, u(1-u) - \alpha u, \tag{2.38}$$

where

$$J(u) = \int_{-\infty}^{\infty} \phi(x-y)u(y,t)dy,$$

$\phi(x)$ is a non-negative function with a bounded support and $\int_{-\infty}^{\infty} \phi(x)dx = 1$. If we replace ϕ by a δ-function, then instead of (2.38) we obtain the reaction-diffusion equation

$$\frac{\partial u}{\partial t} = \frac{\partial^2 u}{\partial x^2} + u^2(1-u) - \alpha u. \tag{2.39}$$

In population dynamics it describes evolution of a population density. The reproduction term $u^2(1-u)$ is proportional to the square of the density (sexual reproduction) and to available resources $(1-u)$. The last term in the right-hand side describes mortality of the population. In some cases the interaction of the individuals in the population can be nonlocal. This can be for example plants that can distribute their pollen in some area around their location or biological cells which can send signalling molecules stimulating other cells to proliferate. In this case, instead of the reaction-diffusion equation we should consider the integro-differential equation (2.38).

The properties of the reaction-diffusion equation (2.39) are well-known. If $0 < \alpha < 1/4$, then the nonlinearity

$$F(u) = u^2(1-u) - \alpha u$$

has three zeros :

$$w_+ = 0, \quad w_0 = \frac{1}{2} - \sqrt{\frac{1}{4} - \alpha}, \quad w_- = \frac{1}{2} + \sqrt{\frac{1}{4} - \alpha}\,.$$

In this case equation (2.39) has a travelling wave solution, that is solution of the form $u(x,t) = w(x-ct)$, with the limits $w(\pm\infty) = w_\pm$ at infinity. It is unique up to translation in space, and globally stable.

We study the existence of waves for equation (2.38). In the other words, we look for solutions of the problem

$$w'' + cw' + J(w)w(1-w) - \alpha w = 0. \tag{2.40}$$

$$\lim_{x\to\pm\infty} w(x) = w_{\pm}. \tag{2.41}$$

This particular equation represents, for example, cell communitation during the process of haematopoiesis. The main result is stated in the following theorem.

Theorem 2. *There exists a monotone travelling wave, that is a constant* c *and a twice continuously differentiable monotone function* $w(x)$ *satisfying* (2.40)*,* (2.41)*.*

In the case of the scalar reaction-diffusion equation, the proof of the wave existence is simple. It is sufficient to reduce the equation

$$w'' + cw' + F(w) = 0$$

to the system of first order equations and to prove the existence of a heteroclinic trajectory. For obvious reasons, this method is not applicable for the integro-differential equation. The proof becomes much more involved and requires a rather sophisticated mathematical construction. It is based on the Leray-Schauder method which implies the existence of a topological degree for the corresponding operators and a priori estimates solutions.

Topological degree for elliptic operators in unbounded domains is constructed using the properties of Fredholm and proper operators with the zero index [117, 119, 120]. The same construction can be used for the nonlocal reaction-diffusion operators. We discuss this question in Section 9.2. We need to use here weighted spaces. Otherwise the degree may not be defined.

The method to obtain a priori estimates of solutions is similar to the method developed for monotone reaction-diffusion systems [119]. It is based on the maximum principle which appears to be applicable for the equations under consideration. This is an important point which should be emphasised. If the integral enters the nonlinearity in a different way, for example $u(1 - J)$, as it is the case for the nonlocal Fisher equation, then the maximum principle is not applicable. In this case, the properties of the equation become quite different. It possesses an interesting nonlinear dynamics [23, 52] but the wave existence can be proved only in the case of functions ϕ with a small support where the perturbation methods are applicable [9, 10]. Here we do not assume that the support is small. A priori estimates of solutions are proved in Section 9.3.

9.2 Operators, spaces, topological degree

9.2.1 Operators and spaces

We recall that the Leray-Schauder method, which is used here to prove the existence of waves, implies that the topological degree for the corresponding operators is defined. If it is the case, a homotopy of a given operator to some model operator with known properties should be constructed, and a priori estimates of solutions in the process of this deformation of the operator should be obtained.

When we consider unbounded domains, we should use some specially chosen weighted spaces. Otherwise, the degree with the usual properties may not exist. Here we use weighted Hölder spaces $C^{k+\alpha}_{\mu}(\mathbb{R})$ with the norm

$$\|u\|_{C^{k+\alpha}_{\mu}(\mathbb{R})} = \|u\mu\|_{C^{k+\alpha}(\mathbb{R})},$$

where k is a non-negative integer, $0 < \alpha < 1$, $C^{k+\alpha}(\mathbb{R})$ is the usual Hölder space. Parameter α here is different from constant α introduced in (2.38). The weight function $\mu(x)$ has a polynomial growth at infinity. We take $\mu(x) = 1 + x^2$.

Obviously, any function $u \in C^{k+\alpha}_{\mu}(\mathbb{R})$ tends to zero at infinity. On the other hand, we look for solutions of equation (2.40) with the limits (2.41). Therefore, we introduce an infinitely differentiable function $\psi(x)$ such that $\psi(x) = w_+$ for $x \geqslant 1$ and $\psi(x) = w_-$ for $x \leqslant -1$ and put $w = u + \psi$. Hence we can write equation (2.40) in the form

$$(u+\psi)'' + c(u+\psi)' + J(u+\psi)(u+\psi)(1-u-\psi) - \alpha(u+\psi) = 0. \tag{2.42}$$

Consider the operator $A(u)$ corresponding to the left-hand side of the previous equation,

$$A(u) = (u+\psi)'' + c(u+\psi)' + J(u+\psi)(u+\psi)(1-u-\psi) - \alpha(u+\psi) \tag{2.43}$$

and acting in weighted Hölder spaces, $A : C^{2+\alpha}_{\mu}(\mathbb{R}) \to C^{\alpha}_{\mu}(\mathbb{R})$.

9.2.2 Homotopy

In [10] the authors have proved the existence of solutions in the form of monotone travelling waves for a similar integro-differential equation, in which function ϕ had a small support $[-\varepsilon_0, \varepsilon_0]$. In this section we construct a homotopy that relies equation (2.40) to the equation with function ϕ having a small support. Let us introduce a family of operators A_τ : $C^{2+\alpha}_\mu(\mathbb{R}) \times [0,1] \to C^\alpha_\mu(\mathbb{R})$:

$$A_\tau(u) = (u+\psi)'' + c(u+\psi)' + J_\tau(u+\psi)(u+\psi)(1-u-\psi) - \alpha(u+\psi) \tag{2.44}$$

with

$$J_\tau(u) = \int_{-\infty}^{\infty} \phi_\tau(x-y)u(y)dy, \tag{2.45}$$

where

$$\phi_\tau(x) = \frac{(\varepsilon_0 - 1)\tau + 1}{\varepsilon_0}\, \phi\left(\frac{((\varepsilon_0 - 1)\tau + 1)x}{\varepsilon_0}\right). \tag{2.46}$$

We study the following equation,

$$w'' + cw' + J_\tau(w)w(1-w) - \alpha w = 0 \tag{2.47}$$

If $\tau = 0$ then we obtain operator A_0 with function $\phi(x)$, which has a small support, and, thus, the existence of a solution of equation $A_0(u) = 0$ is known [10]. When $\tau = 1$ we obtain equation (2.40).

Linearised near function $u_1(x)$ operator A_τ, introduced in (2.44), is

$$L_\tau u = \lim_{t\to 0} \frac{A_\tau(u_1 + tu) - A_\tau u_1}{t} = u'' + cu' + J_\tau(w_1)(1-2w_1)u + w_1(1-w_1)J_\tau(u) - \alpha u, \tag{2.48}$$

where $w_1 = u_1 + \psi$. Let us introduce limiting operators of operator L,

$$L_{\tau\pm}u = u'' + cu' + w_\pm(1-2w_\pm)u + w_\pm(1-w_\pm)J_\tau(u) - \alpha u. \tag{2.49}$$

Let us recall the definition of a proper operator and of Condition NS.

Definition 3 (Properness)**.** *Operator $A(u) : E_0 \to E$ is proper if intersection of an inverse*

image of a compact set with any bounded closed ball $B \in E_0$ is compact.

Definition 4 (Condition NS)**.** *We say that the operator L satisfies Condition NS if the limiting equations $L_{\pm}u = 0$ do not have nonzero solutions. in $C^{2+\alpha}(\mathbb{R})$.*

Lemma 5 (Schauder estimate)**.** *For any solution u of equation $L_\tau u = f \in C^\alpha(\mathbb{R})$, the following estimate holds :*

$$\|u\|_{C^{2+\alpha}(\mathbb{R})} \leqslant K(\|L_\tau u\|_{C^\alpha(\mathbb{R})} + \|u\|_{C(\mathbb{R})}) \tag{2.50}$$

where K is a constant.

Proof. The proof of this lemma for similar integro-differential operator can be found in [10].

□

9.2.3 Fredholm operator with zero index

We recall that an operator satisfies the Fredholm property if it is normally solvable, its kernel has a finite dimension and the codimension of its image is also finite. Elliptic operators in unbounded domains are normally solvable with a finite dimensional kernel if the Condition NS is satisfied [116]. Invertibility of limiting operators provides the Fredholm property.

The operator L_τ acting from $C^{2+\alpha}(\mathbb{R})$ into $C^\alpha(\mathbb{R})$ satisfies the Fredholm property and has the zero index. The proof of this assertion follows the same lines as for elliptic operators (cf. [10]). We should verify that the Fredholm property remains valid in the weighted spaces, $L_\tau : C^{2+\alpha}_\mu(\mathbb{R}) \to C^\alpha_\mu(\mathbb{R})$, and the index equals zero. From Lemma 2.24 in [119] it follows that it is sufficient to verify that the operator

$$Ku = \mu L_\tau u - L_\tau(\mu u), \quad K : C^{2+\alpha}_\mu(\mathbb{R}) \to C^\alpha(\mathbb{R})$$

is compact. Consider a sequence $\{u_i\}$ such that $\|u_i\|_{C^{2+\alpha}_\mu(\mathbb{R})} \leqslant M$. We should prove that from the sequence $\{Ku_i\}$ we can find a convergent in $C^\alpha(\mathbb{R})$ subsequence. Put $v_i = u_i\mu$. Then $\|v_i\|_{C^{2+\alpha}(\mathbb{R})} \leqslant M$. From the sequence $\{v_i\}$ we can find a subsequence, denoted again by $\{v_i\}$, convergent locally in C^2 to some function v_0. Denote $z_i = v_i - v_0$, then

$$\|Ku_i - Ku_0\|_{C^\alpha(\mathbb{R})} = \|K\frac{z_i}{\mu}\|_{C^\alpha(\mathbb{R})},$$

where $\|z_i\|_{C^{2+\alpha}(\mathbb{R})} \leqslant M_1$, $z_i \to 0$ in C^2 locally. Denote $y_i = K(z_i/\mu)$. We should prove that $\|y_i\|_{C^\alpha} \to 0$. The definition of the operator K gives

$$y_i = \mu L_\tau(z_i/\mu) - L_\tau z_i =$$
$$\left(-z_i\frac{\mu''}{\mu} - 2z_i'\frac{\mu'}{\mu} + 2z_i\left(\frac{\mu'}{\mu}\right)^2 - cz_i\frac{\mu'}{\mu}\right) + w_1(1-w_1)(\mu J(z_i/\mu) - J(z_i)). \tag{2.51}$$

We have

$$\mu J(z_i/\mu) - J(z_i) = \int_{-\infty}^{\infty} \phi(\xi) z_i(x-\xi)\left(\frac{\mu(x)}{\mu(x-\xi)} - 1\right) d\xi.$$

Both terms in the right-hand side of (2.51) uniformly tends to zero at infinity. From this and from the local convergence $z_i \to 0$ in C^2, it follows that y_i converges to zero in $C^\alpha(\mathbb{R})$.

9.2.4 Properness

In this section we show that operator A_τ, defined in (2.44), is proper. First, let us prove the following lemma.

Lemma 6. *For any $u, u_0 \in C^{2+\alpha}_\mu$ and $\tau, \tau_0 \in [0,1]$ the following representation holds*

$$A_\tau(u) - A_{\tau_0}(u_0) = A'_{\tau_0}(u_0)(u-u_0) + \varphi(u, u_0, \tau, \tau_0), \tag{2.52}$$

where $A'_{\tau_0}(u_0)(u-u_0) = L_{\tau_0}(u_0)(u-u_0)$ and

$$\varphi(u, u_0, \tau, \tau_0) = J_\tau(w)w(1-w) - J_{\tau_0}(w)w_0(1-w_0) - J_{\tau_0}(w_0)(1-2w_0)(w-w_0),$$

where $w = u + \psi$ and $w_0 = u_0 + \psi$. Moreover

$$\varphi(u, u_0, \tau_0, \tau_0) = (u-u_0)(J_{\tau_0}(w)(1-w-w_0) - J_{\tau_0}(w_0)(1-2w_0)). \tag{2.53}$$

Proof. Let us denote the difference $A_\tau(u) - A_{\tau_0}(u_0) - L_{\tau_0}(u_0)(u-u_0)$ by $\varphi(u, u_0, \tau, \tau_0)$, then

using (2.44) and (2.48) we obtain

$$\varphi(u,u_0,\tau,\tau_0)=(u-u_0)''+c(u-u_0)'+J_\tau(w)w(1-w)-J_{\tau_0}(w_0)w_0(1-w_0)-\alpha(u-u_0)-$$
$$(u-u_0)''-c(u-u_0)'-J_{\tau_0}(w_0)(1-2w_0)(w-w_0)-w_0(1-w_0)J_{\tau_0}(w-w_0)+\alpha(u-u_0)=$$
$$J_\tau(w)w(1-w)-J_{\tau_0}(w_0)w_0(1-w_0)-J_{\tau_0}(w_0)(1-2w_0)(w-w_0)-w_0(1-w_0)J_{\tau_0}(w-w_0)=$$
$$J_\tau(w)w(1-w)-J_{\tau_0}(w)w_0(1-w_0)-J_{\tau_0}(w_0)(1-2w_0)(w-w_0).$$

Simple transformation of $\varphi(u,u_0,\tau_0,\tau_0)$ gives (2.53). The lemma is proved.

□

Theorem 7 (properness of operator A_τ)**.** *If the operator L_τ, defined in* (2.48)*, satisfies Condition NS, then the operator $A_\tau(u)$, defined in* (2.44)*, is proper with respect to both u and τ.*

Proof. Consider a convergent in $C^\alpha_\mu(\mathbb{R})$ sequence $\{f_n\}\to f_0$ and solutions of the equations

$$A_{\tau_n}(u_n)=f_n \tag{2.54}$$

bounded in $C^{2+\alpha}_\mu(\mathbb{R})\times[0,1]$, $\|u_n\|_{C^{2+\alpha}_\mu(\mathbb{R})}\leqslant M$. We should prove the existence of a subsequence $\{u_{m_n}\}$ that is convergent in $C^{2+\alpha}_\mu(\mathbb{R})$ to a function $u_0\in C^{2+\alpha}_\mu(\mathbb{R})$.

Since $\{u_n\}$ is bounded in $C^{2+\alpha}_\mu(\mathbb{R})$, it admits a subsequence $\{u_{n_m}\}$, which is convergent to a function u_0, uniformly on any bounded interval $I\subset\mathbb{R}$. By diagonalisation process we prolong u_0 to all $\mathbb{R}$. The limit function $u_0\in C^{2+\alpha}_\mu(\mathbb{R})$. Passing to the limit $m\to\infty$ in equation $A_{\tau_{n_m}}(u_{n_m})=f_{n_m}$ we obtain

$$A_{\tau_0}(u_0)=f_0. \tag{2.55}$$

We know that $u_{n_m}\to u_0$ uniformly on any bounded interval I. Let us show that the convergence is uniform with respect to x on the whole axis, $u_{n_m}\to u_0$ in $C(\mathbb{R})$.

Let us write the subscript n instead of n_m and denote

$$v_n=u_n\mu,\quad v_0=u_0\mu,\quad z_n=v_n-v_0,\quad g_n=f_n\mu,\quad g_0=f_0\mu. \tag{2.56}$$

Subtracting (2.55) from (2.54) and multiplying it by μ we obtain

$$(A_{\tau_n}(u_n) - A_{\tau_0}(u_n))\mu + (A_{\tau_0}(u_n) - A_{\tau_0}(u_0))\mu = g_n - g_0. \tag{2.57}$$

Denote

$$r_n = (A_{\tau_n}(u_n) - A_{\tau_0}(u_n))\mu, \tag{2.58}$$

then we have

$$\|r_n\|_{C^\alpha(\mathbb{R})} \to 0, \quad n \to \infty.$$

Injecting (2.56), (2.58), operator definition (2.44) into (2.57) and taking into account Lemma 6 we obtain

$$\begin{aligned} z_n'' + z_n' + J_{\tau_0}(w_0)(1-2w_0)z_n + w_0(1-w_0)J_{\tau_0}(u_n - u_0)\mu - \alpha z_n + \\ \left(-z_n\frac{\mu''}{\mu} - 2z_n'\frac{\mu'}{\mu} + 2z_n\left(\frac{\mu'}{\mu}\right)^2 - cz_n\frac{\mu'}{\mu}\right) + \varphi(u_n, u_0, \tau_0, \tau_0)\mu = g_n - g_0 - r_n. \end{aligned} \tag{2.59}$$

We should prove that there exists a subsequence $\{z_{n_k}\}$ convergent uniformly on the whole axis, $z_{n_k} \to 0$ in $C(\mathbb{R})$. Suppose that it is not true. Then there exists an unbounded sequence $\{x_m\}$, such that $|z_m(x_m)| \geqslant \varepsilon > 0$. Let us introduce shifted functions,

$$\tilde{z}_m(x) = z_m(x + x_m).$$

Since $\|\tilde{z}_m\|_{C^{2+\alpha}(\mathbb{R})} \leqslant M$, from sequence $\{\tilde{z}_m\}$ we can choose a subsequence $\{\tilde{z}_{m_k}(x)\}$ converging to a limiting function $\tilde{z}_0 \in C^{2+\alpha}(\mathbb{R})$ in C^2 uniformly on any bounded interval $I \subset \mathbb{R}$ (the same reasoning as above). We have $|\tilde{z}_0(0)| \geqslant \varepsilon > 0$. Functions $\tilde{z}_{m_k}(x)$ with shifted arguments satisfy equation (2.59). From definition of weight function μ we obtain

$$\frac{\mu'(x + x_m)}{\mu(x + x_m)} \to 0, \quad \frac{\mu''(x + x_m)}{\mu(x + x_m)} \to 0 \quad \text{as} \quad x_m \to \infty.$$

From (2.53) :

$$\varphi(u_m(x+x_m), u_0(x+x_m), \tau_0, \tau_0)\mu =$$
$$\tilde{z}_m(x)(J_{\tau_0}(w_m(x+x_m))(1-w_m(x+x_m)-w_0(x+x_m)) - J_{\tau_0}(w_0(x+x_m))(1-2w_0(x+x_m))).$$

Since $w_0(x+x_m), w_m(x+x_m) \to w_0^{\pm}$ as $m \to \infty$, we obtain that

$$\|\varphi(u_m(x+x_m), u_0(x+x_m), \tau_0, \tau_0)\mu\|_{C^\alpha} \to 0 \quad \text{as} \quad m \to \infty.$$

By definition of g_m and g_0, $\|g_m - g_0\|_{C^\alpha(\mathbb{R})} \to 0$ as $m \to \infty$. In the limit $m \to \infty$, equation (2.59) becomes

$$\widehat{L}\tilde{z}_0 = 0,$$

which means that limiting operator $\widehat{L}$ admits a nonzero solution. This contradicts Condition NS. Thus, convergence $z_m \to 0$ is uniform in $C(\mathbb{R})$. Using this convergence and Schauder estimate (Lemma 5) we obtain convergence $z_m \to 0$ in $C^{2+\alpha}(\mathbb{R})$, which means the convergence $u_m \to u_0$ in $C^{2+\alpha}_\mu(\mathbb{R})$. This completes the proof.

□

9.2.5 Functionalisation of parameter c

We recall that parameter c in (2.40) is an unknown constant that should be found along with function $w(x)$. Note that solutions of (2.40) are invariant with respect to translation, i.e. if $w(x) = u(x) + \psi(x)$ is a solution of (2.40), then $w(x+h) = u(x+h) + \psi(x+h)$ is also a solution of this equation for all $h \in \mathbb{R}$. Then the weighted norm $\|u(x+h)\mu(x)\|_{C^{2+\alpha}}$ tends to infinity as $h \to \pm\infty$. Hence the set of solutions of the equation $A(u) = 0$ is not bounded in the space $C^{2+\alpha}_\mu(\mathbb{R})$, and the topological degree cannot be applied.

To get rid of the invariance of solutions with respect to translation, we apply functionalisation of parameter c first used for travelling waves in [117, 118]. We introduce a functional $c = c(u)$ that satisfies the following properties :

1. $c(u)$ satisfies Lipschitz condition on every bounded set in $C^{2+\alpha}_\mu(\mathbb{R})$ and has a continuous Fréchet derivative,

2. function $\tilde{c}(h) = c(u(x+h))$ is a decreasing function of h, such that $\tilde{c}(-\infty) = +\infty$ and $\tilde{c}(+\infty) = -\infty$,
3. the solution $w = u + \psi$ of equation (2.40) satisfies

$$\langle c'(u), w' \rangle \neq 0.$$

We introduce the following function

$$c(u) = \ln \int_R (u(x) + \psi(x) - w_+)^2 \sigma(x) dx,$$

where $\sigma(x)$ is an increasing function, with $\sigma(-\infty) = 0$, $\sigma(+\infty) = 1$ and

$$\int_{-\infty}^{0} \sigma(x) dx < \infty.$$

The function $c(u)$ introduced in this way satisfies the conditions enumerated above, the proof can be found in [117]. Equation (2.40) is equivalent to the equation

$$(u+\psi)'' + c(u)(u+\psi)' + J(u+\psi)(u+\psi)(1-u-\psi) - \alpha(u+\psi) = 0. \tag{2.60}$$

9.2.6 Construction of topological degree

Consider an operator A acting from a Banach space E into another Banach space F. By definition, topological degree is an integer number $\gamma(A, D)$ which depends on the operator and on the domain D in the function space E. Topological degree for elliptic operators in unbounded domains is constructed in [119, 120] on the basis of the theory of Fredholm and proper operators. The results on the Fredholm property and properness of the integro-differential operators presented above allow us to use the same construction.

One of the main applications of the topological degree is related to the Leray-Schauder method widely used to prove existence of solutions of various problems. We briefly recall the main ideas of this method. If the operator A_τ continuously depends on the parameter τ and

$$A_\tau(u) \neq 0, \quad u \in \partial D, \quad \tau \in [0, 1], \tag{2.61}$$

then the value $\gamma(A_\tau, D)$ of the degree does not depend on τ. This property is called homotopy invariance. If we can reduce the operator $A = A_1$ by a continuous deformation to a model operator A_0 for which $\gamma(A_0, D) \neq 0$ and (2.61) is satisfied, then $\gamma(A, D) \neq 0$. Another property of the degree, nonzero rotation, ensures that the equation $A(u) = 0$ has a solutions in the domain D.

Let us take as a domain D a ball B of the radius R. Then condition (2.61) will be satisfied if all solutions of the equation $A_\tau(u) = 0$ satisfy the inequality $\|u\| \leqslant R$. These are a priori estimates of solutions. They play a crucial role in the proof of the existence of solutions. We discuss them in the next section.

9.3 A priori estimates

A priori estimates of travelling wave solutions have some specific features. We note first of all that they imply not only the estimate of the function $w(x)$ but also of the wave velocity. Moreover, the function $w(x)$ should be estimated in the weighted space. We consider in fact the function $u(x) = w(x) - \psi(x)$ with the zero limits at infinity. It decays exponentially at infinity, so its weighted norm with a polynomial weight is limited. The difficulty is to estimate it "far" from infinity.

To explain the origin of this difficulty, let us consider the following geometrical interpretation. Travelling wave is a heteroclinic trajectory of some first order ordinary differential system of equations. Suppose that this trajectory approaches some intermediate stationary point during the deformation of the system. In the limit we can obtain two heteroclinic trajectories which connect consecutively three stationary points.This situation corresponds to loss of a priori estimates in the weighted space. Thus, we need to prove that the trajectory, which corresponds to the travelling wave, cannot approach intermediate stationary points or other invariant manifolds.

We will follow here the method developed in [117, 118] for monotone reaction-diffusion systems. It consists of two steps. First of all, we separate monotone and non-monotone solutions $w(x)$ of problem (2.40), (2.41). This means that two sequences of solutions, $w_M^j(x)$ and $w_N^j(x)$, where the former are monotone with respect to x and the latter non-monotone, cannot converge in $C^2(\mathbb{R})$ to the same limiting function. This result allows us to deal only with

monotone solutions. At the second step, we obtain a priori estimates of monotone solutions. According to the geometrical interpretation given above, we prove that the trajectory cannot be attracted by an intermediate stationary point. This will follow from the sign of the wave velocity. Here we use the monotonicity of solutions. Otherwise, the intermediate manifold can have a more complex structure, and the method is not applicable.

9.3.1 Monotonicity

In this section we show that monotone solutions of equation (2.47) are strictly monotone. We begin with an auxiliary result on the positiveness of solutions of the linear parabolic equation

$$\frac{\partial v}{\partial t} = \frac{\partial^2 v}{\partial x^2} + a(x,t)J(v) + b(x,t)v \tag{2.62}$$

in $x \in \mathbb{R}$ assuming that $a(x,t)$ and $b(x,t)$ are continuous functions, $a(x,t) \geqslant 0$. We cannot directly use the classical positiveness theorems here because of the integral term in the right-hand side.

Lemma 8. *Suppose that* $a(x,t) + b(x,t) < 0$ *for* $|x| \geqslant N$, $0 \leqslant t \leqslant T$ *with some positive* N *and* T. *If* $v(x,0) \geqslant 0$ *and* $v(x,0) \not\equiv 0$, *then* $v(x,t) > 0$ *for* $0 \leqslant t \leqslant T$.

Proof. Suppose that the assertion of the lemma does not hold. If there exists such (x_0, t_0) that $v(x_0,t_0) = 0,\ v(x,t_0) \geqslant 0$ for all $x \in \mathbb{R}$, and $v(x,t) > 0$ for all $x \in \mathbb{R}$ and $0 < t < t_0$, then we obtain a contradiction with the classical positiveness theorem [48]. Indeed, we can write equation (2.62) in the form

$$\frac{\partial v}{\partial t} = \frac{\partial^2 v}{\partial x^2} + b(x,t)v + c(x,t),$$

where $c(x,t) = a(x,t)J(v) \geqslant 0$ for all x and $0 \leqslant t \leqslant t_0$. Since $v(x,0)$ is non-negative and not identically zero, then $v(x,t_0)$ should be strictly positive.

Otherwise, the solution becomes negative for some $t_1 > 0$. Then there exists such $t_0, 0 \leqslant t_0 \leqslant t_1$ that $v(x,t_0) \geqslant 0$ for all $x \in \mathbb{R}$ and $v(x_k,t_k) < 0$ for some sequences x_k and $t_k > t_0$, $t_k \to t_0$ as $k \to \infty$. If the sequence x_k is bounded, then we can find a convergent subsequence.

Denote its limit by x_0. Then $v(x,t_0) \geqslant 0$ for all x and $v(x_0,t_0) = 0$. As above, we obtain the contradiction with the positiveness theorem.

Hence, the sequence x_k does not have bounded limiting points. Without loss of generality we can assume that $x_k \to +\infty$. For each fixed t we have $v(x,t) \to 0$ as $x \to \infty$. Therefore, the function $v(x,t)$ has a negative minimum that we denote by x_k^m. As before, $x_k^m \to +\infty$.

Let us choose k sufficiently large such that $x_k^m > N$. Put $z = v + \epsilon$ where $\epsilon = |v(x_k^m, t_k)|$. Then z satisfies the equation

$$\frac{\partial z}{\partial t} = \frac{\partial^2 z}{\partial x^2} + a(x,t)J(z) + b(x,t)z - (a(x,t) + b(x,t))\epsilon. \tag{2.63}$$

Moreover, $z(x,t_k) \geqslant 0$ for all x, $0 \leqslant t \leqslant t_k$ and $z(x_k,t_k) = 0$. We obtain a contradiction in signs in the last equation. Indeed, the time derivative at the point $x = x_k, t = t_k$ is non-positive, while all all terms in the right-hand side are non-negative. The last term is strictly positive. The lemma is proved.

□

Lemma 9. *If $w_0(x)$ is a non-constant solution of equation* (2.47) *such that $w_0'(x) \leqslant 0$ for all $x \in \mathbb{R}$, then $w_0'(x) < 0$.*

Proof. Denote $v = -w'$. Differentiating equation (2.47) and taking into account that $J'(w) = J(v)$, we obtain

$$v'' + cv' + a(x)J(v) + b(x)v = 0,$$

where

$$a(x) = w(1-w), \quad b(x) = J(w)(1-2w) - \alpha,$$

$a(x) + b(x) < 0$ for $|x|$ sufficiently large. We should prove that solution of this equation, which satisfies $v \geqslant 0$, is strictly positive. This follows from Lemma 8 if we take function $v(x)$ as initial condition.

□

Lemma 10. *If $w_j(x)$ is a sequence of solutions of problem* (2.47), (2.41) *such that $w_j \to w_0$ in $C^1(\mathbb{R})$, where $w_0'(x) \leqslant 0$, $x \in \mathbb{R}$, then for all j sufficiently large $0 < w_j(x) < 1$ and $w_j'(x) < 0$, $x \in \mathbb{R}$.*

Proof. Let us first prove the inequality $0 < w_j(x) < 1$. The right inequality holds for j sufficiently large because of the uniform convergence $w_j \to w_0$ and $0 < w_0(x) < w_- < 1$. We now verify that $w_j(x)$ is positive for all x. If this is not the case, then each of these functions has a negative minimum x_j. From the uniform convergence $w_j \to w_0$ it follows that $x_j \to +\infty$ and $J(w_j(x_j)) \to 0$. Hence,

$$w_j''(x_j) \geqslant 0, \quad w_j'(x_j) = 0, \quad J(w_j(x_j))(1 - w_j(x_j)) - \alpha < 0, \quad w_j(x_j) < 0.$$

This gives a contradiction in signs in the equation

$$w_j'' + cw_j' + (J(w_j)(1 - w_j) - \alpha)w_j = 0.$$

Next, we prove that the functions w_j are decreasing. Suppose that this assertion does not hold and there exists a sequence x_j such that $w_j'(x_j) = 0$. If it is bounded, then there exists a subsequence converging to some point x_0. Hence $w_0'(x_0) = 0$. We obtain a contradiction with Lemma 9.

Consider now the case where $x_j \to +\infty$. Denote $v = -w'$. Differentiating equation (2.47) and taking into account that $J'(w) = J(v)$, we obtain

$$v'' + cv' + a(x)J(v) + b(x)v = 0,$$

where

$$a(x) = w(1 - w), \quad b(x) = J(w)(1 - 2w) - \alpha.$$

If $v_j(x) \geqslant 0$ for all x, then the existence of x_j such that $v_j(x_j) = 0$ contradicts Lemma 9. Therefore, there exist negative values of this function for each j. On the other hand, from the convergence $w_j' \to w_0'$ it follows that v_j is positive in each given interval for j sufficiently large. Finally, note that $v_j(x) \to 0$ as $x \to \pm\infty$. Hence, there exists a sequence $\hat{x}_j \to \infty$ such that it is a negative minimum of the function $v_j(x)$. The uniform convergence $w_j'(x) \to w_0'(x)$ implies that $v_j(\hat{x}_j) \to 0$ as $j \to \infty$.

Put $\epsilon = v_j(\hat{x}_j)$ for some j sufficiently large and $z(x) = v_j(x) + \epsilon$. Then

$$z'' + cz' + a(x)J(z) + b(x)z - (a(x) + b(x))\epsilon = 0. \tag{2.64}$$

Moreover, $z(x) \geqslant 0$ for $-\infty < x < \infty$, $z(x_j) = 0$. Hence $z''(x_j) \geqslant 0$, $z'(x_j) = 0$, $J(z)(x_j) \geqslant 0$. Since $0 < w_j(x) < 1$, then $a(x_j) > 0$. It remains to note that $a(x_j) + b(x_j) < 0$ for j sufficiently large. Indeed, if $x_j \to +\infty$, then $a(x_j) \to 0$, $b(x_j) \to -\alpha$. If $x_j \to -\infty$, then $a(x_j) \to \alpha$, $b(x_j) \to w_-(1 - 2w_-) - \alpha$, that is

$$a(x_j) + b(x_j) \to w_-(1 - 2w_-) < 0.$$

We obtain a contradiction in signs in equation (2.64). The lemma is proved.

□

9.3.2 Estimates of derivatives

In this section we obtain estimates in $C(-\infty, +\infty)$ of the derivatives $w'(x)$ and $w''(x)$ of the solution $w(x)$ of equation (2.47). We will use the notation $R_2 = \max\limits_{|w| \leqslant R} |J_\tau(w)w(1 - w) - \alpha w|$.

Lemma 11. *Let solution $w(x)$ of equation* (2.47) *satisfy inequality $|w(x)| \leqslant R$ for all x. Then the derivatives $w'(x)$ and $w''(x)$ can be estimated in $C(-\infty, +\infty)$ by a constant, depending only on R and R_2.*

Proof. Let us first obtain an estimate for the first derivative $w'(x)$. We consider two cases, $|c| \geqslant 1$ and $|c| < 1$. Suppose that $|c| \geqslant 1$. The second derivative $w''(x)$ equals zero when $w'(x)$ is at its extremum point, which we denote by x_0. Then from equation (2.47) we obtain

$$|w'(x)| \leqslant |w'(x_0)| \leqslant |J_\tau(w(x_0))w(x_0)(1 - w(x_0)) - \alpha w(x_0))| \leqslant R_2, \quad \forall x \in \mathbb{R}.$$

Suppose now that $|c| < 1$. Consider an interval $[\alpha, \beta]$ where $|w'(x)| \geqslant 1$. Integrating equation (2.47) over the interval $[\alpha, x]$, we obtain

$$w'(x) - w'(\alpha) + c(w(x) - w(\alpha)) + \int\limits_\alpha^x (J_\tau(w(x))w(x)(1 - w(x)) - \alpha w(x))dx = 0.$$

This provides

$$|w'(x)| \leqslant 1 + |c||w(x) - w(\alpha)| + R_2(\beta - \alpha) \leqslant 1 + 2R + R_2(\beta - \alpha).$$

The mean-value theorem gives

$$|w(\beta) - w(\alpha)| = |w'(x_0)|(\beta - \alpha) \geqslant (\beta - \alpha),$$

which provides that $\beta - \alpha \leqslant 2R$ and thus finally we obtain

$$|w'(x)| \leqslant 1 + 2R + 2R\,R_2.$$

So we have estimated the first derivative of the function $w(x)$. Let us now estimate the second derivative. From equation (2.47) we obtain

$$|w''(x)| \leqslant |cw'(x)| + R_2.$$

The first term in the right-hand side has its maximum when $w'(x)$ reaches its extremum, that is $w''(x) = 0$ at this point. Therefore, from equation (2.47)

$$|cw'(x)| \leqslant R_2.$$

Hence

$$|w''(x)| \leqslant 2R_2,$$

which completes the proof of the lemma.

□

9.3.3 A priori estimates of the speed

In this section we obtain a priori estimates of the speed c of monotone waves. Suppose that there exists a solution $w(x)$ of equation (2.40) for some $c = c_0$ with the limits (2.41) at infinity.

Let us estimate the value c_0 of the speed. For this purpose we consider the evolution equation

$$\frac{\partial u}{\partial t} = \frac{\partial^2 u}{\partial x^2} + c_0 \frac{\partial u}{\partial x} + J(u)u(1-u) - \alpha u. \tag{2.65}$$

So that $w(x)$ is a stationary solution of this equation. Let $u(x,t)$ be a solution of equation (2.65) and $v = u - w_0$, where $w_0 < 1/2$ satisfies $w_0(1-w_0) = \alpha$. Then v satisfies the equation

$$\frac{\partial v}{\partial t} = \frac{\partial^2 v}{\partial x^2} + c_0 \frac{\partial v}{\partial x} + J(v)(1-w_0)u - J(u)uv. \tag{2.66}$$

Suppose that $0 < u < 1$ and $v > 0$. Then

$$J(v)(1-w_0)u - J(u)uv \leqslant J(v). \tag{2.67}$$

Next, consider the equation

$$\frac{\partial z}{\partial t} = \frac{\partial^2 z}{\partial x^2} + c_0 \frac{\partial z}{\partial x} + J_\eta(z), \tag{2.68}$$

where

$$J_\eta(z) = \int_{-\infty}^{\infty} \eta(x-y)z(y,t)dy,$$

$\eta(x)$ is a piece-wise constant function equal $M = \sup_x \phi(x)$ in the support of the function $\phi(x)$ and zero otherwise. Let the support of the function $\eta(x)$ be $[-N, N]$. Let us look for a solution of the equation

$$w'' + cw' + J_\eta(w) = 0 \tag{2.69}$$

for some c possibly different from c_0 in the form of the exponential $w(x) = e^{-\lambda x}$. We obtain

$$\lambda^2 - c\lambda + \frac{M}{\lambda}\left(e^{\lambda N} - e^{-\lambda N}\right) = 0.$$

For any M and N, if c is sufficiently large, then this equation has a solution λ. Let us take these values of c and λ and consider the corresponding solution $w(x)$ of equation (2.69). Then $z(x,t) = w(x - (c-c_0)t)$ is a solution of equation (2.68), which has a constant profile and moves to the right with the speed $(c - c_0)$. The function $\hat{u}(x,t) = z(x,t) + w_0$ satisfies the

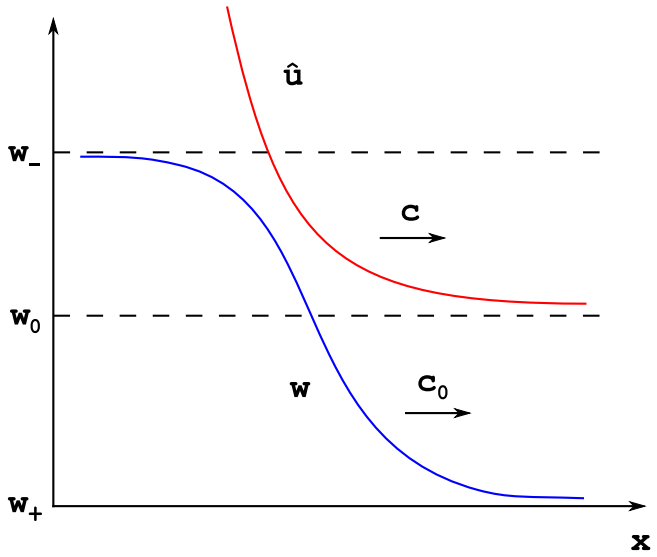

FIGURE 28 – The estimate of the speed of the travelling wave solution of equation (2.38). The wave w propagates with the speed c_0, the solution $\hat{u}$ with the speed c. The wave remains below the solution. If it touches it, this will contradict the comparison of solutions. Hence $c > c_0$.

equation

$$\frac{\partial \hat{u}}{\partial t} = \frac{\partial^2 \hat{u}}{\partial x^2} + c_0 \frac{\partial \hat{u}}{\partial x} + J_\eta(\hat{u} - u_0) \tag{2.70}$$

Let us now compare the solution $u(x,t)$ of equation (2.65) and the solution $\hat{u}(x,t)$ of equation (2.70) (Figure 1). We recall that $u(x,t) \to w_\pm$ as $x \to \pm\infty$ for each $t \geqslant 0$ and $\hat{u}(x,t)$ is a strictly decreasing function converging to w_0 as $x \to +\infty$ and exponentially growing at $-\infty$. Hence, we can choose a constant h such that $u(x,0) < \hat{u}(x-h,0)$ for all $x \in \mathbb{R}$. We are going to prove that $u(x,t) < \hat{u}(x-h,t)$ for all $x \in \mathbb{R}$ and $t \geqslant 0$. Suppose that this is not true. Then there exists $t_0 > 0$ such that $u(x,t_0) \leqslant \hat{u}(x-h,t_0)$ for all $x \in \mathbb{R}$ and $u(x_0,t_0) = \hat{u}(x_0-h,t_0)$ for some x_0. Since $\hat{u}(x_0-h,t_0) > w_0$, then $v(x_0,t_0) > 0$. This inequality holds in some neighborhood $\delta(x_0)$ of $x = x_0$. Moreover, $0 < u(x,t) < 1$, $J(u) > 0$. Hence, by virtue of (2.67),

$$J(u)u(1-u)-\alpha u = J(v)(1-w_0)u - J(u)uv \leqslant J(v) = J(u-w_0) \leqslant J_\eta(\hat{u}-w_0), \quad x \in \delta(x_0).$$

We obtain a contradiction with the positiveness theorem. Thus, if there exists a stationary solution $w(x)$ of equation (2.65), then we put $u(x,0) = w(x)$ and obtain $w(x) \equiv u(x,t) < \hat{u}(x,t)$.

Therefore, $c_0 < c$, where c is the value of the speed chosen above.

In order to estimate the speed c from below, we repeat a similar construction with a solution $w(x)$ such that $w(x) \to w_0$ as $x \to \infty$ and exponentially decreasing as $x \to +\infty$. It propagates to the left with a certain speed $(c - c_0)$. We thus have proved the following theorem.

Theorem 12. *For any arbitrary solution (c, w) of problem* (2.47), (2.41)*, where $w(x)$ is monotonically decreasing function, there exists an estimate of the speed c independent of τ.*

9.3.4 Sign of the speed

In this section we consider behaviour of solutions of equation (2.47) as $x \to \pm\infty$. The subscript τ is omitted. We prove that the waves connecting a stable point with an unstable point can exist only with the speed of a certain sign. This will be used below in order to obtain a priori estimates of solutions. We begin with an auxiliary result.

Lemma 13. *Suppose that $v(x)$ is a decreasing positive function, $\phi(x)$ is even and non-negative. Then for any N*

$$\int_N^\infty dx \int_{-\infty}^\infty \phi(x-y)v(y)dy \geqslant \int_N^\infty dx \int_{-\infty}^\infty \phi(x-y)v(x)dy. \tag{2.71}$$

If v is a positive and increasing function, then

$$\int_{-\infty}^N dx \int_{-\infty}^\infty \phi(x-y)v(y)dy \geqslant \int_{-\infty}^N dx \int_{-\infty}^\infty \phi(x-y)v(x)dy. \tag{2.72}$$

It is assumed that all these integrals exist.

Proof. We have

$$\int_N^\infty dx \int_N^\infty \phi(x-y)v(y)dy = \int_N^\infty dx \int_N^\infty \phi(x-y)v(x)dy.$$

If v is decreasing, then

$$\int_N^\infty dx \int_{-\infty}^N \phi(x-y)v(y)dy \geqslant \int_N^\infty dx \int_{-\infty}^N \phi(x-y)v(x)dy$$

since $y \leqslant N \leqslant x$ in the domain of integration and, consequently, $v(y) \geqslant v(N) \geqslant v(x)$. Taking a sum of the last two relations, we obtain (2.71).

Consider now the second case. From the equality

$$\int_{-\infty}^{N} dx \int_{-\infty}^{N} \phi(x-y)v(y)dy = \int_{-\infty}^{N} dx \int_{-\infty}^{N} \phi(x-y)v(x)dy$$

and inequality

$$\int_{-\infty}^{N} dx \int_{N}^{\infty} \phi(x-y)v(y)dy \geqslant \int_{-\infty}^{N} dx \int_{N}^{\infty} \phi(x-y)v(x)dy,$$

which takes place since in the domain of integration $x \leqslant N \leqslant y$ and $v(x) \leqslant v(N) \leqslant v(y)$, we obtain (2.72). The lemma is proved.

□

Let $w_0 < 1/2$ be a solution of the equation $u(1-u) = \alpha$. Suppose that there exists a decreasing solution $u(x)$ of equation (2.47) such that $u(x) \to w_0$ as $x \to +\infty$. Put $u(x) = w_0 + v(x)$. Then

$$v'' + cv' + (J(v)(1-w_0) - (w_0 + J(v))v)(w_0 + v) = 0. \tag{2.73}$$

Consider first the linear equation

$$v'' + cv' + (J(v)(1-w_0) - w_0 v)w_0 = 0 \tag{2.74}$$

and integrate it from N to $+\infty$:

$$-v'(N) - cv(N) + I_+(N) = 0, \tag{2.75}$$

where

$$I_+(N) = w_0(1-w_0) \int_{N}^{\infty} dx \int_{-\infty}^{\infty} \phi(x-y)v(y)dy - w_0^2 \int_{N}^{\infty} dx \int_{-\infty}^{\infty} \phi(x-y)v(x)dy.$$

Since $1 - w_0 > w_0$, then by virtue of Lemma 13, $I_+(N) > 0$ for any N. We recall that $v(x)$ is

positive and decreasing. Therefore, equality (2.75) can take place only if $c > 0$.

The corresponding integral remains positive for equation (2.73) since $J(v) \to 0$ as $x \to +\infty$ and for any $\epsilon > 0$, $w_0 + J(v) \leqslant w_0 + \epsilon$, $x \geqslant N$ for N sufficiently large. Therefore, integrating (2.73), we obtain, as before, that $c > 0$.

Suppose now that there exists a decreasing solution $u(x)$ of equation (2.47) such that $u(x) \to w_0$ as $x \to -\infty$. Put $v(x) = w_0 - u(x)$. Then $v(x)$ is a positive increasing function. As above, we obtain equation (2.74). Integrating it from $-\infty$ to N, we obtain

$$v'(N) + cv(N) + I_-(N) = 0, \tag{2.76}$$

where

$$I_-(N) = w_0(1 - w_0) \int_{-\infty}^{N} dx \int_{-\infty}^{\infty} \phi(x - y)v(y)dy - w_0^2 \int_{-\infty}^{N} dx \int_{-\infty}^{\infty} \phi(x - y)v(x)dy.$$

It follows from (2.72) that $I_-(N) \geqslant 0$. Then from (2.76), $c < 0$. Thus, we have proved the following lemma.

Lemma 14. *If there exists a decreasing solution of equation (2.47) with the limits* $w(-\infty) = w_-$, $w(+\infty) = w_0$, *then* $c > 0$. *If such solution has the limits* $w(-\infty) = w_0$, $w(+\infty) = w_+$, *then* $c < 0$.

9.3.5 A priori estimates of solutions

In this section we obtain a priori estimates of monotone solutions of equation (2.47) with conditions (2.41). We begin with the lemma which states exponential behaviour of solutions at infinity.

Lemma 15. *There exists a constant* $\varepsilon > 0$ *such that the following estimates of monotone solutions* $w_\tau(x)$ *of problem* (2.47), (2.41) *hold*

$$|w_\tau(x) - w_+| \leqslant Ke^{-ax} \tag{2.77}$$

for such x *that* $|w_\tau(x) - w_+| \leqslant \varepsilon$, *and*

$$|w_\tau(x) - w_-| \leqslant Ke^{-bx} \tag{2.78}$$

for such x *that* $|w_\tau(x) - w_-| \leqslant \varepsilon$. *Moreover, constants* $K > 0, a > 0$ *and* $b > 0$ *are independent of* τ *and of solution* $w_\tau(x)$.

Proof. Consider first behavior of solutions of equation (2.47) as $x \to \infty$. Since $w_\tau \to w_+ = 0$, and it is monotonically decreasing, then for sufficiently large x we can estimate the integral $J_\tau(w)$ by a small constant $\beta > 0$ such that $\beta < \alpha$,

$$J_\tau(w(x)) \leqslant \beta, \quad \forall x > x_0,$$

which provides

$$J_\tau(w(x))w(x)(1 - w(x)) - \alpha w(x) \leqslant (\beta - \alpha)w(x), \quad \forall x > x_0.$$

We can now compare solutions of equation (2.47) with the equation

$$v'' + cv' + (\beta - \alpha)v = 0, \quad \beta < \alpha$$

Exponential behaviour of solutions of this equation is well known. It remains to prove that monotone solutions $w(x)$ of equation (2.47) can be majorated by solutions $v(x)$ of the previous equation, i.e.

$$w(x) \leqslant v(x), \quad \forall x > x_0. \tag{2.79}$$

To do so, consider the difference $z(x) = v(x) - w(x)$. It satisfies the following equation :

$$z'' + cz' + (\beta - \alpha)z + ((\beta - \alpha)w - J_\tau(w)w(1 - w) - \alpha w) = 0.$$

It can be rewritten as

$$z'' + cz' + (\beta - \alpha)z + g(x) = 0, \tag{2.80}$$

where $g(x) \geqslant 0$ for all $x > x_0$. Consider this equation on the half-axis $[x_0, +\infty)$ with the boundary conditions $z(x_0) = 0$ and $z(x_0) \to 0$ as $x \to 0$. If we prove that solutions of this problem satisfy $z(x) \geqslant 0$ for all $x \geqslant x_0$, then estimate (2.79) will be proved. Let us assume that this is not true. Hence $z(x)$ has negative values. Since it converges to zero at infinity, then there exists a point $x_2 > x_0$ where the function $z(x)$ attains its negative minimum. At this point we have $z''(x_2) \geqslant 0, z'(x_2) = 0, (\beta - \alpha)z(x_2) > 0$ and $g(x_2) > 0$. We obtain a contradiction in signs in equation (2.80). Estimate (2.77) follows from (2.79). Estimate (2.78) can be proved in a similar way.

□

Lemma 16. *There exists a constant $\chi > 0$ such that outside of the ε-neighbourhoods of the points w_+ and w_- the following estimate holds $|w'_\tau(x)| \geqslant \chi$ for arbitrary monotone solution $w_\tau(x)$ of the problem* (2.47), (2.41). *Constant χ is independent of the parameter τ and of solution $w_\tau(x)$, constant ε is defined in Lemma 15.*

Proof. Let us assume that the assertion of the lemma does not hold. Then there exist sequences $\{\tau_k\}, \{w_{\tau_k}\}, \{x_k\}$ such that $w'_{\tau_k}(x_k) \to 0$ and points x_k do not belong to ε-neighbourhoods of points w_- and w_+. We can assume that $\tau_k \to \tau_0$ and $c_k \to c_0$, where $\tau_0 \in [0, 1]$, c_0 is a constant, and c_k is the speed of the wave w_{τ_k}.

Since solutions of equation (2.47) are invariant relative to translation with respect to x, we can assume that $|w_{\tau_k}(0) - w_-| = \varepsilon$. We can also assume that the sequences $\{w_{\tau_k}(0)\}$ and $\{w'_{\tau_k}(0)\}$ are convergent with limits y and z, respectively. Denote by $v^{(1)}(x)$ the solution of equation (2.47) for $c = c_0, \tau = \tau_0$ with initial conditions $v^{(1)}(0) = y, v^{(1)\prime}(0) = z$. It is clear that $v^{(1)}(x) \to w_-$ as $x \to -\infty$.

Let us suppose that $v^{(1)}(x) \to w_+$ as $x \to \infty$. Then, outside of the ε-neighbourhoods of the points w_-, w_+, function $v^{(1)}(x)$ exists on a finite interval with respect to x. Since solutions $w_{\tau_k}(x)$ converge to $v^{(1)}(x)$, then, for some $x = x_0$, we have $v^{(1)\prime}(x_0) = 0$, and the point $v^{(1)}(x_0)$ lies outside the ε-neighbourhoods of the points w_-, w_+. This contradicts Lemma 9. Thus $v^{(1)}(x)$ is a monotone (not necessarily strict) function not tending towards w_+. Then $v^{(1)}(x)$ tends to w_0 as $x \to \infty$, where w_0 is such that $w_0(1 - w_0) - \alpha = 0$.

In a similar way we may prove existence of function $v^{(2)}(x)$ having limits w_0 as $x \to -\infty$

and w_+ as $x \to \infty$. Thus we have simultaneously two solutions of equation (2.47) with the same wave speed $c = c_0$. This contradicts Lemma 14, which completes the proof of the lemma.

□

Lemma 17. *Let $\mathfrak{M}_r$ $(r \geqslant 0)$ be the set of all monotone solutions of problem* (2.47),(2.41) *for all τ such that for x_0 defined by*

$$w_\tau(x_0) = w_0$$

holds the estimation $|x_0| \leqslant r$. Then there exists such a constant M_r that for all $w \in \mathfrak{M}_r$ the following estimate holds,

$$\|w - \psi\|_{C_\mu^{2+\alpha}(\mathbb{R})} \leqslant M_r. \tag{2.81}$$

Proof. Let w be from $\mathfrak{M}_r$ and points x_1 and x_2 be defined by the equalities

$$|w(x_1) - w_-| = \varepsilon, \quad |w(x_2) - w_+| = \varepsilon,$$

where the constant ε is defined in Lemma 15, $\varepsilon < w_0$. Then

$$x_1 < x_0 < x_2, \quad |x_0| \leqslant r. \tag{2.82}$$

Let χ be the constant in the estimate of $w'(x)$, presented in Lemma 16. Then

$$0 < x_2 - x_1 < (w_- - w_+)/\chi := N. \tag{2.83}$$

We suppose that $\chi < 1$. From (2.82) and (2.83) we obtain that

$$|x_1| \leqslant N + r, \quad |x_2| \leqslant N + r.$$

From Lemma 15 we conclude that solutions $w(x)$ approach $\psi(x)$ exponentially outside the interval $[x_1, x_2]$. Thus we conclude that

$$\|w - \psi\|_{C_\mu^{2+\alpha}(\mathbb{R})} = \|w - \psi\|_{C_\mu^{2+\alpha}([x_1,x_2])}.$$

This norm, in turn, is

$$\|w-\psi\|_{C^{2+\alpha}_{\mu}([x_1,x_2])} = \|(w-\psi)\mu\|_{C^{2+\alpha}([x_1,x_2])}.$$

The estimate of the norm in the right-hand side follows from the estimate of the Hölder norm of the functions w and μ. The former follows from Lemma 11 for the function itself and its first two derivative. The norm C^{α} of the second derivative can be obtained from the equation. The estimate of the Hölder norm of μ follows from the boundedness of the interval.

□

Proposition 18. *Consider the homotopy defined in Section 9.2.2 and the equation*

$$w'' + cw' + J_{\tau}(w)w(1-w) - \alpha w = 0, \qquad (\tau \in [0,1]).$$

1) The following estimate holds for all monotone solutions $w(x)$ of problem (2.47)*,* (2.41)*,*

$$\|w-\psi\|_{C^{2+\alpha}_{\mu}} \leqslant R,$$

where $R > 0$ is some constant.

2) For some $r > 0$ we have the estimate

$$\|w_M - w_N\|_{C^{2+\alpha}_{\mu}} \geqslant r,$$

where w_M and w_N are, respectively, an arbitrary monotone and a nonmonotone solution of problem (2.47)*,* (2.41)*.*

Proof. Up to now we considered c as a constant, now we consider it as a functional $c(u)$ introduced previously, $u(x) = w(x) - \psi(x)$. Let us denote the solution of equation $w(x) = w_0$ by x_0 and prove that there exists a constant $r > 0$ such that $|x_0| < r$ for all monotone solutions of our problem and for all $\tau \in [0,1]$. Let us assume the contrary. Then there exists a sequence $\{x_k\}$ such that $|x_k| \to \infty$ with $k \to \infty$ and a sequence of solutions $\{w_k(x)\}$ with $c = c(u_k)$,

$u_k(x) = w_k(x) - \psi(x)$ are such that $w_k(x_k) = w_0$. Let

$$v_k(x) = w_k(x + x_k) - \psi(x),$$

so that $v_k + \psi \in \mathfrak{M}_0$ (see Lemma 17), and, thus, we have the estimate

$$\|v_k\|_{C^{2+\alpha}_\mu} \leqslant M_0.$$

From functionalisation of parameter c we have

$$\rho(u) = \left(\int_R (u(x) + \psi(x) - w^+)^2 \sigma(x) dx \right)^{1/2},$$

which provides

$$\rho(u_k) = \left(\int_R (v_k(x) + \psi(x) - w^+)^2 \sigma(x + x_k) dx \right)^{1/2}.$$

Further we show that $c(u_k) = \ln \rho(u_k)$ is unbounded, which leads to a contradiction with the a priori estimates of the speed obtained in Section 9.3.3. When $x_k \to \infty$, $\sigma(x + x_k) \to 1$ and $|v_k| \to 0$. Function $\psi(x)$ is different from w_+ when $-x$ is big, thus $\rho(x_k) \to \infty$ as $x_k \to \infty$. We should consider as well the case when $x_k \to -\infty$. From the definition of the norm in Hölder spaces we obtain that $|v_k(x)| \leqslant N(\mu(x))^{1/2}$. Thus there exists square summarible function $y(x)$ such that $|v_k(x)| < y(x)$. This allows the conclusion that $\rho(u_k) \to 0$ as $x_k \to -\infty$.

Thus we have shown that all monotone solutions of problem (2.47),(2.41), in which $c = c(u)$, belong to $\mathfrak{M}_r$ for some $r > 0$ and validity of the first part of the proposition follows from Lemma 17.

Let us now prove the second part of the proposition. Introduce the notation,

$$u_M = w_M - \psi, \qquad u_N = w_N + \psi.$$

Assume that the assertion of the second part of the proposition does not hold. We can then find

sequences of solutions of equation (2.47) $\{u_M^{(k)}\}$ and $\{u_N^{(k)}\}$ such that

$$\|u_M^{(k)} - u_N^{(k)}\|_{C_\mu^{2+\alpha}} \xrightarrow[k\to\infty]{} 0. \tag{2.84}$$

Since all the functions $u_M^{(k)}$ are in the ball of radius R of the space $C_\mu^{2+\alpha}(\mathbb{R})$, we obtain the strong convergence of $\{u_M^{(k)}\}$ to some $u_M^{(0)}$,

$$\|u_M^{(k)} - u_M^{(0)}\|_{C^2} \xrightarrow[k\to\infty]{} 0$$

We let $w^{(0)} = u_M^{(0)} + \psi$. Then function $w^{(0)}$ is a solution of problem (2.47),(2.41) for some τ and c and

$$\|w_M^{(k)} - w^{(0)}\|_{C^2} \xrightarrow[k\to\infty]{} 0 \tag{2.85}$$

Then from (2.84) and (2.85) we have

$$\|w_N^{(k)} - w^{(0)}\|_{C^2} \xrightarrow[k\to\infty]{} 0 \tag{2.86}$$

Applying Lemma 10 to sequence $\{w_N^{(k)}\}$ we obtain a contradiction, which completes the proof of the proposition.

□

Consider a ball $\|u\|_{C_\mu^{2+\alpha}} \leqslant R$ of space $C_\mu^{2+\alpha}(\mathbb{R})$, in which all solutions of equation (2.47) are contained. We set $R_1 = R+1$ and select $r, 0 < r < 1$, such that for solutions of equation (2.47) in the ball $\|u\|_{C_\mu^{2+\alpha}} \leqslant R_1$ we have the inequality

$$\|w_M - w_N\|_{C_\mu^{2+\alpha}} \geqslant r.$$

In Theorem 7 we have proved that operator $A_\tau(u)$ is proper with respect to both τ and u. This means that the set of solutions of equation $A_\tau(u) = 0$ is compact in the ball $\|u\|_{C_\mu^{2+\alpha}} \leqslant R_1$. For a fixed solution $u_M(x)$ we construct the ball $K(u_M)$ of radius r and center at the point u_M. By virtue of compactness of the set of solutions u_M, we can select from a covering of this set by balls $K(u_M)$ a finite subcovering. We denote by $G_k, k = 1, \ldots, N$, the set of domains formed by the union of the balls from this subcovering, Γ_k are boundaries of these domains.

It is obvious that any $u_N \notin \bigcup_{k=1}^{N}[G_k + \Gamma_k]$ and all solutions u_M belong to $\bigcup_{k=1}^{N} G_k$ for all $\tau \in [0,1]$. We thus have separated all monotone solutions from all nonmonotone solutions, which allows us to prove the main result of this work stated in Theorem 2.

Proof. Consider the homotopy (2.45)-(2.47). As it is shown in Section 9.2, the topological degree can be introduced for the operator A_τ. By virtue of a priori estimates obtained in this section we can use the Leray-Schauder method. As shown in [10], equation (2.47) with conditions (2.41) has a solution in the form of monotone travelling wave when $\tau = 0$. Thus topological degree for the operator $A_\tau(u)$, introduced in (2.44), equals 1 for $\tau = 0$. Consequently, the topological degree for operator A_1, corresponding to the initial equation (2.40) also equals 1, whence the existence of a solution follows.

□

Troisième partie

Individual Based Modelling Approach

Cell-to-cell communications are very important for the erythropoiesis regulation. One of the appropriate approaches that allows taking into account this communication is the individual based modelling. This considers each cell as an independent element of the whole system and, thus, allows considering communications of every single cell with its neighbours that can provide additional insights into the behaviour of cell populations.

In Section 10 a multi-agent software that describes such a communication is presented. It allows us to numerically study spatial distribution of erythroid progenitors in the bone marrow, see Section 11. Using this software we demonstrate that cell division can generate random cell motion (Section 12). Random cell motion, in turn, can be described by a diffusion term when dealing with continuous models.

10 Description of "Cell Dynamics" software

"Cell Dynamics" is an original software developed by N. Bessonov [21]. Several versions of the software are available. In this section some features of version *BC.v27c,* which was released in spring 2009, are presented. The software can be used to study various types of cell-to-cell interactions. For instance, cell interactions that occur in the bone marrow during haematopoiesis.

10.1 User interface

In Figure 29 the main window of the application is shown. It consists of the plot area and several buttons. The plot area is a domain of calculation, cells that leave this domain are removed from the calculation. Several buttons of the interface are used to set up model parameters. Panels presented in Figure 30 are accessible through the button "Tree". An example can be saved or opened using the menu "File". The button "Data" allows to define some parameters determining cell-to-cell interaction. In the current version only mechanical interaction is taken into account. Note that this version does not take into account the exchange of chemical signals. Button "Output" allows to determine a representation of output results. Other buttons are interface related and ease the usage of the software.

Panels presented in Figure 30 are used to define domain settings and cell types. Domain dimensions are defined in Panel A. Button "Create" creates the domain. To restart calculation,

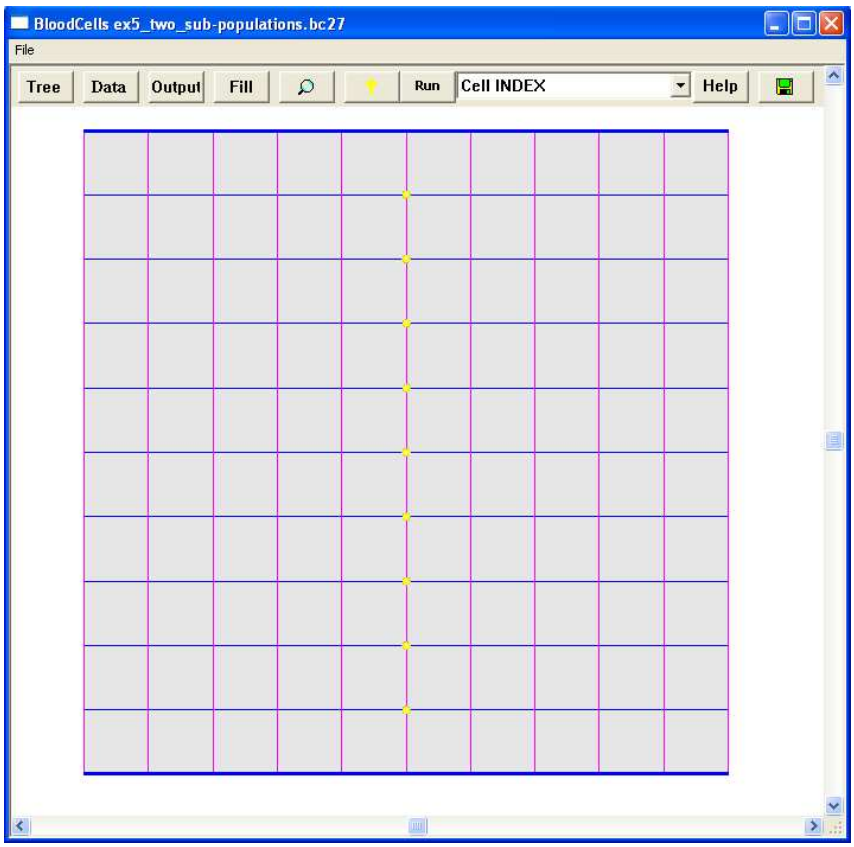

FIGURE 29 – Software description. Main window.

A B C

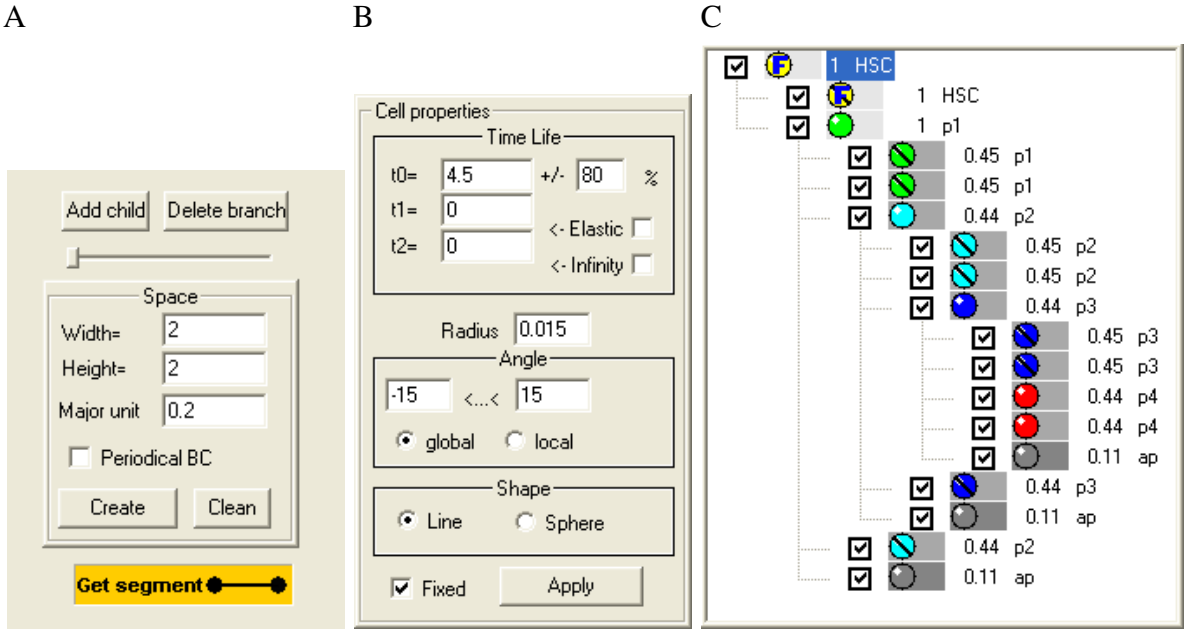

FIGURE 30 – Software description. The genealogical tree.

all current cells and segments can be removed using button "Clean". "Get segment" button allows to create obstacles in the domain, which cells cannot overpass. For example, in Figure 29 the top and bottom borders of the calculation area are such obstacles. This option can also be used to model fibres of the bone marrow, which represent obstacles for cell motion. Several cell types (generations), describing maturation process are defined in Panel C. Lifetime of cells is defined in Panel B, edit-box "t_0" defines average lifetime, edit-box "+/-" defines an interval of stochasticity. The Panel C shows genealogical tree of cell generations. Letter "F" means that cells of this type are fixed and do not move. A user can choose a color and a name for every cell type. At the end of the cell cycle the cell makes a choice, which is described in the tree. Let us explain how this tree is organised. Cells of type "p3" (Figure 30.C, blue discs) are produced by cells of type "p2". In turn, a "p3" cell produces two daughter "p3" cells with probability 0.45 (self-renewal), two daughter cells of type "p4" with probability 0.44 (differentiation) and with probability 0.11 one cell of type "ap". Cells of type "ap", which do not have children, are used to model apoptosis, i.e. a "p3" cell produces an apoptotic cell that will die at the end of its cell cycle with probability 0.11. Cell type "HSC" models haematopoietic stem cells. A cell of this type gives birth to two daughter cells, one of the same type as mother cell, which replaces it, and one cell of another type (an immature progenitor).

Cells push each other out of the domain that results in the cell motion. Stochastic cell division results in homogeneous diffusion. This aspect is discussed in detail in Section 12.

An example of simulation can be found in Figure 31. Panel A represents configuration of the plot area and stem cells inside (yellow discs in the middle) before starting the calculation. Panel B shows the computational domain after some time. Stem cells (yellow discs) are fixed and do not move. They give birth to their offsprings. The offsprings, in turn, proliferate and move. After some time the domain is partially filled with cells of different types as shown in Panel B.

The software can be used as well to model the appearance of malignant cells and their propagation. This is demonstrated in Figures 32 and 33. The probability of appearance of malignant cells (yellow) is small, equals 0.001 (Figure 32), which models a rare genetic mutation. Once such a cell appears, it proliferates and, if it survives producing enough daughter cells, then malignant cells propagate and finally fill the whole domain. Such application of the software can

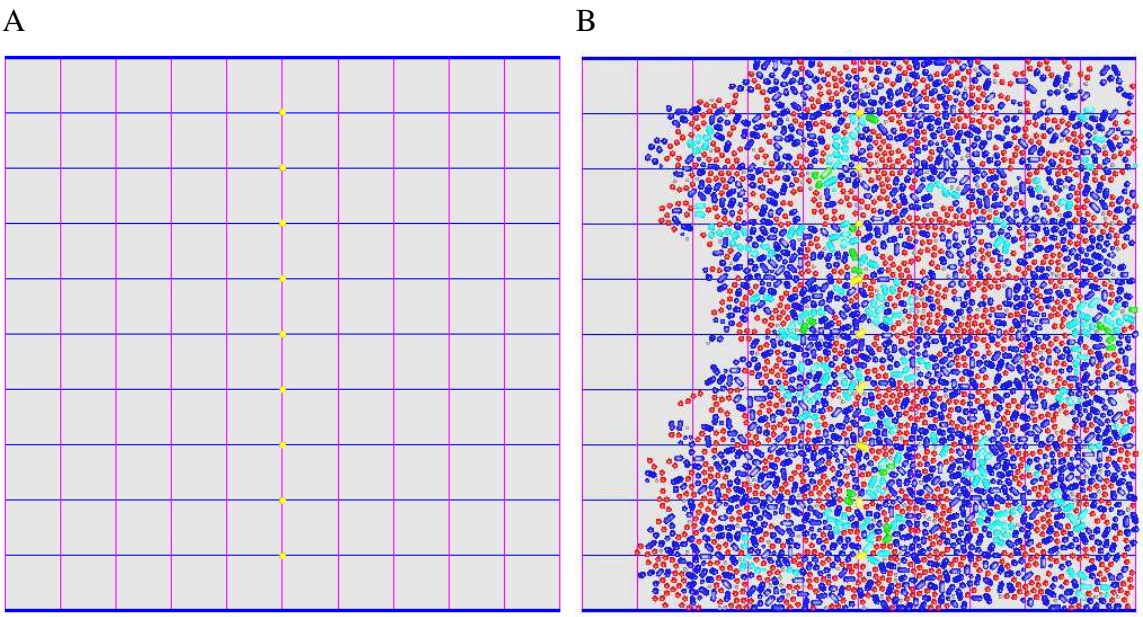

FIGURE 31 – Software description. An example of simulation.

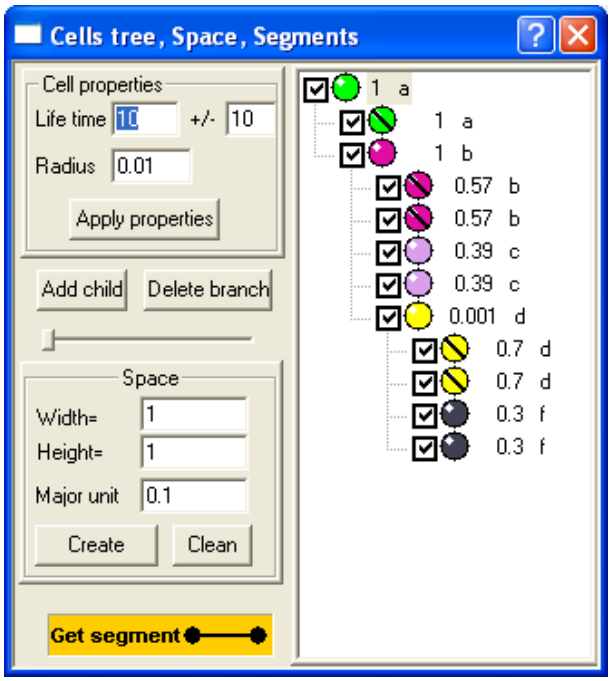

FIGURE 32 – Demonstration of the software. Propagation of malignant cells. Genealogical tree.

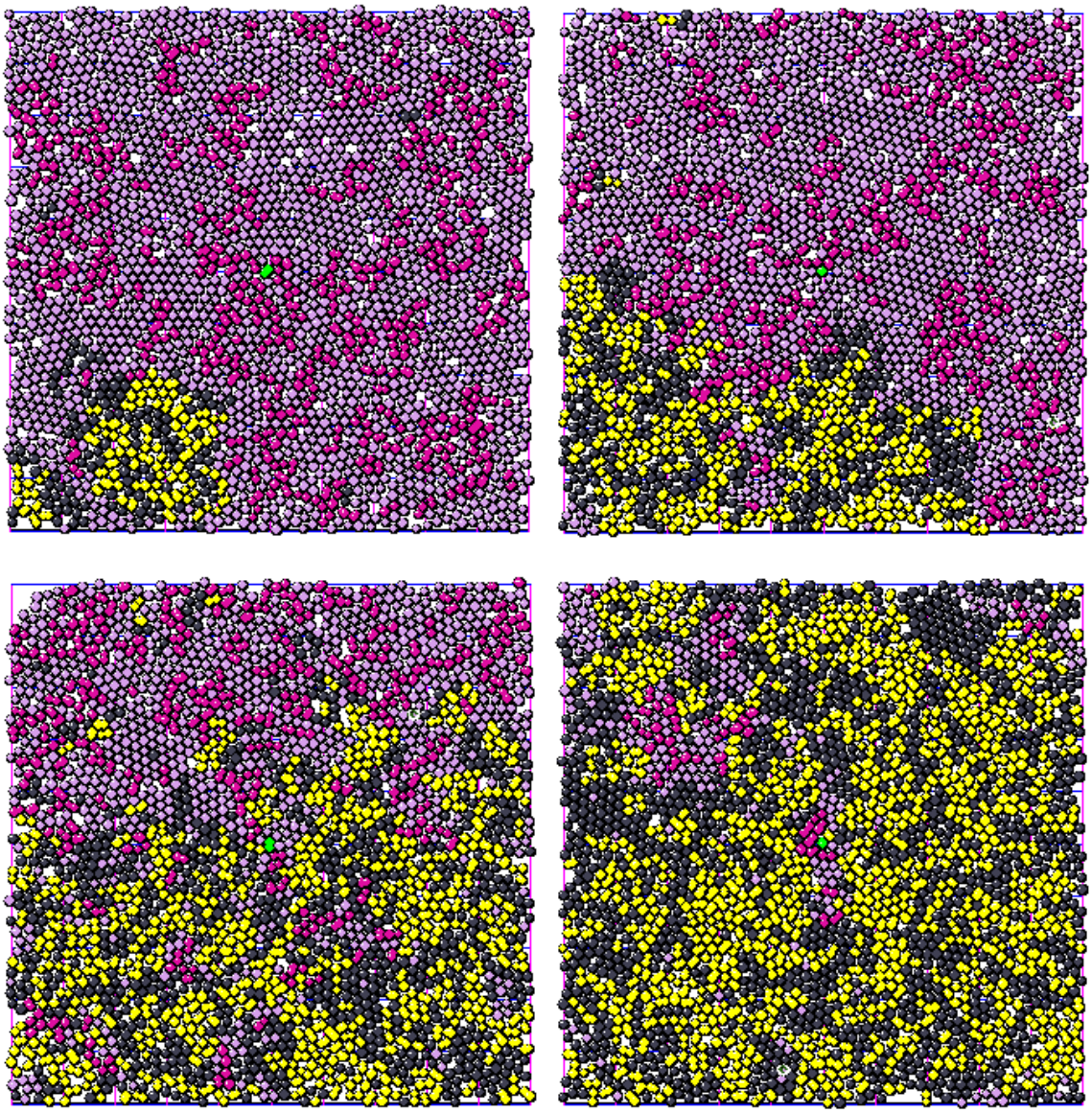

FIGURE 33 – Demonstration of the software. Propagation of malignant cells (yellow).

be done in order to study leukaemias. In the next section we present how the software can be used to study spatial aspects of erythropoiesis.

10.2 Cell displacement

Each cell is considered as a disk in the plane. Cells of different types are shown with different colors. Cell behaviour is characterised by its interactions with other cells, its proliferation, differentiation and apoptosis properties.

Interaction of two neighboring cells is determined by the interaction potential. The sum of forces acting on each cell from other cells determines the cell motion according to Newton's law with a possible damping because of the friction with other cells. Thus, we use an approach similar to molecular dynamics simulations even though the potential is different. We have

$$x_i^{''} - \epsilon x_i^{'} + \frac{1}{m} \sum_{i \neq j} f_{ij} = 0,$$

where x_i is the coordinate of the center of the i-th cell, m is its mass, ϵ is the damping coefficient, f_{ij} is the force acting between the cells i and j. We put

$$f_{ij} = -\phi(|x_i - x_j|),$$

where the function $\phi(r,t)$ equals zero for $r \geqslant r_i + r_j$ and it goes to infinity as r decreases. Here r_i and r_j are the radii of the cells i and j, respectively (which can depend on time). Thus, two cells push each other when the distance between their centers is less than the sum of their radii.

11 Simulations of erythropoiesis

In this section we present simulations of normal erythropoiesis. In the part I, devoted to multi-scale modelling of erythropoiesis, we assumed that 8 maturity levels of erythroid progenitors can be distinguished. That modelling provided values of self-renewal, differentiation and apoptosis rates in normal erythropoiesis. Here we consider 8 cell types with the rates of self-renewal, differentiation and apoptosis as obtained in Section 6.2. The objective of the si-

mulations presented hereafter is to study spatial distributions of erythroid cells in the bone marrow.

The multi-agent approach implies calculations for every single element of the system, i.e. for every single cell, which is very resource-demanding. The number of individual elements in the simulations is about 80 000. The number of primary cells in the domain that give birth to all other cells is 9 with daily influx equals 2 cells per day (each primary cell divides every 4.5 days). These cells are called "HSC" that means haematopoietic stem cells. The hierarchic tree of cell generations is presented in Figure 34. Cell types "p1",...,"p8" model erythroid progenitor sub-

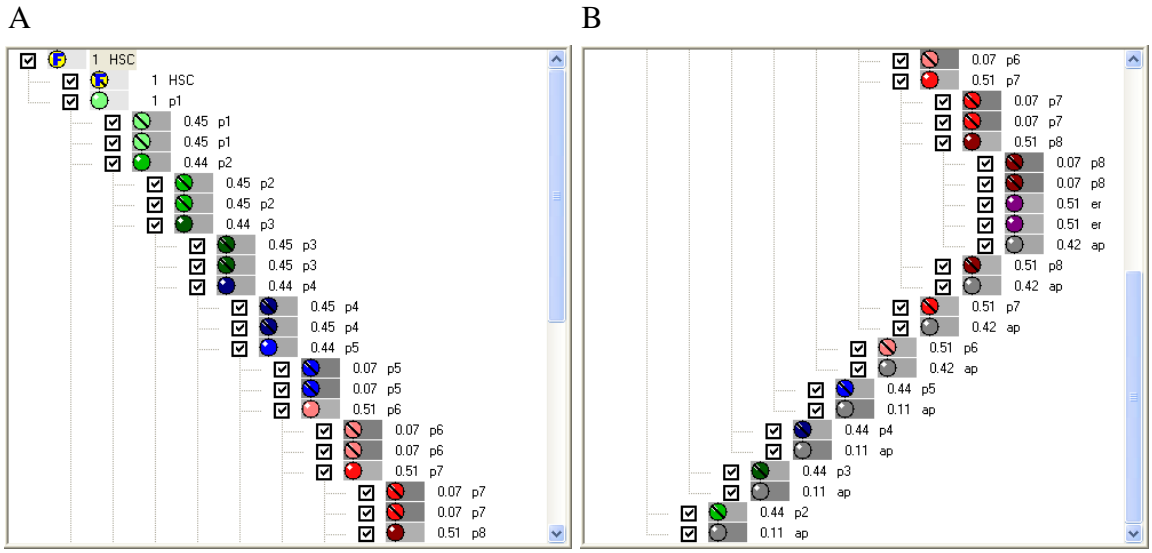

FIGURE 34 – Genealogical tree of cell types for a model of erythropoiesis.

populations, "ap" – apoptotic cells, "er" – population of mature erythrocytes. Sub-populations "p1",...,"p4" are self-renewing (means inclined preferentially to the self-renewal, discussed in detail in Section 6), "p5",...,"p8" are differentiating. All progenitors are supposed to have average lifetime of 1 day, erythrocytes have average lifetime of 40 days. This particular number describes average lifetime of erythrocytes for mice. Progenitor volume decreases with maturation from 0.015 to 0.01 units.

The calculation domain has the same form as that presented previously in Figure 31 with two closed borders (top and bottom) and two others (left and right), through which cells leave the domain. This domain is a schematic representation of bone marrow, cells leaving the domain are supposed to get into the blood stream. To calculate cell densities, the domain is divided into

11 vertical stripes, with one stripe in the middle of the domain, where stem cells are located. All stripes have the same dimensions. We calculate the total number of cells as well as percentages of erythrocytes, reticulocytes and of apoptotic cells in every stripe. These calculations are carried out for several time moments. The results of spatial distributions of cells with respect to the stripes are presented in Figure 35.

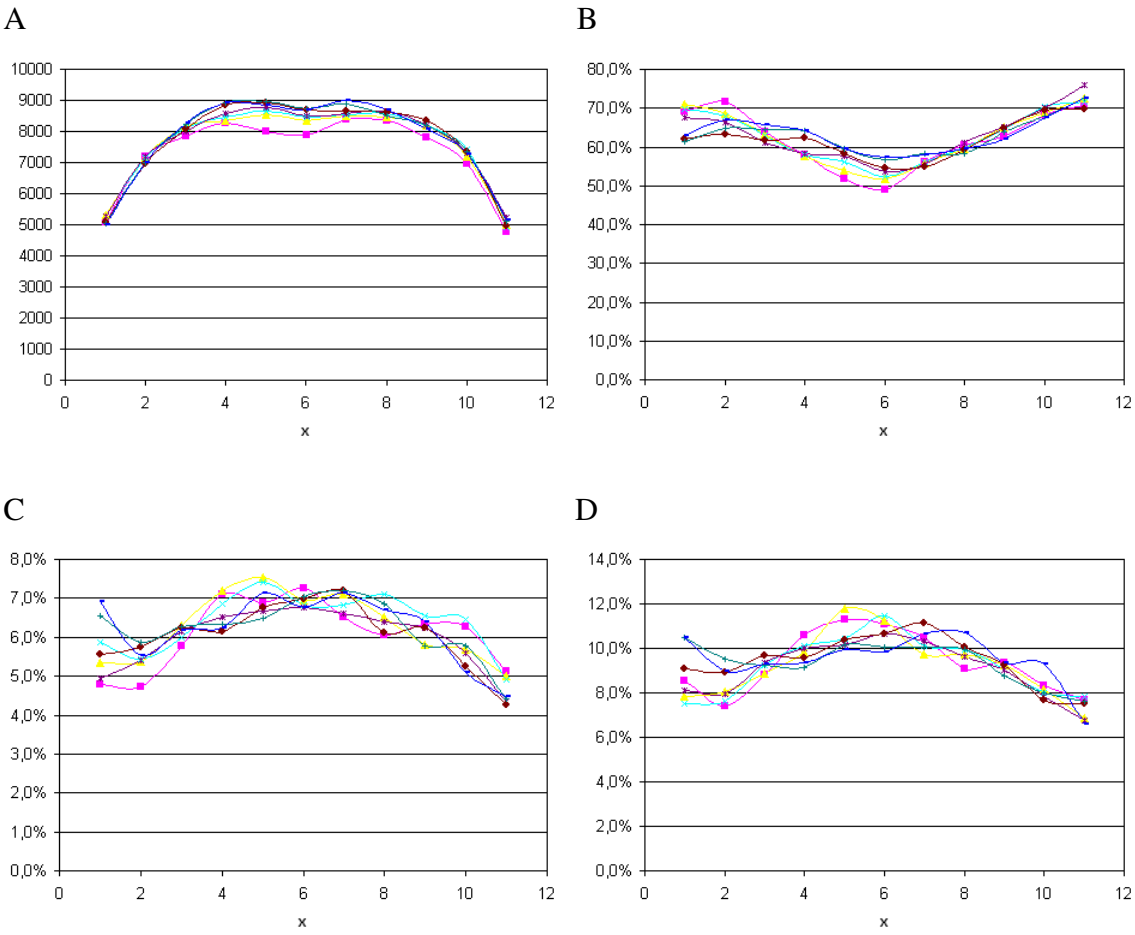

FIGURE 35 – Simulations of normal erythropoiesis. Cell distributions in the bone marrow, which is divided into 11 vertical stripes, $x = 6$ is the center stripe that contains stem cells. Panel A : total cell count in the bone marrow, Panel B : percentage of erythrocytes, Panel C : percentage of reticulocytes, Panel D : percentage of apoptotic cells.

Horizontal axis x denotes the stripe number, $x = 6$ corresponds to the middle stripe with stem cells, $x = 1$ and $x = 11$ correspond to the stripes located closely to open borders of the domain. Since the domain and all model conditions are homogeneous (no preferred direction is introduced), the distributions should be symmetric with respect to $x = 6$. It should be noted that

the approach implies stochasticity, that is why the obtained results do not possess this symmetry. Figure 35.A demonstrates that cell count decreases from the center to the exit borders with a maximum value in the second or third stripe. The modelling provides that among erythroid cells of the bone marrow $55\% - 70\%$ are mature erythrocytes, $4.5\% - 7\%$ are reticulocytes, $7\% - 12\%$ are apoptotic cells and others are immature progenitors. The percentage of erythrocytes is maximal near open borders of the bone marrow.

12 Cell division and displacement in individual based modelling

We show the existence of random motion due to cell division and of directed motion due to cell pressure. The contribution of each of these two factors can be different. In particular, if the cell density is low, then their random motion prevails over directed motion. In this case we can use reaction-diffusion systems of equations in order to describe the evolution of cell populations.

Spatial cell distribution in the bone marrow should be taken into account in order to specify the conditions of leukaemia development. This distribution is closely related to cell division and displacement. In this section we investigate both cell division and displacement with the individual based modelling approach. We also use it to explain the origin of random cell motion due to division. This justifies the usage of reaction-diffusion systems in the next section. Simulations are performed using the software "Cell dynamics", version "Soft sphere model", presented in Section 10.

As presented in Section 10.2, each particle moves according to the equation

$$\ddot{x}_i + \nu \dot{x}_i + \sum_{j \neq i} f(r_{ij}) = 0, \tag{3.1}$$

where the second term in the left-hand side of this equation describes the friction of the particle by the medium, the last term represents the force acting on the particle by all other particles. This is one of possible models in the approach called dissipative particle dynamics [21]. The force $f(r_{ij})$ between the i-th and the j-th particle depends on the distance r_{ij} between them. In

molecular dynamics this is the Van der Waals force, which is nonlocal and usually described by the Lennard-Jones potential. In the case of cell dynamics, the force between two particles is nonzero only when they touch each other, that is when the distance between the centers of the spherical particles is less than the sum of their radii.

Equation (3.1) allows us to determine the position of each cell in time. In addition, the process of cell division, which changes the number of cells and the forces acting between them, must be specified. This is done hereafter.

12.1 Cell division

When haematopoietic cells in the bone marrow divide, they push each other resulting in their displacement. This mechanism determines motion of immature red blood cells, which are the most represented cells in the bone marrow. Therefore, in order to study cell motion, we need to begin with cell division.

When a cell divides, it is replaced by two other cells. If we neglect the mechanical interaction with other cells, then the center of mass of the body composed by the two daughter cells does not change in comparison with the center of mass of the mother cell. Hence, after each division, each daughter cell is shifted with respect to its mother cell. Figure 36 shows several first consecutive divisions simulated with the software “Cell dynamics”, version “Soft sphere model”. Cell size and the frequency of division are given as parameters of the model.

There is one more parameter which should be specified in order to describe cell division : the direction of division, that is the direction of the straight line connecting the centers of the new cells. In some cases, the direction of division can be determined by the position of the mother cell with respect to the surrounding cells. In particular, this can be the case in embryogenesis or in plant growth. However, in the case of haematopoiesis, we can assume that this direction is arbitrary. Therefore the angle of the straight line connecting the centers with respect to the x-axis is chosen in a random way with a uniform distribution.

Let now focus on cell motion. Consider the following division process $A \to A + B$ (Figure 36) under the assumptions formulated above. After each division the cell A gives one cell, which is identical to itself (self-renewal), and another cell which is different (differentiation). Hence,

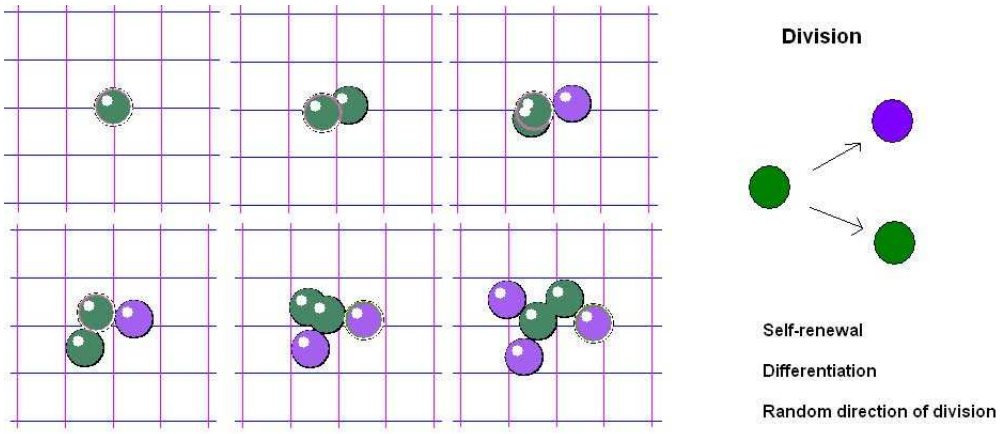

FIGURE 36 – Successive cell divisions simulated with the software "Cell dynamics", version "Soft sphere model". Every division gives birth to two daughter cells (green for a self-renewing division, purple for differentiating division). The direction of division is not specified.

there will always be one cell of the type A and a growing number of cells B. After each division the cell A moves in a random direction at the distance equal to its radius. This means that the cell A moves along the plane in a random way. In the case where there are many such cells and we can consider them as a continuous medium, this motion becomes similar to diffusion and can be described in a similar way. We discuss this question in more detail in the next section.

Each cell defined in the individual-based model must be able to divide, change its type, or die (either by apoptosis or necrosis). Hence probabilities for such events are provided by the user, for each type of cell defined. These probabilities are determined by intracellular regulatory networks. In the case of erythroid progenitors they are discussed in Section 3.

In the example shown in Figure 37 (left), there is one stem cell (green) that divides in two cells at each division, one cell is identical (this is self-renewal) and the other cell is of another type (red). In turn, the red cell can self-renew with the probability 0.57, differentiate with the probability 0.39, or die by apoptosis with the probability 0.04 (this probability does not appear on Figure 37, it is obtained from the two other probabilities). In the first case, it divides giving two cells identical to itself. In the second case, it gives two different cells (violet). If the cell dies, it is removed from the computational domain. Red cells can also mutate with the probability 0.001. When this happens, a mutated cell (yellow) appears. Its properties are different in comparison with the original cell (red). It self-renews with the probability 0.7, differentiates with the probability 0.3, and does not die by apoptosis. These assumptions correspond, for ins-

tance, to properties of malignant cells. Their self-renewal ability is greater than for normal cells, while differentiation and apoptosis abilities are lower (or absent). Therefore, we can expect that after some time malignant cells will appear and will take over the normal cells. It is numerically observed that malignant cells push out normal cells and gradually fill the whole computational domain (Figure 37, right). This replacement corresponds to reaction-diffusion waves discussed in Section 14.2.1, Theorem 19. Cell division occurs according to the algorithm described above, presented in Figure 36.

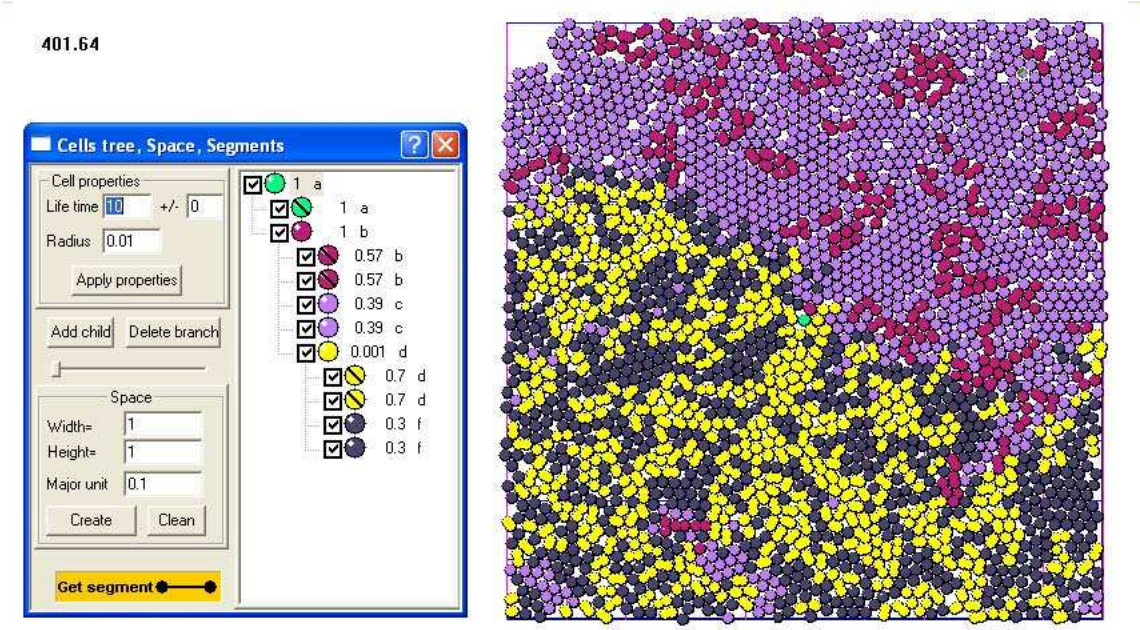

FIGURE 37 – Simulation obtained with the software “Cell dynamics”. Left : Properties of the different cells involved in the computations are listed, as self-renewing (same color), differentiating (different color) and mutation (yellow) probabilities. Right : Computational domain, filled with cells defined on the left panel.

12.2 Cell displacement

There are various mechanisms of cell displacement in the bone marrow. We discuss here random cell motion, which is to some extent similar to diffusion, and directed cell motion, similar to convection. Since biological cells are macroscopical objects, the usual Fickian diffusion is not applicable for them. However they can move in a random way due to division.

Let us discuss the motion of a single dividing cell when it is surrounded by other cells.

Obviously, cells push each other and create a preferential direction of motion. It is easier for a cell to move in the direction where there are less cells. In order to study this phenomenon, we consider the following numerical experiment. The cell A is placed at the bottom of an empty rectangular box (Figure 38, left). It divides reproducing itself and some other cells which fill the box. These latter cells do not divide and do not move unless they are pushed by other cells. What will be the position of the cell A in time ? If it moves in a random way, its distance from the initial position will grow proportionally to $\sqrt{t}$ (with random perturbations). However, when there are many other cells around it, they will influence its motion pushing it to the direction where cell concentration is lower. If we introduce pressure, that is the force exerted by cells on the unit surface, then, similar to Darcy's law, cell velocity will be determined by pressure gradient [27]. It can be verified on model examples that the cell will move in this case with a constant speed, that is its displacement will be proportional to t.

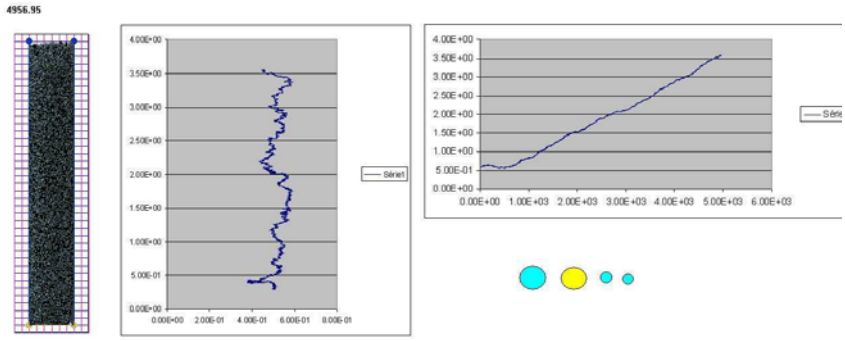

FIGURE 38 – Trajectory and displacement of a cell A dividing according to the process $A \to A + B + 2C$. Left : Rectangular domain, center : cell trajectory, right : cell displacement.

We can vary the ratio of the directed and random motion. In order to do this, let us consider the division scheme in the form $A \to A + B + 2C$ and assume that the cells A and B have the same radius, the radius of the cell C is twice less, the cell B is located on one side of the cell A after the division, and the cells C on the diametrically opposite side. The cell A is shown in yellow in Figure 38, B and C in blue. Clearly, such a cell division is not realistic from the biological point of view. We consider it in order to explain the mechanisms of cell motion. We use here the advantage of mathematical modelling, which allows us to consider idealised models, in order to study a symmetric division where the center of the cell A does not shift after

cell division, and various asymmetric divisions where this center displaces due to division. In the real biological situation, division is asymmetric. We will see below that it results in a random cell motion. However, if cell density is sufficiently high, convective cell motion becomes also important. To study it more precisely and independently of the random motion, we need to consider a symmetric division.

With the division scheme shown in Figure 38, the center of the cell A before and after the division remains at the same place. In fact, we consider here not the center of mass of the system of cells but its geometrical center. Hence, cell division in this case does not provide random motion. Figure 38 shows the cell trajectory and its displacement from the initial position. We can see that its displacement is close to a linear function. Therefore, it is a directed motion with a weak random component.

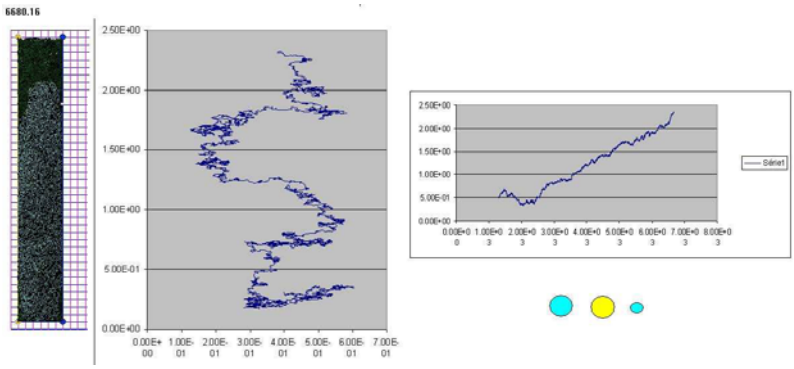

FIGURE 39 – Trajectory and displacement of a cell A dividing according to the process $A \to A + B + C$, where B and A have the same radius, and the radius of C equals one half of the radius of A. Left : Rectangular domain, center : Cell trajectory, right : Cell displacement.

Figure 39 shows another scheme of cell division, $A \to A + B + C$, where B and C are from the opposite sides of A. Since the radius r_C of C is twice less than the radius r_B of B, then the center of the cell A moves at $r_C/2$ after each division. The cell displacement remains practically linear. However its trajectory essentially changes in comparison with the previous case. The projection of the cell speed on the vertical direction remains the same since it is determined by the frequency of its division. In other words, by the rate with which it fills the box with other cells. However, its local mobility becomes higher because of the increased random motion. The cell motion has two components : small random displacements and large scale sinusoidal motion from one side to another and upwards. This horizontal motion of the cell is caused by the

pressure difference. Since the box is sufficiently large, the cell first fills one side, then another side of the box. Its increased mobility makes it more sensitive to the pressure difference.

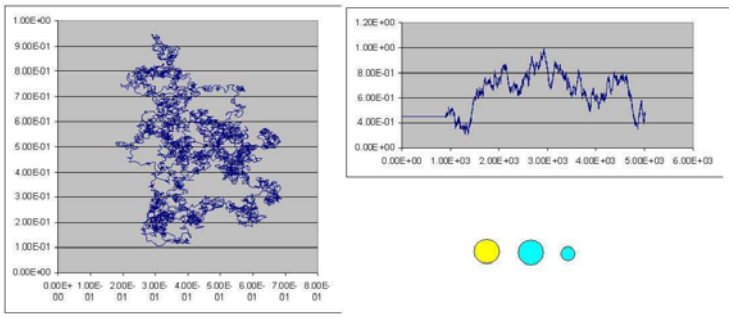

FIGURE 40 – Cell trajectory (left) and displacement (right) in the case of a strong random component.

If we increase even more the random component of the cell motion by appropriately choosing division scheme, then the directed component of its motion is not visible any more (Figure 40). Another parameter which determines the relative contribution of the random and directed components of the cell motion is their concentration. If it is low, then mechanical interaction with the surrounding cells will be negligible.

In Section 8 we modelled the evolution of cell populations by reaction-diffusion-convection equations. We took into account their random motion described by the diffusion-terms and their directed motion. Directed or convective motion should be taken into account if the density of cell population is sufficiently high. In this case it can be described by reaction-diffusion equations coupled with fluid dynamics in a porous medium. Such a model has been studied in previous works [21, 44].

We note finally that the diffusion coefficient depends on the cell adhesion to the extracellular matrix. In particular, leukaemic cells have a weaker adhesion and, consequently, a bigger diffusion coefficient.

13 Discussion

In this part we presented the software which is based on the individual based modelling and which can be applied to study cell interaction processes. The presented version of the soft-

ware considers mechanical cell-to-cell interactions. Using this software we studied spatial cell distributions of erythroid progenitors in bone marrow.

Models of cell populations are often semi-empiric and based on some intuitive assumptions, which seem in agreement with biological observations. We attempted to give here some more rigorous justification of one of such assumptions about cell displacement. Although there are different mechanisms of cell motion in the bone marrow, we did not discuss here biologically active mechanisms such as chemotaxis but concentrated only on pure mechanical cell interaction. Since new cells appear due to proliferation, cells push each other creating random motion, which can be described by diffusion, and directed motion determined by pressure difference. We carried out some analysis of this motion with individual based modelling.

Quatrième partie

PK/PD Modelling of AML Treatment with AraC

Acute myeloid leukaemia (known also as non-lymphocytic or myelogenous) is a type of leukaemia characterised by abnormal proliferation of myeloid cells. One of the most common and effective chemotherapeutic agents against AML is AraC (cytosine arabinoside, cytarabine), which is used in combination with other drugs. Pharmacokinetics-pharmacodynamics approach is one of modern ways to study drug outcome on the disease. The last part of my work is devoted to the PK/PD modelling of AML treatment with AraC.

We consider dynamics of normal and malignant cells, which are determined by AraC concentration. We built a mathematical model of AraC distribution in the body and of its action. The model consists of two parts. First part describes pharmacokinetics of AraC, that is drug delivery to the bone marrow, penetration through cell membrane and its metabolism, which is a set of interactions between the drug and intracellular proteins, its degradation, phosphorylation and deamination. Then we describe AraC action on cells, that is pharmacodynamics.

We consider AraC distribution between two compartments, blood and bone marrow. Transmembrane transport is described as a process of passive diffusion that goes until concentrations of AraC inside and outside cells are equal. Metabolism of AraC is described as a set of chemical reactions and is modelled using Michaelis-Menten kinetics. Drug action on DNA synthesis and thus on cell proliferation is presented as a dependance of proliferation rates and apoptosis on AraCTP concentrations. This constitutes pharmacodynamics part.

14 Cell population dynamics

14.1 Normal erythropoiesis

In Section 4 we considered several erythroid progenitor sub-populations denoted by $P_1, \ldots, P_n$. Each of them consists of identical cells with given rates of self-renewal s_i, differentiation d_i and apoptosis a_i, $i = 1, \ldots, n$. As discussed in Section 3, these rates and their dependence on the parameters are determined by the Erk/Fas regulatory system (see Figure 7). In the framework of the model described in Section 3, they are determined by the basins of attraction of the corresponding stationary points.

Evolution of these population densities is described by the ordinary differential system of

equations

$$\begin{cases} \dfrac{dP_1}{dt} &= H + (s_1 - d_1 - a_1)P_1, \\ \dfrac{dP_i}{dt} &= (s_i - d_i - a_i)P_i + 2d_{i-1}P_{i-1}, \qquad i = 2, \ldots, n, \end{cases} \tag{4.1}$$

where H denotes a constant flux of haematopoietic stem cells differentiating in erythroid progenitors, the coefficients s_i, d_i and a_i depend on the values of the concentrations of intracellular proteins Erk and Fas, E_i and F_i. These concentrations are regulated by intracellular networks (see Section 3). In this section we do not take into account the external control feedback by hormones (glucocorticoids or erythropoietin) discussed in Section 5. Hence, the source term α in System (1.6) is assumed to be constant. Fas-ligand, the main external source for Fas activation is produced by mature cells [39], hence we assume γ, in (1.6), is a function of P_j, $j = 1, \ldots, n$. Consequently, the protein concentrations are governed by the equations

$$\begin{cases} \dfrac{dE_i}{dt} &= \Phi(\alpha, E_i, F_i), \\ \dfrac{dF_i}{dt} &= \Psi\left(\sum_{j=1}^{n} \mu_{ij} P_j, E_i, F_i\right), \end{cases} \tag{4.2}$$

where the functions Φ and Ψ are defined in (1.6), and μ_{ij} are constant parameters accounting for the weight of mature cell populations in the production of Fas-ligand.

We now introduce spatial cell distribution. We consider a one-dimensional problem with the space variable x and assume cells can move in space in a random way. This motion can be described by diffusion (see Section 12). The intracellular concentrations E_i and F_i are supposed to be the same for all cells in the i-th population, therefore they do not depend on the space variable, but can depend on time.

We also take into account a limitation of cell proliferation when cell density exceeds some threshold level, by means of a chemical cell interaction. Let P_0 be the maximal cell density. Then System (4.1) can be rewritten in order to take into account both diffusion and the dependence

of cell proliferation (self-renewal and differentiation) on $P_0 - \bar{P}$, where $\bar{P} = \sum_{i=1}^{n} P_i$,

$$\begin{aligned} \frac{\partial P_1}{\partial t} &= D\frac{\partial^2 P_1}{\partial x^2} + H + (s_1 - d_1)P_1(P_0 - \bar{P}) - a_1 P_1, \\ \frac{\partial P_i}{\partial t} &= D\frac{\partial^2 P_i}{\partial x^2} + (s_i - d_i)P_i(P_0 - \bar{P}) - a_i P_i + 2d_{i-1}P_{i-1}(P_0 - \bar{P}), \quad i = 2, \ldots, n. \end{aligned} \tag{4.3}$$

In order to be able to analyse the model, we first assume intracellular reactions are fast in the time scale related to cell motion. Then, instead of System (4.2), we can consider the stationary equations

$$\Phi(\alpha, E_i, F_i) = 0, \qquad \Psi\left(\sum_{j=1}^{n} \mu_{ij} P_j, E_i, F_i\right) = 0. \tag{4.4}$$

Therefore, E_i and F_i can be expressed as functions of P_j, $j = 1, \ldots, n$. As a consequence, coefficients s_i, d_i, a_i in (4.1) also become functions of P_j.

System (4.3) and (4.4) describes erythroid progenitor dynamics in normal erythropoiesis under the assumption of fast intracellular reactions. Consider first the case of a single cell population P_1. Then System (4.3) is reduced to the first equation where $\bar{P} = P_1$:

$$\frac{\partial P_1}{\partial t} = D\frac{\partial^2 P_1}{\partial x^2} + H + (s_1 - d_1)P_1(P_0 - \frac{a_1}{s_1 - d_1} - P_1). \tag{4.5}$$

Equation

$$H + (s_1 - d_1)P_1(P_0 - \frac{a_1}{s_1 - d_1} - P_1) = 0$$

has a unique positive solution $P_1 = P_1^*$ if $s_1 - d_1 > 0$. It is a globally asymptotically stable stationary solution of equation (4.5), that satisfies $P_1^* \geqslant \max\{0, P_0 - a_1/(s_1 - d_1)\}$.

If $P_0 > a_1/(s_1 - d_1)$, then $P_1^* \geqslant P_0 - a_1/(s_1 - d_1)$, and P_1^* is positive even if $H = 0$. This means that even in the absence of haematopoietic stem cells, erythroid progenitors keep a positive concentration due to self-sustained proliferation. This case seems to be unrealistic from the biological point of view. Therefore, we assume in what follows $P_0 \leqslant a_1/(s_1 - d_1)$.

In the next section, we introduce a population of leukaemic cells and investigate the dynamics of the model. In particular, the attention is focused on the existence of a leukaemic equilibrium.

14.2 Erythroleukaemia

Consider two cell lineages, normal and mutated. The lineage of mutated cells will differ by the rates of self-renewal, differentiation and apoptosis. Denote by P_i cells from the normal lineage and by Q_i cells from the mutated lineage. Both of them are described by the same model (4.3) as in the previous section. However, we should take here into account that the total number of cells include both lineages,

$$\bar{P} = P_1 + \cdots + P_n + Q_1 + \cdots + Q_n.$$

In what follows we restrict ourselves to the case where each of these two lineages consists of a single cell type. This is equivalent to the assumption that we neglect in the previous equality all cell densities except for P_1 and Q_1. Then equations for P_1 and Q_1 become independent of other equations and can be written in the form :

$$\begin{cases} \dfrac{\partial P}{\partial t} &= D_P \dfrac{\partial^2 P}{\partial x^2} + H + (s-d)P(P_0 - P - Q) - aP, \\ \dfrac{\partial Q}{\partial t} &= D_Q \dfrac{\partial^2 Q}{\partial x^2} + (s_m - d_m)Q(P_0 - P - Q) - a_m Q, \end{cases} \tag{4.6}$$

where the subscripts are omitted for simplicity of notation, and s_m, d_m, a_m denote the rates of self-renewal, differentiation and apoptosis of mutated cells, respectively. In particular, since there is only one generation of erythroid progenitors, denoted by P, the influence of progenitor densities on the activation of Fas is neglected, so that (4.4) becomes

$$\Phi(\alpha, E, F) = 0, \qquad \Psi(\gamma, E, F) = 0,$$

with $\alpha > 0$ and $\gamma > 0$ constant. Consequently, E and F no longer depend on P and, similarly, the different rates do not depend on cell densities. This assumption has then strong consequences, yet it allows drawing comprehensive conclusions on the existence of a leukaemic equilibrium and treatment of the disease (see below).

The constant source H is absent in the second equation of (4.6) because it is assumed in the case of erythroleukaemia there is no permanent influx of mutated cells from the stem cell

compartment. Different assumptions could of course be considered.

14.2.1 Existence of a Leukaemic Equilibrium

In order to analyse reaction-diffusion System (4.6), we first consider the system without diffusion,

$$\left\{ \begin{array}{rcl} \dfrac{dP}{dt} & = & H + (s-d)P(P_0 - P - Q) - aP, \\ \dfrac{dQ}{dt} & = & (s_m - d_m)Q(P_0 - P - Q) - a_m Q, \end{array} \right. \tag{4.7}$$

and we assume $s-d>0$, $s_m-d_m>0$, and $a_m/(s_m-d_m) < P_0 < a/(s-d)$. The assumption $a_m/(s_m - d_m) < P_0$ ensures the possibility to have a leukaemic equilibrium (see (4.8)), as shown below.

Zero lines of the right-hand side of (4.7) are given by the equalities

$$H + kP(-b - P - Q) = 0, \qquad k_m Q(b_m - P - Q) = 0, \tag{4.8}$$

where

$$k = s - d, \quad k_m = s_m - d_m, \quad b = -P_0 + \frac{a}{k}, \quad b_m = P_0 - \frac{a_m}{k_m}.$$

According to the above assumptions, all parameters, k, k_m, b and b_m are positive.

From the first equation in (4.8),

$$Q = -b - P + \frac{H}{kP}, \tag{4.9}$$

and from the second equation

$$Q = 0 \qquad \text{or} \qquad Q = b_m - P. \tag{4.10}$$

System (4.9)–(4.10) can have one or two stationary points (Figure 41). If we put $Q = 0$ in (4.9), and denote by P^* the positive solution of this equation, then we find

$$P^* = \frac{b}{2}\left(\sqrt{1 + \frac{4H}{kb^2}} - 1\right).$$

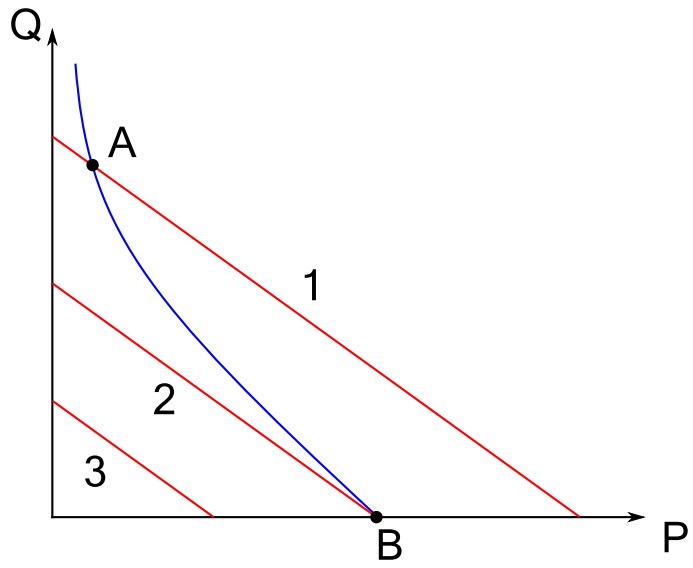

FIGURE 41 – Graphical solution of System (4.9)–(4.10). Case 1 corresponds to the existence of two stationary points, A and B, the case 3 to the existence of only one stationary point, B. In case 2, the points A and B have the same location.

The stationary solution $(P, Q) = (P^*, 0)$ always exists.

On the other hand, from (4.9) and the second equation in (4.10), we obtain

$$P_m^* + Q_m^* = -b + \frac{H}{kP_m^*} \qquad \text{and} \qquad P_m^* + Q_m^* = b_m.$$

If $b_m > P^*$, then we have the case 1 in Figure 41. There exist two stationary points : A with the coordinates (P_m^*, Q_m^*), and B with the coordinates $(P^*, 0)$. If $b_m < P^*$, then we have the case 3 in Figure 41, there exists a unique stationary point $B = (P^*, 0)$. It follows that leukaemia may develop only if $b_m > P^*$.

Condition $b_m > P^*$ can be written as

$$b_m(b_m + b) > \frac{H}{k}$$

or equivalently

$$\left(\mu - \frac{P_0 k}{a}\right)(\mu - 1) > \frac{Hk}{a^2}, \tag{4.11}$$

where

$$\mu = \frac{a_m}{a}\,\frac{k}{k_m} = \frac{a_m}{a}\,\frac{s-d}{s_m-d_m}. \tag{4.12}$$

We call the inverse parameter $1/\mu$ the *strength of mutation*. If a malignant mutation decreases the rate of apoptosis and differentiation and increases the rate of proliferation, then $\mu < 1$. This means that the strength of mutation is greater than 1.

We recall that the assumption $b > 0$ implies that $P_0 k/a < 1$. Moreover, from (4.12) and the assumption $b_m > 0$, one deduces $\mu < P_0 k/a$. Consequently, the left-hand side of (4.11) is positive. Furthermore, it is straightforward that inequality (4.11) is satisfied if and only if

$$P_0 > \frac{H}{a}. \tag{4.13}$$

This condition means that (4.11) is true for $\mu = 0$. Indeed, the set of values of μ satisfying (4.11) is an interval in the form $[0, \mu^*)$ with $\mu^* < P_0 k/a < 1$. If (4.13) is not satisfied, then leukaemia will not develop, independently of the strength of mutation. This occurs if the influx of normal cells from the stem cell compartment is sufficiently large.

If (4.11) is satisfied, that is the mutation is sufficiently strong and the influx is not strong enough, then System (4.7) has two stationary points A and B (Figure 41). It can be verified that A is stable while B is unstable. This means that the disease will develop. The values of the concentrations P_m^* and Q_m^* in the leukaemic equilibrium depend on μ. In particular, the concentration Q_m^* of malignant cells can be rather low if μ is close to the critical value. If (4.11) is not satisfied (weak mutation or strong influx), then there exists a unique stable stationary point B, which corresponds to the disease free situation.

The analysis of the ordinary differential system of equations (4.7) allows us to do some conclusions about the behaviour of solutions of (4.6). More precisely, classical results on monotone systems allow to conclude the existence of a travelling wave providing a transition from the unstable disease free equilibrium B to the leukaemic equilibrium A, when (4.11) is satisfied. The existence and stability of travelling waves for monostable monotone reaction-diffusion systems are well known [117]. The existence result is stated in the next theorem.

Theorem 19. Let condition (4.11) be satisfied. Then the endemic equilibrium (P_m^*, Q_m^*) of System (4.6) considered on the whole axis is globally asymptotically stable in the sense that

any solution with the initial condition $(P_0(x), Q_0(x))$, where $P_0(x) \geqslant \epsilon$, $Q_0(x) \geqslant \epsilon$, ϵ is a positive constant, converges uniformly to $(P, Q) = (P_m^*, Q_m^*)$ as $t \to \infty$. The disease free solution $(P^*, 0)$ is unstable.

Moreover there exists a minimal speed c_0 such that for all speeds $c \geqslant c_0$ there exist travelling wave solutions of System (4.6), that is solutions of the form $P(x,t) = p(x - ct)$, $Q(x,t) = q(x - ct)$. The functions $p(x)$ and $q(x)$ are monotone with respect to x and satisfy the system

$$D_P\, p'' + cp' + H + (s - d)P(P_0 - P - Q) - aP = 0,$$

$$D_Q\, q'' + cq' + (s_m - d_m)Q(P_0 - P - Q) - a_m Q = 0$$

and the conditions at infinity :

$$p(-\infty) = P_m^*, \quad q(-\infty) = Q_m^*, \quad p(+\infty) = P^*, \quad q(+\infty) = 0.$$

For $c < c_0$ such solutions do not exist.

The proof of the theorem is based on the reduction of System (4.6) to a monotone system and on the application of the comparison principle. The interested reader may refer to [117] for details.

It is known that the appearance of malignant cells is due to several rare consecutive mutations. Once this event occurs, malignant cells start proliferating. If malignant cells appear then they persist and spread in the whole bone marrow in the form of a travelling wave. Their existence is stated in Theorem 19.

15 Pharmacokinetics modelling

Pharmacokinetics study drug distribution in the body and its delivery to target organs. Three stages can be distinguished, delivery to target organs, transport inside cells and drug metabolism.

To describe drug distribution in the body, several anatomical compartments should be chosen. In [31] the authors suggest that it can be gastrointestinal tract, blood, liver, non eliminating

tissue, efficacy and toxicity compartments. Efficacy compartment in leukaemic case is the bone marrow. Considering many compartments introduce more complexity because of many unknown parameters that should be estimated. In [54] the authors proposed methods of model reduction, which can be used in PK/PD modelling. They presented how some compartments can be removed without loosing relevant information in the model. In order to render our model simpler with a few parameters to estimate, we choose two compartments, blood and bone marrow, and consider drug concentrations inside them (Section 15.1). Drug distribution in other organs can be introduced, for example, as clearance from the blood.

Second step, membrane penetration, is very drug-specific, different drugs go through membrane by different transport mechanism. AraC is brought into cells by nucleoside transporters and can be considered as passive diffusion. A simple model of the transport is presented in Section 15.2. For other drugs transmembrane transport can be due to different mechanisms.

Metabolism scheme is also drug-specific. Nevertheless, some similarities can be found for certain drugs, for example for AraC and gemcitabine. This last stage of pharmacokinetics is often described as a set of chemical reactions. Each reaction can be described using Michaelis-Menten mechanism, the law of mass action or by other methods depending on the concrete chemical reactions. We use Michaelis-Menten mechanism to describe the scheme of metabolism of AraC, which is presented in Section 15.4. In Section 15.3 we explain this mechanism on three example chemical reactions.

15.1 Drug distribution

In this section we propose a simple model of drug distribution in the body. We distinguish two compartments, blood and bone marrow, see Figure 42. Let us denote by $a_b(t)$ and $a_m(t)$ respectively extracellular concentrations of AraC in the blood and in the bone marrow at time t. Then their dynamics can be described by the following equations,

$$\dot{a}_b = I(t) - k_{bm}(a_b - a_m) - \gamma_b a_b, \tag{4.14}$$

$$\dot{a}_m = k_{bm}(a_b - a_m) - g(a_m, a_{mi}) - \gamma_m a_m. \tag{4.15}$$

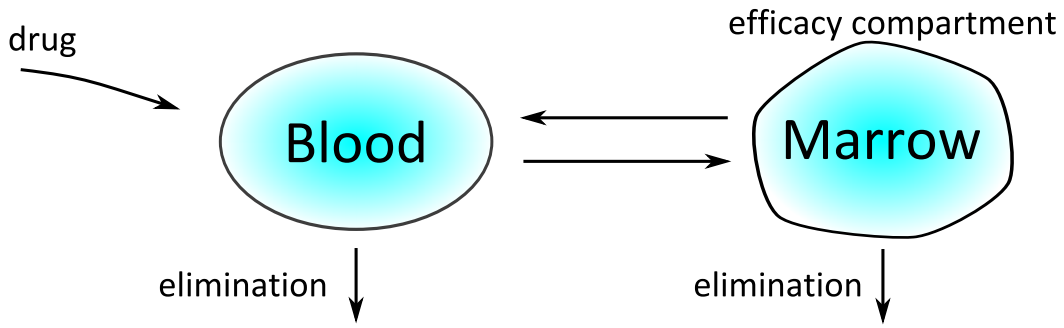

FIGURE 42 – Two compartment model of AraC distribution in the body is considered in the modelling.

The term $I(t)$ describes drug administration protocol, last term in each equation describes AraC clearance, i.e. its destruction. The term $k_{bm}(a_b - a_m)$ describes AraC transition between the two compartments, in which constant k_{bm} determines the rate of the distribution. The term $g(a_m, a_{mi})$ describes AraC transmembrane transport inside the bone marrow and is discussed in Section 15.2.

15.2 Transmembrane transport of AraC

In Section 15.1 we considered a model that describes drug distribution in the body. We included two compartments, blood and bone marrow. The term $g(a_m, a_{mi})$ described transmembrane transport.

AraC penetrates inside a cell by a mechanism relayed essentially by human equivibrative nucleoside transporter-1 (hENT1), which can be considered as facilitated diffusion, see Figure 43. The process does not need energy and goes in accordance with the gradient of concentration up

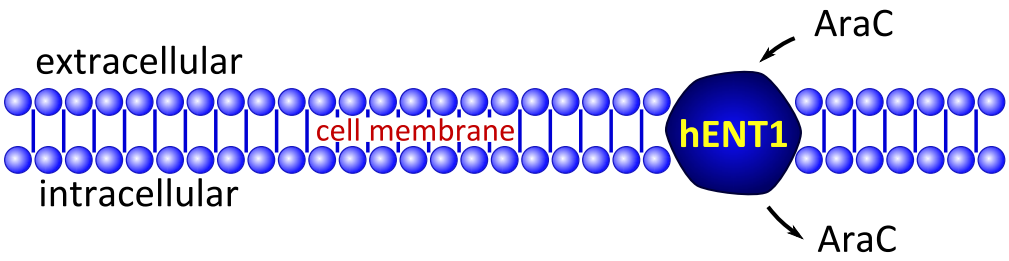

FIGURE 43 – Transmembrane transport of AraC is implemented by hENT1 transporter.

to the equilibrium between intracellular and extracellular concentrations of AraC [62, 125].

For weak AraC plasma concentrations (less than 0.5–1μM), obtained after administration of a standard dose of AraC (100–200 mg/m^2) the transmembrane transport is a limiting factor for AraCTP formation. In case of strong AraC plasma concentrations (more than 10μM), obtained after administration of a strong dose of AraC, the transmembrane transport is no more a limiting factor. In this case intracellular processes such as phosphorylation, deamination, nucleoside half-life and AraCTP incorporation into DNA determine drug efficacy.

We propose the following simple model of the transmembrane transport. The rate of intracellular AraC accumulation due to transmembrane transport is

$$g(a_m, a_{mi}) = k_{hENT1}(a_m - a_{mi}),$$

where a_{mi} is intracellular concentration of AraC, a_m is extracellular concentration of AraC, k_{hENT1} is a constant that describes the rate of transmembrane penetration and is determined by the activity of hENT transporter. If extracellular concentration is greater than intracellular concentration ($a_m > a_{mi}$), then intracellular concentration increases, extracellular decreases and vice versa. When both concentrations are equal, the transport stops.

Hence, Equations (4.14), (4.15) describing dynamics of extracellular concentrations of AraC in the blood and in the bone marrow become

$$\dot{a}_b = I(t) - k_{bm}(a_b - a_m) - \gamma_b a_b, \tag{4.16}$$

$$\dot{a}_m = k_{bm}(a_b - a_m) - k_{hENT1}(a_m - a_{mi}) - \gamma_m a_m. \tag{4.17}$$

This simple model allows us to take into account the transmembrane transport.

In Section 15.4 we describe kinetics of intracellular AraC, determined by the scheme of metabolism, using Michaelis-Menten kinetics presented in the next section.

15.3 Michaelis-Menten kinetics

The Michaelis-Menten mechanism for the catalysis of biological chemical reactions is one of the most common approaches in biochemistry. Catalysis is a process in which the rate of

a chemical reaction is either increased or decreased by a catalyst. Enzymes are large protein molecules that are natural catalysts. The vast majority of chemical reactions that keep living systems alive are too slow without a catalyst to sustain life and it becomes rapid in presence of a catalyst. Let us demonstrate this mechanism on several example chemical reactions.

15.3.1 Enzyme without inhibitor

Consider a chemical reaction,

$$E + S \underset{k_{-1}}{\overset{k_1}{\rightarrow}} ES \overset{k_2}{\rightarrow} E + \text{products}, \tag{4.18}$$

where E is the enzyme, S is the "substrate" (the molecule on which the enzyme does its work), and ES is an enzyme-substrate complex. It is presumed that the substrate binds somehow to the enzyme before the enzyme can do its work. The step of complex formation of $[ES]$ goes very fast with respect to the product formation. Constants k_1, k_{-1} denote rates of reaction in both directions.

Let us show how the approach is generally used in chemical kinetics. The rate of formation of product, called the reaction rate, v, is defined as

$$v = \frac{[\text{product}]}{dt} = k_2[ES]. \tag{4.19}$$

The enzyme-substrate complex, ES, is an intermediate complex. A steady-state approximation provides

$$\frac{d[ES]}{dt} = k_1[E][S] - k_{-1}[ES] - k_2[ES] \approx 0, \tag{4.20}$$

where $[E]$ is the concentration of free (uncomplexed) enzyme, which is usually unknown. The concentration of the substrate is defined by $[S]$. From Equation (4.20) we obtain

$$[ES] = \frac{k_1[E][S]}{k_{-1} + k_2} = \frac{[E][S]}{K_M}, \tag{4.21}$$

where

$$K_M = \frac{k_{-1} + k_2}{k_1}.$$

This constant is called the Michaelis-Menten constant. Substitute (4.21) into Equation (4.19),

$$v = \frac{d[\text{product}]}{dt} = k_2 \frac{[E][S]}{K_M}. \tag{4.22}$$

Total concentration $[E]_0$ of the enzyme, which is supposed to remain constant, is

$$[E]_0 = [E] + [ES] = [E] + \frac{[E][S]}{K_M} = [E]\left(1 + \frac{[S]}{K_M}\right).$$

Deriving from this equation $[E]$ and substituting it into (4.22) we obtain

$$v = k_2 \frac{[E]_0[S]}{K_M + [S]}. \tag{4.23}$$

The reaction velocity, v, is zero when $[S]$ is zero and it increases if $[S]$ increases. It reaches its maximum when $[S]$ becomes very large. Define the maximal velocity, $v_{\max}$, as

$$v_{\max} = \lim_{[S]\to\infty} k_2 \frac{[E]_0[S]}{K_M + [S]} = k_2[E]_0.$$

Then Equation (4.23) can be written as

$$v = \frac{v_{\max}[S]}{K_M + [S]}.$$

The kinetics of the reaction are characterised by two parameters, $v_{\max}$ and K_M. These are the parameters that are usually given in the literature in studies of the kinetics of biochemical reactions.

15.3.2 Enzyme with inhibitor

Let us suppose now that for the chemical reaction defined in (4.18), an inhibitor I interferes with enzyme E but not with the complex ES,

$$E + I \underset{k'_{-1}}{\overset{k'_1}{\longrightarrow}} EI.$$

The condition of quasi-steady state for the complex $[EI]$ provides

$$\frac{d[EI]}{dt} = k_1'[E][I] - k_{-1}'[EI] \approx 0,$$

which gives

$$[EI] = \frac{k_1'}{k_{-1}'}[E][I]. \tag{4.24}$$

Expression (4.22) remains valid in this case, the only difference that should be introduced in the reasoning presented in the previous section is that now the total quantity of the enzyme is

$$[E]_0 = [E] + [ES] + [EI]. \tag{4.25}$$

Substituting (4.21), (4.24) into (4.25) we obtain

$$[E]_0 = [E]\left(1 + \frac{[S]}{K_M} + \frac{k_1'}{k_{-1}'}[I]\right).$$

Resolve $[E]$ from this equation and substitute it into (4.22),

$$v = k_2 \frac{[E_0][S]}{K_M + [S] + K_M \frac{k_1'}{k_{-1}'}[I]}.$$

The maximal velocity $v_{\max} = k_2 E_0$ in this case remains the same as in the previous section, then

$$v = \frac{v_{\max}[S]}{K_M + [S] + K_M \frac{k_1'}{k_{-1}'}[I]}.$$

15.3.3 Mixed inhibition

Consider the same chemical reaction (4.18) and the case when inhibitor can bind to both $[E]$ and $[ES]$,

$$E + I \underset{k_{-1}'}{\overset{k_1'}{\longrightarrow}} EI,$$
$$ES + I \underset{k_{-1}''}{\overset{k_1''}{\longrightarrow}} ESI.$$

Conditions for quasi steady states for complexes $[EI]$ and $[ESI]$ are

$$\frac{d[EI]}{dt} = k'_1[E][I] - k'_{-1}[EI] \approx 0,$$
$$\frac{d[ESI]}{dt} = k''_1[ES][I] - k''_{-1}[ESI] \approx 0,$$

which provide

$$[EI] = \frac{k'_1}{k'_{-1}}[E][I], \tag{4.26}$$
$$[ESI] = \frac{k''_1}{k''_{-1}}[ES][I]. \tag{4.27}$$

The total quantity of the enzyme is

$$[E]_0 = [E] + [ES] + [EI] + [ESI]. \tag{4.28}$$

Substituting (4.21), (4.26) and (4.27) into (4.28) we obtain

$$[E]_0 = [E]\left(1 + \frac{[S]}{K_M}\left(1 + \frac{k''_1}{k''_{-1}}[I]\right) + \frac{k'_1}{k'_{-1}}[I]\right).$$

Resolve $[E]$ from this equation and substitute it into (4.22),

$$v = k_2 \frac{[E_0][S]}{K_M + [S]\left(1 + \frac{k''_1}{k''_{-1}}[I]\right) + K_M \frac{k'_1}{k'_{-1}}[I]}.$$

When $[S]$ tends to infinity very small amount of free inhibitor remains, thus $[I] \to 0$. The maximal velocity is then as before $v_{\max} = k_2 E_0$, so

$$v = \frac{v_{\max}[S]}{K_M + [S]\left(1 + \frac{k''_1}{k''_{-1}}[I]\right) + K_M \frac{k'_1}{k'_{-1}}[I]}.$$

We demonstrated how Michaelis-Menten mechanism is applied to describe kinetics of chemical reactions. In the next section we describe the metabolism of AraC using this approach.

15.4 Metabolism of AraC

Metabolism scheme of AraC is presented in Figure 44. The enzymatic paths of AraC me-

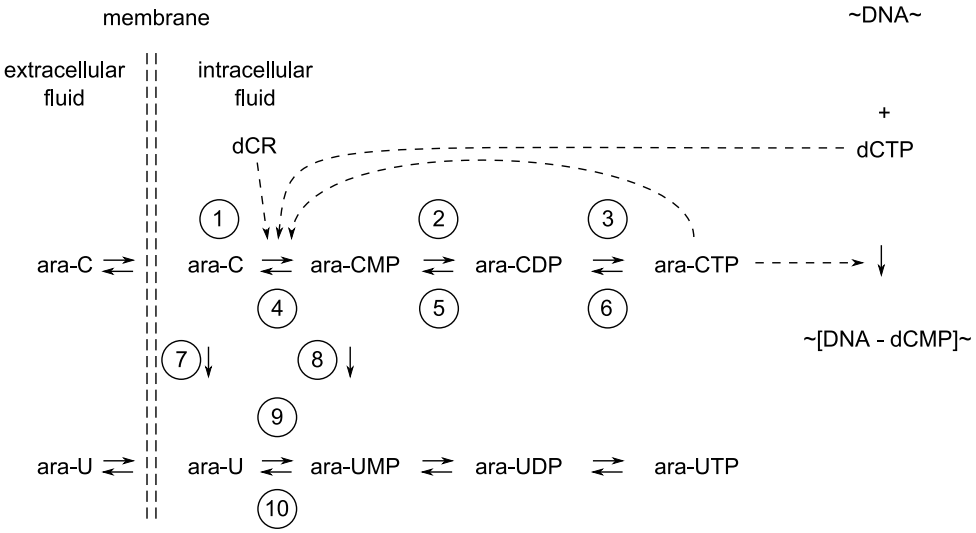

FIGURE 44 – The metabolism of AraC, adapted from [76].

tabolism are the same as that of deoxycytidine dC [73]. AraC should pass through three steps of phosphorylation to form its active metabolite AraC triphosphate (AraCTP), which arrests the DNA synthesis and thus prevents cells from proliferating.

Let us briefly present the most important components of the metabolism. Monophosphorylation is catalysed by deoxycytidine kinase (dCK). This step of AraC phosphorylation is rate determining. The activity of dCK is inhibited by dCTP (regulation by retroinhibition) and AraCTP. The phosphate is taken from ATP (adenosine triphosphate) and UTP (uridine triphosphate), see [11, 101] for more details. The diphosphorylation and triphosphorylation are catalysed by other kinases and the phosphate is taken from ATP. These two stages go fast with respect to the monophosphorylation. Dephosphorylation AraCMP $\rightarrow$ AraC is catalysed by 5'-nucleotidases [6]. Deamination AraC $\rightarrow$ AraU is catalysed by cytidine deaminase (CDA). Deamination AraCMP $\rightarrow$ AraUMP is catalysed by deoxycytidilate deaminase (dCMPDA). This step of the deamination is of secondary importance and is not introduced in the model. The phosphorylation AraU $\rightarrow$ araUMP is observed *in vitro*. In human leukaemic cells this phosphorylation is not observed, the only source of AraUMP, which accumulates in cells, is due to deamination of AraCMP by dCMPDA.

First step of AraC phosphorylation, which is catalysed by dCK, is of particular importance. Its mixed kinetics for AraC phosphorylation appears in Figure 45. Deoxycytidine kinase is

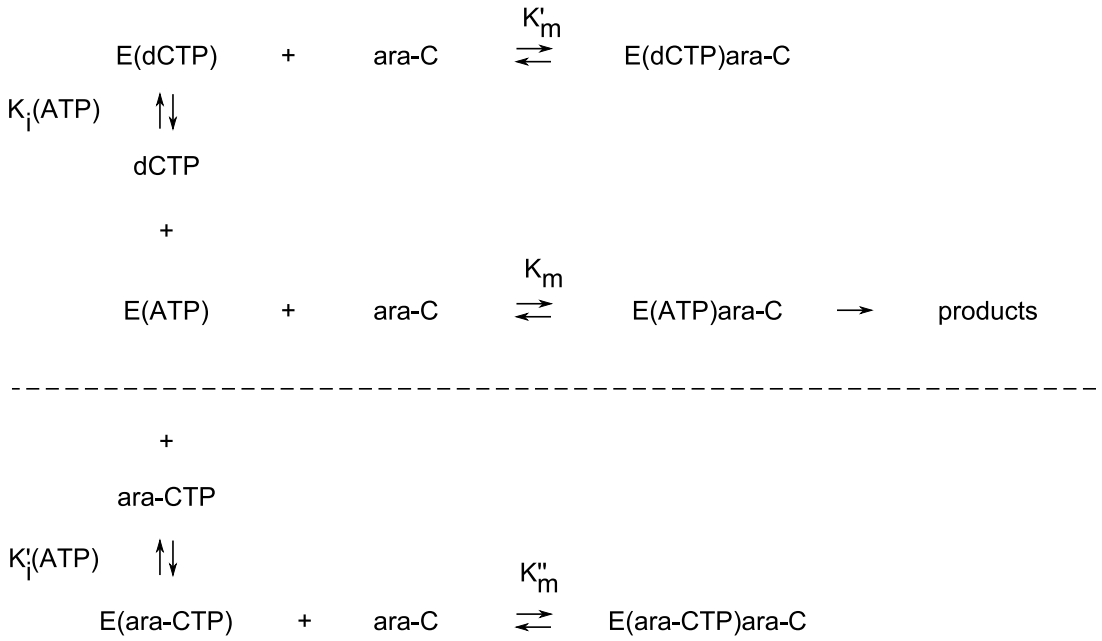

FIGURE 45 – The monosubstrate kinetics of deoxycytidine kinase and AraC at saturating levels of ATP. The equilibrium constants are given here in the mixed inhibition notation used commonly in enzyme kinetics. The figure is adapted from [76].

inhibited by both dCTP and AraCTP. Normal substrate, deoxycytidine (dC), is also an inhibitor of the enzyme with respect to AraC phosphorylation. dCTP and AraCTP form a complex with dCK that interferes with AraC.

Let us describe the first step of phosphorylation using Michaelis-Menten kinetics for mixed inhibition as explained in Section 15.3. Introduce the following notations,

- a_{mi} – intracellular AraC concentration ;
- ap_3 – intracellular AraCTP concentration ;
- ap_1, ap_2 – AraCMP and AraCDP concentrations respectively ;
- c – dCTP (deoxycytidine triphosphate) concentration ;
- dC – deoxycytidine concentration ;

Then phosphorylation rate of AraC is given by

$$\dot{r}_p \equiv \left[\frac{d(ap_1+ap_2+ap_3)}{dt}\right]_p = \frac{V_k}{1+\frac{K_m}{a_{mi}}\left(1+\frac{c}{K_i}+\frac{dC}{K_I}+\frac{ap_3}{K_i'}\right)+K_m\left(\frac{c}{K_iK_m'}+\frac{ap_3}{K_i'K_m''}\right)}, \tag{4.29}$$

where K_I is the deoxycytidine inhibitor constant, K_m is the competitive Michaelis-Menten constant, K_i, K_i', K_m', K_m'' are mixed inhibition constants, V_k is the kinase activity. It should be noted that in the left part of (4.29) we should write the sum of all three forms of AraC. This is because two other steps of phosphorylation go very fast with respect to the first step and, thus, a part of obtained by phosphorylation AraCMP is transmitted rapidly to AraCDP and AraCTP. We can suppose that the fractions ap_3/ap_2 and ap_2/ap_1 are constant,

$$\frac{ap_3}{ap_2}=\alpha_1, \quad \frac{ap_2}{ap_1}=\alpha_2,$$

which provides

$$\dot{r}_p = \left(1+\frac{1}{\alpha_1}+\frac{1}{\alpha_1\alpha_2}\right)\frac{d\,ap_3}{dt}.$$

The $5'$-nucleotidase is the most important enzyme that catalyses the dephosphorylation of AraCMP $\rightarrow$ AraC. We do not consider mixed inhibition for this enzyme, hence the dephosphorylation rate of intracellular AraC is given by a simple Michaelis-Menten equation,

$$\dot{r}_{dp} \equiv \left[\frac{d(ap_1+ap_2+ap_3)}{dt}\right]_{dp} = \left(1+\frac{1}{\alpha_1\alpha_2}+\frac{1}{\alpha_1}\right)\left[\frac{d\,ap_3}{dt}\right]_{dp} = \frac{V_{dp}}{1+\frac{\alpha_1\alpha_2K_{dp}}{ap_3}}, \tag{4.30}$$

where K_{dp} is the Michaelis constant, V_{dp} is the nucleotidase activity, $\frac{ap_3}{\alpha_1\alpha_2}=ap_1$.

The last component, which we take into account, is deamination AraC $\rightarrow$ AraU. We consider the deamination only by cytidine deaminase (CDA) and other mechanisms are omitted due to their minor effects. To describe it we use a simple Michelis-Menten equation,

$$\dot{r}_{da} = \frac{da}{dt} = \frac{V_{da}}{1+\frac{K_{da}}{a_{mi}}}, \tag{4.31}$$

where K_{da} is the Michaelis constant and V_{da} is CDA activity.

The overall kinetics of intracellular AraC is then described by the following equation,

$$\frac{da_{mi}}{dt} = -\dot{r}_p + \dot{r}_{dp} - \dot{r}_{da}.$$

Taking into account transmembrane transport (see Section 15.2) of AraC this equation becomes

$$\frac{da_{mi}}{dt} = k_{hENT1}(a_m - a_{mi}) - \dot{r}_p + \dot{r}_{dp} - \dot{r}_{da}, \tag{4.32}$$

where a_m is extracellular AraC concentration in bone marrow. Denote for brievity,

$$\widetilde{\alpha} = \left(1 + \frac{1}{\alpha_1} + \frac{1}{\alpha_1\alpha_2}\right). \tag{4.33}$$

Then, dynamics of intracellular AraCTP (ap_3) is described by the following equation,

$$\frac{dap_3}{dt} = (\dot{r}_p - \dot{r}_{dp})/\widetilde{\alpha}. \tag{4.34}$$

Hence Equations (4.29)-(4.34) describe intracellular kinetics of AraC and AraCTP inside bone marrow cells. Let us note that AraCTP consumption due to its incorporation into DNA is not included into the model, which can slightly modify AraCTP kinetics.

15.5 Resistances

Several mechanisms of resistance to AraC are known nowadays, deficiency of transmembrane transport, problems with dCK kinase and high CDA activity, which deaminate AraC to its inactive form AraU. It has been demonstrated that relapsed leukaemia patients show decreased dCK mRNA expression [59]. In addition, reduced dCK mRNA expression and a deficiency of functional dCK have often been associated with resistance to AraC [82]. The deamination of AraC into AraU by CDA prevents the formation of AraCTP and decreases the cytotoxicity of AraC. In [60] the authors concluded that decreased hENT-1 expression and function is responsible for the acquisition of Ara-C resistance. In Section 17.2 we study numerically these mechanisms of resistance.

16 Pharmacodynamics modelling

Pharmacodynamics describes what drug does to organism. In Section 14 we introduced System (4.7) that describes a model of cell populations, in which a population of malignant and a population of normal cells are considered. We introduced self-renewal, differentiation and apoptosis rates for each cell population. AraCTP exerts cytotoxic effect on all dividing cells arresting DNA synthesis. This results in increased apoptosis rate and reduced proliferation rate. We describe drug action as a dependence of the three rates on AraCTP concentration,

$$s = s(ap_3), \quad d = d(ap_3), \quad a = a(ap_3), \tag{4.35}$$

where $s(ap_3)$ and $d(ap_3)$ are decreasing bounded functions. Hill functions can be used to describe such dependencies. Let us denote rates of self-renewal, differentiation and apoptosis by s^*, d^*, a^* for population of normal cells and by s^*_m, d^*_m, a^*_m for population of malignant cells in non-treated case, which provides,

$$s(0) = s^*, \quad d(0) = d^*, \quad a(0) = a^*.$$

17 Simulations

In previous sections of this chapter we constructed WBPBPK/PD model that consists of cell population dynamics (4.7), AraC distribution in the body (4.16)-(4.17), Equations (4.29)-(4.34) describing AraC metabolism inside bone marrow cells and drug action described by Equation (4.35). In Section 17.1 we present simulations of the Whole Body Physiologically Based PharmacoKinetic (WBPBPK) model. The simulations demonstrate AraC distribution in the body and kinetics of AraCTP (AraC active form) under some protocols of administration, including high-dose and standard dose AraC. We introduce the notions of minimal cytotoxic and cytostatic AraCTP concentrations and study the efficacy of treatment with respect to them. In Section 17.2 we present simulations of WBPBPK model within resistant cells. Then, in Section 17.3 we present PK/PD model of AraC, which provides the dynamics of malignant as well as of normal bone marrow cells under chemotherapy treatment.

17.1 WBPBPK model

Let us first introduce parameters of metabolism scheme, their values are taken from [76] and correspond to AraC metabolism in mice, see Table 6. In Section 15.4 we introduced two

TABLE 6 – Parameter values of the metabolism scheme of AraC.

Parameter		Value	Unit
V_k	deoxycytidine kinase activity	1.28	μM.min^{-1}
K_m		27.0	μM
K_i		1.0	μM
K_i'		17.9	μM
K_I		0.84	μM
K_m'		309	μM
K_m''		101.9	μM
V_{dp}	nucleotidase activity	300	μM.min^{-1}
K_{dp}	Michaelis-Menten constant	900	μM
V_{da}	CDA activity	16.45	μM.min^{-1}
K_{da}	Michaelis-Menten constant	1011.7	μM

parameters, α_1 and α_2 which denote proportions between concentrations AraCTP/AraCDP and AraCDP/AraCMP respectively. We took the following values for them, $\alpha_1 = 7.83$ and $\alpha_2 = 5.67$, which provided $\widetilde{\alpha} = 1.30$, see (4.33). Deoxycytidine triphosphate (dCTP) concentration was supposed to equal 10μM and deoxycytidine concentration (dC) equals to 4μM.

Two phases of AraC distribution in the body can be distinguished. Each stage is characterised by its own half-life and different processes interfere into its fate. Once administered in the blood, AraC is distributed between different compartments and penetrates into cells. Clearance is also present during this initial phase, but is less important than physiological processes. On the second phase, when drug concentrations are equalised in different compartments and inside cells, clearance becomes important. Secondary half-life, which represents AraC clearance, is known to equal one to three hours. We choose two hours, which provides $\gamma_b = 0.0058\text{min}^{-1}$. We suppose that AraC clearance in the blood and in the bone marrow is the same, $\gamma_m = 0.0058\text{min}^{-1}$. In Section 6.2.1 we presented how to obtain clearance constant γ of a degradating substance if its half-life is known.

Let us now describe transmembrane transport. To determine the rate of transmembrane penetration, we introduce the notion of half-exchange. Let us explain it. Consider a substrate that

is able to penetrate through cell membrane. Suppose that its transmembrane transport rate is constant and equals k. The exchange stops when intracellular and extracellular concentrations are equal, otherwise it goes from the compartment with greater concentration to that with lower concentration. Denote by $c_e(t)$ and $c_i(t)$ respectively its extracellular and intracellular concentrations at time t. Then, the substrate behaviour can be described by the following equations,

$$\frac{dc_i(t)}{dt} = k(c_e(t) - c_i(t)), \quad \frac{dc_e(t)}{dt} = k(c_i(t) - c_e(t)). \tag{4.36}$$

The total concentration of the substrate remains constant, denote it by c_T. Then, $c_e(t) = c_T - c_i(t)$. Substitute it into the first equation of (4.36),

$$\frac{dc_i(t)}{dt} = k(c_T - 2c_i(t)).$$

The solution is given by

$$c_i = \frac{c_T}{2} - \frac{c_{i0}}{2}e^{-2kt}, \quad c_e = \frac{c_T}{2} + \frac{c_{i0}}{2}e^{-2kt}.$$

This provides $c_e(t) - c_i(t) = c_{i0}e^{-2kt}$. At time $t_0 = 0$ the difference is $c_e(0) - c_i(0) = c_{i0}$. We call the half-exchange time, the time T_2 such that

$$c_e(T_2) - c_i(T_2) = \frac{1}{2}\left(c_e(0) - c_i(0)\right),$$

i.e. the time after which the difference between intracellular and extracellular concentrations is decreased twice. This provides

$$k = \frac{\ln 2}{2T_2}.$$

This formulae allows the estimation of constant k_{hENT1} in Equation (4.17). We suppose that the difference between intracellular and extracellular concentrations decreases twice in a half an hour, i.e. half-exchange time equals 30 minutes. Then, we obtain $k_{hENT1} = 0.0116\text{min}^{-1}$.

In [76] the authors determined limits of cytotoxic and cytostatic effects of AraCTP. As minimum cytotoxic level of AraCTP concentration, below which AraCTP is no more cytotoxic, they determined 1μM. As minimum cytostatic level of AraCTP concentration 0.1μM was deter-

mined. With this concentration, AraCTP is supposed to inhibit 50% of DNA synthesis. Thus for the simulations, we assume that AraC treatment kills cells when intracellular AraCTP concentration is above 1μM. Cytostatic effect is not included in the model.

Results of simulations of different regimens of AraC administration are presented in Figure 46 and Figure 47. Figure 46 demonstrates kinetics of AraC in blood, bone marrow and inside bone marrow cells as well as kinetics of intracellular AraCTP concentrations. For standard protocol (200mg/m^2), AraC is cytotoxic during about 7 hours (Panel A), for high-dose protocol (3g/m^2), AraC is cytotoxic during about 14 hours (Panel B). Let us note that high dose of AraC represents 15-fold standard dose of AraC. Panel C demonstrates that similar cytotoxic effect can be obtained through two standard dose injections of AraC, one at the beginning and another after 7 hours after the first dose. Similar cytotoxic effect can be obtained through three injections of 100mg/m^2 at hours 0, 4 and 10, which divides the amount of administered drug by 10 with respect to high-dose. Hence, our model suggests that high-dose regimen can be not benefit for patients, taking into account many side effects that emerge during chemotherapy. Figure 47 demonstrates another treatment protocol, with continuous infusion of AraC, that allows obtaining similar cytotoxic effect as high-dose treatment.

Standard protocol used in induction therapy on patients diagnosed with AML consists of 100-200mg/m^2/day given in bolus (impulse doses) or as continuous intravenous infusion during first 7 days. AraC is generally given in combination with daunorubicin. Results of simulations of standard protocol are presented in Figure 48.

17.2 Pharmacokinetics of AraC within resistant cells

As discussed in Section 15.5, three mechanisms of resistance are known nowadays, decreased dCK activity, problems with transmembrane transport and high deamination rate of AraC to its inactive form AraU. In this section we carry out simulations which describe these mechanisms.

In normal cells we use the following parameter values, dCK activity is $V_k^n = 1.28\mu$M.min^{-1}, half-exchange time equals 30 minutes, which provides $k_{hENT1}^n = 0.0116$min^{-1} and cytidine deaminase activity equals $V_{da}^n = 16.45\mu$M.min^{-1}. We consider the three sources of resistance

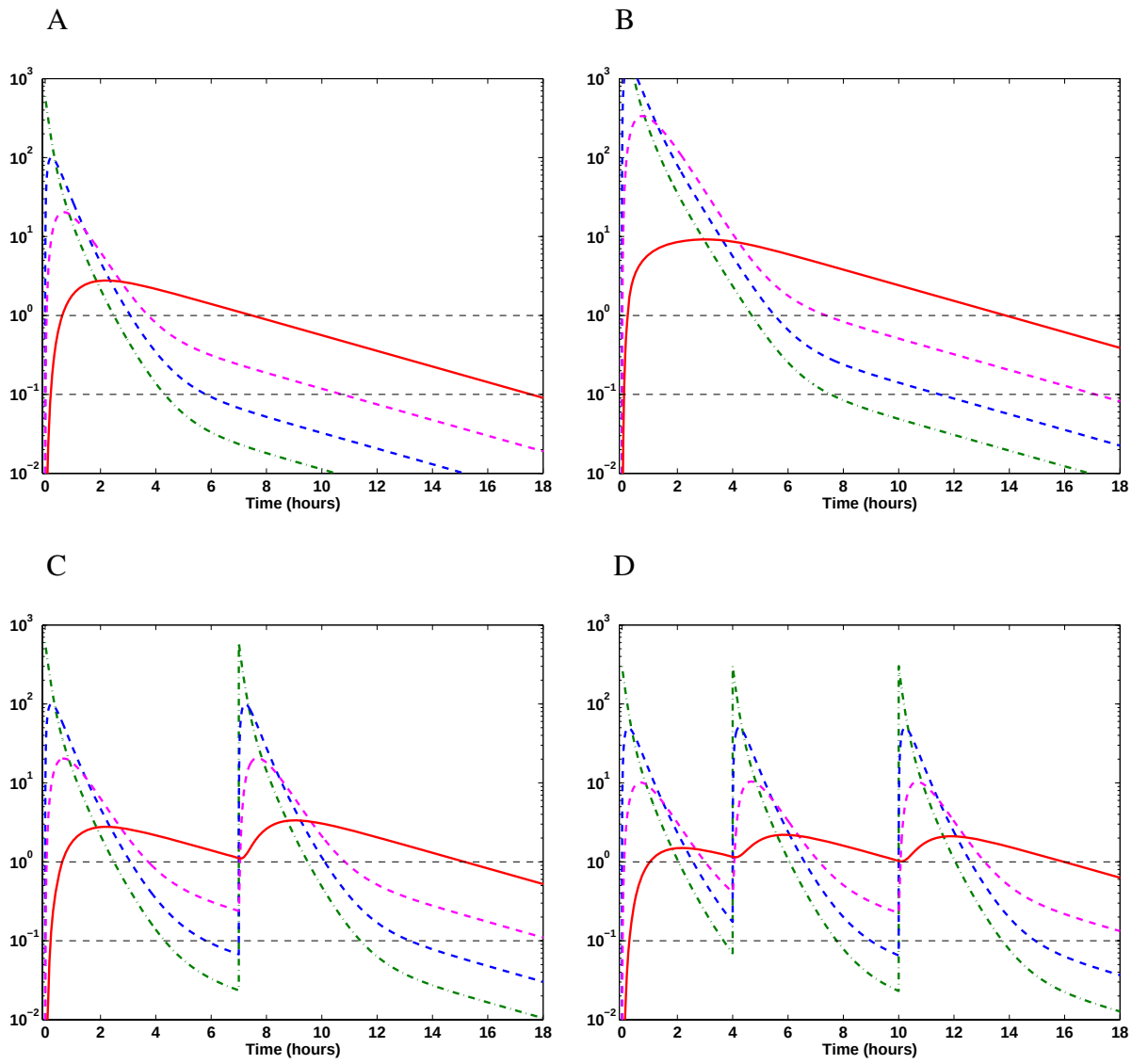

FIGURE 46 – WBPBPK modelling of AraC. Panel A : Standard dose treatment (200mg/m^2), Panel B : High dose treatment (3g/m^2). Panel C : Two injections of standard dose of AraC (200mg/m^2) at hours 0 and 7. Panel D : Three injections of low dose of AraC (100mg/m^2) at hours 0, 4 and 10. Parameters of metabolism are taken for murine L1210 cell line. Red solid lines represent AraCTP concentration, green dash-dot lines represent extracellular AraC concentration in blood, blue dash lines represent extracellular AraC concentration in bone marrow, magenta dash lines represent intracellular AraC concentration in bone marrow cells.

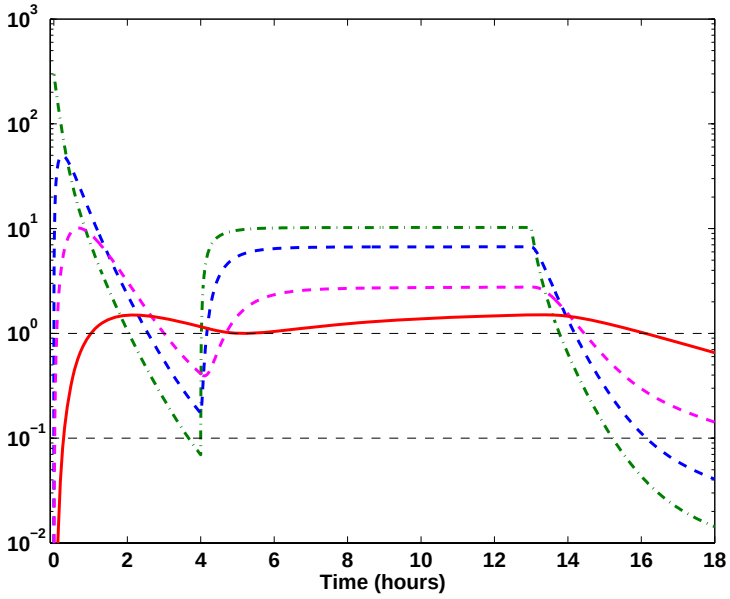

FIGURE 47 – WBPBPK modelling of AraC. Standard dose injection at the beginning (200mg/m^2), followed by continuous infusion of 150mg/m^2 administered during hours 4-13.

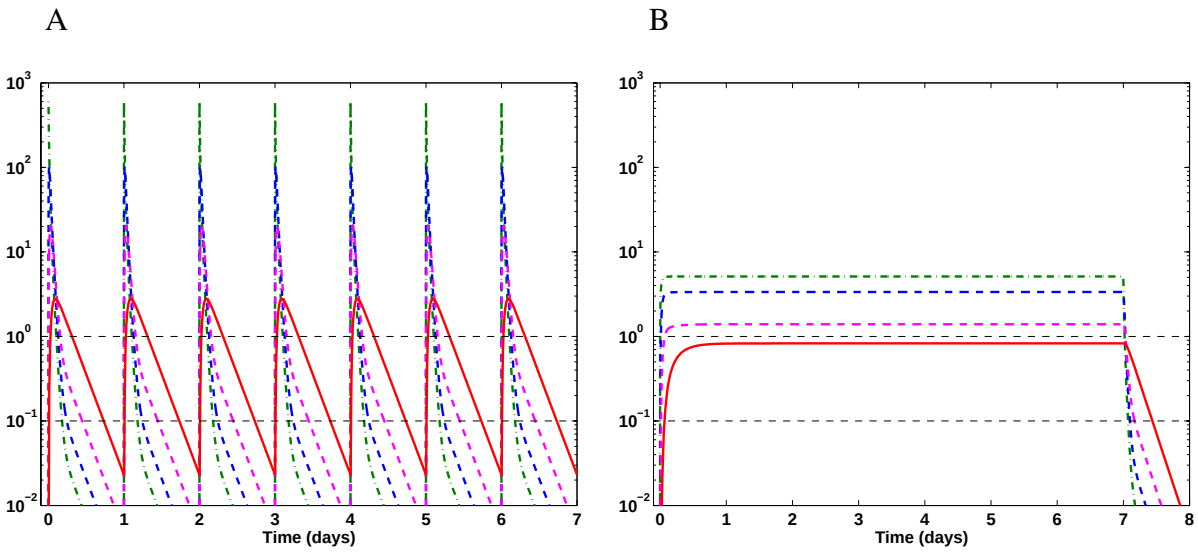

FIGURE 48 – Simulations of AraC/AraCTP kinetics during standard protocol of induction therapy. Panel A : in bolus intravenous injection of standard dose (200mg/m^2) of AraC, Panel B : continuous infusion of standard dose (200mg/m^2) of AraC. Parameters of metabolism are taken for murine L1210 cell line. Red solid lines represent AraCTP concentration, green dash-dot lines represent extracellular AraC concentration in blood, blue dash lines represent extracellular AraC concentration in bone marrow, magenta dash lines represent intracellular AraC concentration in bone marrow cells.

separately. We suppose that dCK activity within resistant cells is twice lower than in normal cells, $V_k^r = V_k^n/2 = 0.64\mu$M.min^{-1}, half-exchange time is doubled, to equal one hours, which provides $k_{hENT1}^r = k_{hENT1}^n/2 = 0.0058$min^{-1} and and deaminase activity is doubled and equals $V_{da}^r = 2V_{da}^n = 32.9\mu$M.min^{-1}. Below we compare AraCTP kinetics within normal cells and within defected cells with three sources of resistances.

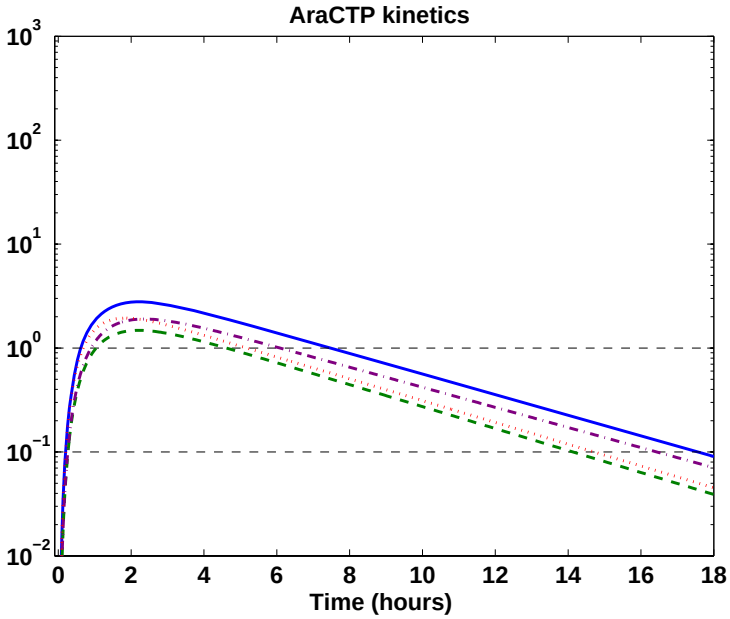

FIGURE 49 – Kinetics of AraCTP within normal cells (blue solid line) and resistance cells. Three types of resistance are considered separately, resistance due to low dCK activity (green dash line), to problems with transmembrane transport (violet dash dot line) and due to high cytidine deaminase activity (red dot line).

Results of simulations for standard dose of AraC are presented in Figure 49. As shown in this Figure, all the three mechanisms of resistance decrease cytotoxic time of AraC and, thus, its efficacy. We can conclude that mechanism of resistance due to dCK deficiency is stronger than the two others, reducing almost twice the period when AraC is cytotoxic.

17.3 PK/PD model

Dynamics of cell sub-populations are defined in (4.7), where rates s, d, a and s_m, d_m, a_m depend on AraCTP concentration. We should then introduce functions $s(ap_3), d(ap_3), a(ap_3)$ and $s_m(ap_3), d_m(ap_3), a_m(ap_3)$. As said above, $s(ap_3), d(ap_3)$ are decreasing bounded functions.

We use Hill functions to describe these dependencies,

$$s(ap_3) = s^* \frac{\theta_s^{n_s}}{\theta_s^{n_s} + ap_3^{n_s}}, \quad d(ap_3) = d^* \frac{\theta_d^{n_d}}{\theta_d^{n_d} + ap_3^{n_d}}, \tag{4.37}$$

where s^* and d^* represent self-renewal and differentiation rates of untreated bone marrow cells. Hence, greater AraCTP concentrations in the body, smaller self-renewal and differentiation rates. Cells killed by AraCTP increase apoptosis rate, which provides

$$a(ap_3) = a^* + s^* \frac{ap_3^{n_s}}{\theta_s^{n_s} + ap_3^{n_s}} + d^* \frac{ap_3^{n_d}}{\theta_d^{n_d} + ap_3^{n_d}}, \tag{4.38}$$

where a^* represents apoptosis rate of untreated bone marrow cells. The rates for malignant cell population are defined by similar functions, denoted respectively by $s_m(ap_3), d_m(ap_3)$ and $a_m(ap_3)$. In previous section we obtained that even during high-dose AraC treatment, intracellular AraCTP concentration does not exceed 10μM. Hence, we assume that functions $s(ap_3)$ and $d(ap_3)$ are only relevant on the interval $ap_3 \in [0, 10]$. Plots of functions $s(ap_3), d(ap_3), a(ap_3)$

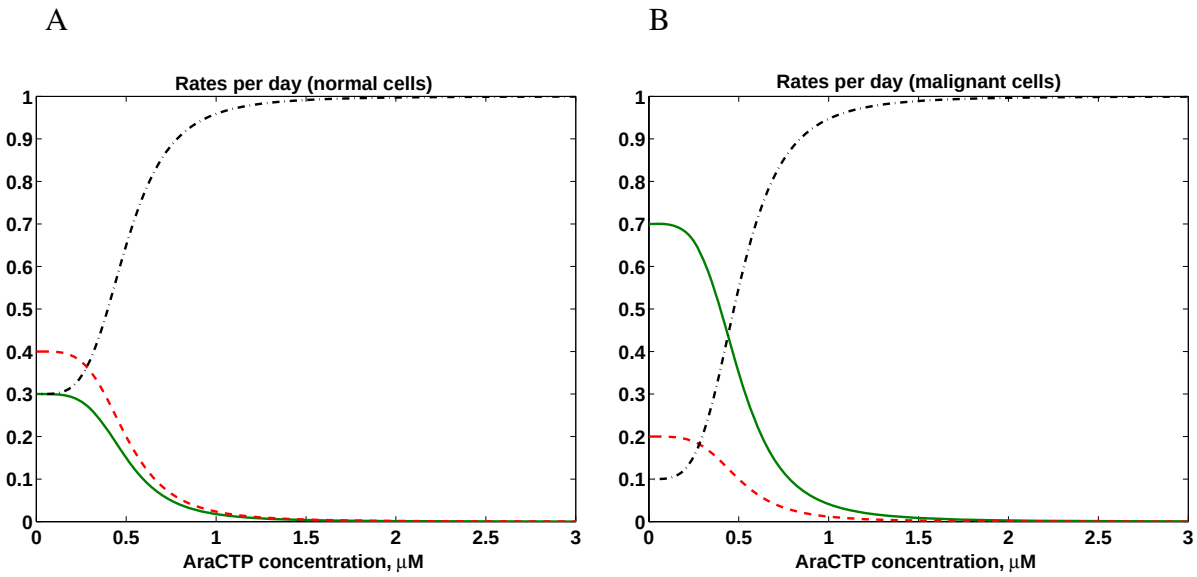

FIGURE 50 – Functions $s(ap_3), d(ap_3), a(ap_3)$ as well as $s_m(ap_3), d_m(ap_3), a_m(ap_3)$ describing self-renewal, differentiation and apoptosis rates of normal and malignant cells as a function of intracellular AraCTP concentration. Panel A : the three rates in sub-population of normal cells, Panel B : the three rates in sub-population of malignant cells. Green solid lines represent self-renewal rates, red dash lines represent differentiation rates, black dash-dot lines represent apoptosis rates.

and $s_m(ap_3), d_m(ap_3), a_m(ap_3)$ can be found in Figure 50, their parameter values are indicated in Table 7. Dynamics of cell populations are presented in Figure 51.

TABLE 7 – Parameters that define how self-renewal, differentiation and apoptosis rates depend on AraCTP concentrations, see (4.37)-(4.38), their plots can be found in Figure 50.

Parameter		Value	Unit
s^*	normal self-renewal rate	0.3	d^{-1}
n_s	sensitivity of $s(ap_3)$	5	N.U.
θ_s	threshold value of $s(ap_3)$	0.5	μM
d^*	normal differentiation rate	0.4	d^{-1}
n_d	sensitivity of $d(ap_3)$	5	N.U.
θ_d	threshold value of $d(ap_3)$	0.5	μM
a^*	normal apoptosis rate	0.3	d^{-1}
s_m^*	normal self-renewal rate	0.7	d^{-1}
n_{sm}	sensitivity of $s_m(ap_3)$	5	N.U.
θ_{sm}	threshold value of $s_m(ap_3)$	0.5	μM
d_m^*	normal differentiation rate	0.2	d^{-1}
n_{dm}	sensitivity of $d_m(ap_3)$	5	N.U.
θ_{dm}	threshold value of $d_m(ap_3)$	0.5	μM
a_m^*	normal apoptosis rate	0.1	d^{-1}

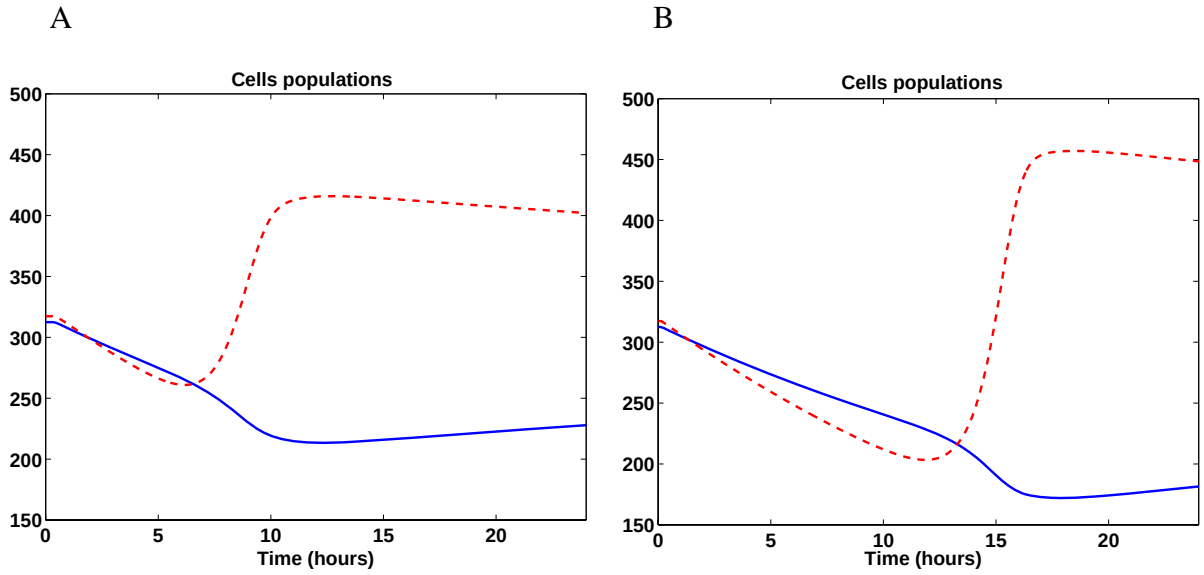

FIGURE 51 – Dynamics of cell populations during standard dose treatment (Panel A) and high dose treatment (Panel B). Blue solid line represents normal cell population, red dash line represents malignant cell population. Kinetics of AraCTP concentrations for these two examples are presented in Figure 46.A-B.

One can notice, even the high-dose protocol does not allow killing all malignant cells. This can be due to the parameter values which are not well estimated. Nevertheless, the dynamics of populations demonstrates that if the administered dose of AraC is increased then all malignant cells are killed and some of the normal cells remain alive (not shown here). On the contrary, if not all malignant cells are removed, then they recover much faster than normal cells, once the chemotherapy effect is over.

18 Discussion

In this chapter we presented a PK/PD model of AML treatment with AraC. We first introduced a model of cell populations, in which we considered a population of normal and a population of malignant cells. We studied steady states of this system and found conditions when leukaemic steady state is stable. Dynamics of cell populations were described by their self-renewal, differentiation and apoptosis rates. Pharmacodynamics was modelled as the dependence of these rates upon AraC active form.

Pharmacokinetics model consists of several parts. We introduced a model of drug distribution between two compartments, blood and bone marrow. Drug penetration through cell membrane was described as passive diffusion. We explained the Michaelis-Menten mechanism on several model reactions and then applied it to describe the AraC metabolism scheme.

We carried out simulations of pharmacokinetic model of the whole body. Several treatment protocols were studied. The values of parameters were chosen to describe AraC metabolism in mice. Simulations have shown different kinetics of AraC and AraCTP concentrations. AraCTP remains longer within cells than AraC. We tested standard dose treatment and high dose treatment. Simulations demonstrated that high dose treatment is not advantageous and can be replaced by several injections of standard dose in order to reduce the overall administered dose and thus its toxicity to organism. We carried out several simulations, in which the total dose is reduced with respect to high-dose and which have similar effect on malignant cells. This allows stating an optimal control problem, to find a treatment protocol with a given administered dose to maximise its efficacy.

We also studied numerically AraC distribution within resistant cells. We considered sepa-

rately three possible mechanisms of resistance (due to transmembrane transport, due to dCK deficiency and due to increased CDA activity). We concluded with simulations of PK/PD model.

Thus, the model presented in this chapter can serve as a basis of the modelling of AML treatment with AraC. It can be used to describe treatment of humans. To do so, the values of parameters should be experimentally estimated.

Cinquième partie

Conclusions and Perspectives

This PhD thesis is devoted to mathematical modelling of haematopoiesis and blood diseases. We investigated several models, which consider different aspects of blood production process.

First we studied a multi-scale model of erythropoiesis in which we coupled intracellular protein interactions, which determine cell behaviour, with dynamics of cell sub-populations. The model allowed the evaluation of the roles of different feedback mechanisms in response to stress erythropoiesis.

We studied spatial distribution of cells in bone marrow, using a system of reaction-diffusion-convection equations. We demonstrated the existence of a solution of this system and computed the speed of propagation of malignant cells. Bone marrow cells exchange different signals that regulate cell behaviour. We considered an integro-differential equation which describes cell communication. We proved the existence of travelling wave solutions using topological degree and the Leray-Schauder method. Individual based approach was used to study mechanical cell interactions and cell distributions in bone marrow. Using this approach we demonstrated that cell division can result in random cell motion.

Erythropoiesis can sometimes exhibit disorders, such as excessive proliferation of immature cells, as observed in acute leukaemias. We then considered a physiologically based pharmacokinetics-pharmacodynamics model of treatment of acute myeloid leukaemia with AraC. We investigated numerically pharmacokinetics of AraC and efficacy of several treatment protocols. Below we discuss possible perspectives for this work.

Multiscale modelling of haematopoiesis. The intracellular regulatory network studied in this work is simplified. A more sophisticated model can be considered (Figure 52). Every protein-protein interaction can be presented as a chemical reaction. Taking into account particular conditions of these interactions, they could be described by different chemical kinetics mechanisms (Michaelis-Menten kinetics, law of mass action, etc.). However, such a regulatory network would necessitate to go deeper in the nature of proteins involved in erythropoiesis regulation and their interactions. Although meaningful, such an approach will also add complexity to the model. It is however expected to obtain in a future work a more precise model of intracellular regulatory mechanisms.

In this work we assumed that all erythroid progenitors with the same maturity had similar

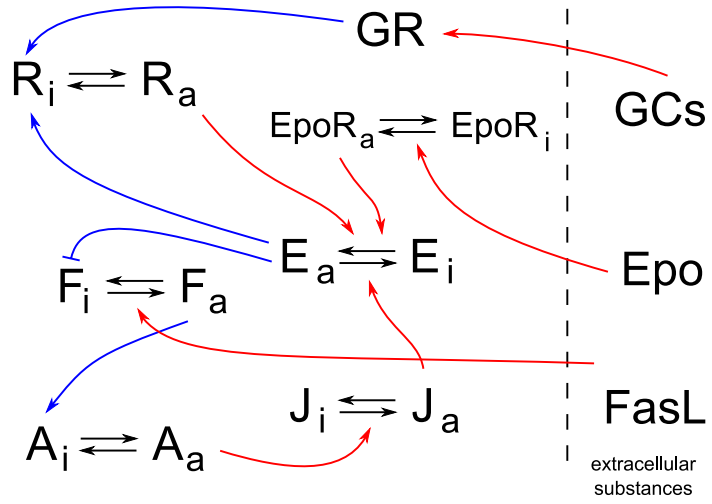

FIGURE 52 – Intracellular regulatory network that controls erythroid progenitor fate. Red flashes represent fast reactions, blue flashes represent slow reactions. For notations, see Section 3.

concentrations of Erk and Fas. Thus, our model does not take into account stochasticity in these expressions, which can play an important role in the regulation of erythropoiesis. One of the appropriate approaches that would allow taking into account the stochasticity is the individual based modelling, presented in Chapter III. It considers each cell as an independent element of the whole system and, consequently, every cell can have its own properties and protein concentrations.

It is known that Epo level rises due to the lack of haemoglobin. In this work we did not consider haemoglobin and we assumed that erythrocyte count alters Epo levels (thus implicitly supposing that erythrocyte count and haemoglobin are linearly dependent). Nevertheless, as shown in [29], there is no linear dependence between haemoglobin and erythrocyte (or red blood cell) count during anaemia. This point can be relevant for the modelling of the response to anaemia. Studies like [5, 115] can clarify dependencies between haemoglobin, erythrocyte count and reticulocyte count in stress erythropoiesis. It should be noted as well that during anaemia there is no clear distinctions between erythrocytes and circulating reticulocytes, both circulate in the blood and fulfil functions of red blood cells. Here, we only considered erythrocytes to be red blood cells, which is not exact. Reticulocytes also contain haemoglobin but in smaller volumes. Another point is that no information is currently available about how sensiti-

vity to Epo evolves with maturation. All these aspects of Epo regulation should be investigated to improve erythropoiesis modelling.

Spatial modelling of haematopoiesis. Spatial models of haematopoiesis considered in this work are generic from the mathematical point of view but do not take into account detailed biological mechanisms. In the future we will consider more specific models that allow taking into account more biological information.

Individual based modelling. The software presented in this work takes into account mechanical cell interactions. Nevertheless, it is well known that chemical interactions between cells can play an important role for cell population behaviour. Moreover, cell proliferation is controlled by certain extracellular substances, such as nutrients, oxygen, growth factors, etc. Thus, introducing chemical interactions between cells into the modelling as well as cell interactions with extracellular substances will allow approaching the biological reality of the processes under consideration.

One of the applications of the software is modelling of haematopoiesis and, in particular, of erythropoiesis. As we demonstrated in Chapter I, during erythropoiesis cell behaviour crucially depends on the intracellular regulatory network. This regulatory network is controlled by growth factors, which are extracellular substances, and by some enzymes which are expressed on the surface of mature cells. This means that cell fate depends also on neighbouring cells. Considering the intracellular regulatory network for every single cell would additionally improve the individual based modelling.

PK/PD modelling. The considered PK/PD model of AML treatment with AraC consisted of two parts, drug pharmacokinetics and pharmacodynamics. In order to describe the pharmacodynamics, we introduced two interacting between each other cell populations, a population of normal and a population of malignant cells. Drug action on cell proliferation was modelled by a simple dependence of the proliferation and apoptosis rates on the concentration of drug active form. This is a simplified pharmacodynamics model. Considering several sub-populations of malignant and of normal cells depending on the cell cycle phase (including quiescent cells) will

allow introducing a cell cycle model. In this more precise model, we can take into account that the considered drug is a cycle active agent and kills only cells that are in S-phase.

The metabolism scheme is well described in the model. To carry out simulations, we considered the values of parameters that describe murine metabolism. Although the scheme of metabolism remains similar for humans, chemical constants are not the same, they should be estimated experimentally. Thresholds of cytotoxic and cytostatic effects will also change. In the present model we did not consider cytostatic effect of the drug, which should also be taken into account.

When we describe drug distribution in the body, in order to reduce the number of constants to estimate, we considered two compartments, blood and the bone marrow. To study a more precise model of drug distribution we can introduce additional compartments. To estimate all the necessary constants, experimental data will be needed.

Bibliographie

[1] A.S. Ackleh, K. Deng, C.E. Cole, and H.T. Tran, *Existence-uniqueness and monotone approximation for an erythropoiesis age-structured model*, J. Math. Anal. Appl. **289** (2004), 530–544.

[2] A.S. Ackleh, K. Deng, K. Ito, and J. Thibodeaux, *A structured erythropoiesis model with nonlinear cell maturation velocity and hormone decay rate*, Mathematical Biosciences **204** (2006), 21–48.

[3] M. Adimy and F. Crauste, *Modelling and asymptotic stability of a growth factor-dependent stem cells dynamics model with distributed delay*, Discrete Cont. Dyn. Syst. Ser. B **8** (2007), 19–38.

[4] E. Afenya, *Acute leukemia and chemotherapy : a modeling viewpoint*, Mathematical biosciences **138** (1996), 79–100.

[5] N.H. Al-Huniti, J.A. Widness, R.L. Schmidt, and P. Veng-Pedersen, *Pharmacodynamic analysis of changes in reticulocyte subtype distribution in phlebotomy-induced stress erythropoiesis*, Journal of Pharmacokinetics and Pharmacodynamics **32** (2005), 359–376.

[6] A. Amici, M. Emanuelli, G. Magni, N. Raffaelli, and S. Ruggieri, *Pyrimidine nucleotidases from human erythrocyte possess phosphotransferase activities specific for pyrimidine nucleotides*, FEBS Lett. **419** (1997), 263–267.

[7] A.R.A. Anderson, K.A. Rejniak, P. Gerlee, and V. Quaranta, *Modelling of cancer growth, evolution and invasion : Bridging scales and models*, Math. Model. Nat. Phenom. **2** (2007), 1–27.

[8] A. Aouba, F. Péquignot, A. Le Toullec, and E. Jougla, *Les causes médicales de décès en france en 2004 et leur évolution / medical causes of death in france in 2004 and*

trends 1980-2004 (english abstract), Bulletin épidémiologique hebdomadaire de l'INVS (2007), 305–316.

[9] N. Apreutesei, A. Ducrot, and V. Volpert, *Competition of species with intra-specific competition*, Math. Model. Nat. Phenom. **3** (2008), 1–27.

[10] ———, *Travelling waves for integro-differential equations in population dynamics*, Discrete Cont. Dyn. Syst. Ser. B **11** (2009), 541–561.

[11] E.S. Arnér and S. Eriksson, *Mammalian deoxyribonucleoside kinases*, Pharmacol. Ther. **67** (1995), 155–186.

[12] H.T. Banks, C.E. Cole, P.M. Schlosser, and H.T. Tran, *Modeling and optimal regulation of erythropoiesis subject to benzene intoxication*, Mathematical biosciences and engineering **1** (2004), 15–48.

[13] A. Bauer, F. Tronche, O. Wessely, C. Kellendonk, H.M. Reichardt, P. Steinlein, G. Schutz, and H. Beug, *The glucocorticoid receptor is required for stress erythropoiesis*, Genes Dev. **13** (1999), 2996–3002.

[14] Swenson CE. Bayne WF, Mayer LD, *Pharmacokinetics of cpx-351 (cytarabine/daunorubicin hcl) liposome injection in the mouse*, J. Pharm. Sci. **98** (2009), 2540–2548.

[15] J. Bélair, M.C. Mackey, and J.M. Mahaffy, *Age-structured and two delay models for erythropoiesis*, Math. Biosci. **128** (1995), 317–346.

[16] M.C. Béné, M. Bernier, G. Castoldi, G.C. Faure, W. Knapp, W.D. Ludwig, E. Matutes, A. Orfao, and M. van't Veer, *Impact of immunophenotyping on management of acute leukemias*, Haematologica **84** (1999), 1024–1034.

[17] S. Bernard, J. Bélair, and M.C. Mackey, *Oscillations in cyclical neutropenia : new evidence based on mathematical modeling*, J. Theor. Biol. **2003** (223), 283–298.

[18] M. Bessis, C. Mize, and M. Prenant, *Erythropoiesis : Comparison of in vivo and in vitro amplification*, Blood Cells **4** (1978), 155–174.

[19] N. Bessonov, F. Crauste, I. Demin, and V. Volpert, *Dynamics of erythroid progenitors and erythroleukemia*, Math. Model. Nat. Phenom. **4** (2009), 210–232.

[20] N. Bessonov, I. Demin, L. Pujo-Menjouet, and V. Volpert, *A multi-agent model describing self-renewal or differentiation effect of blood cell population*, Mathematical and computer modelling **49** (2009), 2116–2127.

[21] N. Bessonov, L. Pujo-Menjouet, and V. Volpert, *Cell modelling of hematopoiesis*, Math. Model. Nat. Phenom. **1** (2006), 81–103.

[22] D. Bonnet, *Haematopoietic stem cells*, Pathol. **197** (2002), 430–440.

[23] N.F. Britton, *Spatial structures and periodic travelling waves in an integro-differential reaction-diffusion population model*, SIAM J. Appl. Math. **6** (1990), 1663–1688.

[24] T. Büchner, C. Schoch, T. Haferlach, M.C. Sauerland, and A. Heinecke, *Acute myeloid leukaemia (aml) : treatment of the older patient*, Best Practice and Research Clinical Haematology **14** (2001), 139–151.

[25] L. Bueno, D.P. de Alwis, C. Pitou, J. Yingling, M. Lahn, S. Glatt, and I.F. Trocóniz, *Semi-mechanistic modelling of the tumour growth inhibitory effects of LY2157299, a new type I receptor TGF-β kinase antagonist, in mice*, European Journal of Cancer **44** (2008), 142–150.

[26] H.M. Byrne and D. Drasdo, *Individual-based and continuum models of growing cell populations : a comparison.*, J. Math. Biol. **58** (2009), 657–687.

[27] V. Capasso and D. Bakstein, *An introduction to continuous-time stochastic processes. theory, models, and applications to finance, biology, and medicine series : modeling and simulation in science, engineering and technology*, Birkhuser Boston, Inc., Boston, MA, 2005.

[28] D. Chappell, P.A. Tilbrook, T. Bittorf, S.M. Colley, G.T. Meyer, and S.P. Klinken, *Prevention of apoptosis in J2E erythroid cells by erythropoietin : involvement of JAK2 but not MAP kinases*, Cell Death Differ. **4** (1997), 105–113.

[29] S. Cherukuri, N.A. Tripoulas, S. Nurko, and P.L. Fox, *Anemia and impaired stress-induced erythropoiesis in aceruloplasminemic mice*, Blood Cells, Molecules, and Diseases **33** (2004), 346–355.

[30] V. Chickarmane, T. Enver, and C. Peterson, *Computational modeling of the hematopoie-*

tic erythroid-myeloid switch reveals insights into cooperativity, PLoS Comput. Biol. **5** (2009), doi :10.1371/journal.pcbi.1000268.

[31] J. Clairambault, *Modelling physiological and pharmacological control on cell proliferation to optimise cancer treatments*, Math. Model. Nat. Phenom. **4** (2009), doi :10.1051/mmnp :20083701.

[32] C. Colijn and M.C. Mackey, *A mathematical model of haematopoiesis-i. periodic chronic myelogenous leukemia*, J. Theor. Biol. **237** (2005), 117–132.

[33] _____, *A mathematical model of haematopoiesis-ii. cyclical neutropenia*, J. Theor. Biol. **237** (2005), 133–146.

[34] C. Crauste, I. Lefebvre, M. Hovaneissian, J.Y. Puy, B. Roy, S. Peyrottes, S. Cohen, J. Guitton, C. Dumontet, and C. Perigaud, *Development of a sensitive and selective LC/MS/MS method for the simultaneous determination of intracellular 1-beta-d-arabinofuranosylcytosine triphosphate (araCTP), cytidine triphosphate (CTP) and deoxycytidine triphosphate (dCTP) in a human follicular lymphoma cell line*, J. Chromatogr. B Analyt. Technol. Biomed. Life Sci. **877** (2009), 1417–1425.

[35] F. Crauste, I. Demin, O. Gandrillon, and V. Volpert, *Mathematical study of feedback control roles and relevance in stress erythropoiesis*, submitted, 2009.

[36] F. Crauste, L. Pujo-Menjouet, S. Génieys, C. Molina, and O. Gandrillon, *Adding self-renewal in committed erythroid progenitors improves the biological relevance of a mathematical model of erythropoiesis*, J. Theor. Biol. **250** (2008), 322–338.

[37] Y.F. Cui, B.I. Lord, L.B. Woolford, and N.G. Testa, *The relative spatial distribution of in vitro-cfcs in the bone marrow, responding to specific growth factors*, Cell Prolif. **29** (1996), 243–257.

[38] S. Dazy, F. Damiola, N. Parisey, H. Beug, and O. Gandrillon, *The MEK-1/ ERKs signalling pathway is differentially involved in the self-renewal of early and late avian erythroid progenitor cells*, Oncogene **22** (2003), 9205–9216.

[39] R. De Maria, U. Testa, L. Luchetti, A. Zeuner, G. Stassi, E. Pelosi, R. Riccioni, N. Felli, P. Samoggia, and C. Peschle, *Apoptotic role of Fas/Fas ligand system in the regulation of erythropoiesis*, Blood **93** (1999), 796–803.

[40] I. Demin, F. Crauste, O. Gandrillon, and V. Volpert, *A multi-scale model of erythropoiesis*, Journal of Biological Dynamics **4** (2010), 59–70.

[41] I. Demin, A. Ducrot, and V. Volpert, *Spatial distribution of cell populations in the process of erythropoiesis*, 2009.

[42] I. Demin and V. Volpert, *Existence of waves for a nonlocal reaction-diffusion equation*.

[43] D. Drasdo, S. Höhme, and M. Block, *On the role of physics in the growth and pattern formation of multi-cellular systems : What can we learn from individual-cell based models ?*, J. Stat. Phys. **128** (2007), 287–345.

[44] A. Ducrot and V. Volpert, *On a model of leukemia development with a spatial cell distribution*, Math. Model. Nat. Phenom. **3** (2007), 101–120.

[45] C.A. Finch, M.L. Hanson, and D.M. Donohue, *Kinetics of erythropoiesis. A comparison of response to anemia induced by phenylhydrazine and by blood loss*, Am. J. Physiol. **197** (1959), 761–764.

[46] P. Fortin and M.C. Mackey, *Periodic chronic myelogenous leukemia : Spectral analysis of blood cell counts and aetiological implications*, Brit. J. Haematol. **104** (1999), 336–345.

[47] F. Frassoni, N.G. Testa, and B.I. Lord, *The relative spatial distribution of erythroid progenitor cells (BFUe and CFUe) in the normal mouse femur*, Cell Tissue Kinet. **15** (1982), 447–455.

[48] A. Friedman, *Partial differential equations of parabolic type*, Prentice-Hall, Englewood Cliffs, 1964.

[49] A. Friedman and B. Hu, *Bifurcation from stability to instability for a free boundary problem arising in a tumor model*, Arch. Rational Mech. Anal. **180** (2006), 293–330.

[50] J. Galle, G. Aust, G. Schaller, T. Beyer, and D. Drasdo, *Individual cell-based models of the spatio-temporal organisation of multicellular systems - achievements and limitations*, Cytometry A **69A** (2006), 704–710.

[51] O. Gandrillon, U. Schmidt, H. Beug, and J. Samarut, *TGF-beta cooperates with TGF-alpha to induce the self-renewal of normal erythrocytic progenitors : evidence for an autocrine mechanism*, EMBO J. **18** (1999), 2764–2781.

[52] S. Génieys, V. Volpert, and P. Auger, *Pattern and waves for a model in population dynamics with nonlocal consumption of resources*, Math. Model. Nat. Phenom. **1** (2006), 63–80.

[53] T. Gregory, C. Yu, A. Ma, S.H. Orkin, G.A. Blobel, and M.J. Weiss, *GATA-1 and erythropoietin cooperate to promote erythroid cell survival by regulating bcl-xL expression*, Blood **94** (1999), 87–96.

[54] I. Gueorguieva, I.A. Nestorov, and M. Rowland, *Reducing whole body physiologically based pharmacokinetic models using global sensitivity analysis : diazepam case study*, J. Pharmacokinet. Pharmacodyn. **33** (2006), 1–27.

[55] S. Huang, Y.-P. Guo, G. May, and T. Enver, *Bifurcation dynamics in lineage-commitment in bipotent progenitor cells*, Dev. biol. **305** (2007), 695–713.

[56] F. Jacob, *Le monde des cellules souches*, C. R. Biologies **315** (2002), 999–1002.

[57] C.T. Jordan, *The leukemic stem cell*, Best Practice and Research Clinical Haematology **20** (2007), 13–18.

[58] L.P. Jordheim, C.M. Galmarini, and C. Dumontet, *Metabolism, mechanism of action and resistance to cytotoxic nucleoside analogue*, Bull. Cancer **92** (2005), 239–248.

[59] T. Kakihara, T. Fukuda, A. Tanaka, I. Emura, K. Kishi, K. Asami, and M. Uchiyama, *Expression of deoxycytidine kinase (dCK) gene in leukemic cells in childhood : decreased expression of dCK gene in relapsed leukemia*, Leuk. Lymphoma **31** (1998), 405–409.

[60] S. Kanno, T. Hiura, T. Ohtake, K. Koiwai, H. Suzuki, M. Ujibe, and M. Ishikawa, *Characterization of resistance to cytosine arabinoside (Ara-C) in NALM-6 human B leukemia cells*, Clin. Chim. Acta **377** (2007), 144–149.

[61] W. Kern and E.H. Estey, *High-dose cytosine arabinoside in the treatment of acute myeloid leukemia*, Cancer **107** (2006), 116–124.

[62] W. Kong, K. Engel, and J. Wang, *Mammalian nucleoside transporters*, Curr. Drug Metab. **5** (2004), 63–84.

[63] M.J. Koury and M.C. Bondurant, *Erythropoietin retards DNA breakdown and prevents programmed death in erythroid progenitor cells*, Science **248** (1990), 378–381.

[64] A. Kowal-Vern, F.M. Mazzella, J.D. Cotelingam, M.A. Shrit, J.T. Rector, and H.R. Schumacher, *Diagnosis and characterization of acute erythroleukemia subsets by determining the percentages of myeloblasts and proerythroblasts in 69 cases*, Am. J. Hematol. **65** (2000), 5–13.

[65] T.L. Lincoln, P.F. Morrison, J. Aroesty, and G. Carter, *Computer simulation of leukemia therapy : combined pharmacokinetics, intracellular enzyme kinetics, and cell kinetics of the treatment of l1210 leukemia by cytosine arabinoside.*, Cancer Treat. Rep. **60** (1976), 1723–1739.

[66] B.I. Lord, *The architecture of bone marrow cell populations*, Int. J. Cell Cloning **8** (1990), 317–331.

[67] M.C. Mackey, *Unified hypothesis of the origin of aplastic anaemia and periodic haematopoiesis*, Blood **51** (1978), 941–956.

[68] ———, *Dynamic hematological disorders of stem cell origin.*, Biophysical and Biochemical Information Transfer in Recognition (1979), 373–409.

[69] M.C. Mackey and R. Rudnicki, *Global stability in a delayed partial differential equation describing cellular replication*, J. Math. Biol. **33** (1994), 89–109.

[70] A. Madan, C. Lin, Z. Wang, and P.T. Curtin, *Autocrine stimulation by erythropoietin in transgenic mice results in erythroid proliferation without neoplastic transformation*, Blood Cells, Molecules and Diseases **30** (2003), 82–89.

[71] J.M. Mahaffy, J. Bélair, and M.C. Mackey, *Hematopoietic model with moving boundary condition and state dependent delay : applications in erythropoiesis*, J. Theor. Biol. **190** (1998), 135–146.

[72] D Manwani and J.J. Bieker, *The erythroblastic island*, Curr. Top. Dev. Biol. **82** (2008), 23–53.

[73] A. Matsuda and T. Sasaki, *Antitumor activity of sugar-modified cytosine nucleosides*, Cancer Sci. **95** (2004), 105–111.

[74] F.M. Mazzella, C. Alvares, A. Kowal-Vern, and H.R. Schumacher, *The acute erythroleukemias*, Clin. Lab. Med. **20** (2000), 119–137.

[75] K.A. Moore and I.R. Lemischka, *Stem cells and their niches*, Science **311** (2006), 1880–1885.

[76] P.F. Morrison, T.L. Lincoln, and J. Aroesty, *The disposition of ara-c and its metabolites : a pharmacokinetic simulation*, Cancer Chemother. Rep. **59** (1975), 861–876.

[77] V. Munugalavadla and R. Kapur, *Role of c-Kit and erythropoietin receptor in erythropoiesis*, Critical Reviews in Oncology/Hematology **54** (2005), 63–75.

[78] J.D. Murray, *Mathematical biology*, Springer, New York, 2004.

[79] Y. Nagata, N. Takahashi, R.J. Davis, and K. Todokoro, *Activation of p38 MAP kinase and JNK but not ERK is required for erythropoietin-induced erythroid differentiation*, Blood **92** (1998), 1859–1869.

[80] S.K. Nilsson, H.M. Johnston, and J.A. Coverdale, *Spatial localization of transplanted hemopoietic stem cells : inferences for the localization of stem cell niches*, Blood **97** (2001), 2293–2299.

[81] S.K. Nilsson, H.M. Johnston, G.A. Whitty, B. Williams, R.J. Webb, D.T. Denhardt, I. Bertoncello, L.J. Bendall, P.J. Simmons, and D.N. Haylock, *Osteopontin, a key component of the hematopoietic stem cell niche and regulator of primitive hematopoietic progenitor cells*, Blood **15** (2005), 1232–1239.

[82] J.K. Owens, D.S. Shewach, B. Ullman, and B.S. Mitchell, *Resistance to 1-beta-D-arabinofuranosylcytosine in human T-lymphoblasts mediated by mutations within the deoxycytidine kinase gene*, Cancer Res. **52** (1992), 2389–2399.

[83] B. Pain, C.M. Woods, J. Saez, T. Flickinger, M. Raines, S. Peyroll, C. Moscovici, M. G. Moscovici, H.-J. Kung, P. Jurdic, E. Lazarides, and J. Samarut, *Egf-r as a hemopoietic growth factor receptor : the c-erbb product is present in normal chicken erythrocytic progenitor cells and controls their self-renewal*, Cell **65** (1991), 37–46.

[84] K. Parmar, P. Mauch, J.A. Vergilio, R. Sackstein, and J.D. Down, *Distribution of hematopoietic stem cells in the bone marrow according to regional hypoxia*, Proc. Natl. Acad. Sci. USA **104** (2007), 5431–5436.

[85] E. Piroso, A.J. Erslev, K.K. Flaharty, and J. Caro, *Erythropoietin life span in rats with hypoplastic and hyperplastic bone marrows*, Am. J. Hematol. **36** (1991), 105–110.

[86] A. Plesa, G. Ciuperca, V. Louvet, L. Pujo-Menjouet, S. Génieys, C. Dumontet, X. Thomas, and V. Volpert, *Diagnostics of the AML with immunophenotypical data*, Math. Model. Nat. Phenom. **2** (2009), 104–123.

[87] L. Preziosi, *Cancer modelling and simulation*, Chapman & Hall/CRC Mathematical Biology and Medicine Series, 2003.

[88] I. Rajman, *PK/PD modelling and simulations : utility in drug development*, Drug Discovery Today **13** (2008), 341–346.

[89] B. Ribba, K. Marron, Z. Agur, T. Alarcón, and P.K. Maini, *A mathematical model of doxorubicin treatment efficacy for non-hodgkin's lymphoma : investigation of the current protocol through theoretical modelling results*, Bulletin of Mathematical Biology **67** (2005), 79–99.

[90] D.M. Ridley, F. Dawkins, and E. Perlin, *Erythropoietin : a review*, J. Natl. Med. Assoc. **86** (1994), 129–135.

[91] I. Roeder, *Quantitative stem cell biology : computational studies in the hematopoietic system*, Curr. Opinion Hematol. **13** (2006), 222–228.

[92] I. Roeder and I. Glauche, *Towards an understanding of lineage specification in hematopoietic stem cells : A mathematical model for the interaction of transcription factors GATA-1 and PU.1*, J. Theor. Biol. **241** (2006), 852–865.

[93] I. Roeder and M. Loeffler, *A novel dynamic model of hematopoietic stem cell organization based on the concept of within-tissue plasticity*, Exp. Hematol. **30** (2002), 853–861.

[94] S.I. Rubinow and J.L. Lebowitz, *A mathematical model of the acute myeloblastic leukemic state in man.*, Biophys. J. **16** (1976), 897–910.

[95] ———, *A mathematical model of the chemotherapeutic treatment of acute myeloblastic leukemia*, Biophys. J. **16** (1976), 1257–1271.

[96] C. Rubiolo, D. Piazzolla, K. Meissl, H. Beug, J.C. Huber, A. Kolbus, and M. Baccarini, *A balance between Raf-1 and Fas expression sets the pace of erythroid differentiation*, Blood **108** (2006), 152–159.

[97] Y.M. Rustum and H.D. Preisler, *Correlation between leukemic cell retention of 1-β-d-arabinofuranosylcytosine 5'-triphosphate and response to therapy*, Cancer Res. **39** (1979), 42–49.

[98] S.T. Sawyer and S.M. Jacobs-Helber, *Unraveling distinct intracellular signals that promote survival and proliferation : study of erythropoietin, stem cell factor, and constitutive signaling in leukemic cells*, J. Hematother. Stem Cell Res. **9** (2000), 21–29.

[99] Y. Shiozawa, A.M. Havens, K.J. Pienta, and R.S. Taichman, *The bone marrow niche : habitat to hematopoietic and mesenchymal stem cells, and unwitting host to molecular parasites*, Leukaemia **22** (2008), 941–950.

[100] E.L.J.M. Smits, Z.N. Berneman, and V.F.I. van Tendeloo, *Immunotherapy of acute myeloid leukemia : Current approaches*, The Oncologist **14** (2009), 240–252.

[101] H. Someya, S.C. Shaddix, K.N. Tiwari, J.A. 3rd. Secrist, and W.B. Parker, *Phosphorylation of 4'-thio-beta-d-arabinofuranosylcytosine and its analogs by human deoxycytidine kinase*, J. Pharmacol. Exp. Ther. **304** (2003), 1314–1322.

[102] P. Sonneveld and A.F. List, *Chemotherapy resistance in acute myeloid leukaemia*, Best Practice and Research Clinical Haematology **14** (2001), 211–233.

[103] J.L. Spivak, T. Pham, M. Isaacs, and W.D. Hankins, *Erythropoietin is both a mitogen and a survival factor*, Blood **77** (1991), 1228–1233.

[104] X. Sui, S.B. Krantz, M. You, and Z.J. Zhao, *Synergistic activation of MAP kinase (ERK1/2) by erythropoietin and stem cell factor is essential for expanded erythropoiesis*, Blood **92** (1998), 1142–1149.

[105] X. Sui, S.B. Krantz, and Z.J. Zhao, *Stem cell factor and erythropoietin inhibit apoptosis of human erythroid progenitor cells through different signalling pathways*, Br. J. Haematol. **110** (2000), 63–70.

[106] D.M. Swirsky and S.J. Richards, *Laboratory diagnosis of acute myeloid leukaemia*, Best Practice and Research Clinical Haematology **14** (2001), 1–17.

[107] R.S. Taichman, *Blood and bone : two tissues whose fates are intertwined to create the hematopoietic stem-cell niche*, Blood **105** (2005), 2631–2639.

[108] U. Testa, *Apoptotic mechanisms in the control of erythropoiesis*, Leukemia **18** (2004), 1176–1199.

[109] J. E. Till and E. A. McCulloch, *A direct measurement of the radiation sensitivity of normal mouse bone marrow cells*, Radiat. Res. **14** (1961), 213–222.

[110] K. Tokoyoda, T. Egawa, T. Sugiyama, B. Choi, and T. Nagasawa, *Cellular niches controlling b lymphocyte behavior within bone marrow during development*, Immunity **20** (2004), 707–718.

[111] T.N. Tozer and M. Rowland, *Introduction to pharmacokinetics and pharmacodynamics : The quantitative basis of drug therapy.*, Lippincott, Philadelphia, 2006.

[112] D.A. Tsakiris and A. Tichelli, *Thrombotic complications after haematopoietic stem cell transplantation : early and late effects*, Best Practice and Research Clinical Haematology **22** (2009), 137–145.

[113] Y. Tsukamoto, Y. Kato, M. Ura, I. Horii, T. Ishikawa, H. Ishitsuka, and Y. Sugiyama, *Investigation of 5-FU disposition after oral administration of capecitabine, a triple-prodrug of 5-FU, using a physiologically based pharmacokinetic model in a human cancer xenograft model : comparison of the simulated 5-FU exposures in the tumour tissue between human and xenograft model*, Biopharm. Drug Dispos. **22** (2001), 1–14.

[114] W. Vainchenker, A. Dusa, and S.N. Constantinescu, *JAKs in pathologies : Role of Janus kinases in hematopoietic malignancies and immunodeficiencies*, Seminars in Cell and Developmental Biology **19** (2008), 385–393.

[115] P. Veng-Pedersen, S. Chapel, R.L. Schmidt, N.H. Al-Huniti, R.T. Cook, and J.A. Widness, *An integrated pharmacodynamic analysis of erythropoietin, reticulocyte, and hemoglobin responses in acute anemia*, Pharmaceutical Research **19** (2002), 1630–1635.

[116] A. Volpert and V. Volpert, *Normal solvability of general linear elliptic problems*, Abstract and Applied Analysis **7** (2005), 733–756.

[117] A. Volpert, Vl. Volpert, and Vit. Volpert, *Travelling wave solutions of parabolic systems*, AMS, Providence, 1994.

[118] A.I. Volpert and V.A. Volpert, *Applications of the rotation theory of vector fields to the*

study of wave solutions of parabolic equations, Trans. Moscow Math. Soc. **52** (1990), 59–108.

[119] V. Volpert and A. Volpert, *Properness and topological degree for general elliptic operators*, Abstract and Applied Analysis **2003** (2003), 129–181.

[120] V. Volpert, A. Volpert, and J.F. Collet, *Topological degree for elliptic operators in unbounded cylinders*, Adv. Diff. Eq. **4** (1999), 777–812.

[121] M. von Kleist and W. Huisinga, *Physiologically based pharmacokinetic modelling : a subcompartmentalized model of tissue distribution*, J Pharmacokinet Pharmacodyn. **34** (2007), 789–806.

[122] C.J. Watchman, A.V. Bourke, J.R. Lyon, A.E. Knowlton, S.L. Butler, D.D. Grier, J.R. Wingard, R.C. Braylan, and V.E. Bolch, *Spatial distribution of blood vessels and CD34$^+$ hematopoietic stem and progenitor cells within the marrow cavities of human cancellous bone*, J. Nucl. Med. **48** (2007), 645–654.

[123] F.M. Watt and B.L. Hogan, *Out of eden : stem cells and their niches*, Science **287** (2000), 1427–1430.

[124] I.L. Weissman, *Stem cells : units of development, units of regeneration, and units in evolution*, Cell **100** (2000), 157–168.

[125] J.C. White, J.P. Rathmell, and R.L. Capizzi, *Membrane transport influences the rate of accumulation of cytosine arabinoside in human leukemia cells*, J. Clin. Invest. **79** (1987), 380–387.

[126] H.E. Wichmann and M. Loeffler, *Mathematical modeling of cell proliferation*, CRC Press, Boca Raton, Florida, 1985.

[127] H.E. Wichmann, M. Loeffler, K. Pantel, and H. Wulff, *A mathematical model of erythropoiesis in mice and rats. Part 2. Stimulated erythropoiesis*, Cell Tissue Kinet. **22** (1989), 31–49.

[128] H. Wulff, H.E. Wichmann, M. Loeffler, and K. Pantel, *A mathematical model of erythropoiesis in mice and rats. Part 3. Suppressed erythropoiesis*, Cell Tissue Kinet. **22** (1989), 51–61.

[129] S.J. Yaffe and J.V. Aranda, *Pediatric pharmacology*, 2nd ed., ch. 41, pp. 466–475, W.B. Saunders Company, Philadelphia, 1992.

Résumé

Cette thèse est consacrée à la modélisation mathématique de l'hématopoïèse et des maladies sanguines. Plusieurs modèles traitant d'aspects différents et complémentaires de l'hématopoïèse y sont étudiés.

Tout d'abord, un modèle multi-échelle de l'érythropoïèse est analysé, dans lequel sont décrits à la fois le réseau intracellulaire, qui détermine le comportement individuel des cellules, et la dynamique des populations de cellules. En utilisant des données expérimentales sur les souris, nous évaluons les rôles des divers mécanismes de retro-contrôle en réponse aux situations de stress.

Ensuite, nous tenons compte de la distribution spatiale des cellules dans la mœlle osseuse, question qui n'avait pas été étudiée auparavant. Nous décrivons l'hématopoïèse normale à l'aide d'un système d'équations de réaction-diffusion-convection et nous démontrons l'existence d'une distribution stationnaire des cellules. Puis, nous introduisons dans le modèle les cellules malignes. Pour certaines valeurs des paramètres, la solution "disease-free" devient instable et une autre solution, qui correspond à la leucémie, apparaît. Cela mène à la formation d'une tumeur qui se propage dans la mœlle osseuse comme une onde progressive. La vitesse de cette propagation est étudiée analytiquement et numériquement. Les cellules de la mœlle osseuse échangent des signaux qui régulent le comportement cellulaire. Nous étudions ensuite une équation integro-différentielle qui décrit la communication cellulaire et nous prouvons l'existence d'une solution du type onde progressive en utilisant la théorie du degré topologique et la méthode de Leray et Schauder. L'approche multi-agent est utilisée afin d'étudier la distribution des differents types de cellules dans la mœlle osseuse.

Finalement, nous étudions un modèle de type "Physiologically Based Pharmacokinetics-Pharmacodynamics" du traitement de la leucémie par l'AraC. L'AraC agit comme chimiothérapie et induit l'apoptose de toutes les cellules proliférantes, saines et malignes. La pharmacocinétique donne accès à la concentration intracellulaire d'AraC. Cette dernière, à son tour, détermine la dynamique des populations cellulaires et, par conséquent, l'efficacité de différents protocoles de traitement.

Mots-clés: modèle multi-échelle de l'érythropoïèse, réseau de régulation intracellulaire, ondes progressives, équation integro-différentielle, modèle multi-agent, méthode de Leray-Schauder, PK/PD, modélisation du traitement de leucémie.

Mathematical modelling of haematopoiesis and blood diseases

Abstract

This PhD thesis is devoted to mathematical modelling of haematopoiesis and blood diseases. We investigate several models, which deal with different and complementary aspects of haematopoiesis.

The first part of the thesis concerns a multi-scale model of erythropoiesis where intracellular regulatory networks, which determine cell choice between self-renewal, differentiation and apoptosis, are coupled with dynamics of cell populations. Using experimental data on anemia in mice, we evaluate the roles of different feedback mechanisms in response to stress situations.

At the next stage of modelling, spatial cell distribution in the bone marrow is taken into account, the question which has not been studied before. We describe normal haematopoiesis with a system of reaction-diffusion-convection equations and prove existence of a stationary cell distribution. We then introduce malignant cells into the model. For some parameter values the disease free solution becomes unstable and another one, which corresponds to leukaemia, appears. This leads to the formation of tumour which spreads in the bone marrow as a travelling wave. The speed of its propagation is studied analytically and numerically. Bone marrow cells exchange different signals that regulate cell behaviour. We study, next, an integro-differential equation which describes cell communication and prove the existence of travelling wave solutions using topological degree and the Leray-Schauder method. Individual based approach is used to study distribution of different cell types in the bone marrow.

Finally, we investigate a Physiologically Based Pharmacokinetics-Pharmacodynamics model of leukaemia treatment with AraC drug. AraC acts as chemotherapy, inducing apoptosis of all proliferating cells, normal and malignant. Pharmacokinetics provides the evolution of intracellular AraC. This, in turn, determines cell population dynamics and, consequently, efficacy of treatment with different protocols.

Keywords: multi-scale model of erythropoiesis, intracellular regulatory network, travelling wave solutions, integro-differential equation, individual based model, Leray-Schauder method, PK/PD, Michaelis-Menten kinetics.